Technische Universität München

TUM School of Life Sciences

PIN-FORMED PROTEINs from *Arabidopsis thaliana*: Biochemical characterization of functional domains and transport properties

Dorina P. Janacek

Vollständiger Abdruck der von der TUM School of Life Sciences der Technischen Universität München zur Erlangung des akademischen Grades einer

Doktorin der Naturwissenschaften (Dr. rer. nat.)

genehmigten Dissertation.

Vorsitz:	Prof. Dr. Ralph Hückelhoven
Prüfer der Dissertation:	1. Priv.-Doz. Dr. Ulrich Z. Hammes
	2. Prof. Dr. Kay H. Schneitz

Die Dissertation wurde am 30.03.2023 bei der Technischen Universität München eingereicht und durch die TUM School of Life Sciences am 26.07.2023 angenommen.

In the soil below
Lies a seed, waiting to grow
Tiny, fragile, yet full of life
Ready to break free from strife

As the seedling emerges
Auxin guides its every verge
Sending signals down the roots
Telling them which way to shoot

Through the soil, the roots they reach
Absorbing water, nutrients—each
Growing stronger day by day
As they seek the home they'll stay

And from above, the plant's abloom
Through sunshine, rain, and thunder's boom
A testament of growth and life
Fueled by seeds, roots, auxin, and strife.

— ChatGTP 3.5

Abstract

PIN-FORMED PROTEINs (PINs) are the main factors in polar auxin transport (PAT). Their cell biology has been studied extensively over the last decades and members of the AGCVIII kinase family were identified as regulators of cellular localization and activation of PINs.

In this thesis I determined the transport properties of canonical PINs and the impact of the PIN protein domains on transport. PINs consist of two transmembrane (TM) domains and a cytosolic loop domain. The loop domain contributes to the regulation of localization and has been viewed mainly as on/off switch for transport activity upon phosphorylation, whereas the TM domains form the transporter unit in the plasma membrane (PM). Using *Xenopus laevis* oocytes, the concentration-dependent transport properties of PINs were investigated and more members of the AGCVIII kinase family and of other kinase families were tested with respect to their potential to activate transport. The agravitropic root phenotype of the *pin2* mutant was used to monitor the impact of modulating auxin flow on gravitropic root growth and root bending rates.

Through domain swapping of canonical and noncanonical PINs, additional layers of PIN-mediated transport regulation were identified. The loop contributes to transport itself by intramolecular interactions with the TM domains. It is suggested that the loop modulates the TM domain context and that some regulatory aspects are dependent on the combination of the PIN domains. Neither all AGVIII kinases nor members of other kinase families could activate PIN transport. Further, the kinase directly impacts the PIN transport properties, which underlines the importance of the kinase identity. This suggests distinct structural interactions of the kinase with the TM domains and the loop domain.

It was concluded that the level of (activated) PIN in the PM determines the net flux over the membrane, the loop domain and the kinase impact the transport properties through structural interactions with the TM domains and/or the loop domain, but that the observed differences in transport activity might be compensated in the plant and that activation of transport is limited to some members of the AGCVIII kinase family.

The transport data are in line with the data obtained *in planta*, which contributes to explain the auxin levels in the root. The results demonstrate that PAT and auxin flow cannot be explained solely by the cellular localization of PINs. Polar localization to the PM is necessary for PAT, but not sufficient to explain auxin distribution by PIN-mediated transport. In the future, it will be necessary to understand which molecular mechanisms lead to the differences in transport rates observed for different PINs.

Zusammenfassung

PIN-FORMED Proteine (PINs) sind maßgeblich für den polaren Auxintransport in Pflanzen verantwortlich. Ihre Zellbiologie wurde in den letzten Jahrzehnten eingehend untersucht und Kinasen der AGCVIII-Kinasefamilie wurden als Regulatoren der zellulären Lokalisierung und Aktivierung der PINs identifiziert.

Ziel dieser Arbeit war es die Transporteigenschaften von kanonischen PINs und den Beitrag der Proteindomänen zum Transport zu bestimmen. Die PINs setzen sich aus zwei Transmembran (TM)-Domänen und der zytosolischen Loop-Domäne zusammen. Die Loop-Domäne ist an der Lokalisierungsregulation beteiligt und wurde bisher als phosphorylierungsabhängiger Aktivierungsschalter betrachtet, wohingegen die Transmembran (TM)-Domänen die Transporter-Einheit in der Plasmamembran (PM) bilden. In Oozyten von *Xenopus laevis* wurden die Transporteigenschaften in Abhängigkeit von der Substratkonzentration der PINs untersucht und weitere Mitglieder der AGCVIII-Kinasefamilie und anderer Kinasefamilien hinsichtlich ihres Potentiales PINs zu aktiveren untersucht. Mittels des agravitropen Wurzelphänotyps der *pin2* Mutante wurde der Einfluss von modifizierten Auxinflüssen anhand von Wurzelwachstum und Biegung der Wurzelspitze nach Änderung des Gravitationsvektors untersucht.

Durch das Austauschen von Proteindomänen kanonischer und nichtkanonischer PINs konnten weitere Ebenen der Transportregulierung identifiziert werden. Die Loop-Domäne trägt durch intramolekulare Interaktionen mit den TM-Domänen zum Transport bei. Es wird vermutet, dass die Loop-Domäne den Kontext der TM-Domänen moduliert und dass manche regulatorischen Aspekte durch bestimmte Kombinationen der PIN-Domänen beeinflusst werden können. Der PIN-Transport wurde weder von allen Mitgliedern der AGCVIII-Kinasefamilie, noch von Mitgliedern anderer Kinasefamilien aktiviert. Zudem beeinflusst die aktivierende Kinase direkt die Transporteigenschaften eines PINs, was die Notwendigkeit nach kompatiblen PIN-Kinase-Kombinationen unterstreicht. Dies legt eine strukturelle Interaktion zwischen der Kinase und den TM-Domänen, sowie der Loop-Domäne nahe.

Daraus ergibt sich, dass die Menge an (aktivierten) PINs in der PM den Netto-Efflux über die Membran bestimmt, dass Loop-Domäne und Kinase die Transporteigenschaften durch strukturelle Interaktion zwischen TM-Domäne und/oder Loop-Domäne beeinflussen, aber dass die beobachteten Unterschiede in der Pflanze kompensiert werden und dass nur einzelne Mitglieder der AGCVIII-Kinasefamilie PINs aktivieren können.

Anhand der Transporteigenschaften der PINs können die Auxinlevel in der Wurzel besser erklärt werden. Die Ergebnisse dieser Arbeit stellen die gängige Meinung, dass die zelluläre Lokalisierung der PINs ausreiche, um polaren Auxinfluss zu beschreiben, in Frage. Die polare Lokalisierung in der PM ist notwendig, aber nicht hinreichend um die Auxinverteilung zu erklären. In der Zukunft wird es notwendig sein, die molekularen Mechanismen zu verstehen, die zu den beobachteten Unterschieden führen, um PINs mit definierten Charakteristiken zu schaffen.

List of publications

Parts of the thesis will be published in:

Janacek, D.P., Kolb, M., Schulz, L., Glanc, M., Friml, J., Ten Tusscher, K.H., Mergner, J., Küster, B., Schwechheimer, C., Hammes, U.Z. (2023). Transport properties of canonical PIN proteins and the role of the loop in auxin transport. Nat Plants.

Publications from doctoral work not included in this thesis:

Abas, L., Kolb, M., Stadlmann, J., **Janacek, D.P.**, Lukic, K., Schwechheimer, C., Sazanov, L.A., Mach, L., Friml, J., and Hammes, U.Z. (2021). Naphthylphthalamic acid associates with and inhibits PIN auxin transporters. Proc Natl Acad Sci U S A 118.

Marhava, P., Aliaga Fandino, A.C., Koh, S.W.H., Jelinkova, A., Kolb, M., **Janacek, D.P.**, Breda, A.S., Cattaneo, P., Hammes, U.Z., Petrasek, J., and Hardtke, C.S. (2020). Plasma Membrane Domain Patterning and Self-Reinforcing Polarity in Arabidopsis. Dev Cell 52, 223-235 e225.

Roth, O., Yechezkel, S., Serero, O., Eliyahu, A., Vints, I., Tzeela, P., Carignano, A., **Janacek, D.P.**, Peters, V., Kessel, A., Dwivedi, V., Carmeli-Weissberg, M., Shaya, F., Faigenboim-Doron, A., Riov, J., Klavins, E., Dawid, C., Hammes, U.Z., Ben-Tal, N., Napier, R., Sadot, E., and Weinstain, R. (2023). Alleviating the barrier of adventitious roots formation in recalcitrant mature tissue by slow release of a synthetic auxin. bioRxiv, 2023.2003.2013.532257.

Skokan, R., Medvecka, E., Viaene, T., Vosolsobe, S., Zwiewka, M., Muller, K., Skupa, P., Karady, M., Zhang, Y., **Janacek, D.P.**, Hammes, U.Z., Ljung, K., Nodzynski, T., Petrasek, J., and Friml, J. (2019). PIN-driven auxin transport emerged early in streptophyte evolution. Nat Plants 5, 1114-1119.

Ung, K.L., Winkler, M., Schulz, L., Kolb, M., **Janacek, D.P.**, Dedic, E., Stokes, D.L., Hammes, U.Z., and Pedersen, B.P. (2022). Structures and mechanism of the plant PIN-FORMED auxin transporter. Nature 609, 605-610.

Yang, S., de Haan, M., Mayer, J., **Janacek, D.P.**, Hammes, U.Z., Poppenberger, B., and Sieberer, T. (2022). A novel chemical inhibitor of polar auxin transport promotes shoot regeneration by local enhancement of HD-ZIP III transcription. New Phytol 235, 1111-1128.

List of figures

List of tables

Abbreviations

2,4-D ..... 2,4-Dichlorophenoxyacetic acid
AAAP ..... AMINO ACID PERMEASE
ABA ..... Abscisic acid
ABC ..... ATP-BINDING CASSETTE
AnP ..... Antarctic Phosphatase
AUX1 ..... AUXIN RESISTANT 1
BRX ..... BREVIS RADIX
bud1 ..... bushy and dwarf 1
CAMEL ..... CANALIZATION-RELATED AUXIN-REGULATED MALECTIN-TYPE RECEPTOR KINASE
CANAR ..... CANALIZATION-RELATED RECEPTOR-LIKE KINASE
CDS ..... Coding sequence
CRK ..... Ca2+/CALMODULIN-DEPENDENT PROTEIN KINASE-RELATED KINASE
cRNA ..... copy RNA
Cryo-EM ..... Cryogenic electron microscopy
D6PK ..... D6 PROTEIN KINASE
DII ..... Domain II
EDTA ..... Ethylenediaminetetraacetic acid
ENP1 ..... ENHANCER OF PINOID 1
ER ..... Endoplasmatic reticulum
FACS ..... Fluorescence-activated cell sorting
FRAP ..... Fluorescence after photo-bleaching
gDNA ..... genomic DNA, genomic DNA
GFP ..... Green flueorescent protein
GUS ..... β-Glucoronidase
HK1 ..... HISTIDINE KINASE 1
IAA ..... Indole-3-acetic acid
IBA ..... Indole-3-butyric acid
IMAC ..... Immobilized metal affinity chromatography
LAX ..... LIKE-AUX
LFQ ..... Label-free quantification
LRC ..... Lateral root cap
MAB4 ..... MACCHI-BOU 4
MAP ..... MITOGEN-ACTIVATED
MKK ..... MAP KINASE KINASE
MKKK ..... MAP KINASE KINASE KINASE
MPK ..... MAP KINASE
MS ..... Mass spectrometry, Murashige & Skoog
NPA ..... *N*-1-naphthylphthalamic acid
NPF ..... NITRATE TRANSPORTER 1/PEPTIDE TRANSPORTER
PA ..... Phosphatidic acid
PAT ..... Polar auxin transport
PAX ..... PROTEIN KINASE ASSOCIATED WITH BRX

PDK1 ..... 3-PHOSPHOINOSITIDE-DEPENDENT PROTEIN KINASE 1
PI ..... Phosphoinositide
$PI(4,5)P_2$ Phosphatidylinositol-4,5-bisphosphate
PI4P Phosphatidylinositol-4-phosphate
PID ..... PINOID
PIF ..... PDK1-interacting fragment
PILS ..... PIN-LIKE PROTEIN
PIN ..... PIN-FORMED PROTEIN
PIP5K ..... PHOSPHATIDYLINOSITOL 4-PHOSPHATE 5-KINASE
PLD ..... PHOSPHOLIPASE D
PM ..... Plasma membrane
PP2A ..... PROTEIN PHOSPHATASE 2A
PYL ..... PYRABACTIN RESISTANCE 1-LIKE
PYR ..... PYRABACTIN RESISTANCE 1
QC ..... Quiescent center
RCAR ..... REGULATORY COMPONENT OF ABA RECEPTOR
ROI ..... Region of interest
SPR ..... Surface plasmon resonance
TM ..... Transmembrane
TOB1 ..... TRANSPORTER OF IBA 1
UCN ..... UNICORN
UMAMIT ..... USUALLY AMINO ACIDS MOVE IN AND OUT TRANSPORTER
VGI ..... Vertical growth index
WAG1 ..... WAVY ROOT GROWTH 1
WAT1 ..... WALLS ARE THIN 1
YFP ..... Yellow fluorescent protein

Contents

1 Introduction

1.1 The phytohormone auxin

1.1.1 History

Phytohormones occur naturally in plants and act as signaling molecules with a strong impact on plant physiology and development. In 1880, a mobile signal in grass coleoptiles that transports positional information from the plant tip through the plant body was described by Charles Darwin and his son (Darwin and Darwin, 1880). Later this signal was isolated from fermentation media and was identified as indole-3-acetic acid (IAA), that belongs to the group of auxins (Salkowski, 1885; Kögl *et al.*, 1934). Auxins are organic acids with a low molecular weight, consisting of an indole ring with a carboxyl group in close distance (George *et al.*, 2007). Throughout the plant kingdom, auxins are present from Streptophyte algae to flowering plants at low concentrations and play a role in all developmental processes. They are synthesized in dividing tissues, like the leaf tip or locally in the root apex and released from dying tissues (Petersson *et al.*, 2009; Sheldrake, 2021). The most abundant auxin is in most plant species IAA. Comparable to morphogens, which govern pattern formation through an uneven distribution in a tissue, IAA acts through gradients in the plant body, which makes it a suitable molecule to connect plant growth to environmental stimuli.

1.1.2 Physico-chemical properties and necessity of auxin transport

IAA is distributed in the plant by diffusion through plasmodesmata, by long-distance transport through the phloem and by short-distance transport from cell to cell (Goldsmith *et al.*, 1974; Cande and Ray, 1976; Mellor *et al.*, 2020). The cell-to-cell transport occurs in a directional way by polarly localized auxin export transporters and is therefore called polar auxin transport (PAT).

The chemical properties of IAA make it necessary to have a network of importer and exporter proteins to establish auxin gradients, as suggested by the chemiosmotic hypothesis by Rubery, Sheldrake and Raven (Rubery and Sheldrake, 1974; Raven, 1975). IAA is a weak acid with a pK_a of 4.85. In the apoplast, with a pH of 5.5, only 17 % of the IAA fraction is protonated. This population can enter the cell by passive diffusion through the lipid bilayer. The dissociated fraction of IAA is transported by auxin influx proteins into the cell. In the cytosol, the pH is 7.4 and the proportion which favors the dissociated form of IAA. The dissociated IAA cannot cross the membrane and the efflux of IAA from the cytoplasm to the apoplast must be mediated by efflux transport proteins.

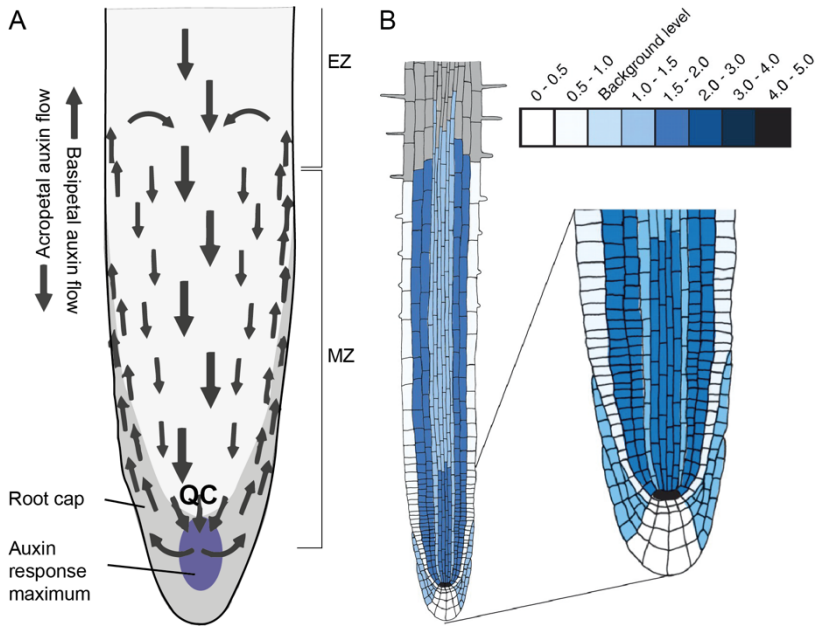

Figure 1 – Auxin flux and levels in the Arabidopsis root. (A) Acropetal auxin flow from the shoot leads to increased auxin levels in the QC. Basipetal transport processes distribute auxin at the lateral sides of the root. Size of arrows correlates with strength of auxin flow. QC: quiescent center. MZ: meristematic zone. EZ: elongation zone. Figure modified from Kepinski and Leyser, 2005. (B) Auxin gradient in the root derived from FACS and MS analyses with maximal auxin levels in the QC. Auxin levels in the cortex, the endodermis and the stele are elevated. Auxin levels in the columella and the epidermis are below average. Figure from Petersson *et al*., 2009.

1.1.3 How auxin flows

The auxin reflux/fountain model (Figure 1A) describes the self-perpetuating flow of auxin from the shoot through the vasculature to the root apical meristem (acropetal auxin flow) and back towards the elongation zone (basipetal auxin flow). It is based on the localization of auxin transporters, the initial observation that horizontally grown pea roots accumulated C14-labelled IAA in the lower half of the root and on mathematical models of the auxin flow (Konings, 1967; Benjamins and Scheres, 2008). An auxin maximum at the quiescent center (QC) is necessary in order to maintain the root meristem. From there, auxin is transported into the root cap away from the QC and distributed laterally from the columella through the epidermis by auxin transporters. An auxin minimum at the transition zone determines the shift from cell division to differentiation (Di Mambro *et al.*, 2017). In the elongation zone, auxin flows back into the vasculature by diffusion and lateral transport. Auxin response can be visualized by transcriptional reporter constructs like *DR5:GUS* or *DR5:GFP*, which show a strong signal in the columella (Ulmasov *et al.*, 1997; Ottenschlager *et al.*, 2003). However, a study combining fluorescence-activated cell sorting (FACS) and mass spectrometry (MS) found that QC cells accumulate the highest IAA concentration, whereas the columella is largely devoid of IAA (Petersson *et al.*, 2009). This indicates that auxin levels and transcriptional response are uncoupled in these cells. The study provided clear evidence of an auxin gradient in the root apex, with elevated IAA levels in the cortex, endodermis and the stele, and lower levels than the average in the epidermis

and the columella (Figure 1 B). In order to sustain the gradient in the root, auxin flow is highly dependent on controlled transport processes.

1.1.4 Plant tropisms

External changes in the plant's environment make it necessary to adapt plant growth to a new situation. Rapid nastic plant movements are determined by the structure of the organ and often depend on changes in turgor pressure, e.g. movement of stomata or closing of the Venus flytrap (Mano and Hasebe, 2021). In contrast, in tropisms the direction of organ movement depends on the direction of the stimulus. Positive tropism describes the movement towards the stimulus, e.g. root growth towards the earth center, and negative tropism describes growth away from the stimulus, e.g. shoot growth against the gravity. These processes are slower compared to nastic movements, because they require signal detection, signal transduction and altered directional growth.

Early experiments established the role of auxin in these processes: In the 1920s, the Cholodny-Went model established the asymmetrical distribution of auxin as reason for differential growth in plant tropisms (Went, 1974). Experiments with illuminated coleoptiles revealed that auxin accumulates at the shady side of the tip, which stimulates cell elongation and results in shoot bending towards the light source. Later the model was expanded to gravitropic growth. It was shown that auxin accumulation in the above ground tissues leads to cell elongation, whereas in the root it has the opposite effect (Swarup *et al.*, 2005; Esmon *et al.*, 2006). The cells on the upper root side expand normally which lead to root bending.

1.2 Auxin and the root

1.2.1 Root growth

Plants are sessile organisms and must find ways to access water and nutrients in changing environments. The decisive reason for successful adaption is the very dynamic root growth, which follows the gravity vector and can adjust to avoid obstacles through modulating its growth direction. This process is also impacted by hormonal crosstalk and cytoskeletal dynamics.

Growth on solid medium is distinct from growth on soil. On high percentages of agar, roots show different classes of movements: tropisms as a reaction to directional cues (e.g. gravitropism), nastic movements that are independent of the plant's position (e.g. closing leaves at night) and nutations through unequal growth rates of organ sides (e.g. circumnutation) (Migliaccio *et al.*, 2013).

The decision whether the root waves or curls, the wavelength and the amplitude are strongly dependent on the environmental factors and can be mainly linked to the tilting angle of the plate (Zhang *et al.*, 2022). On plates tilted by 45 °, roots show strong waviness, whereas on horizontal plates they curl in most cases. This leads to the hypothesis that curling is the basal root growth pattern

and that waving is induced by the gravity vector that is lost on horizontal plates. Thin root hairs anchor the root on the plate but only emerge above the root tip and the meristematic zone, leading to a part of the root that can move freely (Thompson and Holbrook, 2004). Static friction anchors the root tip on the surface, while root growth builds tension between the hair-anchored upper root part and the root tip. Once the tension overcomes the force through static friction, the root slips along the agar. The observations that roots can start curling after a longer period of wavy growth might result from changes in agar composition, i.e. reduced water content (Rizzieri *et al.*, 2006).

Root skewing describes roots that grow leftwards or rightwards away from the gravity vector (imaged from the back of the plate). Like waving, skewing is dependent on the tilting angle of the growth plate (Rutherford and Masson, 1996). The epidermal cell file twists through cell file rotation, which is caused by different expansion rates between the inner and outer cell layer. The outer epidermal cell layer compensates for the growth differences by twisting (Ishida *et al.*, 2007).

Recently, the first molecular players of root circumnutation were identified in *Oryza sativa* (Taylor *et al.*, 2021). Circumnutation takes place 1-2 mm above the root tip in a region of fast cellular elongation with pronounced bending of the root (Takehisa *et al.*, 2012). Mutants of *histidine kinase 1* (*hk1*) were detected in a screen for increased root length and no root circumnutation compared to wildtype. OsHK1 is an active histidine kinase and was shown to regulate the downstream signal transduction of ethylene by restricting root elongation (Zhao *et al.*, 2020). It might act as a regulator of cross-talk between the ethylene and auxin signaling pathways, because root bending after a gravitropic stimulus is reminiscent to root bending during circumnutation. Indeed, the auxin importer mutant of *OsAUX1* showed no root circumnutation but could be rescued by applying 1-NAA.

In contrast to *Arabidopsis thaliana*, root growth patterns of *Oryza sativa* do not follow a fixed chirality which suggests a different mechanism of Arabidopsis waving and rice circumnutation (Piconese *et al.*, 2003; Migliaccio *et al.*, 2013).

1.2.2 Root gravitropism

Roots grow towards the earth's center. That requires sensing of gravity in the first step, followed by transmission of the signal and the actual growth response.

Early diverging vascular plants show a slower response to gravitropic stimuli, compared to flowering plants (Zhang *et al.*, 2019). This can be explained by the localization of statoliths, i.e. starch-filled amyloplasts, that differs drastically compared to seed plants. In lycophytes and ferns, amyloplasts are found at the lateral sides of the root and in the root apex. In seed plants, statoliths are restricted to the root apex and therefore distinct from the elongation zone. Changes in gravity lead to sedimentation of statoliths which triggers a signal transduction cascade (Leitz *et al.*, 2009). The intracellular statolith distribution and interactions with receptors in the PM might be responsible for forwarding the signal (Su *et al.*, 2020). Although the gravity signal is mainly perceived in the root tip in seed plants, the elongation zone is also involved in gravity sensing (Wolverton *et al.*, 2002a;

Wolverton *et al.*, 2002b). The hydrostatic pressure model suggests that gravitational pressure can be sensed by the pressure of protoplasts against the PM and is integrated through activation of mechanosensitive ion channels which modify the cytoskeleton network, as observed in rice root tips (Staves *et al.*, 1997).

After stimulus sensing, the gravitropic signal is transmitted through changes in the auxin distribution in the root tip. Auxin is transported from the middle of the root cap outward to the lateral root cap and root epidermis by an auxin transporter system. This occurs only at the bottom side of the root and leads to a lateral auxin gradient across the root tip. The establishment of directional auxin transport in gravistimulated roots shows the necessity of polar auxin transport to adapt plant growth in response to external stimuli.

1.3 Polar auxin transport

Plant development depends strictly on the controlled distribution of auxin though the plant body. Changes of plant growth to external stimuli require the adaptation of auxin flows in the plant, as described for the lateral auxin gradient in gravistimulated roots. The polarity of auxin flow that is needed to establish auxin gradients is therefore one of the most important and basic requirements for proper plant growth.

1.3.1 History of PAT

After the identification of auxin as the mobile signal that is involved in all developmental processes, its polar distribution was intensively analyzed in physiological assays from the 1930s on. Classically, unlabeled or radiolabeled IAA was applied to one side of a plant segment, e.g. the hypocotyl, and an agar block was placed at the other end as a receiver (Lomax *et al.*, 1995). This revealed that auxin transport through the hypocotyl occurs basipetally and is independent of orientation and gravity. Later, Frits Went used decapitated coleoptiles and auxin-soaked agar blocks to demonstrate that asymmetric auxin distribution lead to coleoptile bending away from the agar block (Went, 1926). This allowed to test other naturally occurring auxins besides IAA or synthetic compounds, like indole-3-butyric acid (IBA) or 2,4-dichlorophenoxyacetic acid (2,4-D).

The identification of auxin flow inhibitors opened a new tool box to further investigate PAT (Morgan and Söding, 1958; Katekar and Geissler, 1977). Experiments with the identified inhibitors, together with auxin transport studies in the 1970s led to the chemiosmotic hypothesis (see Chapter 1.1.2). The hypothesis was proved in pea stem cell fractions, where auxin efflux transporters were detected at the basal side of the cell with the help of monoclonal antibodies (Jacobs and Gilbert, 1983). As proposed, the asymmetric localization of auxin efflux transporters is the reason for the directionality of auxin flow.

One of the most important auxin efflux inhibitors is *N*-1-naphthylphthalamic acid (NPA) (Morgan and Söding, 1958; Hertel and Leopold, 1963; Hertel *et al.*, 1983). Initially developed as a herbicide, it is extensively used to study PAT-depending processes for over 60 years (Teale and Palme, 2018). Plants grown in presence of NPA show severe developmental defects, like no or sterile floral organs or affected phyllotaxis (Okada *et al.*, 1991). By comparing the NPA-induced phenotypes in wildtype plants with mutants impaired in flower morphogenesis, the developmental defects could be linked to auxin transport (Goto *et al.*, 1987; Haughn and Somerville, 1988). Mutants resembling the pin-formed inflorescence were identified as auxin efflux transporter *pin1-1* and the AGCVIII kinase *pinoid* (Okada *et al.*, 1991; Bennett *et al.*, 1995). The molecular mechanism of inhibition through direct binding of NPA to the auxin transporter was based on studies with Xenopus oocytes, and finally proven by the cryo-EM structure of the auxin efflux transporter PIN8 in a complex together with NPA (Abas *et al.*, 2021; Ung *et al.*, 2022).

1.3.2 Uptake of auxin

Besides passive diffusion along the concentration gradient, the major portion of IAA is transported across the membrane. The main importer protein is AUXIN RESISTANT 1 (AUX1) (Bennett *et al.*, 1996). Together with the LIKE-AUX (LAX) proteins – LAX1, LAX2 and LAX3 in *Arabidopsis thaliana* – they form the AUX/LAX family (Peret *et al.*, 2012). AUX/LAX proteins are phylogenetically closely related to the plant-specific AMINO ACID PERMEASEs (AAPs). Together they form the AAAP family.

AUX1 is involved in embryo development, female gametophyte development, phyllotactic patterning and apical hook formation (Swarup *et al.*, 2001; Swarup *et al.*, 2004). It contributes to many developmental processes in the root, like gravitropism, lateral root development and root hair development (Bennett *et al.*, 1996; Grebe *et al.*, 2002; Marchant *et al.*, 2002; Swarup *et al.*, 2005). The polar expression of *AUX1* in the lateral root cap (LRC) and in elongating cells of the root epidermis is necessary to establish an auxin gradient that allows gravitropic growth (Swarup *et al.*, 2005). The most prominent defect of the *aux1* mutant is the agravitropic root growth.

LAX1 and LAX2 act comparable to AUX1 in embryo development and phyllotactic patterning (Peret *et al.*, 2012). In complementation studies of the *aux1* mutant, LAX2 expression only partially rescued the agravitropic root phenotype, indicating that LAX2 is different from LAX1 and LAX3 *in planta* (Peret *et al.*, 2012). Biochemical analyses showed that AUX1, LAX1 und LAX3 share redundant transport properties (Swarup *et al.*, 2008; Peret *et al.*, 2012).

Oocyte experiments demonstrated that AUX1 is a high-affinity IAA transporter with a substrate affinity in the physiological range ($K_m \approx 1$ µM) and a pH optimum in the range of the pH in the apoplast (pH 5.5–6) (Yang et al., 2006). Like AAPs, the proton motion force drives AUX1 to transport the substrate across the plasma membrane (PM) (Lomax *et al.*, 1985; Dindas *et al.*, 2018). Despite the close relationship to AAAPs, no protein structure of AUX1 was published to date and

experiments to show that AUX1 transports amino acids, i.e. the IAA precursor tryptophan, failed (Hammes *et al.*, 2021).

Besides the AUX1/LAX transporter family, several other proteins can import IAA and other auxins into the cytosol. The contribution to PAT is considered minor, because either their preferred substrate is not auxin, they localize apolarly to the PM or to internal membranes.

For example, members of the NITRATE TRANSPORTER 1/PEPTIDE TRANSPORTER (NPF) family are nitrate transporter that can as well mediate auxin transport, e.g. NPF6.3/NRT1.1, NPF7.3/NRT1.5 or NPF5.12/ TOB1 (Krouk *et al.*, 2010; Michniewicz *et al.*, 2019; Watanabe *et al.*, 2020). Mutants of *npf* transporters show defects in lateral root growth (NPF6.3/NRT1.1), root gravitropism (NPF7.3/NRT1.5) or lateral root branching (TOB1).

Another transporter that localizes to the tonoplast is WALLS ARE THIIN 1 (WAT1)/UMAMIT5 of the USUALLY AMINO ACIDS MOVE IN AND OUT TRANSPORTER (UMAMIT) family. Although amino acid transport of WAT1 could not be shown to date, IAA transport was demonstrated in oocyte experiments (Ranocha et al., 2013). Mutants of *wat1* show impaired cell wall thickness.

1.3.3 Efflux of auxin

After import of IAA into the cytosol, the negatively charged IAA molecules are trapped and need transporters that facilitate IAA efflux. The most important family of efflux transporters are the PIN-FORMED PROTEINs (PINs) which will be introduced later in more detail. Two other transporter families regulate the auxin concentration in the cytoplasm through export into the apoplast or the endoplasmatic reticulum (ER).

ABC transporters

Members of the ATP-BINDING CASSETTE (ABC) family can translocate IAA over the PM. ABC transporters use energy from ATP hydrolysis to operate. Some members of the subgroup B (11 of 22 ABCBs) were shown to transport IAA and can be identified by a signature D/E-P motif (Hao *et al.*, 2020). The main functions of ABCB transporters in IAA transport are in the long-distance transport and the nonpolar auxin distribution (Blakeslee et al., 2007). Mutations in *ABCB1, ABCB4, ABCB19* and *ABCB21* led to changes in the auxin distribution in the shoot, leaves, the hypocotyl and the root of *Arabidopsis thaliana* (Blakeslee *et al.*, 2007; Kamimoto *et al.*, 2012; Kubes *et al.*, 2012; Jenness *et al.*, 2019). They were identified as net exporters, but ABCB4 and ABCB21 can change directionality if the cellular IAA concentration is very low. Their contribution to PAT is still a matter of debate, because the auxin transporting ABCBs differ strongly in their localization, depending on the protein and the plant tissue. ABCB1 localizes non-polarly in the root meristem and shows basal localization in endodermal and cortical cells above the elongation zone (Geisler *et al.*, 2005). ABCB4 is either basally or apically localized in the root epidermis (Terasaka *et al.*, 2005) and ABCB19

localized polarly in pro-cambial root cells (Titapiwatanakun et al., 2009). Members of the subgroup G are known to transport other auxins like IBA (Ruzicka *et al.*, 2010).

PILS proteins

PIN-LIKE PROTEINs (PILS) are structurally related to PIN proteins. They evolved independently in the plant lineage and form an own family. Their localization to the ER suggests a function in reducing nuclear auxin concentration by transporting IAA into the ER lumen (Beziat *et al.*, 2017). Besides the homeostatic function to buffer the IAA availability in the cytosol, PILS are known to integrate internal and external cues in auxin-dependent processes. PILS function was connected to brassinosteroids, light and temperature (Feraru *et al.*, 2022). They were not detected at the PM and are not directly involved in PAT. To date, PILS-mediated IAA transport could not be shown experimentally unambiguously.

1.4 PINs as the main auxin efflux transporters

The main group of auxin efflux transporters are the PINs. In *Arabidopsis thaliana*, the PIN family consists of eight members that are grouped into the canonical PINs (PIN1, PIN2, PIN3, PIN4 and PIN7), the noncanonical PINs (PIN5 and PIN8) and the semi-canonical PIN6. The protein structure of PINs consists of ten membrane-spanning helices and an intrinsically disordered cytoplasmic loop domain which connects helix 5 and 6. The classification of PINs is based on four conserved motives in the loop domain of canonical PINs, which are absent in noncanonical PINs (Bennett *et al.*, 2014). In *Arabidopsis thaliana*, this correlates with loop length. The canonical PIN loop domain consists of 294 (in PIN4) to 325 (in PIN2) amino acids, the noncanonical loop domain of 27 amino acids in PIN5 and 40 amino acids in PIN8, and the loop domain of PIN6 is of intermediate length with 248 amino acids (Ung *et al.*, 2022). Phylogenetic analyses showed that the canonical PINs lost characteristic loop motifs selectively. This subfunctionalization gives closely related proteins the ability to perform different tasks in the same cellular context as seen for PIN3, PIN4 and PIN7 in the root (Bennett *et al.*, 2014). The canonical PINs localize polarly in most cell types and give directionality to the auxin flow.

1.4.1 Phenotypes and expression

The transporter family is named according to the eponymous *pin1* mutant that displays a pin-shaped inflorescence without reproductive organs and with other severe developmental defects (Goto *et al.*, 1987). In the shoot apical meristem, PIN1 is necessary to create an auxin maximum in the primordium tip (Reinhardt *et al.*, 2003; Heisler *et al.*, 2005). In roots, PIN1 localizes mainly to the basal cell side in the vasculature (Gälweiler *et al.*, 1998).

Mutations in other canonical *PIN* genes cause impaired reactions to environmental stimuli. The *PIN2* gene is expressed in the root epidermis and cortex. PIN2 localizes apically in the LRC, epidermal cells and in distal cortex cells, and basally in the cortical cell file (Müller *et al.*, 1998; Wisniewska *et al.*, 2006). This dual localization is unique among the PINs in Arabidopsis. The *pin2* mutant is impaired in gravitropic root growth and cannot react properly to a gravitropic stimulus (Luschnig *et al.*, 1998; Müller *et al.*, 1998; Abas *et al.*, 2006).

PIN3, PIN4 and *PIN7* are evolutionary closely related and show overlapping expression profiles. In the root stele, PIN3 and PIN7 localize polarly together with PIN1. In the columella, PIN3 and PIN7 are non-polarly distributed together with PIN4 (Friml *et al.*, 2002b; Friml *et al.*, 2002a; Blilou *et al.*, 2005). A *pin3 pin4 pin7* triple mutant displays impaired phototropic hypocotyl bending (Willige *et al.*, 2013).

PIN3 and PIN7 play an important role in gravity sensing cells in the root columella, redirecting the auxin flux upon a gravitropic stimulus. In a gravistimulated root, PIN3 and PIN7 localize to the bottom side of the PM and transport IAA to the lower side of the root tip (Friml *et al.*, 2002a; Ruiz Rosquete *et al.*, 2018). Auxin is then transported from the root columella through the LRC into the epidermis and the elongation zone by the auxin transporters AUX1 and PIN2, resulting in inhibited cell elongation at the lower root side (Swarup *et al.*, 2005). Consequently, the mutants *aux1* and *pin2* show agravitropic root growth, whereas *pin3* or *pin7* mutants do not show a severe root phenotype (Chen *et al.*, 1998; Luschnig *et al.*, 1998; Müller *et al.*, 1998; Swarup and Bhosale, 2019). In the *pin2* mutant, auxin is still transported into the elongation zone, most likely because of a weak *PIN1* expression in the epidermis (Rashotte *et al.*, 2001; Friml *et al.*, 2003; Blilou *et al.*, 2005; Swarup *et al.*, 2005). It is predicted that a block of the auxin flux in the LRC cells is responsible for the agravitropic root in the *pin2* mutant.

In contrast to the canonical PINs, the noncanonical PINs localize to internal membranes, i.e. the ER and might be involved in intracellular auxin homeostasis (Mravec *et al.*, 2009; Ding *et al.*, 2012). The expression pattern of *PIN5* ranges from the hypocotyl, the cotyledon vasculature and the guard cells to the root pericycle, the root tip and later developmental stages in leaves, stems and flowers (Mravec *et al.*, 2009). The *pin5* mutant has defects in lateral root initiation, root and hypocotyl growth and an enlarged root meristem *(Mravec et al.*, 2009; Di Mambro *et al.*, 2019). The *PIN8* gene is expressed in the pollen and in the phloem along the root stele. The *pin8* mutant has a significantly reduced density of lateral roots (Lee *et al.*, 2019), but the pollen phenotype was less penetrant, ranging from no phenotype to aborted pollen grains (Dal Bosco *et al*., 2012; Ding *et al.*, 2012).

The semicanonical PIN6 shows a dual localization, depending on phosphorylation by MITOGEN-ACTIVATED (MAP) KINASES (MPK) and the gene expression level, i.e. low expression leads to localization to internal membranes in the root, high expression leads to localization to the PM in nectary glands and the inflorescence stem (Ditengou *et al.*, 2018). A *pin6* loss-of-function mutant

showed enhanced inflorescence growth and was impaired in root growth processes and lateral root development (Cazzonelli *et al.*, 2013; Ditengou *et al.*, 2018).

1.4.2 Structure

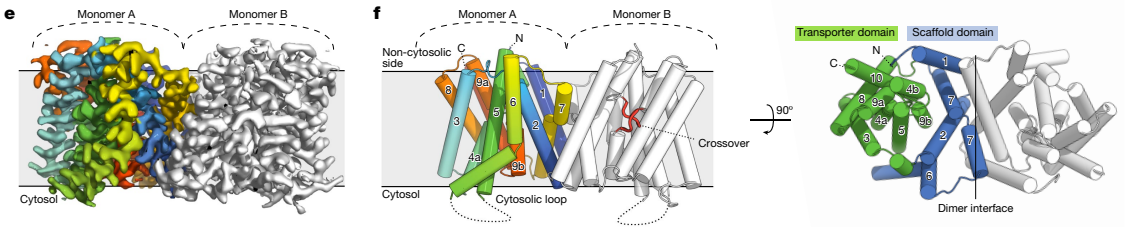

Figure 2 – Protein structure of PIN8. (e) Cryo-EM map of a PIN8 dimer. Individual helices are colored in Monomer A. (f) Model of PIN8 dimer according to Cryo-EM map in (e) and 90 ° turned. Left: Individual helices of Monomer A are colored and labeled. Right: Transporter and scaffold domains are colored in green and blue respectively, individual helices are labeled. The crossover marks the auxin binding site. Figure from Ung *et al*, 2022.

The structures of PIN1, PIN3 and PIN8 where solved by cryogenic electron microscopy (cryo-EM) and revealed that PINs form dimers with one monomer consisting of 10 transmembrane (TM) helices and the N- and C-termini facing the non-cytosolic side (Su *et al.*, 2022; Ung *et al.*, 2022; Yang *et al.*, 2022). The TM domains of all eight PINs are highly conserved and the structure is similar to bicarbonate/sodium symporters, and with an inverted membrane topology also comparable to bile acid/sodium symporters and sodium/proton antiporters (Figure 2) (Hunte *et al.*, 2005; Hu *et al.*, 2011; Lee *et al.*, 2013; Paulino *et al.*, 2014; Wohlert *et al.*, 2014; Fang *et al.*, 2021; Liu *et al.*, 2021). Each monomer is built of a scaffold domain (helices M1, M2, M6 and M7) and a transporter domain (helices M3-5 and M8-10). Comparisons between the structure of PIN8 and its related protein families suggest a cross-over elevator-type movement of the substrate binding site.

In the transporter domain, the helices M4 and M9 form a proline-proline crossover motif that is necessary for auxin binding. The IAA carboxylate group orients towards the crossover, the carbon backbone contacts helix M4 towards the non-cytosolic side and the indole ring contacts helix M9 towards the cytosolic side. Non-specific interactions with the scaffold domain further stabilize the IAA molecule in the binding pocket. The residues involved in the interaction with IAA are fully conserved in all PINs of *Arabidopsis thaliana*, except for PIN5. The PIN-inhibitor NPA binds at the same position as IAA and likely blocks the PIN in the inward facing conformation, because of its larger size compared to IAA. Additionally, the affinity of the transporter is higher for NPA and the NPA molecule showed stronger binding due to more interactions with the scaffold domain.

The helices M5 and M6 are connected by a hydrophilic intrinsically disordered loop domain. Cryo-EM analyses of PIN1 and PIN3 found a short cytosolic segment after helix 5 that forms three β-strands which interact with helices M5, M6 and M9 (Su *et al.*, 2022; Yang *et al.*, 2022). The rest of the loop was not resolved.

1.4.3 Function

The PINs transport negatively charged IAA in a proton- and ion-independent way (Ung *et al.*, 2022). In radiotracer studies with oocytes from *Xenopus laevis*, the IAA transport by canonical PINs was demonstrated for the first time (Zourelidou *et al.*, 2014). This revealed that canonical PINs need AGCVIII kinases for transport activation through phosphorylation of the loop domain. PIN1 and PIN3 were shown to efflux IAA only in presence of D6 PROTEIN KINASE (D6PK) or PINOID, members of the AGC1 and AGC3 clade.

Different to canonical PINs, transport studies of the semi-canonical PIN6 in oocytes revealed a kinase-independent transport component (Martina Kolb, pers. correspondence). The PIN6-mediated transport could be enhanced by co-expression of PINOID, but not D6PK. The PINOID-activated PIN6 transport, as well as the kinase-independent transport component were sensitive to NPA inhibition. Also, the noncanonical PIN8 has a passive transport component which was inhibited by NPA, but the co-expression of any kinase did not increase the transport rate (Ung *et al.*, 2022). For the noncanonical PIN5, no transport activity in oocyte uptake or efflux assays has been observed to date. Interestingly, several key residues for auxin binding are not conserved in the PIN5 sequence, questioning the ability of PIN5 to transport auxin and if so, the transport mechanism.

Domain swapping experiments *in planta* between the TM domains and the loop domains of canonical and noncanonical PINs revealed that characteristic features of PINs, i.e. the subcellular localization in the PM, can be transplanted by providing a canonical loop domain to noncanonical TM domains (Ganguly *et al.*, 2014). In further studies, interspecies complementation experiments showed that not only the loop domain but also the TM domains contribute to the localization. The TM domains of PINs likely co-evolved together with the loop domain (Zhang *et al.*, 2020). Studies on the transport ability of PIN chimeras between the noncanonical PIN8 and the loop domains of the canonical PINs PIN1, PIN2 and PIN3 showed, that also biochemical features can be transferred to TM domains of noncanonical PINs by domain swapping. In the PIN8 chimeras, the steady transport component of PIN8 was inhibited by the loop domain and the transporter became regulatable by kinases. This underlines the importance of the loop domain in terms of transport regulation and as interaction domain with kinases (Janacek *et al.*, 2023, under review).

1.5 Regulation of PINs

PIN-mediated auxin transport is regulated on two temporally distinct levels. First, the transporter itself is activated by phosphorylation. This happens through members of the AGCVIII kinase family and is a fast-occurring process (Zourelidou *et al.*, 2014). Dephosphorylation of the PINs counteracts the transporter's activity (Christensen *et al.*, 2000). Second, auxin transport direction is regulated via the transporter's localization. Members of the AGCVIII kinase family, as well as other protein

families impact endocytosis and polarity control of PINs. Compared to controlling the phosphorylation status, modulating the PM is a rather slow process.

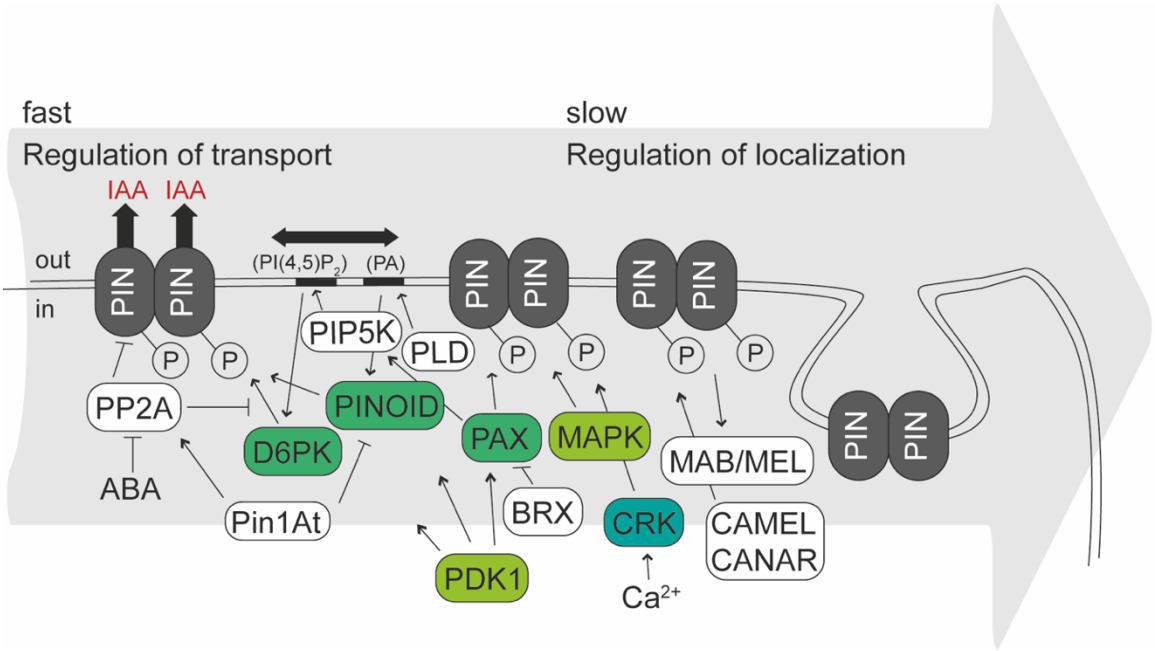

Figure 3 – Time scale of regulation of auxin flow through control of PINs. PP2A: PROTEIN PHOSPHATASE 2A, ABA: Abscisic acid, D6PK: D6 PROTEIN KINASE, PIP5K: PHOSPHATIDYLINOSITOL 4-PHOSPHATE 5-KINASE, PI(4,5)P_2: Phosphatidylinositol-4,5-bisphosphate, PA: Phosphatidic acid, PLD: PHOSPHOLIPASE D, PAX: PROTEIN KINASE ASSOCIATED WITH BRX, BRX: BREVIS RADIX, PDK1: 3-PHOSPHOINOSITDE-DEPENDENT PROTEIN KINASE 1, MAPK: MITOGEN-ACTIVATED KINASE, CRK: Ca^{2+}/CALMODULIN-DEPENDENT PROTEIN KINASE-RELATED KINASE, MAB/MEL: MACCHI-BOU/ENHANCER OF PINOID 1-LIKE, CAMEL: CANALIZATION-RELATED AUXIN-REGULATED MALECTIN-TYPE RECEPTOR KINASE, CANAR: CANALIZATION-RELATED RECEPTOR-LIKE KINASE.

1.5.1 Kinases as master regulators

AGCVIII kinases

The family of AGCVIII kinases is related to the cAMP-, cGMP- and Ca^{2+}-dependent kinases from mammals. It consists of 23 serine-threonine kinases in *Arabidopsis thaliana.* Most phenotypes of *pin* mutants can be phenocopied by mutants or mutant combinations of the AGVIII family members. The inflorescences of the *pinoid* mutant and the higher-order *d6pk* mutant resemble the *pin1* mutant (Bennett *et al.*, 1995; Benjamins *et al.*, 2001; Zourelidou *et al.*, 2009). Also, the mutants *pid, wavy root growth 1* (*wag1*) and *wag2* were impaired in root growth showing stronger root waving on vertical plates (Santner and Watson, 2006). The roots of the *pid wag1 wag2* triple mutant showed agravitropic growth and were shorter, with reduced root bending rate (Santner and Watson, 2006; Grones *et al.*, 2018). The auxin reporter *DR5:GFP* revealed higher transcriptional output that inhibits root growth and leads to reduced gravitropic growth. In contrast, *d6pk* mutants and the single mutants of the closely related *d6pk-like* mutants had only very mild agravitropic defects, suggesting that these kinases do not influence gravitropic growth (Zourelidou *et al.*, 2009; Grones *et al.*, 2018). Root

elongation was reduced in seedlings of the *d6pk d6pkl1 d6pkl2* triple mutant grown on NPA, which suggested a deficiency in auxin transport (Zourelidou *et al.*, 2009).

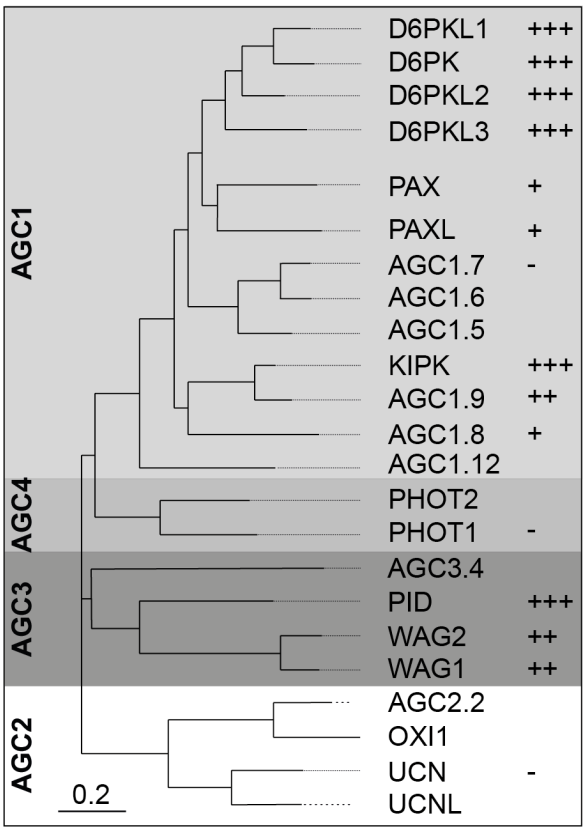

Figure 4 – Phylogenetic tree of AGCVIII kinase family from *Arabidopsis thaliana*. The 23 members are grouped in four clades, based on an alignment of their catalytic domain. (+)/(-) indicate the ability to activate PIN-mediated IAA transport in Xenopus oocytes. (-): no activation of transport, (+): activation of transport, (++): strong activation of transport (+++): maximal activation of transport. Figure created by PD Dr. Ulrich Z. Hammes, modified for this thesis.

Cell biological studies revealed that the kinases are membrane-associated and localize polarly or apolarly in the PM, often together with PINs (Lee and Cho, 2006). Later, transport studies in oocytes of *Xenopus laevis* showed that some AGCVIII kinases activate PIN-mediated IAA transport through phosphorylation of the PIN loop domain (Figure 3) (Zourelidou et al., 2014). The kinase domains of the AGCVIII kinases are conserved. Based on phylogenetic analyses of their catalytic domains, the kinase family was grouped in four clades (Figure 4) (Galvan-Ampudia and Offringa, 2007). In all AGCVIII kinases, the two protein kinase domains I-VII and VIII-XI are separated by an inserted loop domain, the middle (MID) domain, that contains an arginine/lysine(K/R)-rich polybasic motif and serine residues that may neutralize the positive charges. The N- and C-termini vary strongly between the kinases and are less conserved.

PDK1 and PP2A as regulators of AGCVIII kinases

Within the C-terminus of most AGCVIII kinases lays a F(D/E)XF motif, that is supposed to be the 3-PHOSPHOINOSITIDE-DEPENDENT PROTEIN KINASE 1 (PDK1)-interacting fragment (PIF) domain. PDK1 phosphorylates the activation loop segment and therefore acts as an upstream activator of the AGC1 kinases D6PK and PROTEIN KINASE ASSOCIATED WITH BRX (PAX)

(Tan *et al.*, 2020; Xiao and Offringa, 2020), as well as the AGC3 kinase PINOID (Zegzouti *et al.*, 2006a; Zegzouti *et al.*, 2006b). Interestingly, the AGC2 kinase UNICORN (UCN) could not activate auxin transport, but is instead a negative regulator of PDK1 in growth control of integuments and petals (Zourelidou *et al.*, 2014; Scholz *et al.*, 2019).

Besides PDK1 as activator of AGCVIII kinases, the PROTEIN PHOSPHATASE 2A (PP2A) was identified as negative regulator of the AGCVIII kinase PINOID (Li *et al.*, 2020). PINOID genetically interacts with PP2A and directly binds the catalytic subdomains. This might lead to activity control of the kinase by dephosphorylation of the activation loop or to a PINOID-PP2A complex that would act directly on common substrates, like the PIN loop domain (Figure 3).

Lipid interactions

The middle (MID) domain interacts with polyacidic phosphoinositides (PI) which directs the kinases to the PM (Figure 3) (Barbosa *et al.*, 2016). The asymmetric distribution of PIs in the PM is an important tool to create restricted domains within the membrane. The kinases PHOSPHATIDYLINOSITOL 4-PHOSPHATE 5-KINASE 1 (PIP5K) and PIP5K2 produce phosphatidylinositol-4,5-bisphosphate ($PI(4,5)P_2$) from phosphatidylinositol-4-phosphate (PI4P) which is the most abundant phospholipid in PMs of plants (Simon *et al.*, 2016). A PI4P-dependent PM targeting was reported for the AGC3 kinase PINOID and the localization of the AGC1 kinase D6PK depends on a combination of different PIs (Ischebeck *et al.*, 2013; Barbosa *et al.*, 2016; Simon *et al.*, 2016).

In protophloem sieve element cells, PIP5K is recruited to the PM by the PAX-BRX module, which therefore reinforces its own polarity (Marhava *et al.*, 2020). The PM-associated protein BREVIS RADIX (BRX) co-localizes and interacts with PAX and was shown to inhibit PAX activity, leading to inhibited PIN1 transport activity at low cellular auxin concentrations (Marhava *et al.*, 2018; Marhava *et al.*, 2020). Increasing auxin concentrations within the cell lead to migration of BRX to the nucleus, allowing PDK1 to activate PAX and therefore PIN1-mediated transport.

However, the AGC3 kinases PINOID, WAG1 and WAG2 localize apolarly to the PM in epidermal and cortical root cells (Michniewicz *et al.*, 2007; Dhonukshe *et al.*, 2010; Wang *et al.*, 2019). Besides PI4P, PINOID binds phosphatidic acid (PA) that results from PHOSPHOLIPASE D (PLD) activity, but PINOID does not bind $PI(4,5)P_2$ like the D6PKs (Wang *et al.*, 2019) (Figure 3).

Other kinases

The influence of AGCVIII kinases on PAT is well-studied. In the last years, kinases from other kinase families were connected to PIN-mediated PAT by controlling the PIN localization. An evolutionarily conserved family are MPKs, acting in a pathway together with upstream MAP KINASE KINASEs (MKK) and MAP KINASE KINASE KINASEs (MKKK). MPKs target conserved threonine residues in the PIN loop domain. In the *MKK7* gain-of-function mutant *bushy and dwarf 1* (*bud1),*

the shoot and root phenotypes were linked to impaired MPK-dependent internalization of PIN1 (Jia *et al.*, 2016; Dory *et al.*, 2018).

Another kinase family which impacts PIN localization are Ca^{2+}/CALMODULIN-DEPENDENT PROTEIN KINASE-RELATED KINASEs (CRK). CRKs can phosphorylate PINs *in vitro* and localize apolarly to the PM. Especially the localization of PIN2 was impaired in *crk5* mutants with depletion of PIN2 from apical membranes in the epidermis and a basal to apical localization in the cortex of the root transition zone (Rigo *et al.*, 2013). The mutant of *crk5* partially resembles the *pin2* mutant with delayed agravitropic root growth. A recent report links the impact of CRK5 on root gravitropism to the maintenance of redox homeostasis and the feedback regulation of PIN2-mediated auxin transport (Cseplo *et al.*, 2021).

1.5.2 Regulation of transport

Substrate movements across the PM can be controlled by regulating the transporter's activity or by regulating the amount of (active) transporter in the membrane. The latter is under control of different kinase families, whereas direct regulation of the PIN's activity through phosphorylation was only shown for members of the AGC1 and AGC3 clade of the AGCVIII family. In the recent years, important phosphorylation sites in the hydrophilic loop domain of PINs could be linked to transport activation (Bassukas *et al.*, 2022).

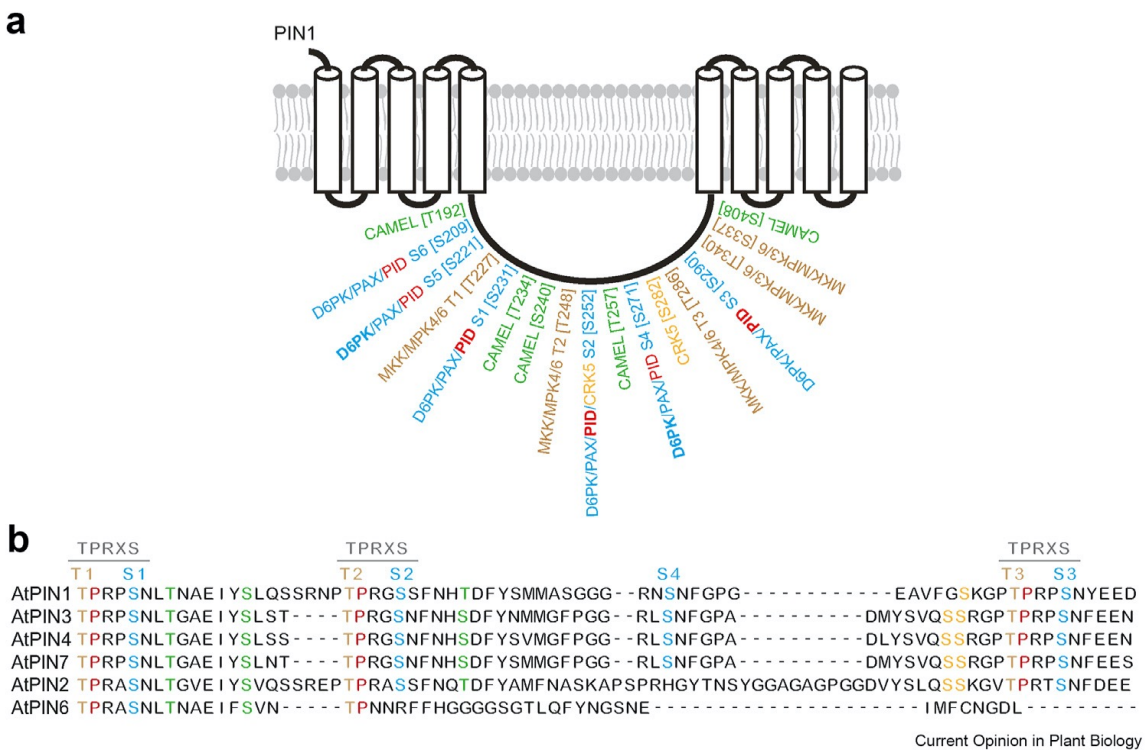

Figure 5 – Phosphorylation sites of PINs from *Arabidopsis thaliana*. (a) PIN1 is phosphorylated at indicated sites by different kinases. (b) Sequence alignment of a loop domain fragment of the canonical and semi-canonical PINs. Important phosphorylation sites in the TPRXS motives and sites for transport activation are highlighted in color. Figure from Bassukas *et al*., 2022.

Of special interest for transport regulation is a strictly conserved TPRXS motif which is repeated three times in the loop domain of canonical PINs (Figure 5). Mutating the serine residues, named S1-S3, to alanine or glutamic acid, reduced the transporter's activity gradually (Zourelidou *et al.*, 2014; Weller, 2017). By using an *in vitro* approach and mass spectrometry, two less conserved phosphosites (S4 and S5) could be identified in PIN3, PIN4 and PIN7. Sequence alignments of the loop domain showed low conversation for S4 and S5 in PIN2 and an aspartic acid at the S5 position in PIN1 (Figure 5 b). The transport activity was completely lost in S1-S4 mutants of PIN1. Experiments with Xenopus oocytes and further *in vitro* studies revealed an overlapping target preference for D6PK and PINOID with small differences for some phosphorylation sites (Zourelidou *et al.*, 2014; Barbosa *et al.*, 2018). Phosphosite-specific antibodies showed that the phosphorylation of PIN1 at all four sites is rapidly lost after internalization of D6PK and that PIN phosphorylation only occurs at the PM, not at internal structures (Weller *et al.*, 2017). This also implies that protein phosphatases antagonize the PIN phosphorylation and might regulate PIN activity through dephosphorylation, as shown for the PP2A complex and PINOID (Michniewicz *et al.*, 2007). Through this regulatory interaction, also the phytohormone abscisic acid (ABA) could be linked to auxin transport (Figure 3). At high ABA concentrations through stress, ABA binds to the PYRABACTIN RESISTANCE 1 (PYR)/PYRABACTIN RESISTANCE 1-LIKE

(PYL)/REGULATORY COMPONENT OF ABA RECEPTOR (RCAR) family of ABA receptors. This inhibits the formation of an active PP2A holoenzyme, leading to increased phosphorylation of PINs through PINOID (Li *et al.*, 2020).

1.5.3 Regulation of localization

The establishment of auxin minima and maxima integrates environmental cues into plant development. External stimuli act through the regulation of auxin transport, and this is mediated through regulation of transporter activity or localization. The PINs are major players in PAT and auxin accumulation in different plant tissues can be explained by the polar PIN localization to one side of the cell. In the root stele, PIN1 localizes basally (rootward). PIN2 localizes apically (shootward) in the epidermis, but basally in the cortex. In the columella and the lateral root cap, PIN3, PIN4 and PIN7 are apolarly distributed in the membrane. This unique localization pattern needs mechanisms to restrict the proteins to certain membrane domains.

Localization control through AGCVIII kinases

Phosphorylation by AGCVIII kinases is crucial for the activity control of PINs, but it also regulates the PIN localization. In *PINOID* overexpression lines, a basal-to-apical polarity shift of PIN1 in the stele was observed (Dhonukshe *et al.*, 2010; Huang *et al.*, 2010). In contrast, PIN1 does not re-localize to the apical PM during shoot differentiation in *pid* mutants (Friml *et al.*, 2004). However, the polarity of PINs is neither affected in *d6pk* mutants nor in *D6PK* overexpression lines indicating that not all AGCVIII kinases can control PIN polarity (Zourelidou *et al.*, 2009; Barbosa *et al.*, 2014; Zourelidou *et al.*, 2014). Phosphorylation events at S1-S3 were mapped as the important sites and phospho-mimicking mutations led to constitutive PIN apicalization. The phosphorylated positions were suggested to be a re-localization signal, but that was falsified later to not be solely responsible for the shift in localization (Kleine-Vehn *et al.*, 2009; Dhonukshe *et al.*, 2010; Huang *et al.*, 2010; Weller *et al.*, 2017). In seedlings expressing a phospho-mimicking version of *PIN3*, gravitropic root growth after gravitropic stimulus was impaired, because the PIN3 variant failed to re-localize, which is similar to the observations in *PINOID* overexpression lines (Grones *et al.*, 2018). For PIN2, the AGC3 kinase WAG1 was identified as the important kinase in dividing epidermal cells that regulate the post-cytokinetic polarity establishment from the cell plate to the apical PM (Glanc *et al.*, 2018).

Localization control through other kinase families

Another kinase family, the CRK family, was found to integrate Ca^{2+} signaling into auxin-dependent processes. It was shown that Ca^{2+}-binding proteins interact with PID and affects PIN polarity through the regulation of PID (Benjamins *et al.*, 2003). Increased Ca^{2+} concentrations led to PID-related polarity shifts of PIN1 in the stele or of PIN2 in the cortex (Zhang *et al.*, 2011). Further, Ca^{2+} was

shown to impact endomembrane trafficking (Himschoot *et al.*, 2017) and CRK5 was identified to decelerate PIN2 endocytosis and to activate its recycling (Rigo *et al.*, 2013).

Besides external stimuli, like light or gravitropism, also wounding leads to the re-direction and canalization of auxin. This is mediated through the receptor kinase CANALIZATION-RELATED AUXIN-REGULATED MALECTIN-TYPE RECEPTOR KINASE (CAMEL) and its interactor CANALIZATION-RELATED RECEPTOR-LIKE KINASE (CANAR) (Hajny *et al.*, 2020). CAMEL and CANAR play a role in leaf venation and vasculature regeneration. In *camel canar* mutants, PIN1 orientation failed and led to regeneration abnormalities. CAMEL can phosphorylate and binds to PINs *in vitro*, but the PIN loop was no substrate for CANAR.

Localization control through diffusion control and protein interactions

After exocytotic trafficking to the PM, the PINs diffuse laterally in the membrane (Kleine-Vehn *et al.*, 2011). To limit the PINs to one cell side, controlling the lateral diffusion is the first point of regulation. Fluorescence after photo-bleaching (FRAP) experiments revealed that the PIN diffusion rate is slow compared to D6PK (Alina Graf, TUM, pers. correspondence). Recently, it was shown that alternative splicing occurs in *PIN4* and *PIN7* (Hrtyan *et al.*, 2015; Kashkan *et al.*, 2022). Alternative splicing of *PIN7* results in two isoforms, PIN7a and PIN7b, which differ in a four amino acid motif in the loop domain. This motif leads to decreased lateral diffusion but not to differences in their expression and localization pattern. PINs form homodimers and interaction of PIN7a and PIN7b could be a mechanism to regulate diffusion in the membrane (Figure 3).

Another way to limit lateral diffusion is through interaction of PINs with other proteins. The loop domain of canonical PINs is predestined to act as an interaction hub, because it faces the cytosol and therefore is accessible for modifications and interactions. It was discovered that the plant-specific proteins of unknown molecular function of the MACCHI-BOU 4 (MAB4)/ENHANCER OF PINOID 1 (ENP1)-LIKE (MAB4/MEL) gene family genetically and physically interact with PINs and PINOID/WAGs (Furutani *et al.*, 2011; Furutani *et al.*, 2014; Glanc *et al.*, 2021). In *mab4/mel* mutants, the polar PIN2 localization is lost and more PIN2 signal was detected at the lateral cell side (Glanc *et al.*, 2021). In newly divided epidermal cells, the PINs localize to the apical PM first and the MAB4/MEL proteins follow the PIN localization. It was shown that this recruitment is dependent on PID-mediated PIN2 phosphorylation and that all three proteins interact *in vitro*.

For PIN1, the PID-dependent phosphorylation at some specific sites is subject to cis/trans isomerization (Xi *et al.*, 2016). The cis/trans prolyl isomerase Pin1At accelerates the conformational change of phosphorylated serine/threonine-proline motifs and exhibits a post-phosphorylation regulatory function (Wang *et al.*, 2010; Xi *et al.*, 2016). Downregulated expression of *Pin1At* led to agravitropic root growth, root meristem collapse and impaired polar localization of PIN1 (Xi *et al.*, 2016). Pin1At isomerizes preferentially S337 in PIN1, and phospho-mimicking variants failed to shift from the basal to apical cell side in the root stele. Also, the threonine residues T1, T2 and T3 in

the TPRXS motif, that were identified as targets of the MAP kinases MPK3, MPK4 and MPK6, are isomerized by Pin1At (Jia *et al.*, 2016; Dory *et al.*, 2018). None of these observations were made for other PINs.

1.6 Objectives of this thesis

PINs, in conjunction with their transport activation and localization regulated by AGCVIII kinases, are the key players in PAT. To date, the cell-biological characteristics of the PIN family were investigated intensively, but little is known about their transport properties. Most studies and models of auxin flow assumed the same transport rates for all PINs (Di Mambro *et al.*, 2017). First results from transport experiments in *Xenopus laevis* oocytes hinted towards different biochemical properties (Zourelidou *et al.*, 2014). In canonical PINs, the cytosolic loop domain is the central point of transport regulation. Besides the regulation of localization, AGCVIII kinases also influence the IAA transport by PINs to different degrees, as shown for D6PK and PAX (Marhava *et al.*, 2018). To gain broader knowledge on PIN activation, the impact of several kinase family members on PIN-mediated IAA transport was investigated. In order to learn more about the impact of the loop domain to transport, PIN chimeras were generated between the respective PINs by domain swapping. The chimeras were analyzed biochemically on their transport properties and physiologically on their ability to rescue the agravitropic *pin2* root phenotype.

The objectives of this thesis were to characterize the transport properties, particularly the kinetics of PIN-mediated IAA transport, to characterize the impact of modulating transport rates in the roots by monitoring the gravitropic root growth and the root bending rate, and to characterize several AGCVIII kinases and members of other kinase families on their ability to active PIN-mediated transport.

2 Materials and methods

2.1 Biological material and constructs for oocyte assay

Escherichia coli (XL1-blue) chemically competent cells were used for molecular cloning. For plant transformation, *Agrobacterium tumefaciens* (GV3101/pSOUP) chemically competent cells were used.

Table 1 – Bacteria strains used in this thesis.

Bacteria strain	**Genotype**	**Reference**
Escherichia coli (XL1-blue)	*recA1 endA1 gyrA96 thi-1 hsdR17 supE44 relA1 lac* F′ proAB lacIqZΔM15 Tn10 Tet^r	Stratagene/Agilent
Agrobacterium tumefaciens (GV3101/pMP90 pSOUP)	pMP90(pTiBo542ΔT-DNA) and pSOUP in C58C1	Koncz and Schell, 1986; Hellens *et al.*, 2000

The genetic background of all plant lines in this thesis is ecotype Columbia-0.

Table 2 – Transgenic lines used in this thesis.

Construct	T-DNA	Background	Reference
pin2 mutant	SALK_042899.22.25.x	Col-0	Willige *et al.*, 2011
PIN1	P_{PIN2}*:PIN1*	*pin2*	This thesis
PIN1-eGFP	P_{PIN2}*:PIN1-eGFP*	*pin2*	This thesis
PIN2	P_{PIN2}*:PIN2*	*pin2*	This thesis
PIN2-eGFP	P_{PIN2}*:PIN2-eGFP*	*pin2*	This thesis
PIN3	P_{PIN2}*:PIN3*	*pin2*	This thesis
PIN3-eGFP	P_{PIN2}*:PIN3-eGFP*	*pin2*	This thesis
PIN1-2-1	P_{PIN2}*:PIN1-2-1*	*pin2*	This thesis
PIN1-2-1-eGFP	P_{PIN2}*:PIN1-2-1-eGFP*	*pin2*	This thesis
PIN1-3-1	P_{PIN2}*:PIN1-3-1*	*pin2*	This thesis
PIN1-3-1-eGFP	P_{PIN2}*:PIN1-3-1-eGFP*	*pin2*	This thesis
PIN2-1-2	P_{PIN2}*:PIN2-1-2*	*pin2*	This thesis
PIN2-3-2	P_{PIN2}*:PIN2-3-2*	*pin2*	This thesis
PIN2-3-2-eGFP	P_{PIN2}*:PIN2-3-2-eGFP*	*pin2*	This thesis
PIN2-2-3	P_{PIN2}*:PIN2-2-3*	*pin2*	This thesis
PIN2-3-3	P_{PIN2}*:PIN2-3-3*	*pin2*	This thesis
PIN3-1-3	P_{PIN2}*:PIN3-1-3*	*pin2*	This thesis
PIN3-1-3-eGFP	P_{PIN2}*:PIN3-1-3-eGFP*	*pin2*	This thesis
PIN3-2-3	P_{PIN2}*:PIN3-2-3*	*pin2*	This thesis
PIN3-2-3-eGFP	P_{PIN2}*:PIN3-2-3-eGFP*	*pin2*	This thesis
PIN3-2-2	P_{PIN2}*:PIN3-2-2*	*pin2*	This thesis
PIN3-3-2	P_{PIN2}*:PIN3-3-2*	*pin2*	This thesis
PIN8	P_{PIN2}*:PIN8*	*pin2*	Martina Kolb (TUM)
PIN8-1-8	P_{PIN2}*:PIN8-1-8*	*pin2*	This thesis
PIN8-2-8	P_{PIN2}*:PIN8-2-8*	*pin2*	Martina Kolb (TUM)
PIN8-2-8-eGFP	P_{PIN2}*:PIN8-2-8-eGFP*	*pin2*	Martina Kolb (TUM)
PIN8-3-8	P_{PIN2}*:PIN8-3-8*	*pin2*	Martina Kolb (TUM)
PIN8-3-8-eGFP	P_{PIN2}*:PIN8-3-8-eGFP*	*pin2*	Martina Kolb (TUM)
DR5v2-GUS	P_{DR5v2}*:GUS*	Col-0	Liao *et al.*, 2015
R2D2	*RPS5A-mDII-ntdTomato; RPS5A-DII-n3xVenus*	Col-0	Liao *et al.*, 2015 and Dr. Yao Xiao (TUM)

Oocytes were isolated from *Xenopus laevis* females by the in-house facility or bought from Ecocyte (Dortmund, Germany). For the oocyte transport assay, the coding sequences (CDS) of all proteins of interest were cloned into the pOO2 backbone and copyRNA (cRNA) was generated for injection (Ludewig *et al.*, 2002).

Table 3 – Constructs for oocyte transport assay used in this thesis.

Name	Details	Reference
PIN1		Zourelidou *et al.*, 2014
PIN1-eGFP		This thesis
PIN2		This thesis
PIN2-eGFP		This thesis
PIN3		Zourelidou *et al.*, 2014
PIN3-eGFP		This thesis
PIN3sc	PIN3 short cut	This thesis
PIN3*		This thesis
PIN3-S294A		This thesis
PIN3-S293A-S294A		This thesis
PIN3-S293D-S294D		This thesis
PIN4		Gütter, 2014
PIN7		Gütter, 2014
PIN8		Kolb, 2015
PIN1-2-1		Invitrogen
PIN1-3-1		Invitrogen
PIN2-1-2		Invitrogen
PIN2-3-2		Invitrogen
PIN2-2-3		Invitrogen
PIN2-3-3		Invitrogen
PIN2-3-3*		This thesis
PIN3-1-3		Invitrogen
PIN3-2-3		Invitrogen
PIN3-2-2		Invitrogen
PIN3-3-2		Invitrogen
PIN8-2-8		Kolb, 2015
PIN8-3-8		Kolb, 2015
AGC1.7		Martina Kolb (TUM)
AGC1.8		Dr. Yao Xiao (TUM)
AGC1.9		Dr. Yao Xiao (TUM)
CRK5		Angela Alkofer (TUM)

Name	Details	Reference
YFP-D6PK		Zourelidou *et al.*, 2014
YFP-D6PKin	inactive	Zourelidou *et al.*, 2014
D6PK-LIKE1		Angela Alkofer (TUM)
D6PK-LIKE2		Angela Alkofer (TUM)
D6PK-LIKE3		Angela Alkofer (TUM)
KIPK	KCBP-INTERACTING PROTEIN KINASE	Dr. Yao Xiao (TUM)
N-1.8-KIPK-C		Dr. Yao Xiao (TUM)
N-KIPK-1.8-C		Dr. Yao Xiao (TUM)
MPK3(D,E)	D193G E197A	Benedikt Pfeilschifter (now FAU)
MPK4(D,E)	D198G E202A	Benedikt Pfeilschifter (now FAU)
MPK4(Y)	Y124C	Benedikt Pfeilschifter (now FAU)
MPK6(D,E)	D218G E222A	Benedikt Pfeilschifter (now FAU)
MPK6(Y)	Y144C	Benedikt Pfeilschifter (now FAU)
PAX		Marhava *et al.*, 2018
YFP-PAX		Lanassa Bassukas (TUM), Angela Alkofer (TUM)
PAX(SMA)	S596A	Lanassa Bassukas (TUM)
PAX(SMD)	S596D	Lanassa Bassukas (TUM)
PAX KD	kinase dead variant	Lanassa Bassukas (TUM)
pax8mut	S15A S68A S136A S137A S138A T227A S269A S316A S596A S735A S737A	Lanassa Bassukas (TUM)
PDK1		Lanassa Bassukas (TUM)
PINOID		Zourelidou *et al.*, 2014
YFP-PINOID		Angela Alkofer (TUM)
WAG1		Angela Alkofer (TUM)

2.2 Oligos and molecular cloning

2.2.1 Oligos

All oligos were ordered from Sigma-Aldrich/Merck (Darmstadt, Germany).

Table 4 – Primers for GreenGate cloning to generate plant expression constructs.

Construct	Oligo	Sequence 5'→3'	Description
PIN1	JAD 007	TATAGGTCTCGACCTAGACCAACGAATTGATGGAG	Promoter FWD
	JAD 008	TATAGGTCTCGCATTTTGATTTACTTTTTCCGGCG	Promoter REV
	JAD 009	TATAGGTCTCGAATGATTACGGCGGCGGACT	TM1 FWD
	JAD 060	TATAGGTCTCGTCCACGGTACTCAAAGAGAAAGAG	TM1 REV
	JAD 061	TATAGGTCTCGTGGAGCTAAGCTTTTGATCTCCG	Loop FWD
	JAD 062	TATAGGTCTCGTGTGATGACAAGACTCATTCTC	Loop REV
	JAD 063	TATAGGTCTCGTCCACGGTACTCAAAGAGAAAGAG	TM2 FWD
	JAD 010	TATAGGTCTCGCTCATAGACCCAAGAGAATGTAGTAGAG	TM2 REV
	JAD 011	TATAGGTCTCGTGAGTTATTATCAAAACGTATTTGC	Terminator FWD
	JAD 012	TATAGGTCTCGTAGTATATATAAGACAAAAGAAATGAAA	Terminator REV
PIN1-eGFP	JAD 007	TATAGGTCTCGACCTAGACCAACGAATTGATGGAG	Promoter FWD
	JAD 008	TATAGGTCTCGCATTTTGATTTACTTTTTCCGGCG	Promoter REV
	JAD 009	TATAGGTCTCGAATGATTACGGCGGCGGACT	CDS FWD
	JAD 010	TATAGGTCTCGCTCATAGACCCAAGAGAATGTAGTAGAG	CDS REV
	JAD 011	TATAGGTCTCGTGAGTTATTATCAAAACGTATTTGC	Terminator FWD
	JAD 012	TATAGGTCTCGTAGTATATATAAGACAAAAGAAATGAAA	Terminator REV
PIN2	JAD 007	TATAGGTCTCGACCTAGACCAACGAATTGATGGAG	Promoter FWD
	JAD	TATAGGTCTCGCATTTTGATTTACTTTTTCCGGCG	Promoter REV

Construct	Oligo	Sequence 5'→3'	Description
	008		
	JAD 025	TATAGGTCTCGAATGATCACCGGCAAAGACATG	CDS FWD
	JAD 026	TATAGGTCTCGCTTAAAGCCCCAAAAGAACGTAGTAG	CDS REV
	JAD 015	TATAGGTCTCGTAAGTTATTATCAAAACGTATTTGC	Terminator FWD
	JAD 012	TATAGGTCTCGTAGTATATATAAGACAAAAGAAATGAAA	Terminator REV
PIN2-eGFP	JAD 007	TATAGGTCTCGACCTAGACCAACGAATTGATGGAG	Promoter FWD
	JAD 008	TATAGGTCTCGCATTTTGATTTACTTTTTCCGGCG	Promoter REV
	JAD 025	TATAGGTCTCGAATGATCACCGGCAAAGACATG	CDS FWD
	JAD 026	TATAGGTCTCGCTTAAAGCCCCAAAAGAACGTAGTAG	CDS REV
	JAD 015	TATAGGTCTCGTAAGTTATTATCAAAACGTATTTGC	Terminator FWD
	JAD 012	TATAGGTCTCGTAGTATATATAAGACAAAAGAAATGAAA	Terminator REV
PIN3	JAD 007	TATAGGTCTCGACCTAGACCAACGAATTGATGGAG	Promoter FWD
	JAD 008	TATAGGTCTCGCATTTTGATTTACTTTTTCCGGCG	Promoter REV
	JAD 013	TATAGGTCTCGAATGATCTCATGGCACGACCT	TM1 FWD
	JAD 054	TATAGGTCTCGCTTGGCGCCACGAAACTCGAAGAGAA	TM1 REV
	JAD 055	TATAGGTCTCGCAAGATGCTCATCATGGAGC	Loop FWD
	JAD 056	TATAGGTCTCGTCGCCGGAGGCATATTTTTTCGTTGACT	Loop REV
	JAD 057	TATAGGTCTCGGCGAGTGTGATGACAAGGCTGATACT	TM2 FWD
	JAD 014	TATAGGTCTCGCTTATAACCCGAGTAGAATGTAGTAAAC	TM2 REV
	JAD 015	TATAGGTCTCGTAAGTTATTATCAAAACGTATTTGC	Terminator FWD
	JAD 012	TATAGGTCTCGTAGTATATATAAGACAAAAGAAATGAAA	Terminator REV
PIN3-eGFP	JAD 007	TATAGGTCTCGACCTAGACCAACGAATTGATGGAG	Promoter FWD

Construct	Oligo	Sequence 5'→3'	Description
	JAD 008	TATAGGTCTCGCATTTTGATTTACTTTTTCCGGCG	Promoter REV
	JAD 013	TATAGGTCTCGAATGATCTCATGGCACGACCT	CDS FWD
	JAD 014	TATAGGTCTCGCTTATAACCCGAGTAGAATGTAGTAAAC	CDS REV
	JAD 015	TATAGGTCTCGTAAGTTATTATCAAAACGTATTTGC	Terminator FWD
	JAD 012	TATAGGTCTCGTAGTATATATAAGACAAAAGAAATGAAA	Terminator REV
PIN 1-2-1	JAD 007	TATAGGTCTCGACCTAGACCAACGAATTGATGGAG	Promoter FWD
	JAD 008	TATAGGTCTCGCATTTTGATTTACTTTTTCCGGCG	Promoter REV
	JAD 009	TATAGGTCTCGAATGATTACGGCGGCGGACT	CDS FWD
	JAD 010	TATAGGTCTCGCTCATAGACCCAAGAGAATGTAGTAGAG	CDS REV
	JAD 011	TATAGGTCTCGTGAGTTATTATCAAAACGTATTTGC	Terminator FWD
	JAD 012	TATAGGTCTCGTAGTATATATAAGACAAAAGAAATGAAA	Terminator REV
PIN 1-2-1-eGFP	JAD 007	TATAGGTCTCGACCTAGACCAACGAATTGATGGAG	Promoter FWD
	JAD 008	TATAGGTCTCGCATTTTGATTTACTTTTTCCGGCG	Promoter REV
	JAD 009	TATAGGTCTCGAATGATTACGGCGGCGGACT	CDS FWD
	JAD 072	TATAGGTCTCGTTTCCCCCGTTATTACCGTCTTG	CDS REV
	JAD 073	TATAGGTCTCGGAAAGATGGTGAGCAAGGGCGAGGAGC	eGFP FWD
	JAD 074	TATAGGTCTCGACAGCTCGTCCATGCCGAGAGTGATC	eGFP REV
	JAD 075	TATAGGTCTCGCTGTACAAGTCACCTTACATGGGCAAAAAAG	CDS FWD
	JAD 010	TATAGGTCTCGCTCATAGACCCAAGAGAATGTAGTAGAG	CDS REV
PIN 1-3-1	JAD 007	TATAGGTCTCGACCTAGACCAACGAATTGATGGAG	Promoter FWD
	JAD 008	TATAGGTCTCGCATTTTGATTTACTTTTTCCGGCG	Promoter REV
	JAD	TATAGGTCTCGAATGATTACGGCGGCGGACT	CDS FWD

Construct	Oligo	Sequence 5'→3'	Description
	009		
	JAD 010	TATAGGTCTCGCTCATAGACCCAAGAGAATGTAGTAGAG	CDS REV
	JAD 011	TATAGGTCTCGTGAGTTATTATCAAAACGTATTTGC	Terminator FWD
	JAD 012	TATAGGTCTCGTAGTATATATAAGACAAAAGAAATGAAA	Terminator REV
PIN 1-3-1-eGFP	JAD 007	TATAGGTCTCGACCTAGACCAACGAATTGATGGAG	Promoter FWD
	JAD 008	TATAGGTCTCGCATTTTGATTTACTTTTTCCGGCG	Promoter REV
	JAD 009	TATAGGTCTCGAATGATTACGGCGGCGGACT	CDS FWD
	JAD 010	TATAGGTCTCGCTCATAGACCCAAGAGAATGTAGTAGAG	CDS REV
	JAD 011	TATAGGTCTCGTGAGTTATTATCAAAACGTATTTGC	Terminator FWD
	JAD 012	TATAGGTCTCGTAGTATATATAAGACAAAAGAAATGAAA	Terminator REV
PIN 2-1-2	JAD 007	TATAGGTCTCGACCTAGACCAACGAATTGATGGAG	Promoter FWD
	JAD 008	TATAGGTCTCGCATTTTGATTTACTTTTTCCGGCG	Promoter REV
	JAD 025	TATAGGTCTCGAATGATCACCGGCAAAGACATG	CDS FWD
	JAD 026	TATAGGTCTCGCTTAAAGCCCCAAAAGAACGTAGTAG	CDS REV
	JAD 015	TATAGGTCTCGTAAGTTATTATCAAAACGTATTTGC	Terminator FWD
	JAD 012	TATAGGTCTCGTAGTATATATAAGACAAAAGAAATGAAA	Terminator REV
PIN 2-3-2	JAD 007	TATAGGTCTCGACCTAGACCAACGAATTGATGGAG	Promoter FWD
	JAD 008	TATAGGTCTCGCATTTTGATTTACTTTTTCCGGCG	Promoter REV
	JAD 025	TATAGGTCTCGAATGATCACCGGCAAAGACATG	CDS FWD
	JAD 026	TATAGGTCTCGCTTAAAGCCCCAAAAGAACGTAGTAG	CDS REV
	JAD 015	TATAGGTCTCGTAAGTTATTATCAAAACGTATTTGC	Terminator FWD
	JAD 012	TATAGGTCTCGTAGTATATATAAGACAAAAGAAATGAAA	Terminator REV

Construct	Oligo	Sequence 5'→3'	Description
PIN 2-3-2-eGFP	JAD 007	TATAGGTCTCGACCTAGACCAACGAATTGATGGAG	Promoter FWD
	JAD 008	TATAGGTCTCGCATTTTGATTTACTTTTTCCGGCG	Promoter REV
	JAD 025	TATAGGTCTCGAATGATCACCGGCAAAGACATG	CDS FWD
	JAD 026	TATAGGTCTCGCTTAAAGCCCCAAAAGAACGTAGTAG	CDS REV
	JAD 015	TATAGGTCTCGTAAGTTATTATCAAAACGTATTTGC	Terminator FWD
	JAD 012	TATAGGTCTCGTAGTATATATAAGACAAAAGAAATGAAA	Terminator REV
PIN 2-2-3	JAD 007	TATAGGTCTCGACCTAGACCAACGAATTGATGGAG	Promoter FWD
	JAD 008	TATAGGTCTCGCATTTTGATTTACTTTTTCCGGCG	Promoter REV
	JAD 025	TATAGGTCTCGAATGATCACCGGCAAAGACATG	CDS FWD
	JAD 014	TATAGGTCTCGCTTATAACCCGAGTAGAATGTAGTAAAC	CDS REV
	JAD 015	TATAGGTCTCGTAAGTTATTATCAAAACGTATTTGC	Terminator FWD
	JAD 012	TATAGGTCTCGTAGTATATATAAGACAAAAGAAATGAAA	Terminator REV
PIN 2-3-3	JAD 007	TATAGGTCTCGACCTAGACCAACGAATTGATGGAG	Promoter FWD
	JAD 008	TATAGGTCTCGCATTTTGATTTACTTTTTCCGGCG	Promoter REV
	JAD 025	TATAGGTCTCGAATGATCACCGGCAAAGACATG	CDS FWD
	JAD 014	TATAGGTCTCGCTTATAACCCGAGTAGAATGTAGTAAAC	CDS REV
	JAD 015	TATAGGTCTCGTAAGTTATTATCAAAACGTATTTGC	Terminator FWD
	JAD 012	TATAGGTCTCGTAGTATATATAAGACAAAAGAAATGAAA	Terminator REV
PIN 3-1-3	JAD 007	TATAGGTCTCGACCTAGACCAACGAATTGATGGAG	Promoter FWD
	JAD 008	TATAGGTCTCGCATTTTGATTTACTTTTTCCGGCG	Promoter REV
	JAD 013	TATAGGTCTCGAATGATCTCATGGCACGACCT	CDS FWD
	JAD	TATAGGTCTCGCTTATAACCCGAGTAGAATGTAGTAAAC	CDS REV

Construct	Oligo	Sequence 5'→3'	Description
	014		
	JAD 015	TATAGGTCTCGTAAGTTATTATCAAAACGTATTTGC	Terminator FWD
	JAD 012	TATAGGTCTCGTAGTATATATAAGACAAAAGAAATGAAA	Terminator REV
PIN 3-1-3-eGFP	JAD 007	TATAGGTCTCGACCTAGACCAACGAATTGATGGAG	Promoter FWD
	JAD 008	TATAGGTCTCGCATTTTGATTTACTTTTTCCGGCG	Promoter REV
	JAD 013	TATAGGTCTCGAATGATCTCATGGCACGACCT	CDS FWD
	JAD 014	TATAGGTCTCGCTTATAACCCGAGTAGAATGTAGTAAAC	CDS REV
	JAD 015	TATAGGTCTCGTAAGTTATTATCAAAACGTATTTGC	Terminator FWD
	JAD 012	TATAGGTCTCGTAGTATATATAAGACAAAAGAAATGAAA	Terminator REV
PIN 3-2-3	JAD 007	TATAGGTCTCGACCTAGACCAACGAATTGATGGAG	Promoter FWD
	JAD 008	TATAGGTCTCGCATTTTGATTTACTTTTTCCGGCG	Promoter REV
	JAD 013	TATAGGTCTCGAATGATCTCATGGCACGACCT	CDS FWD
	JAD 014	TATAGGTCTCGCTTATAACCCGAGTAGAATGTAGTAAAC	CDS REV
	JAD 015	TATAGGTCTCGTAAGTTATTATCAAAACGTATTTGC	Terminator FWD
	JAD 012	TATAGGTCTCGTAGTATATATAAGACAAAAGAAATGAAA	Terminator REV
PIN 3-2-3-eGFP	JAD 007	TATAGGTCTCGACCTAGACCAACGAATTGATGGAG	Promoter FWD
	JAD 008	TATAGGTCTCGCATTTTGATTTACTTTTTCCGGCG	Promoter REV
	JAD 013	TATAGGTCTCGAATGATCTCATGGCACGACCT	CDS FWD
	JAD 014	TATAGGTCTCGCTTATAACCCGAGTAGAATGTAGTAAAC	CDS REV
	JAD 015	TATAGGTCTCGTAAGTTATTATCAAAACGTATTTGC	Terminator FWD
	JAD 012	TATAGGTCTCGTAGTATATATAAGACAAAAGAAATGAAA	Terminator REV
PIN 3-2-2	JAD 007	TATAGGTCTCGACCTAGACCAACGAATTGATGGAG	Promoter FWD

Construct	Oligo	Sequence 5'→3'	Description
	JAD 008	TATAGGTCTCGCATTTTGATTTACTTTTTCCGGCG	Promoter REV
	JAD 013	TATAGGTCTCGAATGATCTCATGGCACGACCT	CDS FWD
	JAD 026	TATAGGTCTCGCTTAAAGCCCCAAAAGAACGTAGTAG	CDS REV
	JAD 015	TATAGGTCTCGTAAGTTATTATCAAAACGTATTTGC	Terminator FWD
	JAD 012	TATAGGTCTCGTAGTATATATAAGACAAAAGAAATGAAA	Terminator REV
PIN 3-3-2	JAD 007	TATAGGTCTCGACCTAGACCAACGAATTGATGGAG	Promoter FWD
	JAD 008	TATAGGTCTCGCATTTTGATTTACTTTTTCCGGCG	Promoter REV
	JAD 013	TATAGGTCTCGAATGATCTCATGGCACGACCT	CDS FWD
	JAD 026	TATAGGTCTCGCTTAAAGCCCCAAAAGAACGTAGTAG	CDS REV
	JAD 015	TATAGGTCTCGTAAGTTATTATCAAAACGTATTTGC	Terminator FWD
	JAD 012	TATAGGTCTCGTAGTATATATAAGACAAAAGAAATGAAA	Terminator REV
PIN 8-1-8	KOM 304	TATAGGTCTCGACCTGTCTTTGCTACGGATTGTGGAA	Promoter FWD
	KOM 305	TATAGGTCTCGCATTTTGATTTACTTTTTCCGGCGAGAG	Promoter REV
	KOM 306	TATAGGTCTCGAATGATCTCCTGGCTCGATATCTAC	CDS FWD
	KOM 307	TATAGGTCTCGCTCATAGGTCCAATAGAAAATAATATGC	CDS REV
	KOM 308	TATAGGTCTCGTGAGTTATTATCAAAACGTATTTGCAA	Terminator FWD
	KOM 309	TATAGGTCTCGTAGTATATATAAGACAAAAGAAATGAA	Terminator REV

Table 5 – Primer combinations for genotyping transgenic plant lines used in this thesis.

Construct	Oligo	Sequence 5'→3'	Fragment (bp)
PIN1, PIN8-1-8	KOM157	AACACAAACAACATTAATTAAATATCGTCTCAAGGAAC	600
	KOM152	TCTGGAAACTGCTCGGAGATCAAAAGCTTAGC	
PIN1-eGFP	PIN1loop_fwd	GCTAAGCTTTTGATCTCCGAGCAGTTTC	840
	GFP_anchor_rev	CAGCTCCTCGCCCTTGCTCACCAT	
PIN2	JAD081	AAACGCCTGCCAAAGAAAGAGTGCGGCGAGG	1500
	GTSpGGZ003_RB	CAATATATCCTGTCAAGGCTCGAAC	
PIN2-eGFP	AtPIN2loop_fwd	GCTAAGCTTCTCATCTCCGAGCAGTTCCCGG	900
	GFPanc_rev	CAGCTCCTCGCCCTTGCTCACCAT	
PIN3, PIN3-eGFP, PIN3-1-3, PIN3-1-3-eGFP, PIN3-2-3, PIN3-2-3-eGFP, PIN3-3-2	KOM157	AACACAAACAACATTAATTAAATATCGTCTCAAGGAAC	500, 500, 500, 500, 380, 380, 450
	JAD083	GAAATTAGCCCATAGGACTAAAAGTGACAACATGATG	
PIN1-2-1	KOM160	GTCCCGGTCCTAGGAAACAGCAGATGCCGCCGGCGAG	500
	PIN1TM_rev	TCATAGACCCAAGAGAATGT	
PIN1-2-1-eGFP	KOM151	GGGATCACTCTCGGCATGGACGAGCTGTACAAG	600
	JAD084	GCAAATACGTTTTGATAATAAC	

Construct	Oligo	Sequence 5'→3'	Fragment (bp)
PIN1-3-1, PIN1-3-1-eGFP, PIN2-3-2, PIN2-3-2-eGFP, PIN2-3-3	KOM157	AACACAAACAACATTAATTAAATATCGTCTCAAGGAAC	600
	KOM153	CAGGGAACTGCTCCATGATGAGCATCTTGGC	
PIN2-1-2	PIN2TMfwd_anchor	ATGATCACCGGCAAAGACATGTACGATG	470
	KOM152	TCTGGAAACTGCTCGGAGATCAAAAGCTTAGC	
PIN3-2-2	PIN3TMfwdanc	ATGATCTCATGGCACGACCTCTACACGGTC	470
	KOM147	CCGGGAACTGCTCGGAGATGAGAAGCTTAGC	
DR5v2-GUS	JAD114	GAGACAAAAGGGAGACAAAAGGGAGACAAAAGGG	300
	GUS_anc_rev	TTCCACAGTTTTCGCGATCCAGACTGAATG	
pin2 mutant background	pin2_LP01	AACCCTGCTACTGATTTTCCG	~1100
	pin2_RP01	TATGGTCAGTTCCGTCGTACC	
	LBb1.3	ATTTTGCCGATTTCGGAAC	750

2.2.2 Cloning procedure

Standard methods of molecular biology were performed as described with molecular grade reagents from Carl Roth, Sigma-Aldrich or the Thermo Fisher group (Sambrook *et al.*, 1989). All enzymes were purchased from Thermo Fisher Scientific (Waltham, USA) or Kapa Biosystems (Wilmington, USA) and used according to the manual. Amplified DNA fragments by PCR were purified by gel electrophoresis and the NucleoSpin gel and PCR kit from Machery & Nagel (Düren, Germany). For plasmid preparation, the NucleoSpin Plasmid kit from Macherey & Nagel was used. For cRNA

synthesis, the mMESSAGE mMACHINE™ SP6 Transcription kit and the MEGAclear Purification of Transcription Reactions kit from Thermo Fisher Scientific were used.

Plant expression vectors were generated by a modified GreenGate cloning protocol (Lampropoulos *et al.*, 2013). Contrary to the original protocol, the BsaI-recognition site and, if necessary, suitable overhangs were added to the DNA fragments through the oligos at the 5' end (TATAGGTCTCG…). The DNA fragments of interest were amplified from genomic DNA (gDNA) or CDS synthesized by Invitrogen (Waltham, USA). The inserts were directly ligated into the destination vector pGGZ003 in a molecular ratio of 1:1 – 1:3. The Basta resistance gene ("F" module) was provided by the entry vector pGGF009.

The protein domains of PIN1, PIN2, PIN3 and PIN8 were defined as the following and derived from (Ganguly *et al.*, 2014): PIN1: TM1 1–156 aa, loop 157–459 aa, TM2 460–623 aa. PIN2: TM1 1–156 aa, loop 157–484 aa, TM2 485–623 aa. PIN3: TM1 1–156 aa, loop 157–477 aa, TM2 478–641 aa. PIN8: TM1 1–163 aa, loop 164–204 aa, TM2 205–367 aa. The CDS of eGFP was inserted C-terminally of amino acid positions 432 (PIN1), 301 (PIN2) and 451 (PIN3) or at equivalent positions in the loop domain in the PIN chimeras. The loops of PIN1, PIN2 or PIN3 were inserted C-terminally of position 163 in PIN8 (Kolb, 2015).

For cloning into pOO2, the CDS was amplified with 5'-phosphorylated oligos and purified by gel electrophoreses. The backbone was linearized with SmaI and dephosphorylated with Antarctic Phosphatase (AnP). Insert and backbone were ligated in a molecular ratio of 1:3 by T4 DNA ligase. The ligation reaction contained the restriction enzyme SmaI to digest re-ligated pOO2 backbones, in order to minimize re-transformants and increase the success rate. The ligation reaction was incubated at 28 °C for 5 min, followed by 37 °C for 5 min (30x) and finally heat-inactivated.

2.3 Work with oocytes

2.3.1 Transport assay

The efflux experiments were performed as described (Fastner *et al.*, 2017). Oocytes were injected with 150 ng/µl PIN cRNA and 75 ng/µl cRNA of respective kinase. The ^{3}H-IAA was purchased by ARC (Saint Louis, USA) or RC Tritec (Teufen, Switzerland). After 4 days, oocytes were injected with the substrate to reach the indicated internal IAA concentration. For the kinetic studies, all concentrations were spiked with non-labelled IAA (SigmaAldrich). Each time point (0, 5, 10, 15 min for PIN3, PIN2-3-2, PIN3-1-3, PIN3-2-3, PIN8 or 0, 7.5, 15, 30 min for PIN1, PIN2, PIN1-2-1, PIN2-1-2, PIN8-2-8, PIN8-3-8) resembles the mean and SEM of 7-10 oocytes. The transport rates

were calculated by linear regression. Experiments were performed at least three times with oocytes from different *X. laevis* females if not indicated differently.

2.3.2 Phospho-MS analysis

Oocytes (n = 50) expressing either PIN1, PIN2, PIN3 alone or PIN co-expressed with YFP-D6PK or PINOID were collected without oocyte buffer in a reaction tube (2 ml). The oocytes were homogenized in 2 ml Lysis buffer (Tris-HCl pH 8.0 50 mM, ½ tablet PhosSTOP (Roche), 1x cOmplete™ EDTA-free proteinase inhibitor cocktail (Sigma-Aldrich), 1 % SDC) and centrifuged (2000 *g*, 10 min, 4 °C). The supernatant without yolk was transferred to a reaction tube suitable for ultracentrifugation and centrifuged (150 000 *g*, 30 min, 4 °C). The cytosolic fraction (supernatant) and the membrane fraction (pellet) were split and the membrane fraction was resuspended in 400 µl Lysis buffer. All samples were stored at –80 °C before preparation for LC-MS/MS analysis.

Samples were prepared with the help of Dr. Julia Mergner (BayBioMS, Freising/Munich) and a detailed protocol can be found in Janacek *et al.*, 2023, under review.

2.3.3 Western blot analysis

Western blot analysis was performed as described in (Fastner *et al.*, 2017). Oocytes (n = 8) were transferred to a reaction tube (1.5 ml) and homogenized with 320 µl Homogenization buffer (50 mM Tris-HCl pH 7.6, 100 mM NaCl, 1 mM EDTA, ½ tablet PhosSTOP (Roche), 1x cOmplete™ EDTA-free proteinase inhibitor cocktail (Sigma-Aldrich)) The samples were centrifuged (2000 *g*, 10 min, 4 °C) and 300 µl of the supernatant were transferred to a reaction cup suitable for ultracentrifugation. After ultracentrifugation (150 000 *g*, 30 min, 4 °C), the supernatant (cytosolic fraction) and the pellet (membrane fraction) were split. To the cytosolic fraction, 75 µl of 4x SDS-loading dye were added and the sample was boiled at 95 °C for 5 min. The membrane fraction was resuspended in 64 µl Homogenization buffer + 16 µl 4x SDS-loading dye and incubated at 42 °C for 15 min. Samples were loaded on a 10 % SDS gel with and blotted on nitrocellulose membrane (Amersham Protran Premium 0.2 µm pore size) by semi-dry protein transfer. The membrane was blocked over night at 4 °C in 5 % milk solution (TBS buffer, 0.2 % Tween-20, 5 % (w/v) milk powder). The membrane was rinsed in TBS buffer after each step and primary and secondary antibodies were used as indicated (Table 6). The membrane was developed with SuperSignal West Femto Stable Peroxide Substrate Buffer Kit (Thermo Fisher Scientific) according to the manual. Signal of the kinases (2 min) and the PIN3 (1 min) was detected with the ImageQuant LAS4000 luminescence imager.

Table 6 – Primary and secondary antibodies for Western Blot analysis.

Name	Dilution	Carrier		Source
anti-GFP	1:3000	rabbit	IgG fraction, polyclonal antiserum	Pineda Antikörper-Service
anti-PIN3	1:5000	sheep	crude antiserum	NASC N782251
anti-rabbit-HRP	1:100 000	goat		Sigma-Aldrich
anti-goat-HRP	1:8000	rabbit		Sigma-Aldrich

2.4 Work with plants

2.4.1 Growth conditions

For growth in pots, the seeds were spread on moist soil and incubated in the growth chamber with a cover under long day conditions (16 h light, 8 h dark, 21-23 °C). After one week, the cover was removed and the plants were separated to individual pots, if necessary.

For growth on plates, the seeds were sterilized with chlorine gas (6 %(v/v), 1 h) and homogenously spread on the agar or placed individually with an autoclaved toothpick. Plates were sealed and incubated at 4 °C in the dark for two days. Afterwards the plates were placed vertically in plant growth chambers (Sanyo or Panasonic) under long day conditions (16 h light, 8 h dark, 21 °C).

Solid 0.5 MS medium contained 2.15 g/l Murashige & Skoog (MS) medium, including B5 vitamins incl. gamborg B5 vitamins (Duchefa Farma, Harleem, Netherlands), 0.5 g/l MES monohydrate (Carl Roth, Karlsruhe, Germany) and 0.8 % (w/v) plant agar (Duchefa Farma).

Solid Growth medium contained 4.3 g/l MS medium, including B5 vitamins incl. gamborg B5 vitamins, 0.5 g/l MES monohydrate, 0.7 % (w/v) plant agar and 1 % (w/v) saccharose.

2.4.2 Plant transformation

Competent *A. tumefaciens* bacteria were transformed with the respective plasmid and incubated for 3-4 days at 30 °C on YEB-plates with rifampicin (20 mg/ml), gentamycin (20 mg/ml) and spectinomycin (300 mg/ml). A single colony was used to inoculate 250 ml of YEB-Rif20-Gent20-Spec300 medium (beef extract (5 g/l,Becton Dickinson), yeast extract (1 g/l, Carl Roth), peptone

(5 g/l, Carl Roth), saccharose (5 g/l), $MgSO_4$ hydrate (0.49 g/l, Carl Roth), supplemented with rifampicin (20 µg/ml), gentamycin (20 µg/ml) and spectinomycin (300 µg/ml)). The overnight culture was centrifuged (4000 *g*, 10 min, 4 °C) and resuspended in 300 ml of buffer (5 % sucrose, 488 µl/l SILVET). The plant pots were dipped upside down into the cell suspension for 5 min and were covered with plastic bags over night. The plants were bagged when the first siliques became brown and allowed to dry.

In order to select for positive transformants, the seeds were brought on soil. After one week, the seedlings were sprayed with a Basta solution (1 % v/v). Seedlings that survived the treatment were transferred to single pots and genotyped.

2.4.3 Genotyping

Genomic DNA (gDNA) was extracted from small leave pieces. The plant material was added to an Eppendorf tube filled with two glass beads (Ø 4 ± 0.3 mm) and several smaller glass beads (Ø 1.25–1.65 mm) and the sample was frozen in liquid nitrogen. The sample was grinded in the TissueLyzer II (Qiagen, Hilden, Germany) for 1 min with a frequency of 30 Hz. Extraction buffer was added (750 µl, 50 mM Tris-HCl pH 8.0, 10 mM EDTA pH 8.0, 100 mM NaCl, 10 mM 2-mercaptoethanol, 1 % (w/v) SDS) and the sample was incubated at 65 °C for 15 min. Afterwards, sodium acetate (200 µl, 5 M stock solution) was added and the sample was incubated on ice for 20 min. After centrifugation (13 000 rpm, 15 min, 4 °C), the supernatant (700 µl) was transferred to a new cup and isopropanol (700 µl) was added. The sample was centrifuged (13 000 rpm, 10 min, 4 °C) and the supernatant was removed. The pellet was washed in 70 % (v/v) ethanol (600 µl) and incubated for 5 min at room temperature. The sample was centrifuged again for 10 min at 13 000 rpm and the pellet was dried overnight. The gDNA was dissolved in 100 µl dH_2O.

The gDNA was used as template in a PCR reaction and was checked for the PIN T-DNA (see Table 5) and the *pin2* mutant background (pin2_LP01 + pin2_RP01, pin2_LP01 + LBb1.3), or the DR5v2-GUS T-DNA.

2.4.4 Crossing

In order to generate DR5-GUS reporter lines, flowers of the respective homozygous PIN rescue line were pollinated with pollen from plants carrying the P_{DR5v2}*:GUS* construct. Positive transformants were identified by PCR in the next plant generation. The R2D2 reporter lines were generated by floral dipping of the respective homozygous PIN rescue line with *Agrobacterium tumefaciens* transformed with the R2D2 construct. Positive transformants were identified by microscopy.

2.4.5 Physiological experiments

Gravitropism assay T2

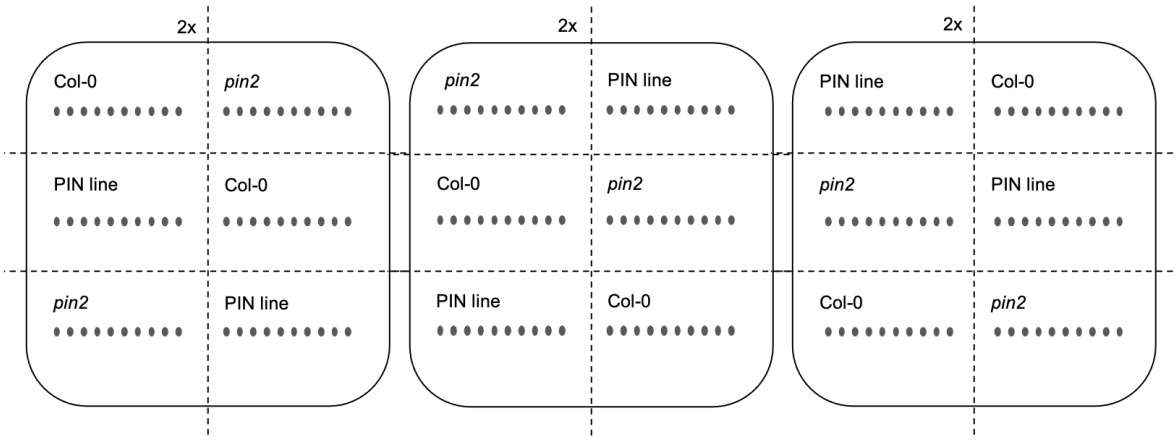

Figure 6 – Plating scheme for the gravitropism assay with T2 lines.

The sterilized seeds of the wildtype control Col-0, the *pin2* mutant and the PIN T-DNA line were plated in two sets of 10 seeds per genotype on the plate containing 0.5 MS + 1 % sucrose (Figure 6). In order to minimize plate effects, the position of the genotypes was rotated on different plates, resulting in six plates and 120 seeds for each genotype per investigated PIN rescue line. The plates were sealed and incubated in the dark at 4 °C for two days. Afterwards the plates were placed vertically into a plant growth chamber and scanned 5 days later. The root angle between the root origin and the root tip was measured for every seedling, using the SNT plugin of FIJI and a script to give the value of the root angle simultaneously, which was kindly provided by Dr. José-Antonio Villaécija-Aguilar (now LMU).

For each PIN construct, 5-10 individual segregating T2 lines were analyzed as described before. One representative line was propagated to the next generation, in order to generate a homozygous line.

Gravitropism assay T3

The representative homozygous PIN T-DNA line was platted with proper controls according to Figure 6, with only one plate per plate layout (n = 60 seeds). The plates were processed as described earlier. The VGI of the homozygous lines was calculated according to (Grabov *et al.*, 2005) using FIJI. The histogram of the root angles was created with GraphPad Prism V9, with a bin width of 15. The rose diagrams were illustrated using Adobe Illustrator 2021.

Root bending assay

The homozygous PIN T-DNA lines of interest, the wildtype Col-0 and the *pin2* mutant were grown on plates containing the indicated medium for five days, after two days of stratification at 4 °C in the dark. Two times five seedlings were transferred to a new plate containing medium as indicated (either

0.5 MS + 1 % sucrose, or 0.5 MS without vitamins) and the root was straightened. The plate was turned 90 ° and was placed into a growth chamber (Sanyo, Moriguchi, Japan), together with an IR LED light module. A Raspberry Pi (Raspberry Pi Foundation, UK) equipped with an IR camera was placed in front of the plate and an image was taken every five minutes. The angle between the root body and the tip was measured every hour from 1-10 hours after turning and after 16 h.

GUS staining

The seeds of homozygous PIN T-DNA lines, the wildtype Col-0 and the *pin2* mutant were grown on plates containing 0.5 MS + 1 % sucrose for five days, after two days of stratification at 4 °C in the dark. The whole seedlings were transferred to a 6-well plate containing GUS staining solution (100 mM $NaPO_4$ pH 7.0, 100 mM EDTA pH 7.0, 1 mM $K_3[Fe(CN)_6]$, 1 mM $K_4[Fe(CN)_6]\cdot 3H_2O$, 0.1 % Triton X-100 in H_2O, 0.5 mg/ml X-Gluc in DMF) and incubated for 1 h at 37 °C with the plate covered in aluminum foil. Afterwards the seedlings were washed three times in buffer (50 mM $NaPO_4$ pH 7.0). The roots were mounted in chloral hydrate solution (50 % (w/v) chloral hydrate, 10 % (v/v) glycerol) and imaged at an Olympus BX61 Upright microscope (Hamburg, Germany).

2.4.6 Microscopy and signal quantification

In order to image the PIN localization in Arabidopsis roots or to image the R2D2 auxin reporter, an Olympus BX61 microscope with a FV1000 confocal laser scanning unit (Olympus, Hamburg, Germany) or a Leica TCS SP8 confocal microscope (Leica, Wetzlar, Germany) were used.

The brightness and contrast were adjusted in all images and the scale bar was automatically included using FIJI. All measurements for the polarity index or the R2D2 signal analysis were performed in FIJI.

The polarity index was determined by calculating the ratio of the GFP signal at the apical and lateral PM of root epidermal cells. A square (3 px x 15 px) was defined as region of interest (ROI) and four cells from two roots of three independent segregating lines were analyzed per genotype.

In order to analyze the R2D2 signal, a maximum projection of 3-8 images with 2.0 µm intervals of either the epidermal or cortical cell file was used. A round ROI covered the nucleus. The R2 (mDII signal) to D2 (DII signal) ratio was calculated of the first five cells after the anticlinal division of the epidermis/lateral root cap initial cell (Q) and five cells at the transition zone (T).

The GUS-stained roots were imaged at an Olympus BX61 Upright microscope (Hamburg, Germany).

2.5 Software

Table 7 – Software used in this thesis.

Name	Distributor
MS Office for Mac	Microsoft, Unterschleißheim, Germany
GraphPad Prism V9	Dotmatics, Boston, USA
FIJI/ImageJ2	NIH, Bethesda, USA
Adobe Illustrator 2021	Adobe Systems, San Jose, USA
EndNote 20	Clarivate, London, UK

2.6 Statistical data processing

All data were plotted with GraphPad Prism V9 (Boston, USA). Statistical analyses were performed using the default settings of GraphPad Prism V9.

3 Results

3.1 Biochemical and physiological analyses of PINs

3.1.1 PIN transport rates are linearly related to auxin concentrations and depend on the activating kinase

The canonical PINs from *Arabidopsis thaliana* must be phosphorylated and thereby activated by AGC kinases to mediate IAA transport (Zourelidou *et al.*, 2014). In order to understand the transport behavior of PINs at physiological IAA concentrations, the transport capacities of all canonical PINs (Figure 7) were tested in a time-dependent oocyte transport assay at a cytosolic IAA concentration of $[IAA]_{in}$ = 1 µM. The PINs were either expressed alone or co-expressed with D6PK or PINOID. PIN3, PIN4 and PIN7 cluster in one phylogenetic group (Krecek *et al.*, 2009; Mravec *et al.*, 2009; De Smet *et al.*, 2011) and act redundantly in terms of their cell biological behavior (Haga and Sakai, 2012; Willige *et al.*, 2013). In the transport assay, similar transport properties to PIN3 were detected for PIN4 and PIN7.

PIN3, PIN4 and PIN7 expressed alone in Xenopus oocytes showed no IAA transport (Figure 7 J, K, L). By co-expressing D6PK, the efflux was activated to rates of 2-3 % x min^{-1} for PIN3 and PIN4, and 0.5 % x min^{-1} for PIN7. The transport rate of PIN3 and PIN4 activated by PINOID was 3-3.5 % x min^{-1} and 1.5 % x min^{-1} for PIN7. Although there were no significant differences between D6PK- and PINOID-activated transport, the transport rates were slightly higher for PINOID as activating kinase. PIN3 was chosen as the representative PIN of this group and all further biochemical and physiological analyses were performed with PIN1, PIN2 and PIN3.

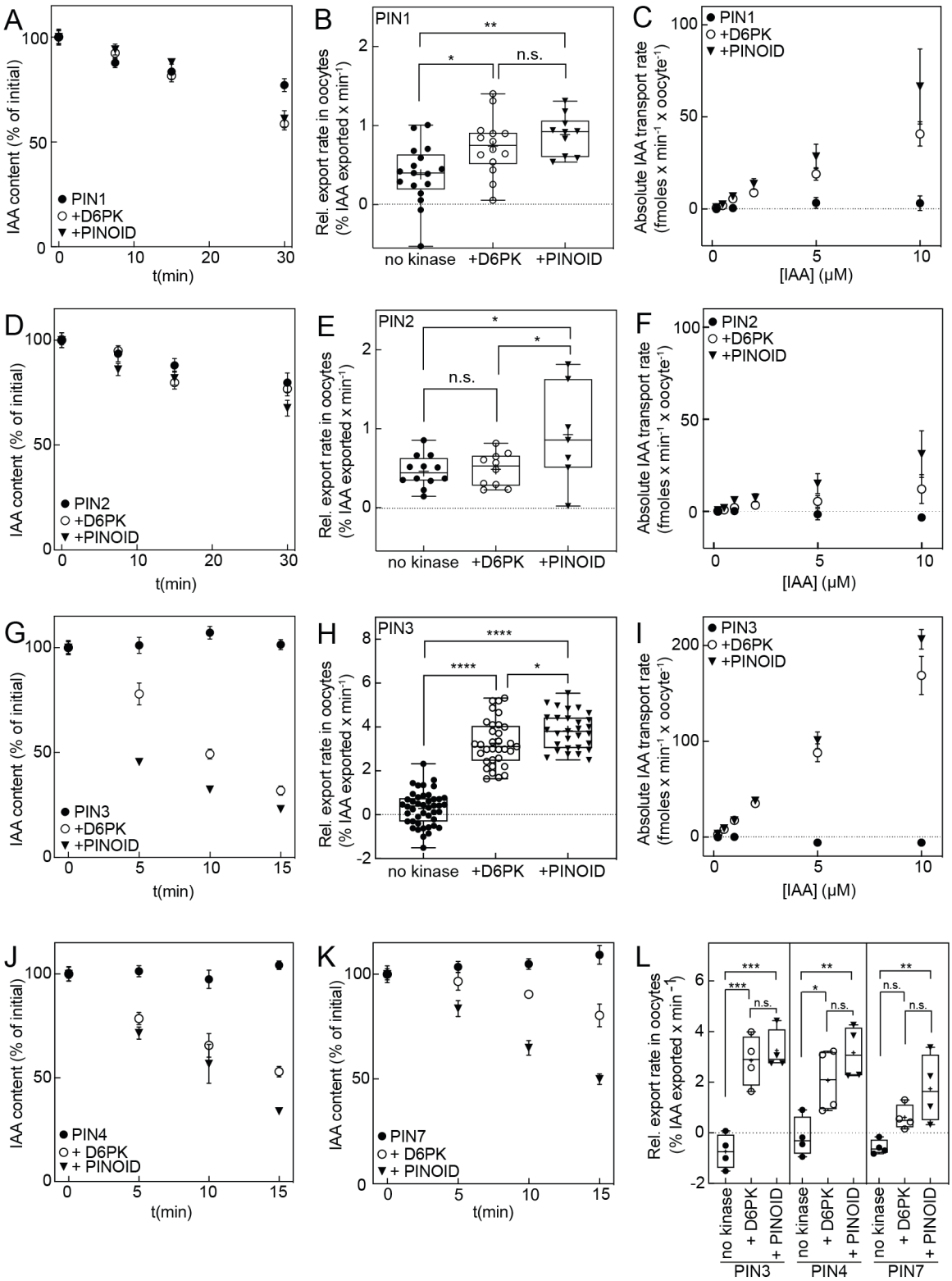
A
IAA content (% of initial)
t(min)
PIN1
+D6PK
+PINOID
B
PIN1
Rel. export rate in oocytes (% IAA exported x min-1)
no kinase
+D6PK
+PINOID
n.s.
C
Absolute IAA transport rate (fmoles x min-1 x oocyte-1)
[IAA] (µM)
D
PIN2
E
PIN2
F
PIN2
G
PIN3
H
PIN3
I
PIN3
J
PIN4
+ D6PK
+ PINOID
K
PIN7
L
no kinase
+ D6PK
+ PINOID
PIN3
PIN4
PIN7

Figure 7 – IAA transport properties of all canonical PINs in Xenopus oocytes. PIN1 (A-C), PIN 2 (D-F) and PIN3 (G-I) were expressed in oocytes without kinase (●) as well as with D6PK (○) or PINOID (▼). (A, D, G, J, K) Representative time-course experiments for PIN1, PIN2, PIN3, PIN4 and PIN7. Time points are mean and SE of n = 8-10 oocytes. (B, E, H) Relative IAA export rates for PIN1, PIN2 and PIN3 (PIN1: n = 10-17, PIN2: n = 7-12, PIN3: n = 30-44). Box plots range from the 25th to 75th percentile and the median is shown, the mean is represented by (+). Groups were compared by one-way ANOVA, followed by Tukey's post-hoc test (PIN1 vs. PIN1 + D6PK: * p-value 0.0178, PIN1 vs. PIN1 + PINOID: ** p-value 0.0021, PIN1 + D6PK vs. PIN1 + PINOID: n.s., not significant, p-value 0.5589; PIN2 vs. PIN2 + D6PK: n.s. p-value 0.9838, PIN2 vs. PIN2 + PINOID: * p-value 0.0265, PIN2 + D6PK vs. PIN2 + PINOID: * p-value 0.0458; PIN3 vs. PIN3 + D6PK: **** p-value <0.0001, PIN3 vs. PIN3 + PINOID: **** p-value <0.0001, PIN3 + D6PK vs. PIN3 + PINOID: * p-value 0.0341). (C, F, I) Transport rates as a function of $[IAA]_{in}$. Data are mean and SE of n = 4 (PIN1), n = 3 (PIN1 + D6PK), n = 3 (PIN1 + PINOID), n = 3 (PIN2), n = 3 (PIN2 + D6PK), n = 3 (PIN2 + PINOID) and n = 3 (PIN3), n = 3 (PIN3 + D6PK), n = 3 (PIN3 + PINOID). (L) Relative IAA export rates for PIN3, PIN4 and PIN7. n = 4 for all constructs. Box plots range from the minimum to maximum percentile and the median is shown, the mean is represented by (+). Groups were compared by one-way ANOVA, followed by Tukey's post-hoc test (PIN3 vs. PIN3 + D6PK: *** p-value 0.0005, PIN3 vs. PIN3 + PINOID: *** p-value 0.0002, PIN3 + D6PK vs. PIN3 + PINOID: n.s., not significant, p-value 0.7894; PIN4 vs. PIN4 + D6PK: * p-value 0.0338, PIN4 vs. PIN4 + PINOID: ** p-value 0.0037, PIN4 + D6PK vs. PIN4 + PINOID: n.s. p-value 0.3447; PIN7 vs. PIN7 + D6PK: n.s. p-value 0.1750, PIN7 vs. PIN7 + PINOID: ** p-value 0.0095, PIN7 + D6PK vs. PIN7 + PINOID: n.s. p-value 0.1931).

For all canonical PINs, a time course assay was performed to monitor the loss of IAA from oocytes over time (Figure 7 A, D, G, J, K). The PIN1-mediated transport was activated by D6PK and PINOID to comparable levels (Figure 7 B). The PIN2-mediated transport was activated significantly only by PINOID at the described assay conditions (Figure 7 E). Overall, the rates of PIN1- and PIN2-mediated IAA transport were found to be in the same range (0.5-0.9 % x min^{-1}). In contrast, PIN3 was strongly activated to transport rates of 3.3 % x min^{-1} by D6PK and 3.8 % x min^{-1} by PINOID (Figure 7 H). The D6PK- and PINOID-activated transport rates of PIN3 were significantly different to each other.

In order to determine the transport properties of PINs at a range of physiological IAA concentrations, a time-dependent efflux assays at cytosolic IAA concentrations ranging from 0.2 µM to 10 µM was performed. The transport rates were plotted as a function of $[IAA]_{in}$ (Figure 7 C, F, I).

Table 8 – IAA transport rates of PIN1, PIN2 and PIN3. The transport activity of PINs was tested at different $[IAA]_{in}$ and linear regression was performed to calculate the IAA transport rate. The transporters were expressed in oocytes either alone or co-expressed with D6PK or PINOID. Table shows the transport rates in fmoles x min^{-1} x $oocyte^{-1}$ of data presented in Figure 1 C, F, I. Mean and SE of n = 4 for PIN1; n = 3 for PIN1 + D6PK, PIN1 + PINOID, PIN2, PIN2 + D6PK, PIN2 + PINOID, PIN3, PIN3 + D6PK and PIN3 + PINOID.

	no kinase	**+ D6PK**	**+ PINOID**
PIN1	0.3 ± 0.3	3.1 ± 0.5	5.4 ± 0.8
PIN2	-0.3 ± 0.2	1.2 ± 0.4	3.0 ± 0.6
PIN3	-0.7 ± 0.2	17.0 ± 0.9	20.8 ± 0.6

PIN1, PIN2 and PIN3 without co-expressed kinase did not show any transport at higher IAA concentrations. Based on these findings, it was concluded that neither canonical PIN is able to efflux IAA without kinase co-expression from oocytes, suggesting that phosphorylation is required to overcome inhibition. PINs co-expressed with D6PK or PINOID showed a linear relationship between transport rate and IAA concentration. This suggests that at physiological IAA concentrations, the transport is limited by the turnover rate of the PIN and the amount of transporter in the PM.

The absolute IAA transport rate for PIN1 + D6PK was 3.1 ± 0.5 fmoles x min^{-1} x $oocyte^{-1}$ and 5.4 ± 0.8 fmoles x min^{-1} x $oocyte^{-1}$ for PIN1 + PINOID. The transport rates were slightly lower for PIN2 + D6PK (1.2 ± 0.4 fmoles x min^{-1} x $oocyte^{-1}$) and PIN2 + PINOID (3.0 ± 0.6 fmoles x min^{-1} x $oocyte^{-1}$). Whereas the transport capacity of PIN3 was strongly enhanced to 17.0 ± 0.9 fmoles x min^{-1} x $oocyte^{-1}$ with D6PK and 20.8 ± 0.6 fmoles x min^{-1} x $oocyte^{-1}$ for PINOID (Table 8). Notably, the PINOID-activated transport was stronger for all three PINs at all tested IAA concentrations. This suggests that the kinase impact on PIN-mediated transport is beyond its function as an activation switch.

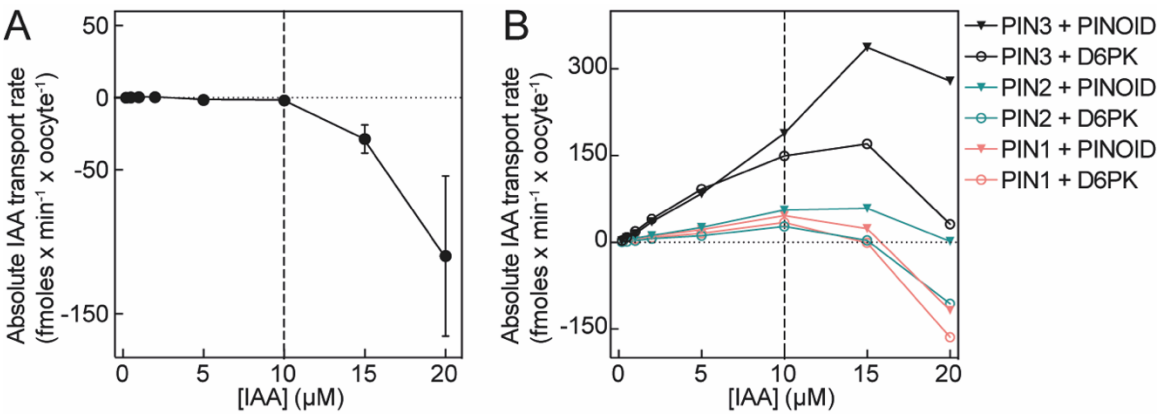

Figure 8 – IAA efflux assay at increasing internal concentrations. (A) Efflux rates of water-injected Xenopus oocytes as a function of $[IAA]_{in}$. Data are mean and SE (n = 4 assays with oocytes from different females). The dashed line indicates the concentration to which the assay was stable. (B) Transport rates of the indicated PIN-kinase combination as a function of $[IAA]_{in}$ in oocytes. (▼) co-expressed with PINOID, (○) co-expressed with D6PK. Data points are transport rate of n = 8-10 oocytes at respective $[IAA]_{in}$.

In all cases transport increased linearly with increasing IAA concentration and in no case, saturation could be reached. Therefore, higher IAA concentrations on PINs in the oocyte assay should have been tested since IAA levels in the Arabidopsis root were described to be in the range of 1–50 µM (Petersson *et al.*, 2009). It was not possible to generate a stable baseline at IAA concentrations between 10 µM and 20 µM with the methodical layout of the assay as described in Chapter 2.3.1 (Figure 8). IAA-injected oocytes without any expressed transporter showed that the assay could be stably used up to $[IAA]_{in}$ of 10 µM (Figure 8 A). At $[IAA]_{in}$ > 10 µM, a technical artefact from the injection scheme led to negative efflux rates. The oocytes that efflux the longest were injected first.

High IAA concentrations in the injection needle drastically increased the diffusion rate of radioactive IAA from the needle into the oocyte without any injection event. Therefore, the IAA levels in the first oocytes were uncontrollably higher than in the later oocytes when the concentration gradient inside the needle was already decreased. Because the last time point was injected first and had the highest artificial diffusion rate, the transport rates became negative after linear regression.
The impact of this became obvious when the described PIN-kinase combinations were tested (Figure 8 B). To test PIN-mediated IAA transport at concentrations higher than 10 µM, SSM-based electrophysiology would be a suitable technique (Ung *et al.*, 2022).

3.1.2 The protein levels and the phosphorylation pattern of PIN1, PIN2 and PIN3 in oocytes are comparable

The AGC kinases D6PK and PINOID phosphorylate serine or threonine residues in PINs and are necessary for activation of PIN-mediated IAA transport. In order to compare kinetics of different PIN transporters, the proteins of interest must be present in comparable levels in the oocyte plasma membrane.
Additionally, the observation that transport rates of PINs depend linearly on the substrate concentration and the fact that the activating kinase affects the transport rates of PINs, opened the question if changes in the PIN's phosphorylation status by the two kinases explain the differences in transport rates. By using a mass spectrometry approach, the membrane and cytosolic fractions of oocytes expressing PIN1, PIN2 or PIN3, and oocytes co-expressing PIN and D6PK or PINOID were analyzed.

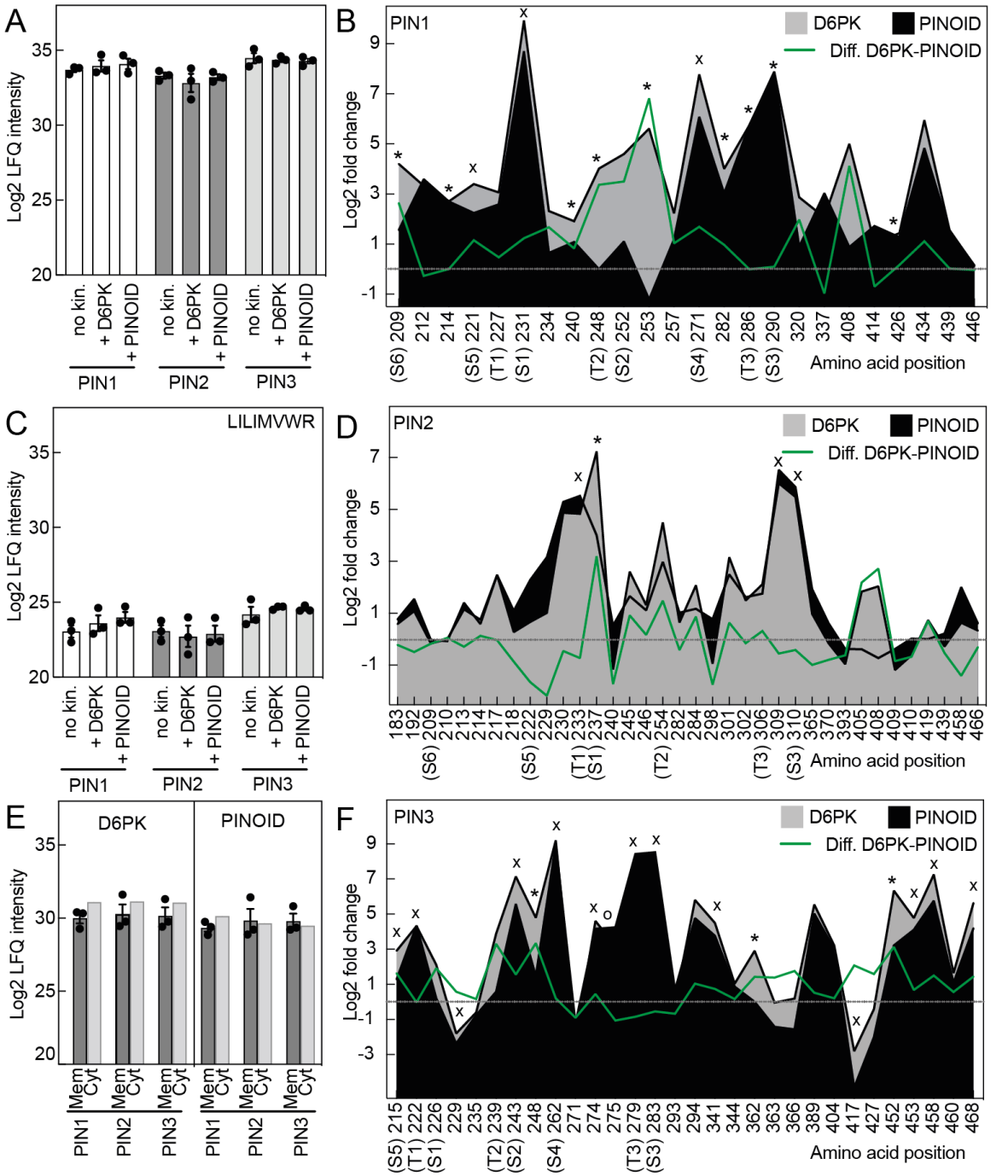
A
Log2 LFQ intensity
no kin.
+ D6PK
+ PINOID
PIN1
PIN2
PIN3
B
PIN1
D6PK
PINOID
Diff. D6PK-PINOID
Log2 fold change
Amino acid position
C
LILIMVWR
D
PIN2
E
D6PK
PINOID
Mem
Cyt
F
PIN3

Figure 9 – Proteome and phospho-proteome analyses of PINs and D6PK or PINOID in Xenopus oocytes. (A) LFQ intensity of all peptides from PIN1, PIN2 and PIN3 in the membrane fraction without kinase (n = 3) and with D6PK (n = 3) or PINOID (n = 3). Data are mean and SE. Data analyzed in their respective group (PIN vs. + D6PK vs. + PINOID) by one-way ANOVA, followed by Tukey's posthoc test showed no significant difference (PIN1 vs. PIN1 + D6PK n.s. 0.8239, PIN1 vs. PIN1 + PINOID n.s. 0.6612, PIN1 + D6PK vs. PIN1 + PINOID n.s. 0.9535. PIN2 vs. PIN2 + D6PK n.s. 0.6559, PIN2 vs. PIN2 + PINOID n.s. 0.9809, PIN2 + D6PK vs. PIN2 + PINOID n.s. 0.7614. PIN3 vs. PIN3 + D6PK n.s. 0.9442, PIN3 vs. PIN3 + PINOID n.s. 0.8343, PIN3 + D6PK vs. PIN3 + PINOID n.s. 0.9642). (B) LFQ intensity of the shared peptide LILIMVWR between the three PINs in the membrane fraction (n = 3). Mean and SE are indicated. Data analyzed by one-way ANOVA, followed by Tukey's posthoc test showed no significant difference between groups. (C) LFQ intensity of D6PK and PINOID in the membrane fraction (n = 3) and the cytosolic fraction (n = 1) of oocytes expressing PIN and the kinase indicated. Mean and SE are indicated. Data analyzed by one-way ANOVA, followed by Tukey's posthoc test showed no significant difference between groups. (D-F) Phosphorylated sites in PIN1, PIN2 and PIN3 in comparison to PIN without kinase after phospho-peptide enrichment by IMAC. The green line indicates the difference between PIN with D6PK or PINOID. (X) marks sites phosphorylation sites that are significantly (p-value < 0.05) increased in response to both kinases, (*) marks phosphorylation sites that are significantly (p-value < 0.05) increased in response to D6PK and (o) marks phosphorylation sites that are significantly (p-value < 0.05) increased in response to PINOID (Student's t-test two sided unpaired, with multiple-testing correction Permutation-based FDR 0.05).

The comparison of the full proteome's label-free quantification (LFQ) intensities revealed that the overall protein levels were comparable between the samples (Figure 9 A). The three PINs shared one unique peptide LILIMVWR that allowed it to compare the PIN protein levels within the group of one PIN, and also between the different PINs (Figure 9 B). No significant differences in the protein amounts were measured and it was concluded that the PINs were expressed to similar levels.

The PINs, both kinases D6PK and PINOID as well as 4556 proteins from *Xenopus laevis* were detected in the membrane fractions, that were enriched before analysis. Additionally, one cytosolic fraction for each PIN co-expressed with the respective kinase was analyzed and 2950 Xenopus proteins were found. D6PK and PINOID were detected in equal levels, likely due to their membrane-association. Neither the expression level of D6PK nor that of PINOID depended on the identity of the PIN co-expressed (Figure 9 C). In contrast to the PINs, the kinases do not share a common peptide. Therefore, it was not possible to directly compare the protein levels between D6PK and PINOID.

In order to identify phosphorylated residues in oocyte-expressed PINs, the membrane fraction of oocytes expressing PIN and D6PK or PINOID was split in the phosphorylated and non-phosphorylated fraction by phospho-peptide enrichment (immobilized metal affinity chromatography, IMAC). By phospho-LC-MS/MS analysis, several phosphorylated residues in PIN1, PIN2 and PIN3 were found, in comparison to the PIN samples without co-expressed kinase (Figure 9 D-F).

In PIN1 (Figure 9 D), three positions (Ser221, Ser231, Ser271) were significantly more phosphorylated by both kinases D6PK and PINOID. In the group of PIN1 + D6PK, nine out of twelve significantly differently phosphorylated positions were detected. For these nine positions, the PINOID samples were variable but showed an overall increase in intensity that did not result in a mathematical significance. Thr248 (T2) and Ser253 (S2) were the only positions with significantly

higher levels of phosphorylation by D6PK, where no increased phosphorylation in the PINOID samples was detected.

The highest number of phosphosites was detected in PIN2 (Figure 9 E). Surprisingly, only four out of 36 measured phosphosites were significantly increased in comparison to samples without kinase (Thr233, Ser237, Thr309, Ser310). Three of them showed increased levels of phosphorylation by both kinases. Ser237 was phosphorylated to significantly higher levels by D6PK.

In PIN3, 17 significantly differently phosphorylated amino acids were detected (Figure 9 F), 13 of them by both kinases. Only three sites were more phosphorylated by D6PK (Ser248, Ser362, Ser452). Ser275 was the only site with increased phosphorylation by PINOID. Thr229 and Ser417 were phosphorylated significantly less compared to samples without kinase, upon co-expression of D6PK or PINOID. That would suggest an oocyte-specific kinase could phosphorylate both positions if only PIN was expressed. If D6PK or PINOID were co-expressed, the positions might be sterically buried either by direct interaction of PIN loop and kinase or by steric effects on the PIN loop structure by phosphorylation events at other positions.

Table 9 – Phosphosite positions in oocyte-expressed D6PK or PINOID. Serine and threonine phosphorylation sites in D6PK and PINOID detected in the phospho-proteome analysis of oocytes expressing D6PK or PINOID and PIN1, PIN2 or PIN3. Intensities of sites marked with (*) were significantly increased (p-value < 0.05, Student's t-test two sided unpaired, with multiple-testing correction Permutation-based FDR 0.05).

	D6PK	**PINOID**
PIN1 +	62 *	54
	264	55
	280	178
	345 *	
PIN2 +	62	54
	264	55
	345 *	178
	408	
PIN3 +	62 *	54
	262	55 *
	264 *	178 *
	345 *	
	408 *	

Besides PIN phosphorylation, phosphorylated serine residues in D6PK and PINOID were detected (Table 9). The amino acid positions 264 and 280 of D6PK are part of the MID domain of D6PK (Barbosa *et al.*, 2016) and position 345 is in the activation loop indicating that a PDK1-like activity is present in oocytes (Xiao and Offringa, 2020). For PINOID, no phosphorylation sites of known protein domains (e.g. ATP binding site, activation loop, DFD motif, PIF domain) were found. The phosphorylated residues detected in PINOID are part of the Ser/Thr-rich N-terminus (Santner and Watson, 2006).

Table 10 – Phosphorylated sites in PIN1, PIN2 or PIN3 expressed in oocytes with D6PK or PINOID in comparison to the *Arabidopsis thaliana* phospho-proteome. PIN1, PIN2 and PIN3 were heterologously co-expressed in oocytes with D6PK or PINOID and compared to the phosphorylation sites from Arabidopsis PIN1, PIN2 or PIN3 found in Mergner et al., 2020 (PIN1 + D6PK n = 24, PIN1 + PINOID n = 22, PIN1 (Arabidopsis) n = 20, PIN2 + D6PK n = 36, PIN2 + PINOID n = 36, PIN2 (Arabidopsis) n = 21, PIN3 + D6PK n = 30, PIN3 + PINOID n = 30, PIN3 (Arabidopsis) n = 28). Sites that were not found in one group are shown as gray empty cells.

		Xenopus oocytes		Arabidopsis
PIN	**AA position**	**PIN + D6PK**	**PIN + PINOID**	**Mergner *et al*., 2020**
PIN1	209	yes	yes	
	212	yes	yes	yes
	214	yes	yes	yes
	221	yes	yes	yes
	227	yes	yes	yes
	231	yes	yes	yes
	234	yes	yes	
	240	yes	yes	yes
	248	yes		yes
	252	yes	yes	yes
	253	yes		yes
	257	yes	yes	yes
	271	yes	yes	yes
	282	yes	yes	yes
	286	yes	yes	yes
	290	yes	yes	yes
	320	yes	yes	yes
	337	yes	yes	yes
	408	yes	yes	
	414	yes	yes	yes
	426	yes	yes	yes

		Xenopus oocytes		Arabidopsis
PIN	**AA position**	**PIN + D6PK**	**PIN + PINOID**	**Mergner *et al*., 2020**
	434	yes	yes	yes
	439	yes	yes	
	446	yes	yes	yes
PIN2	183	yes	yes	yes
	192	yes	yes	
	209	yes	yes	
	210	yes	yes	yes
	213	yes	yes	
	214	yes	yes	
	217	yes	yes	yes
	218	yes	yes	yes
	222	yes	yes	
	229	yes	yes	yes
	230	yes	yes	yes
	233	yes	yes	yes
	237	yes	yes	yes
	240	yes	yes	
	245	yes	yes	yes
	246	yes	yes	
	254	yes	yes	yes
	282	yes	yes	yes
	284	yes	yes	yes
	298	yes	yes	
	301	yes	yes	
	302	yes	yes	yes
	306	yes	yes	yes
	309	yes	yes	yes
	310	yes	yes	yes
	365	yes	yes	
	370	yes	yes	yes
	393	yes	yes	yes
	405	yes	yes	
	408	yes	yes	

		Xenopus oocytes		Arabidopsis
PIN	**AA position**	**PIN + D6PK**	**PIN + PINOID**	**Mergner *et al*., 2020**
	409	yes	yes	
	410	yes	yes	
	419	yes	yes	
	439	yes	yes	yes
	458	yes	yes	yes
	466	yes	yes	yes
PIN3	215	yes	yes	yes
	222	yes	yes	yes
	226	yes	yes	yes
	229	yes	yes	
	235	yes	yes	yes
	239	yes	yes	yes
	243	yes	yes	yes
	248	yes	yes	yes
	262	yes	yes	yes
	271	yes	yes	yes
	274	yes	yes	yes
	275	yes	yes	yes
	279	yes	yes	yes
	283	yes	yes	yes
	293	yes	yes	yes
	294	yes	yes	yes
	341	yes	yes	
	344	yes	yes	yes
	362	yes	yes	yes
	363	yes	yes	yes
	366	yes	yes	yes
	389	yes	yes	yes
	404	yes	yes	yes
	417	yes	yes	yes
	427	yes	yes	yes
	452	yes	yes	yes
	453	yes	yes	yes

		Xenopus oocytes		Arabidopsis
PIN	**AA position**	**PIN + D6PK**	**PIN + PINOID**	**Mergner *et al*., 2020**
	458	yes	yes	yes
	460	yes	yes	yes
	468	yes	yes	yes

In light of the phospho-proteome analysis by Mergner *et al.*, 2020, the detected phosphorylated residues in Xenopus oocytes and in *Arabidopsis thaliana* were to high levels congruent (Table 10). Four phosphorylation sites of oocyte-expressed PIN1 and two sites of oocyte-expressed PIN3 were not detected in *Arabidopsis thaliana*. In PIN2, 15 out of 36 phosphorylated residues were only detected in oocyte-expressed protein, either because the peptides were not detected in the Arabidopsis screen due to technical differences or they were not phosphorylated.

The detailed analysis of PINs in oocytes showed that the differences detected in the transport rates were neither due to variations in the protein levels of the three PINs nor the kinases, nor could the stronger transport activation by PINOID be explained by distinct differences in the phosphorylation status of the PIN loop domain.

3.1.3 PIN1 and PIN3 partially rescue the agravitropic root phenotype of the *pin2* mutant

The transport studies in Xenopus oocytes revealed that the transport properties of PIN1 and PIN2 are more similar to each other than either one of them compared to PIN3. In order to investigate if physiological consequences result from the different transport rates, the coding sequences of *PIN1* and *PIN3* were expressed from a *PIN2* promoter fragment in the *pin2* mutant background and their potential to complement the agravitropic root growth and the lack of response to gravistimulation was investigated (Luschnig *et al.*, 1998; Abas *et al.*, 2006). It is noteworthy that the *pin2* mutant is not fully agravitropic. No root that grew against the gravity vector was detected. The *pin2* mutant was mainly characterized by the wide distribution of root angles between -90 ° and +90 ° around the gravity vector, i.e. 0 °. The angle between the root tip and the gravity vector was used as phenotypic read out in independent segregating T2 lines (Figure 10 A, D, G). One representative T2 line of each genotype was propagated to homozygous T3. The vertical growth index (VGI) and the root angle between the root tip and the gravity vector were measured. The VGI correlates the root length to the distance between the root origin and the root tip (Grabov *et al.*, 2005).

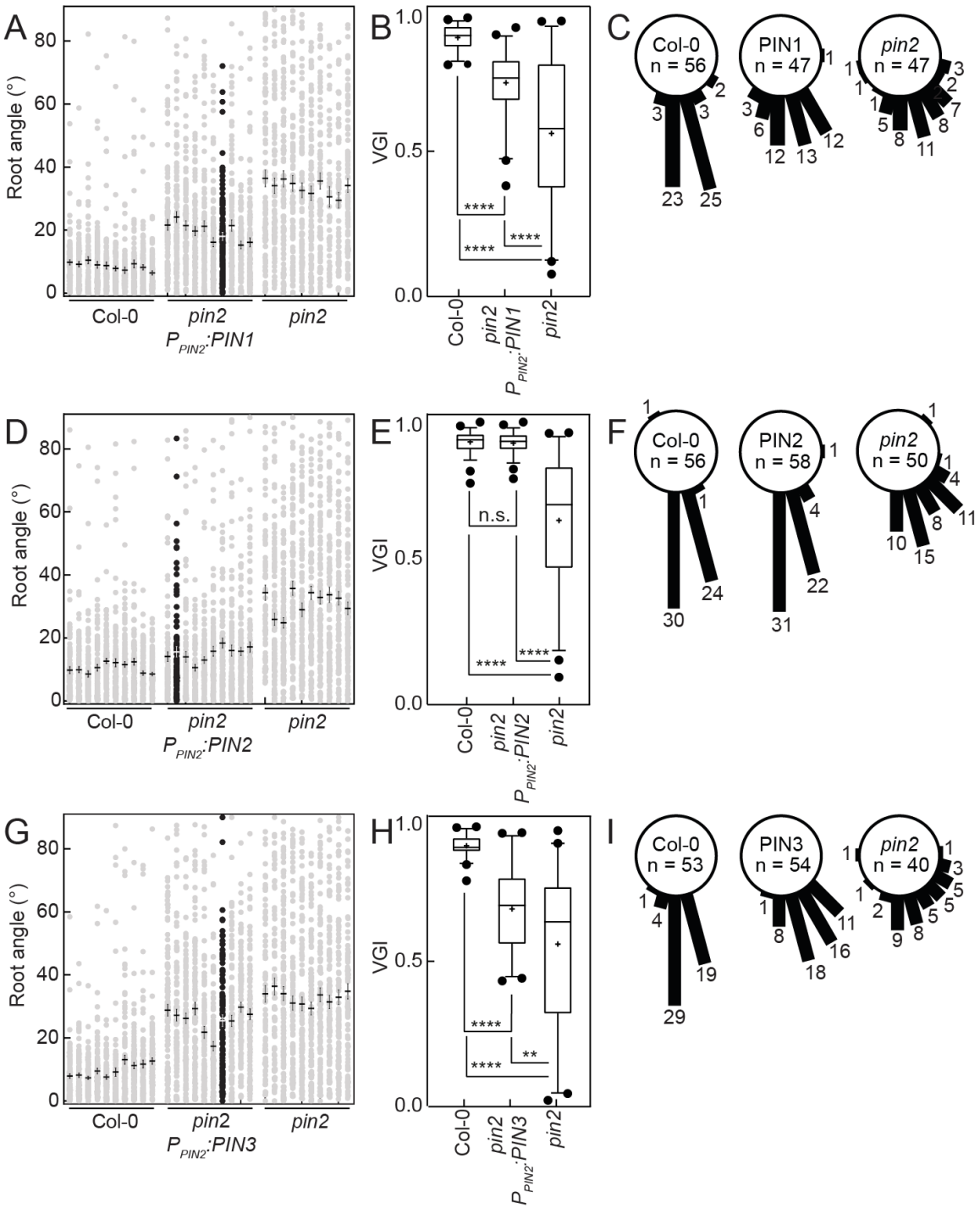
A
Root angle (°)
Col-0
pin2
pin2
P PIN2 :PIN1
B
VGI
****
****
****
Col-0
pin2
P PIN2 :PIN1
pin2
C
Col-0
n = 56
PIN1
n = 47
pin2
n = 47
D
Root angle (°)
Col-0
pin2
pin2
P PIN2 :PIN2
E
VGI
n.s.
****
****
Col-0
pin2
P PIN2 :PIN2
pin2
F
Col-0
n = 56
PIN2
n = 58
pin2
n = 50
G
Root angle (°)
Col-0
pin2
pin2
P PIN2 :PIN3
H
VGI
****
****
**
Col-0
pin2
P PIN2 :PIN3
pin2
I
Col-0
n = 53
PIN3
n = 54
pin2
n = 40

Figure 10 – Potential of PIN1, PIN2 and PIN3 to rescue the *pin2* mutant phenotype. PIN1 (A-C), PIN2 (D-F) or PIN3 (G-I) were expressed from a PIN2 promoter fragment in the *pin2* mutant background. (A, D, G) Root angle of ten independent segregating T2 lines between root tip and gravity vector of *pin2;*P_{PIN2}*:PIN1*, *pin2;*P_{PIN2}*:PIN2* and *pin2;*P_{PIN2}*:PIN3* (n = 103-119, 89-118, 99-116 for PIN1, PIN2 or PIN3, respectively) in comparison to wildtype (n = 98-112 in A, n = 111-117 in D, n = 110-119 in G) and mutant (n = 47-98 in A, n = 83-117 in D, n = 79-119 in G). Data points are individual seedlings. The mean and SE are indicated. The representative line is represented by black dots. (B, E, H) VGI of the representative T3 line of *pin2;*P_{PIN2}*:PIN1*, *pin2;*P_{PIN2}*:PIN2* and *pin2;*P_{PIN2}*:PIN3* (n = 46, n = 56, n = 54 for PIN1, PIN2 or PIN3, respectively) in comparison to wildtype (n = 55 in B, n = 55 in E, n = 53 in H) and mutant (n = 48 in B, n = 50 in E, n = 40 in H). Box plots range from the 25th to 75th percentiles, whiskers mark the 5th and 95th percentiles and the median is shown, the mean is represented by (+), points below and above the whiskers are drawn as individual points. Groups were compared by one-way ANOVA followed by Tukey's posthoc test. n.s. not significant p-value 0.9861, ** p-value 0.0012, **** p-value <0.0001 (C, F, I) Root angles between root tip and gravity vector of the representative homozygous T3 line of *pin2;*P_{PIN2}*:PIN1*, *pin2;*P_{PIN2}*:PIN2* and *pin2;*P_{PIN2}*:PIN3* in comparison to wildtype and mutant. Numbers are individual seedlings.

As expected, PIN2 fully rescued the mutant phenotype (Figure 10 D–F). Due to the proportion of 25 % of *pin2* mutant seedlings that originated from the segregating T2 population, the root angles in all lines were slightly increased (Figure 10 D). In homozygous T3 seedlings, the VGI was not statistically different from the wildtype Col-0 control (Figure 10 E). The root angles were indistinguishable from wildtype (Figure 10 F).

The expression of *PIN1* in the *pin2* mutant resulted in a partial rescue of the agravitropic root growth phenotype (Figure 10 A-C). The VGI of the homozygous *pin2;*P_{PIN2}*:PIN1* line differed significantly from wildtype as well as from the mutant. Additionally, the root angles of the T3 line varied less (SD = 0.11) than the *pin2* mutant (SD = 0.56), but more than wildtype (SD = 0.04).

The expression of *PIN3* in the *pin2* mutant resulted in reduced agravitropic root growth (Figure 10 G–I). The rescue was visible in the reduced variation of the root angle for heterozygous T2 and homozygous T3 seedlings. The VGI of homozygous seedlings was higher as the mutant seedlings, but *pin2;*P_{PIN2}*:PIN3* seedlings still differed significantly from wildtype and mutant. Statistical comparison of the VGIs of *pin2;*P_{PIN2}*:PIN1* and *pin2;*P_{PIN2}*:PIN3* seedlings revealed significant differences between both genotypes (unpaired t-test, p-value 0.0375), suggesting that the ability of PIN1 to rescue the *pin2* phenotype is higher than of PIN3.

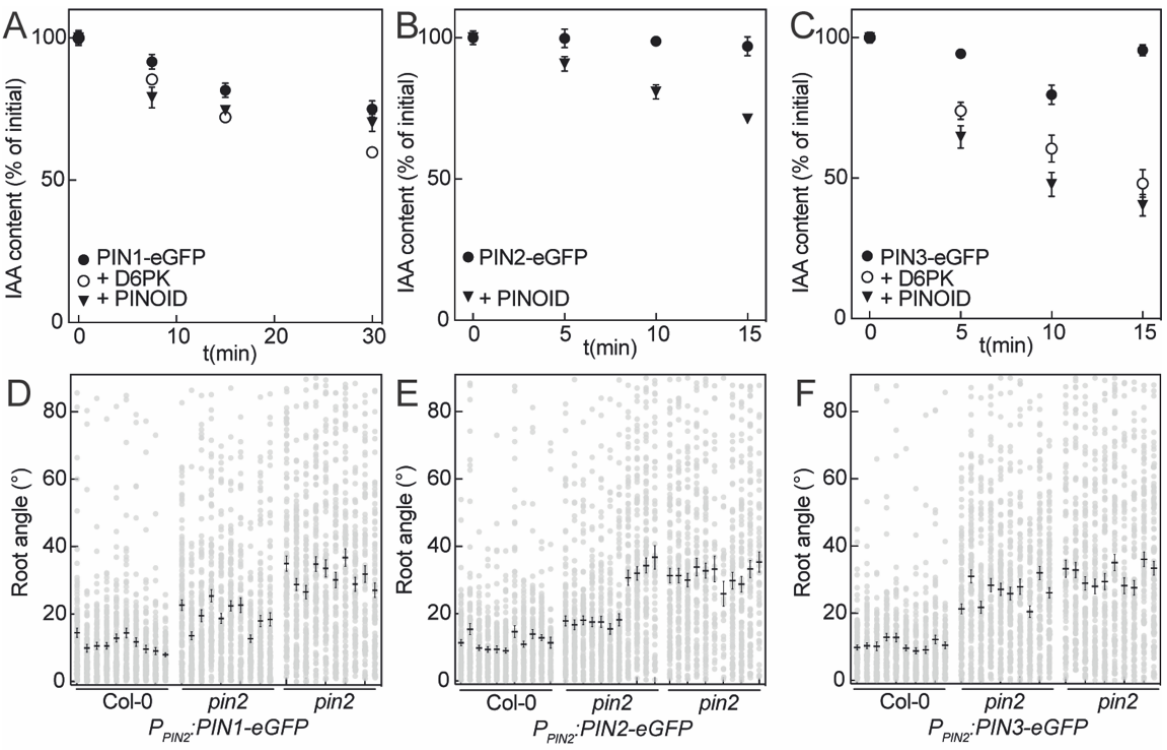

Figure 11 – IAA transport properties and potential to rescue the *pin2* mutant phenotype of GFP-tagged PIN1, PIN2 and PIN3. (A-C) Representative time-course experiments for PIN1-eGFP (A), PIN2-eGFP (B) and PIN3-eGFP (C). PIN1-eGFP, PIN2-eGFP and PIN3-eGFP were expressed in oocytes without (●) as well as with D6PK (○) or PINOID (▼). Time points are mean and SE of n = 8-10 oocytes. (D-F) PIN1-eGFP (D), PIN2-eGFP (E) or PIN3-eGFP (F) were expressed from a *PIN2* promoter fragment in the *pin2* mutant background. Root angle of independent segregating T2 lines (n = 10 lines for PIN1-eGFP, n = 11 lines for PIN2-eGFP and n = 10 lines for PIN3-eGFP) between root tip and gravity vector of *pin2;*P_{PIN2}*:PIN1-eGFP*, *pin2;*P_{PIN2}*:PIN2-eGFP* and *pin2;*P_{PIN2}*:PIN3-eGFP* (n = 77-120, 57-120, 92-117 seedlings for PIN1-eGFP, PIN2-eGFP or PIN3-eGFP, respectively) in comparison to wildtype (n = 95-116 in D, n = 72-117 in E, n = 103-120 in F) and mutant (n = 90-118 in D, n = 40-111 in E, n = 86-115 in F). Data points are individual seedlings. The mean and SE are indicated.

PIN2 is localized polarly to the apical side of the cell in the epidermis and to the basal side in the cortex of the root. In order to investigate if PIN1 and PIN3 localize similarly to PIN2, the fluorophore eGFP was inserted into the loop domain. The eGFP-tagged PINs were tested for their functionality in the oocyte transport assay (Figure 11 A-C). All three PINs behave like untagged PINs and did only transport IAA with a co-expressed kinase. This suggests that inserting eGFP into the loop did not change the biochemical properties of the PINs.

The tagged PINs were expressed from a *PIN2* promoter fragment in the *pin2* mutant and were able to rescue the *pin2* root phenotype like the untagged PINs (Figure 11 D–F), but the root angle of different transformant lines exhibited more variation than their untagged relatives (for PIN1 and PIN1-eGFP SD = 3.0 compared to SD = 4.1; for PIN2 and PIN2-eGFP SD = 2.2 compared to SD = 7.3; for PIN3 and PIN3-eGFP SD = 3.8 compared to SD = 4.0). The population of lines with non-expressing T-DNA was higher in comparison to the untagged PINs (e.g. 4/11 for PIN2-eGFP in contrast to 0/10 for PIN2).

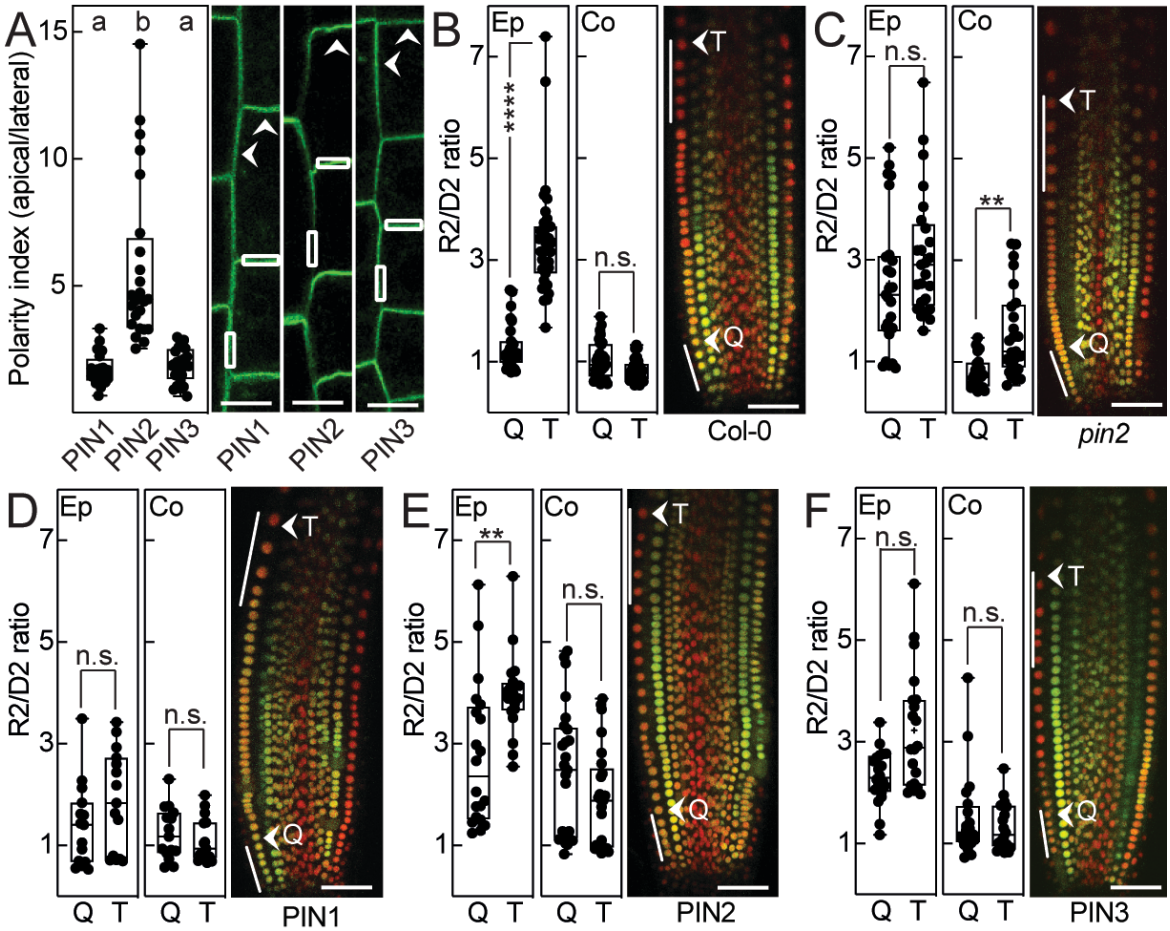

Figure 12 – Localization of PINs and IAA levels in root tips. (A) Polarity index of eGFP-tagged *PIN1*, *PIN2* and *PIN3* expressed from a *PIN2* promoter fragment in epidermal cells in the *pin2* mutant. Representative ROIs are indicated by white boxes. Mean intensities of ROIs at the apical and the lateral side of the cells were used to calculate the ratios. The arrows mark GFP signal. Scale bar represents 10 µm. Box plots range from the 25th to 75th percentiles, whiskers mark the minimum and maximum values and the median is shown. Groups were compared by a one-way ANOVA, followed by Tukey's posthoc test (PIN1 vs. PIN2 <0.0001, PIN1 vs. PIN3 0.9592, PIN2 vs. PIN3 <0.0001), n = 24 per genotype. (B-F) Ratio of mDII to DII signal in epidermis (Ep) and cortex (Co). First five epidermal cells after anticlinal division of the epidermal/LRC initial cell (Q) and five cells at the transition zone as specified by cell elongation (T) were measured for individual roots (n = 15-35 for epidermis and n = 15-30 for cortex). Cells analyzed are indicated by white lines. Picture shows overlay of DII (green) and mDII (red) signal. Scale bar represents 40 µm. Box plots range from the 25th to 75th percentiles, whiskers mark the minimum and maximum values and the median is shown. Whole data set analyzed by one-way ANOVA, followed by Tukey posthoc test (Col-0: **** p-value <0.0001, n.s. not significant p-value 0.9914. *pin2*: n.s. p-value 0.6432, ** p-value 0.0053. PIN1: n.s. (Ep) p-value 0.9513, n.s. (Co) p-value >0.999. PIN2: ** p-value 0.0075, n.s. p-value 0.0.1938. PIN3: n.s. (EP) p-value 0.1419, n.s. (Co) p-value 0.9986).

In order to analyze whether the differences in gravitropism were the result of mislocalized PIN1 or PIN3 transporters, the apical localization and the polarity were checked (Figure 12 A). PIN2-eGFP localized to the apical side of epidermal cells and was almost completely restricted to this side. PIN1-eGFP and PIN3-eGFP showed reduced polarity. The GFP signal of both transporters was detected at the apical side, but also to pronounced levels at the lateral side of the cell. The polarity index was determined by dividing the mean intensities of ROIs from the apical and the lateral sides of the cell.

For PIN1-eGFP and PIN3-eGFP, it was significantly reduced compared to PIN2-eGFP, but PIN1-eGFP and PIN3-eGFP both localized apolarly to a similar degree.

Because the localization of PIN1-eGFP and PIN3-eGFP in the *pin2* background was different compared to the wildtype but in itself coherent, the auxin sensor R2D2 was used to check whether altered auxin levels in the epidermis could explain the different abilities to rescue the gravitropic *pin2* root defect (Figure 12 B–F). R2D2 is a ratiometric reporter that monitors the auxin-sensitive degradation of the yellow DII signal in relation to the red mDII signal in dividing cells (Liao *et al.*, 2015). In Col-0 (Figure 12 B), the auxin level was significantly higher in cells at the transition zone (T) compared to the first epidermal cells (Q) after the anticlinal division of the epidermis/LRC initial cell (Petricka *et al.*, 2012). In the cortex, the auxin level was relatively low and no difference between the developmental zones was detected. In the *pin2* mutant (Figure 12 C), the auxin levels were slightly increased in the transition zone of epidermis and cortex. *pin2;PIN2* seedlings (Figure 12 E) showed the same trend as Col-0, but had increased overall auxin levels. The auxin amount increased between Q and T in epidermal cells, but stayed constant in the cortical cell file. Although a small increase in epidermal auxin levels was detected for *pin2;*P_{PIN2}*:PIN1* and *pin2;*P_{PIN2}*:PIN3* roots, it was not significantly different between younger and older cells. In the cortex, the auxin levels stayed constantly low in both genotypes. Notably, the epidermal R2/D2 ratio of *pin2;*P_{PIN2}*:PIN1* roots was in the same range as Col-0 and the ratio of *pin2;*P_{PIN2}*:PIN3* roots was more comparable to the *pin2* mutant levels. The cortical auxin levels of Col-0, *pin2;*P_{PIN2}*:PIN1* and *pin2;*P_{PIN2}*:PIN3* roots were identical.

Overall, the R2D2 sensor revealed that in wildtype roots the epidermal auxin levels increase from younger to older cells and stay at a constant level in the cortex. By removing PIN2 as the main auxin transporter in epidermis and cortex, the situation was reversed. In the *pin2* mutant, the auxin levels in the epidermis stayed at a constant level between Q and T and showed increased differences in the cortex. By expressing *PIN1* or *PIN3*, the auxin levels in the cortex were balanced between younger and older cells and resembled the wildtype situation. However, the increase of auxin levels in the epidermis could not be restored. This suggests that the modified auxin levels in epidermal cells might lead to the partial rescue of the gravitropism defect in *pin2;*P_{PIN2}*:PIN1* and *pin2;*P_{PIN2}*:PIN3* expressing roots.

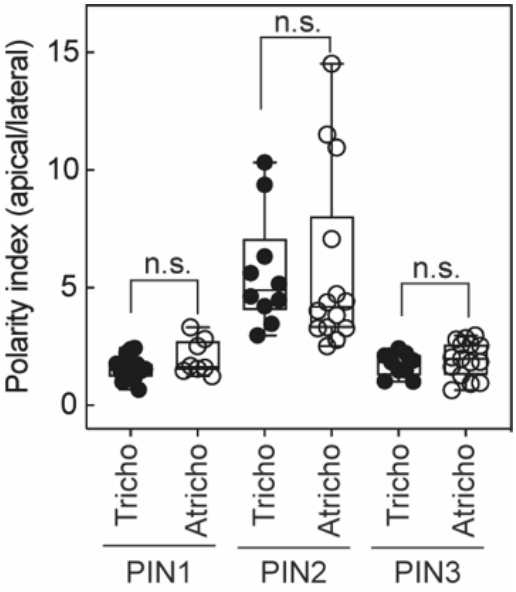

Figure 13 – Polarity index of *PIN1*, *PIN2* and *PIN3* in trichoblasts and atrichoblasts in the root tip of the *pin2* mutant. Polarity index of *pin2;PIN1-eGFP*, *pin2;PIN2-eGFP* and *pin2;PIN3-eGFP*. Comparison between the polarity index of respective *PIN* in trichoblasts (●) and atrichoblasts (○). Box plots range from the 25th and 75th percentiles, whiskers mark the minimum and maximum values and the median is shown. PIN1: n = 16 and n = 8, PIN2: n = 10 and n = 14, PIN3: n = 9 and n = 15. Data sets were compared by unpaired two-tailed t-test (n.s. not significant, PIN1-eGFP 0.0876, PIN2-eGFP 0.9457, PIN3-eGFP 0.3984).

PIN2 is known to cycle differently in trichoblast and atrichoblast cells with a higher PM abundance in atrichoblasts (Lofke *et al.*, 2015). In order to check whether the identity of the epidermal cells impacts the polarity of the transporter, the analyzed cells (Figure 12 A) were reevaluated on their identity as trichoblast or atrichoblast cell. No difference in the polarity of PIN1-eGFP, PIN2-eGFP or PIN3-eGFP was detected between the two cell types (Figure 13).

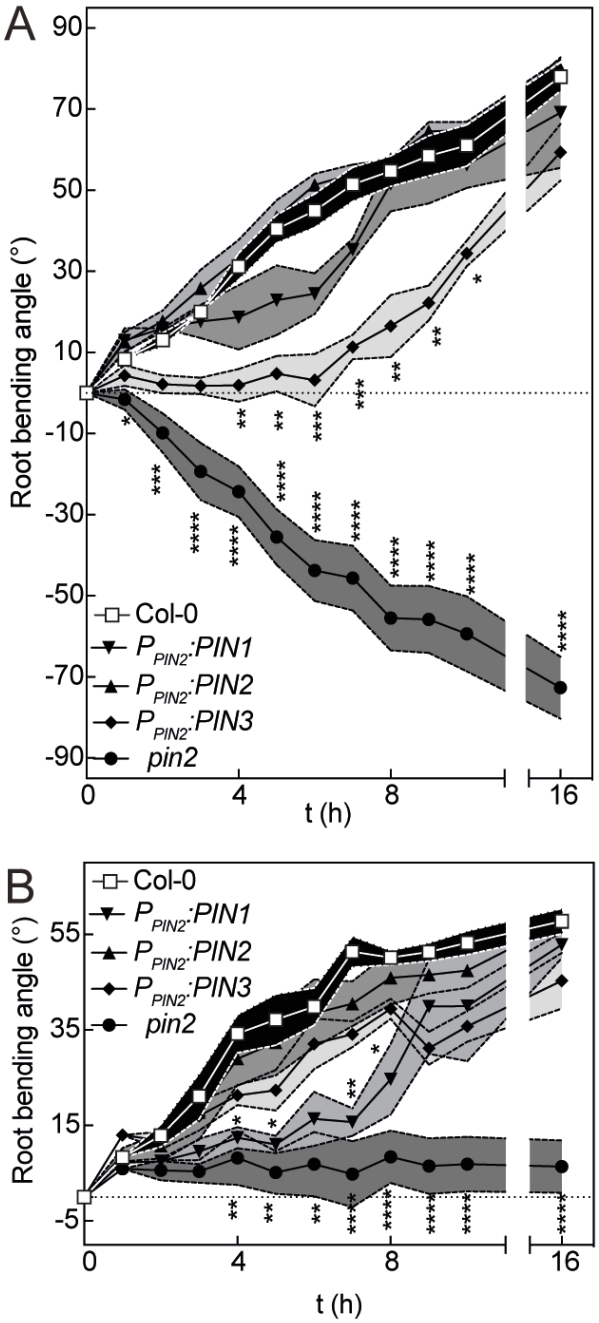

Figure 14 – Response of PIN1, PIN2 or PIN3 to a gravitropic stimulus. Root bending kinetics of *pin2;P$_{PIN2}$:PIN1*, *pin2;P$_{PIN2}$:PIN2* and *pin2;P$_{PIN2}$:PIN3* roots in comparison to wildtype and mutant. (n = 6 for wildtype, mutant and PIN2, n = 3 for PIN1 and PIN3) on plant medium containing 1 % sucrose (A) or neither vitamins nor sucrose (B). PIN1 and PIN3 showed a delayed response to the gravitropic stimulus, but reached wildtype-levels after 16 h. The *pin2* mutant bent against the gravity vector on medium containing sugar (A) and did not react to the stimulus on medium without sugar (B). Data points are mean and SE of 3-6 replicates with 18-20 roots per genotype. Groups were compared by one-way ANOVA, followed by Dunnett posthoc test with Col-0 as control group. Significant differences are indicated by "*". n.s. not significant p-value ≥ 0.05, * p-value 0.01 to 0.05, ** p-value 0.001 to 0.01, *** p-value 0.0001 to 0.001, **** p-value < 0.0001

In order to add a spatiotemporal component, the genotypes of interest were tested on their response to a gravitropic stimulus (Figure 14). After five days, the seedlings were transferred to a new plate and the root was straightened. The plate contained either 1 % sucrose (Figure 14 A) or neither sucrose nor vitamins (Figure 14 B). Afterwards the plate was turned 90 ° and the bending of the root tip was monitored over time in infrared light. On plates containing sugar, the wildtype Col-0 and *pin2;PIN2* plants reacted immediately on the stimulus and bent along the new gravity vector (6-8 ± 0.5-1 ° x h^{-1}). In the beginning, the bending speed of *pin2;P$_{PIN2}$:PIN1* seedlings was comparable to wildtype seedlings (6 ± 1 ° x h^{-1}). The bending velocity decreased after 3 h to 4 ± 2 ° x h^{-1}, but increased again after 7 h. The *pin2;P$_{PIN2}$:PIN3* seedlings did not react to the gravistimulus for the first 6 h (0.4 ± 0.6 ° x h^{-1}) and were significantly different to wildtype from 4-10 h, but from 7-16 h showed

the highest bending velocity (5 ± 0.7 ° x h^{-1}) compared to wildtype, *pin2;*P_{PIN2}*:PIN1* and *pin2;*P_{PIN2}*:PIN2* seedlings (3 ± 0.3-1 ° x h^{-1}). After 16 h, all three genotypes reached wildtype levels. The *pin2* mutant showed root bending against the gravity vector in all replicates and was significantly different to Col-0 from the beginning.

However, on plates without sucrose, the mutant bent in the beginning but stopped at 5-8.5 ° root bending. The differences between the genotypes were smaller under conditions without sucrose. Col-0, *pin2;*P_{PIN2}*:PIN2* and *pin2;*P_{PIN2}*:PIN3* seedlings bent with the same rate for 8 h (4-7 ± 0.4-0.6 ° x h^{-1}). Between 8 and 9 h after stimulus, the *pin2;*P_{PIN2}*:PIN3* seedlings grew against the gravity vector but started bending again after 9 h. After 16 h, they reached ~70 % of the wildtype level. *pin2;*P_{PIN2}*:PIN1* seedlings showed a delayed root bending until 7 h after stimulus with a bending rate of 2 ± 0.4 ° x h^{-1}, but then enhanced the bending rate and overtook the PIN3 group after 9 h. After 16 h, the *pin2;*P_{PIN2}*:PIN1* seedlings reached wildtype levels. This suggests that the PIN's transport properties in the *PIN2* domain have an impact on the early reaction to a gravitropic stimulus, although all genotypes reacted to the stimulus sooner or later. The gravitropic response was influenced by the presence of sucrose in the medium. This showed that besides sugar as an energy source, it can also act as signaling molecule impacting the plants' reaction to environmental stimuli.

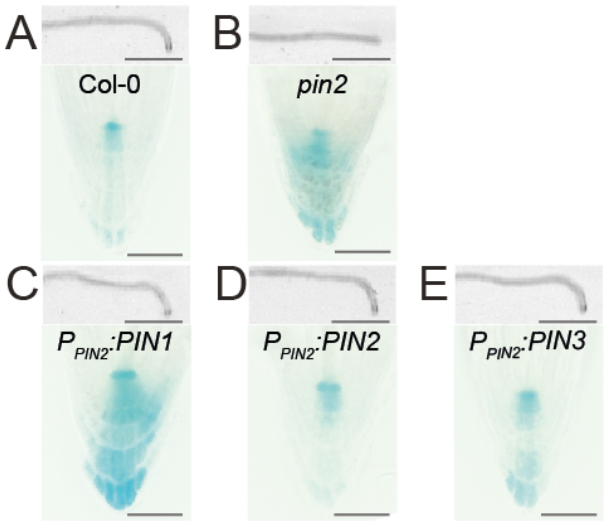

Figure 15 – Root tip growth and DR5 auxin response reporter after gravitropic stimulus. Upper panel: representative root tips of Col-0 (A), the *pin2* mutant (B), P_{PIN2}*:PIN1* (C), P_{PIN2}*:PIN2* (D) and P_{PIN2}*:PIN3* (E) in the *pin2* mutant background after 7 h post gravitropic stimulus. Scale bar represents 1 mm. Lower panel: Roots of respective genotypes crossed with auxin response reporter *DR5rev:GUS*, stained after 7 h post gravitropic stimulus. Scale bar represents 50 µm.

The gravitropism assay on medium containing sucrose revealed a strong influence of sucrose as energy source and signaling molecule. In order to limit the stimulus solely to the gravitropism, assay conditions without sucrose were used in the following. In conditions without sucrose, *pin2;*P_{PIN2}*:PIN1* seedlings showed a delayed response to the gravitropic stimulus in the first 7 h. In order to understand if different auxin levels in the root tip caused the delayed response, the analyzed genotypes were crossed with the auxin response reporter *DR5rev:GUS*. Seedlings expressing the respective *PIN* T-DNA and the *DR5rev:GUS* T-DNA were plated on medium without sucrose, turned

90 ° and allowed to grow along the new gravity vector for 7 h, before performing the staining protocol (Figure 15).

The maximum signal of Col-0 and *pin2;*P_{PIN2}*:PIN2* roots was at the QC and a very faint coloring was detected in the columella (Figure 15 A, D). In the *pin2* mutant, the signal was strongest at the QC, but was also detected in the columella and the LRC in reasonable intensity. The color was asymmetrically distributed in the root tip (Figure 15 B). The *pin2;*P_{PIN2}*:PIN1* seedlings resembled the *pin2* mutant. Compared to the wildtype control, *pin2;*P_{PIN2}*:PIN1* seedlings had very high auxin levels in the QC and in the columella. The signal was limited to those regions and only very faint staining was detected in the LRC (Figure 15 C). In roots of *pin2;*P_{PIN2}*:PIN3*, the signal was strongest at the QC and also detectable in the columella. The signal in the columella was stronger than in Col-0 or *pin2;*P_{PIN2}*:PIN2* seedlings, but the overall intensity was comparable to the wildtype (Figure 15 E). This suggests that differences in the auxin response could be one reason why *pin2;*P_{PIN2}*:PIN1* seedlings were delayed, but still able to bend along the new gravity vector.

In summary, the biochemical and physiological properties showed that PIN1 was more similar to PIN2. At equal protein levels, PIN3 transported more IAA compared to the other PINs, but its potential to rescue the phenotype was lower than that of PIN2 as well as PIN1. It is not sufficient to solely transport IAA, but the auxin flux must be tightly controlled. This can either happen by controlling the amount of transporter in the PM or by regulating the PIN activity. This is possible by regulation of interactions between PIN loop and TM domains or, alternatively by regulation of the PIN transport activity by kinases or a combination of both scenarios.

3.2 Interplay of PIN protein domains

The kinetic and the *in planta* analyses showed that PIN1 and PIN2 display more similar properties to each other than either one of them to PIN3. In order to understand to what extend which protein domain influences the biochemical and physiological functions, a domain swapping approach was used.

The structure of PIN8 revealed that the TM domains use an elevator-type mechanism to transport IAA across the membrane (Ung *et al.*, 2022). As shown by the kinetic studies, the loop domain of canonical PINs is by default inhibitory at physiological IAA concentrations and must be phosphorylated by kinases to overcome this inhibition (Figure 7). Additionally, the loop domain is important for the localization of the transporter (Ganguly *et al.*, 2012; Ganguly *et al.*, 2014) and was thought of as the regulatory part of the PIN transporter (Zourelidou *et al.*, 2014).

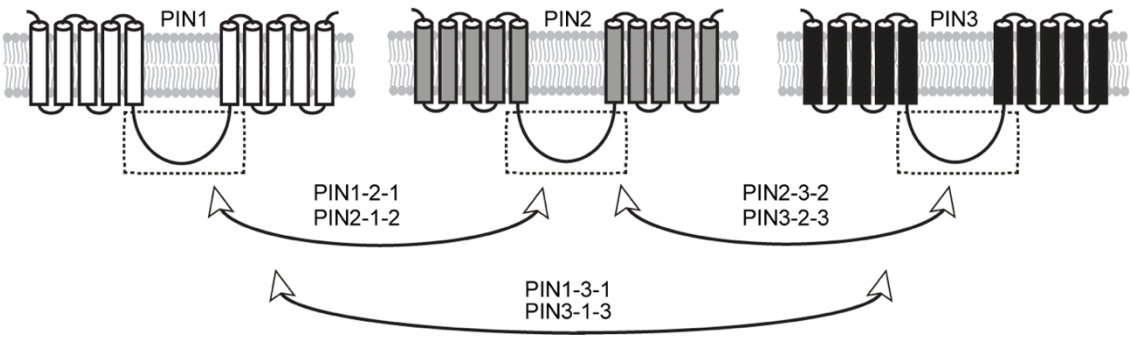

Figure 16 – Canonical PIN chimeras. The loop domain of PIN1, PIN2 or PIN3 was replaced by the loop domain of respective PIN, creating the indicated PIN chimeras.

In order to investigate the interplay of the TM domains and the loop domain, PIN1, PIN2 and PIN3 loop and TM domains were permutated as shown in (Figure 16). The transport properties of the resulting chimeras were subsequently tested in the efflux assay and for their potential to rescue the *pin2* mutant phenotype as explained above.

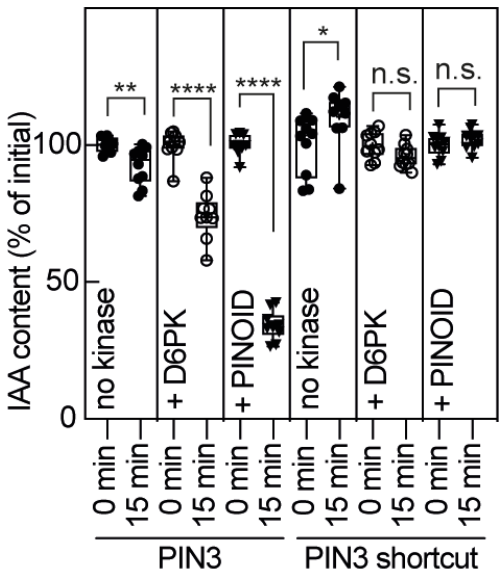

Figure 17 – IAA transport properties of PIN3 without loop domain. PIN3 and PIN3 without loop domain (PIN3 short cut) were expressed in oocytes alone (●) or co-expressed with D6PK (○) or PINOID (▼). The IAA content after 15 min was compared to the initial IAA content by unpaired two-tailed t-test (PIN3: ** p-value 0.0096, **** p-value <0.0001. PIN3 short cut: * p-value 0.0395, n.s. not significant 0.0574 for D6PK and 0.2372 for PINOID). Each data point is one oocyte (n = 8-10). Box plots range from 25th to 75th percentiles, whiskers mark the minimum and maximum values and the mean is indicated.

First, the oocyte transport assay was used to understand if the loop domain is of regulatory nature, or if it is needed for the protein to fulfill a transport cycle. Removing the whole loop domain and putting helix M4b and M5 directly together, rendered the protein non-functional/resulted in the loss of transport under all conditions tested (Figure 17).

3.2.1 PIN1 as TM domain donor

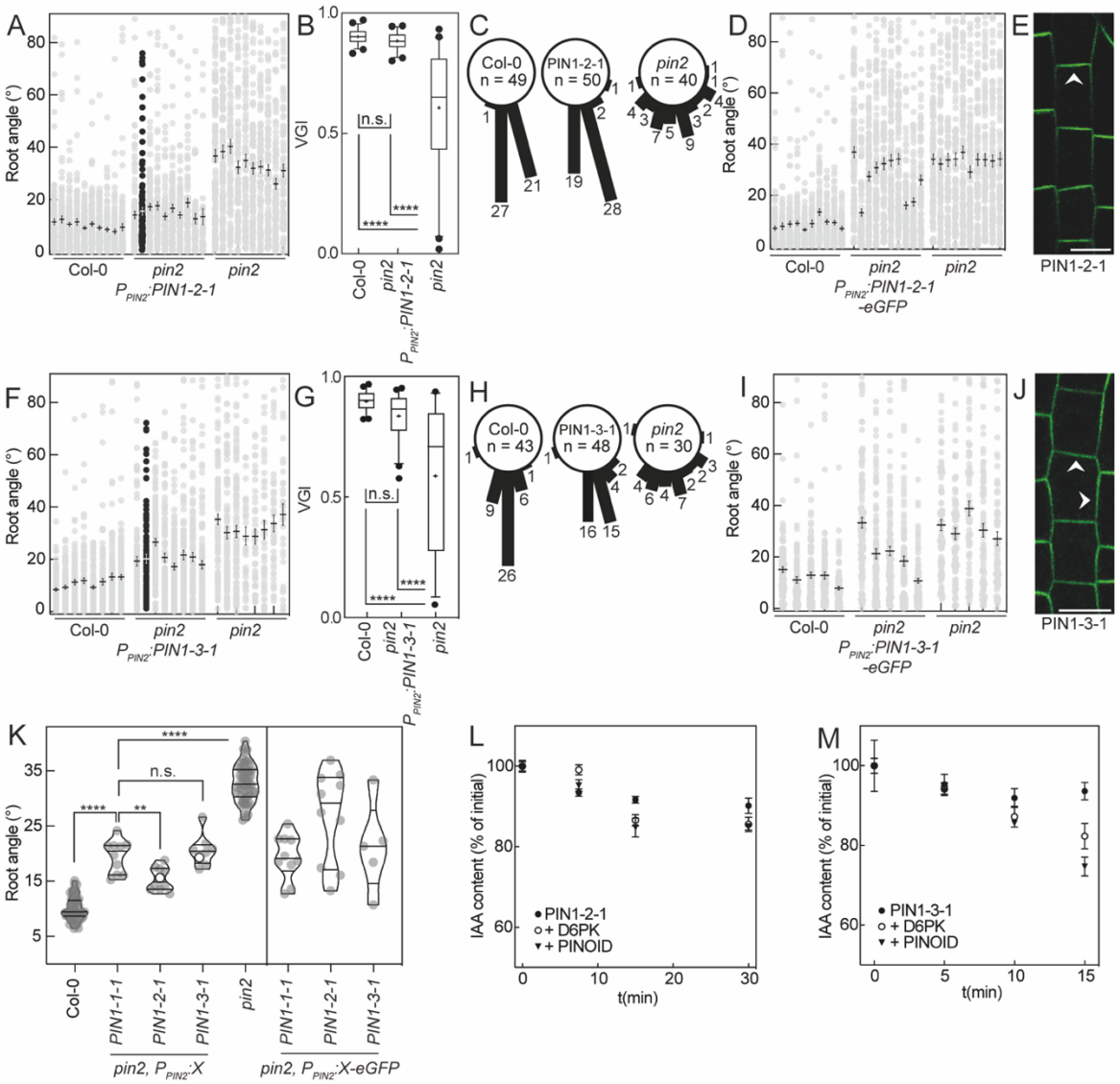

Figure 18 – Potential of *PIN1-2-1* and *PIN1-3-1* chimeras to rescue the *pin2* phenotype, their localization in the root tip and their IAA transport properties. *PIN1-2-1* (A-C), *PIN1-2-1-eGFP* (D-E), *PIN1-3-1* (F-H) or *PIN1-3-1-eGFP* (I-J) were expressed from a *PIN2* promoter fragment in the *pin2* mutant background. (A, D, F, I) Root angle of independent segregating T2 lines (n = 10 in A and D, n = 8 in F, n = 5 in I) between root tip and gravity vector of *pin2;*P_{PIN2}*:PIN1-2-1*, *pin2;*P_{PIN2}*:PIN1-2-1-eGFP*, *pin2;*P_{PIN2}*:PIN1-3-1* and *pin2;*P_{PIN2}*:PIN1-3-1-eGFP* (n = 37-120 for PIN1-2-1, n = 95-118 for PIN1-2-1-eGFP, n = 94-119 for PIN1-3-1, n = 109-115 for PIN1-3-1-eGFP) in comparison to wildtype (n = 103-114 in A, n = 97-107 in D, n = 100-118 in F, n = 109-119 in I) and mutant (n = 91-106 in A, n = 91-106 in D, n = 41-109 in F, n = 71-89 in I). Data points are individual seedlings. The mean and SE are indicated. The representative line is represented by black dots. (B, G) VGI of the one homozygous T3 line of *pin2;*P_{PIN2}*:PIN1-2-1* and *pin2;*P_{PIN2}*:PIN1-3-1* (n = 49 for PIN1-2-1 or n = 45 for PIN1-3-1) in comparison to wildtype (n = 49 in B, n = 42 in G) and mutant (n = 40 in B, n = 30 in G). Box plots range from 25th to 75th percentiles, whiskers mark the 5th and 95th percentiles and the median is indicated. The mean is represented by (+). Points below and above the whiskers are drawn as individual points. Groups were compared by one-way ANOVA followed by Tukey's posthoc test. n.s. not significant p-value 0.7753, **** p-value <0.0001 in B. n.s. p-value 0.1919, **** p-value <0.0001 in G. (C, H) Root angles between root tip and gravity vector of the representative homozygous T3 line of *pin2;*P_{PIN2}*:PIN1-2-1* and *pin2;*P_{PIN2}*:PIN1-3-1* in comparison to wildtype and mutant. Numbers are individual seedlings. (E, J) GFP signal of *pin2;PIN1-2-1-eGFP* and *pin2;PIN1-3-1-eGFP* in epidermal cells. The arrows mark the GFP signal. Scale bar represents 20 µm. (K) Root angle of the indicated *PIN* or *PIN* chimeras expressed from a *PIN2* promoter fragment in the *pin2* mutant background. Frequency distribution of the mean of individual segregating T2 lines shown in (A, D, F, I) in comparison to wildtype (n = 53 in total) and mutant (n = 53 in total). Each data point shows the mean of one independent line. The white dot represents the mean of the representative line of each genotype. Data for *PIN1* and *PIN1-eGFP* are shown in Figure 10 and Figure 11. The line in the plot marks the median. The lower and upper line mark the 25th and 75th percentiles. Groups of untagged PINs were analyzed by one-way ANOVA, followed by Dunnett's test with P_{PIN2}*:PIN1* as control group. n.s. not significant p-value 0.7886 (vs. PIN1-3-1). ** p-value (vs. PIN1-2-1) 0.0045. **** p-value <0.0001. (L, M) Representative time-course experiments for PIN1-2-1 and PIN1-3-1. PIN1-2-1 and PIN1-3-1 were expressed alone (●) or co-expressed with D6PK (○) or PINOID (▼) in oocytes. Time points are mean and SE of (n = 8-10 oocytes). Data for (M) collected during Master thesis (Janacek, 2017).

The exchange of the PIN1 loop domain for the loop domain of PIN2 or PIN3, i.e. PIN1-2-1 or PIN1-3-1, resulted in apparently functional auxin transporters which exhibited characteristics different from the TM domain donor PIN1 (Figure 18). In the gravitropism assay, the PIN1-2-1 chimera rescued the *pin2* root phenotype to wildtype levels. Compared to PIN1, the group of independent T2 lines of PIN1-2-1 were significantly different (Figure 18K). The VGI of a homozygous T3 line did not differ significantly from Col-0 (Figure 18 B). This was also represented by the root angle between root tip and gravity vector (Figure 18 C). Although 7 of 10 lines did not express the transgene for the GFP-tagged PIN1-2-1, the three lines that showed GFP signal rescued the phenotype to the same level as the untagged PIN1-2-1 (Figure 18 K). Comparable to PIN2-eGFP (Figure 12 A), PIN1-2-1-eGFP localized primarily to the apical side of epidermal cells and almost no signal was detected at the lateral sides of the cell. This indicates that by providing the PIN2 loop domain, the physiological characteristics of PIN2 could be transferred to PIN1.

In segregating T2 lines, PIN1-3-1 rescued the *pin2* phenotype to the same levels as PIN1 (Figure 18 K). Compared to PIN1-2-1, the potential to complement the *pin2* phenotype was reduced. However, the VGI of a homozygous PIN1-3-1 line was not significantly different from wildtype, suggesting that the differences were more pronounced in the T2 generation (Figure 18 G). PIN1-3-1-eGFP was only detected in four out of five lines (Figure 18 K). The localization of PIN1-3-1-eGFP was less

polar than PIN1-2-1-eGFP and more similar to PIN1-eGFP (Figure 12 A). The protein was detected with similar intensity at the apical and lateral cell side.

In summary, the root angle of segregating T2 lines revealed that roots expressing *pin2;*P_{PIN2}*:PIN1-2-1* were more gravitropic than its ancestor PIN1. The PIN1-3-1 chimera was more similar to PIN1 in terms of localization and the ability to rescue the *pin2* phenotype. This suggests that the PIN2 loop domain provides the PIN1 TM domains with necessary physiological features that are different compared to the PIN3 loop domain.

The chimeras alone did not transport IAA in the oocyte assay (Figure 18 L/M). Transport was activated by co-expression of either kinase, D6PK or PINOID. The transport rate was very low for PIN1-2-1 and increased for PIN1-3-1. This would suggest that the transport activity can be modulated by providing the PIN1 TM domains with another loop domain. This was supported by the *in planta* data, where PINs with a transport rate similar to PIN2, i.e. PIN1-2-1, rescued the *pin2* phenotype better than PINs that did transport faster, i.e. PIN1-3-1.

3.2.2 PIN2 as TM domain donor

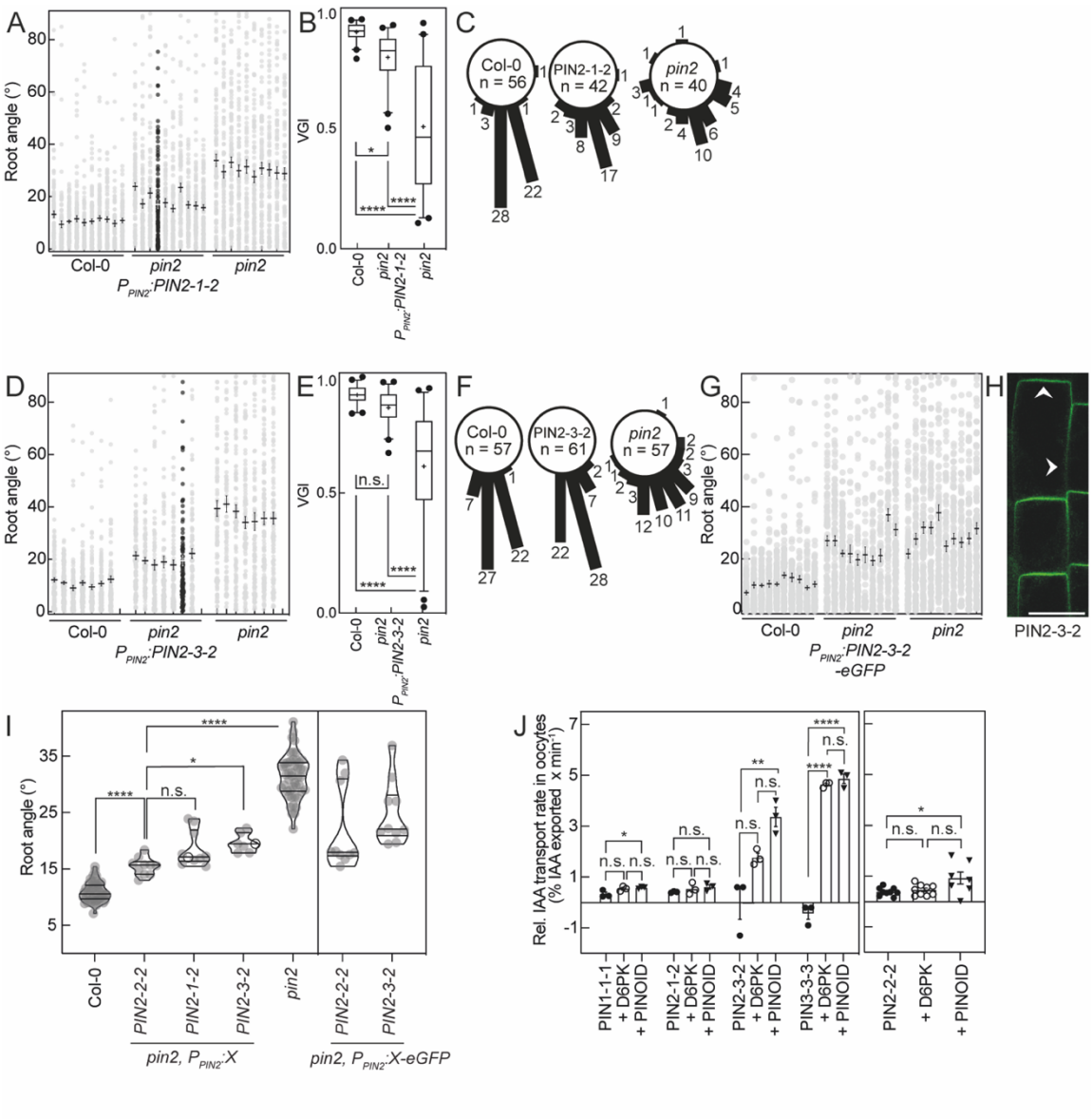

Figure 19 – Potential of PIN2-1-2 and PIN2-3-2 chimeras to rescue the *pin2* phenotype, the localization of PIN2-3-2 in the root tip and the IAA transport properties. PIN2-1-2 (A-C), PIN2-3-2 (D-F) or PIN2-3-2-eGFP (G-H) were expressed from a *PIN2* promoter fragment in the *pin2* mutant background. (A, D, G) Root angle of independent segregating T2 lines (n = 10 in A, n = 7 in D, n = 10 in G) between root tip and gravity vector of *pin2;P_{PIN2}:PIN2-1-2*, *pin2;P_{PIN2}:PIN2-3-2* and *pin2;P_{PIN2}:PIN2-3-2-eGFP* (n = 105-116 for PIN2-1-2, n = 85-114 for PIN2-3-2, n = 60-115 for PIN2-3-2-eGFP) in comparison to wildtype (n = 95-111 in A, n = 104-120 in D, n = 102-116 in G) and mutant (n = 93-107 in A, n = 90-118 in D, n = 99-115 in G). Data points are individual seedlings. The mean and SE are indicated. The representative line is represented by black dots. (B, E) VGI of the homozygous T3 line of *pin2;P_{PIN2}:PIN2-1-2* and *pin2;P_{PIN2}:PIN2-3-2* (n = 41 for PIN2-1-2 and n = 58 for PIN2-3-2) in comparison to wildtype (n = 40 in B, n = 57 in E) and mutant (n = 40 in B, n = 57 in E). Box plots range from 25th to 75th percentiles, whiskers mark the 5th and 95th percentiles and the median is indicated. Points below and above the whiskers are drawn as individual points. The mean is indicated by (+). Groups were compared by one-way ANOVA followed by Tukey's posthoc test. * p-value 0.0140, **** p-value <0.0001 in B. n.s. not significant p-value 0.1123, **** p-value <0.0001 in E. (C, F) Root angles between root tip and gravity vector of the homozygous T3 line of *pin2;P_{PIN2}:PIN2-1-2* and *pin2;P_{PIN2}:PIN2-3-2* in comparison to wildtype and mutant. Numbers are individual seedlings. (H) GFP signal of PIN2-3-2-eGFP expressed from a *PIN2* promoter fragment in epidermal cells of the *pin2* mutant. The arrows mark GFP signal. Scale bar represents 20 µm. (I) Root angle of the indicated PIN or PIN chimeras expressed from a *PIN2* promoter fragment in the *pin2* mutant background. Frequency distribution of the mean of individual segregating T2 lines shown in (A, D, G) in comparison to wildtype (n = 47 in total) and mutant (n = 47 in total). Each data point shows the mean of one independent line. The white dot represents the mean of the representative line shown in (A, D). Data for PIN2 and PIN2-eGFP are shown in Figure 10 and Figure 11. In the plot, the median is indicated. The lower and upper line mark the 25th and 75th percentiles. Groups of untagged PINs were analyzed by one-way ANOVA, followed by Dunnett's test with *P_{PIN2}:PIN2* as control group. n.s. not significant p-value 0.0570. * p-value 0.0145. **** p-value <0.0001. (J) Relative IAA export rates for PIN2-1-2 and PIN2-3-2. PIN2-1-2 and PIN2-3-2 were expressed alone (●) or co-expressed with D6PK (○) or PINOID (▼) in oocytes. PIN1 and PIN3 were used as controls. For comparison, transport rates of PIN2 alone or with D6PK or PINOID are shown. Data points are transport rates of (n = 3 for PIN1, PIN3 and chimeras. n = 9 for PIN2, n = 9 for PIN2 + D6PK, n = 7 for PIN2 + PINOID). Groups were analyzed by one-way ANOVA, followed by Tukey's posthoc test. PIN1: n.s. not significant p-value 0.0962 (vs. + D6PK), * p-value 0.0492 (vs. + PINOID), n.s. p-value 0.8580 (+ D6PK vs. + PINOID). PIN2-1-2: n.s. p-value 0.6263 (vs. + D6PK), n.s. p-value 0.3433 (vs. + PINOID), n.s. p-value 0.8402 (+ D6PK vs. + PINOID). PIN2-3-2: n.s. p-value 0.0607 (vs. + D6PK), ** p-value 0.0037 (vs. + PINOID), n.s. p-value 0.0913 (+ D6PK vs. + PINOID). PIN3: **** p-value <0.0001, n.s. p-value 0.6399 (+ D6PK vs. + PINOID). PIN2: n.s. p-value 0.9002 (vs. + D6PK), * p-value 0.0212 (vs. + PINOID), n.s. p-value 0.0510 (+ D6PK vs. + PINOID). Transport data for PIN2-3-2 were collected during Master thesis (Janacek, 2017).

The PIN chimeras originating from PIN2, PIN2-1-2 and PIN2-3-2, were tested analogously to the PIN1 chimeras. For individual segregating T2 lines, the root angle between the root tip and the gravity vector was measured (Figure 19 A, D, G). For better comparison, the mean of each line was plotted (Figure 19 I). This revealed, that PIN2-1-2 could rescue the agravitropic root phenotype to the same levels as PIN2. PIN2-3-2 was significantly different to its TM domain donor. One representative T2 line was used to generate a homozygous T3 line. The VGI showed that PIN2-1-2 was distinct from Col-0 and PIN2-3-2 behave like wildtype (Figure 19 B, E). This was different to the situation found in segregating T2 lines, where PIN2-1-2 rescued to wildtype levels and PIN2-3-2 was significantly different to Col-0. Also, the root angles of the homozygous T3 lines showed that *pin2;PIN2-3-2* seedlings resembled Col-0 more than *pin2;PIN2-1-2* seedlings (Figure 19 C, F).

In order to analyze the localization of the chimeras, the transporters were tagged with eGFP in their loop domain. Four attempts to generate PIN2-1-2-eGFP transformants, including new cloning of the initial construct, failed. All lines were successfully genotyped for the *PIN* T-DNA but did not show

fluorescence and resembled the *pin2* mutant phenotype (11 out of 11 tested lines), suggesting that the *PIN* T-DNA was suppressed in these transformants. For PIN2-3-2-eGFP, transgenic lines that exhibited fluorescence were found (6 of 10 lines). The root angle between the root tip and the gravity vector was measured (Figure 19 G). The fluorescent lines rescued the *pin2* mutant like their untagged relatives (Figure 19 K), but less than PIN2-eGFP (Figure 11 B). Fluorescence was detected at the apical side of epidermal cells, but also at the lateral cell side (Figure 19 H). The localization was less polar than PIN2-eGFP, but more polar than PIN3-eGFP (Figure 12 A). Indicating that positional information is provided by the PIN2 TM domains and the loop domain. By replacing the PIN2 loop domain by a PIN3 loop, some information is lost and the PIN2-3-2 cannot localize as polar as PIN2. This hints to major differences between the PIN loop domains.

The transport properties of the chimeras were tested in the oocyte assay (Figure 19 J). PIN1 and PIN3 were used as controls in the experiment and the transport rates of PIN2 were shown for better comparison. As described earlier (Figure 7), PIN1 and PIN2 display similar transport properties. The exchange of the PIN2 loop domain for the PIN1 loop domain resulted in a PIN chimera with similar transport characteristics as the domain donors. The transport rates of PIN2-1-2 activated by D6PK or PINOID were very small and mathematical not significantly increased to PIN without kinase. In limited sample sizes and also with some batches of labelled IAA, this was sometimes also the case for PIN1 and PIN2. In contrast, the exchange of the PIN2 loop domain with PIN3 resulted in increased transport rates which did not reach the levels of PIN3. But the transport rates upon activation by D6PK or PINOID were strongly increased compared to PIN1, PIN2 or the PIN2-1-2 chimera. Notably, the difference between D6PK- or PINOID-mediated PIN activation was pronounced in the PIN2-3-2 chimera. This suggests that the biochemical properties of PIN3 could partially be transplanted by the PIN3 loop domain, and that a combination of PIN2 and PIN3 influenced the ability of the transporter to be activated by D6PK or PINOID.

3.2.3 PIN3 as TM domain donor

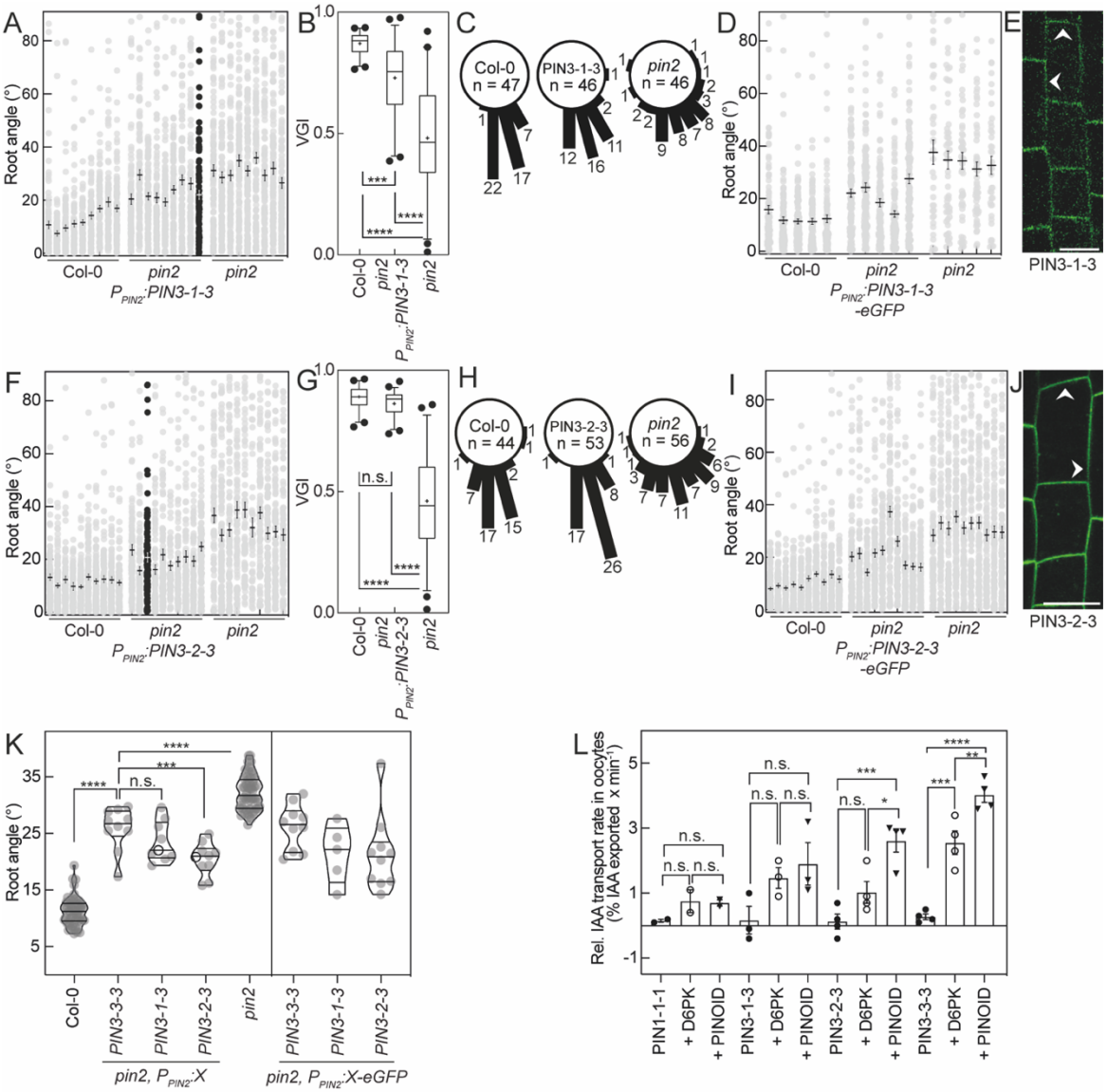

Figure 20 – Potential of PIN3-1-3 and PIN3-2-3 chimeras to rescue the *pin2* phenotype, their localization in the root tip and their IAA transport properties. *PIN3-1-3* (A-C), *PIN3-2-3* (F-H), *PIN3-1-3-eGFP* (D-E) or *PIN2-3-2-eGFP* (I-J) were expressed from a *PIN2* promoter fragment in the *pin2* mutant background. (A, D, F, I) Root angle of independent segregating T2 lines (n = 9 in A, n = 10 in D, n = 5 in F, n = 10 in I) between root tip and gravity vector of *pin2;P_{PIN2}:PIN3-1-3*, *pin2;P_{PIN2}:PIN3-2-3*, *pin2;P_{PIN2}:PIN3-1-3-eGFP* and *pin2;P_{PIN2}:PIN2-3-2-eGFP* (n = 94-117 for PIN3-1-3, n = 64-117 for PIN3-2-3, n = 109-115 for PIN3-1-3-eGFP, n = 91-119 for PIN3-2-3-eGFP) in comparison to wildtype (n = 82-106 in A, n = 95-120 in D, n = 106-115 in F, n = 106-115 in I) and mutant (n = 108-120 in A, n = 47-114 in D, n = 37-52 in F, n = 104-112 in I). Data points are individual seedlings. The mean and SE are indicated. The representative line is represented by black dots. (B, G) VGI of the homozygous T3 line of *pin2;P_{PIN2}:PIN3-1-3* and *pin2;P_{PIN2}:PIN3-2-3* (n = 46 for PIN3-1-3 and n = 51 for PIN3-2-3) in comparison to wildtype (n = 46 in B, n = 40 in G) and mutant (n = 46 in B, n = 56 in G). Box plots range from 25th to 75th percentiles, whiskers mark the 5th and 95th percentiles and the median is indicated. The mean is represented by (+). Points below and above the whiskers are drawn as individual points. Groups were compared by one-way ANOVA followed by Tukey's posthoc test. n.s. not significant 0.6049, *** p-value 0.0002, **** p-value <0.0001. (C, H) Root angles between root tip and gravity vector of the homozygous T3 line of *pin2;P_{PIN2}:PIN3-1-3* and *pin2;P_{PIN2}:PIN3-2-3* in comparison to wildtype and mutant. Numbers are individual seedlings. (E, J) GFP signal of PIN3-1-3-eGFP and PIN3-2-3-eGFP expressed from a *PIN2* promoter fragment in epidermal cells of the *pin2* mutant. The arrows mark the GFP signal. Scale bar represents 20 µm. (K) Root angle of the indicated PIN or PIN chimeras expressed from a PIN2 promoter fragment in the *pin2* mutant background. Frequency distribution of the mean of individual segregating T2 lines shown in (A, D, F, I) in comparison to wildtype (n = 54 in total) and mutant (n = 54 in total). Each data point shows the mean of one independent line. The white dot represents the mean of the representative line shown in (A, F). Data for PIN3 and PIN3-eGFP are shown in Figure 10 and Figure 11. The median is indicated. The lower and upper line mark the 25th and 75th percentiles. Groups of untagged PINs were analyzed by one-way ANOVA, followed by Dunnett's test with *pin2;P_{PIN2}:PIN3* as control group. n.s. not significant p-value 0.2061. *** p-value 0.0002. **** p-value <0.0001. (L) Relative IAA transport rates of PIN3-1-3 and PIN3-2-3. PIN3-1-3 and PIN3-2-3 were expressed alone (●) or co-expressed with D6PK (○) or PINOID (▼) in oocytes. PIN1 and PIN3 were used as controls. Data points are transport rates of (n = 2 for PIN1 /+ D6PK /+ PINOID, n = 4 for PIN3 /+D6PK /+PINOID, n = 3 for PIN3-1-3 /+D6PK /+PINOID, n = 4 for PIN3-2-3 /+D6PK /+PINOID). Groups were analyzed by one-way ANOVA, followed by Tukey's posthoc test. PIN1 vs. PIN1 + D6PK n.s. not significant p-value 0.2588, PIN1 vs. PIN1 + PINOID n.s. p-value 0.3005, PIN1 + D6PK vs. PIN1 + PINOID n.s. p-value 0.9849; PIN3-1-3 vs. PIN3-1-3 + D6PK n.s. p-value 0.2225, PIN3-1-3 vs. PIN3-1-3 + PINOID n.s. p-value 0.1001, PIN3-1-3 + D6PK vs. PIN3-1-3 + PINOID n.s. p-value 0.8104; PIN3-2-3 vs. PIN3-2-3 + D6PK n.s. p-value 0.1454, PIN3-2-3 vs. PIN3-2-3 + PINOID *** p-value 0.0007, PIN3-2-3 + D6PK vs. PIN3-2-3 + PINOID * p-value 0.0129; PIN3 vs. PIN3 + D6PK *** p-value 0.0003, PIN3 vs. PIN3 + PINOID **** p-value <0.0001, PIN3 + D6PK vs. PIN3 + PINOID ** p-value 0.0066. Transport data of PIN3-1-3 and PIN3-2-3 were partially collected during Master thesis (Janacek, 2017).

PIN3 rescued the *pin2* phenotype less than PIN1, although both localized equally apolarly and transport IAA. In order to understand if PIN3 could be modulated towards a PIN protein that rescues like PIN1 or PIN2 in the *pin2* mutant, the impact of the PIN1 or PIN2 loop domains in the PIN3 TM context was investigated. The root angles of independent segregating T2 seedlings of PIN3-1-3 and PIN3-2-3 were analyzed in relation to the gravity vector (Figure 20 A, D). By comparing the means of those T2 lines against the TM domain donor PIN3 (Figure 20 K), it was found that PIN3-1-3 fell into the same statistical group as PIN3, but PIN3-2-3 rescued the *pin2* phenotype significantly better than PIN3. This was also reflected in the VGI of homozygous T3 seedlings. One representative line was used to generate a homozygous T-DNA line. The VGI of PIN3-1-3 (Figure 20 B) was significantly different from both control groups. The *pin2* phenotype was rescued, but not to wildtype levels. In contrast, the VGI of the PIN3-2-3 chimera was identical to the VGI of Col-0 (Figure 20 G). The findings from the VGI analysis were also obvious by plotting the root angle of the homozygous T3 seedlings (Figure 20 C, H). The root angles of PIN3-1-3 seedling varied more than

PIN3-2-3 (SD of PIN3-1-3 = 15.1 vs. SD of PIN3-2-3 = 14.0), but the root angles of both PIN chimeras varied less than those of *pin2* mutant seedlings (SD in data set of PIN3-1-3 = 29.3 and SD in data set of PIN3-2-3 = 22.8).

To check the localization of the chimeras, the PINs were tagged with eGFP. The resulting segregating T2 lines of PIN3-1-3-eGFP and PIN3-2-3-eGFP were analyzed as described. The means of the root angles of independent segregating T2 lines showed a higher variation of the mean (SD of PIN3-1-3-eGFP = 5.2 and SD of PIN3-2-3-eGFP = 6.7) compared to their untagged relatives (SD of PIN3-1-3 = 3.6 and SD of PIN3-2-3 = 2.9; Figure 20 K). The expression was weak, but the signal of the transporter was found at the apical and lateral cell sides. The localization of PIN3-1-3-eGFP in epidermal cells was similar to PIN3-eGFP. For PIN3-2-3-eGFP, the localization was slightly more polar than PIN3-eGFP or PIN3-1-3-eGFP (Figure 12 A; Figure 20 E, F).

The PIN chimeras were tested in the oocyte efflux assay to see how the transport of PIN3 is altered if the loop domain was exchanged against PIN1 or PIN2 (Figure 20 L). PIN1 and PIN3 were included as controls. Both exchanges against PIN1 loop or PIN2 loop resulted in decreased IAA transport properties. The effect was stronger for the PIN1 loop. Although the transport rates of PIN3-2-3 were higher than PIN3-1-3, the difference between D6PK and PINOID was again detectable and significantly different. In this data set, the PIN3 transport rate was also significantly stronger with PINOID than with D6PK. This suggests that the kinase identity influences the PIN-mediated IAA transport and that the role of the kinase is beyond a simple activation mechanism.

3.2.4 Protein domains of PINs work together as functional IAA transporters

One goal of this thesis was to examine the impact of the individual protein domains on the biochemical and physiological functions of PINs. In the oocyte radiotracer transport assay the canonical PINs showed differences in their transport behavior. The AGC kinases D6PK and PINOID were required to activate PIN-mediated transport (Zourelidou *et al.*, 2014). To explore the physiological relevance of IAA transport rates *in planta*, the *pin2* mutant phenotype was again used as described (Luschnig *et al.*, 1998; Abas *et al.*, 2006). The canonical PINs and the chimeras were expressed from a *PIN2* promoter fragment and the main read out was the angle between the root tip and the gravity vector of 5-day old seedlings. GFP-tagged variants allowed it to analyze the localization of the transporters.

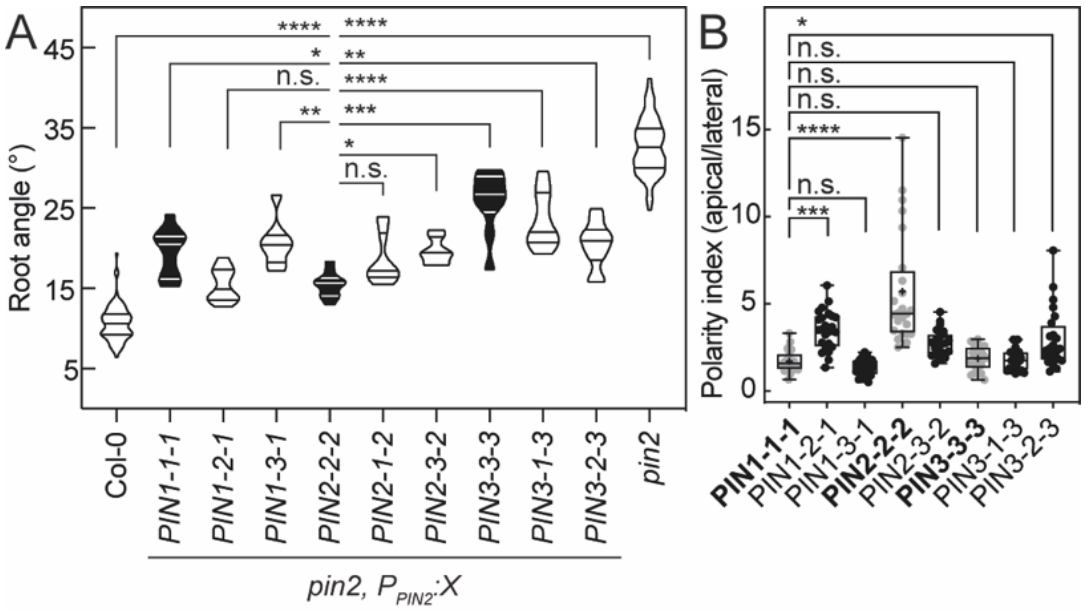

Figure 21 – Potential of PIN chimeras to rescue the *pin2* phenotype and their polarity index. (A) Root angle of the indicated PIN or PIN chimera expressed from a *PIN2* promoter fragment in the *pin2* mutant background. Frequency distribution of the mean of individual segregating T2 lines shown in Figure 10, Figure 18, Figure 19 and Figure 20 (n = 10 for PIN1, PIN1-2-1, PIN2, PIN2-1-2, PIN3, PIN3-2-3. n = 9 for PIN3-1-3. n = 8 for PIN1-3-1. n = 7 for PIN2-3-2) in comparison to wildtype (n = 84 in total) and mutant (n = 84 in total). The black plots show the TM domain-donating PIN. In the plot, the middle line marks the median. The lower and upper line mark the 25th and 75th percentiles. Groups were analyzed by one-way ANOVA, followed by Dunnett's test with *pin2;P$_{PIN2}$:PIN2* as control group. n.s. not significant p-value >0.9999 (vs. PIN1-2-1) and 0.1055 (vs. PIN2-1-2). * p-value 0.0141 (vs. PIN1) and 0.0266 (vs. PIN2-3-2). ** p-value 0.0019 (vs. PIN1-3-1) and 0.0011 (vs. PIN3-2-3). **** p-value <0.0001. (B) Polarity index of eGFP-tagged PIN chimeras expressed from a *PIN2* promoter fragment in epidermal cells in the *pin2* mutant. Mean intensities of ROIs at the apical and the lateral side of the cells were used to calculate the ratios. Data points show individual cells (n = 24 per genotype). TM domain-donating PINs (gray points) are included for comparison with PIN chimeras (black points) and are shown in Figure 10. Box plots ranges from 25th to 75th percentiles, whiskers mark the minimum and maximum values and the median is indicated. The mean is indicated by (+). Groups were analyzed by a one-way ANOVA, followed by Dunnett's posthoc test with PIN1-eGFP as control group. n.s. not significant p-value 0.9994 (vs. PIN3), 0.0803 (vs. PIN2-3-2), 0.9204 (vs. PIN1-3-1), 0.9997 (vs. PIN3-1-3), * p-value 0.0200, **** p-value <0.0001.

The differences between the respective PINs were visible in the T2 generation. The individual lines of each genotype are shown in more detail in Figure 10, Figure 18, Figure 19 and Figure 20.

The frequency distribution of all lines analyzed in the gravitropism assay allowed it to make the following observations (Figure 21 A): PIN1 and PIN3 rescued the *pin2* phenotype partially with increased gravitropic growth by PIN1 than PIN3. Addition of the PIN2 loop domain in the PIN1 or PIN3 TM context improved the degree of rescue by PIN1-2-1 and PIN3-2-3. PIN1-2-1 even was indistinguishable from PIN2 in this assay. In contrast, when provided with a PIN3 loop, PIN1-3-1 and PIN2-3-2 showed reduced ability to rescue the phenotype compared to the TM donors. The impact of the PIN1 loop was smaller than that of the PIN3 loop. The degree of rescue decreased slightly for PIN2-1-2 but increased for PIN3-1-3 compared to the wildtype versions of PIN2 and PIN3, respectively. Particularly in the cases of PIN2 and PIN3, the gradual change of the potential to rescue the mutant phenotype was obvious. In the case of PIN2, PIN2-1-2 and PIN2-3-2, the

potential to rescue the mutant phenotype was decreased. Conversely, in the case of PIN3, the potential to rescue the mutant phenotype was increased for PIN3-1-3 and PIN3-2-3.

The polarity index of respective PINs in epidermal root cells was lower for PIN1 and PIN3 than that of PIN2 (Figure 21 B). In PIN1-2-1 and PIN3-2-3, the polarity index increased compared to the wildtype versions, indicating that the PIN2 loop provides a signal that leads to a more polar localization.

Conversely the PIN3 loop decreased polarity of PIN1-3-1 and PIN2-3-2 compared to the wildtype versions, indicating that the PIN3 loop does not carry the same information as the PIN2 loop.

The impact of the PIN1 loop is not clear. PIN3-1-3 localized as apolar as the wildtype versions and it was not able to find a functional PIN2-1-2-eGFP.

Taken together, PIN1 and PIN2 are similar in terms of transport rates in oocytes. The gravitropism assay showed that PIN1 and combinations of PIN1 and PIN2 almost rescue the *pin2* phenotype to wildtype levels. This indicates that besides their phylogenetic relation, PIN1 and PIN2 share characteristics in terms of transport properties and phylogenetic behavior.

PIN3 displayed the highest transport rates in the oocyte assay but could rescue the root phenotype only partially. Introduction of PIN1 or PIN2 loop, improved the potential to complement the mutant. While the polarity index of chimeras with a PIN2 loop increased, this was not the case when the PIN1 loop was introduced in the PIN3 TM context. This suggests that in addition to polar localization also the transport rate impacts the degree to which the mutant phenotype can be complemented.

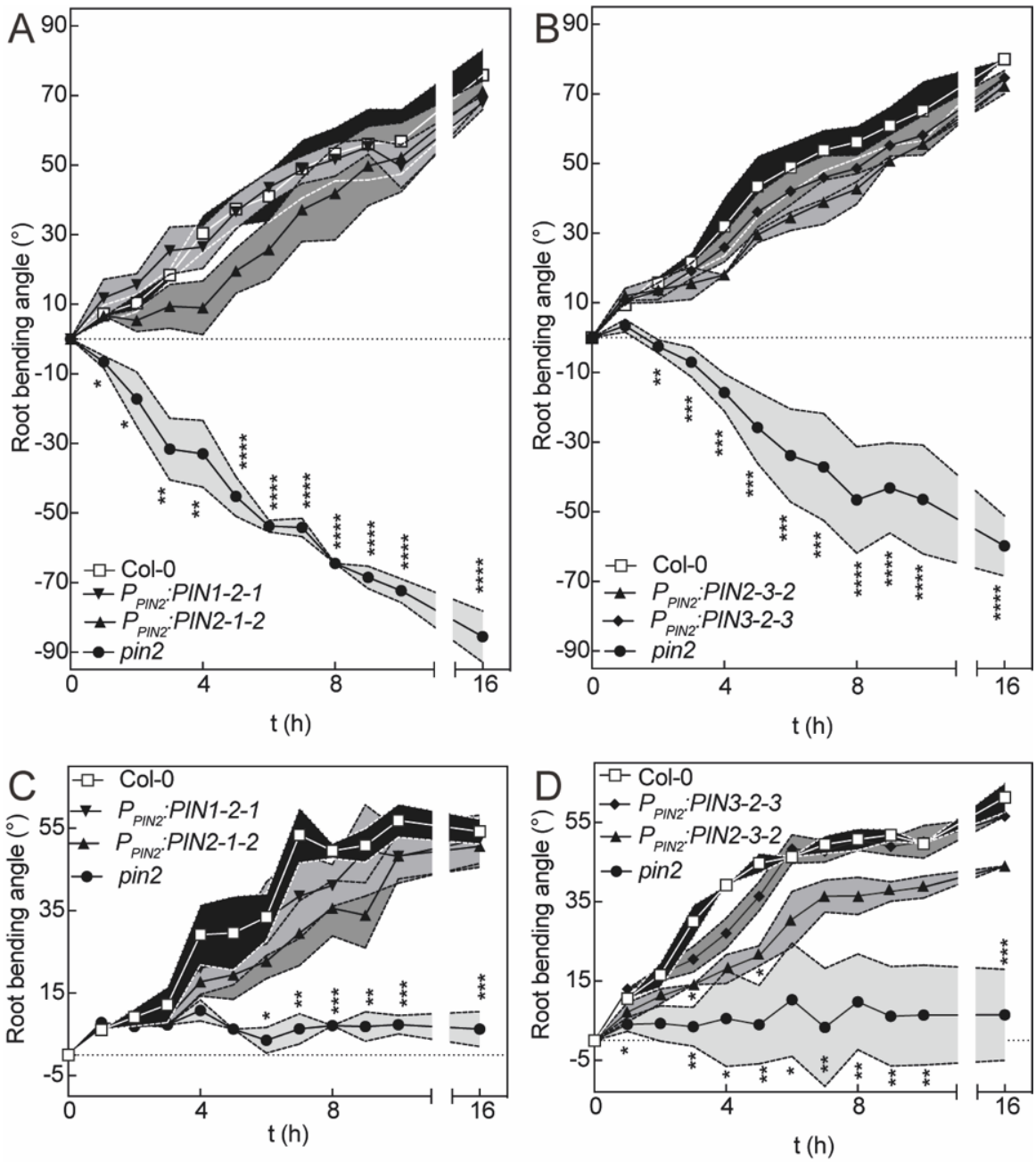

Figure 22 – Response of PIN chimeras to a gravitropic stimulus. Root bending kinetics of *pin2;*P_{PIN2}*:PIN1-2-1* (A, C), *pin2;*P_{PIN2}*:PIN2-1-2* (A, C), *pin2;*P_{PIN2}*:PIN2-3-2* (B, D) and *pin2;*P_{PIN2}*:PIN3-2-3* (B, D) in comparison to wildtype and mutant on plant medium containing 1 % sucrose (A, B) or not (C, D). PIN2-1-2, PIN2-3-2 and PIN3-2-3 showed a delayed response to the gravitropic stimulus, but reached wildtype-levels after 16 h. The *pin2* mutant bent against the gravity vector on medium containing sugar (A, B) and did not react to the stimulus on medium without sugar (C, D). Data points are mean and SE of 3 replicates with 18-20 roots per genotype. Groups were compared by one-way ANOVA, followed by Dunnett posthoc test with Col-0 as control group. Significant differences are indicated by "*". n.s. not significant p-value ≥ 0.05, * p-value 0.01 to 0.05, ** p-value 0.001 to 0.01, *** p-value 0.0001 to 0.001, **** p-value < 0.0001

The described differences between the PIN chimeras were observed in a state of constant auxin flow from the shoot towards the root tip through the vasculature. By applying a gravitropic stimulus, a time-dependent component could be added to the system. In order to test if the gradual differences between the PIN chimeras and the wildtype versions were also relevant for the reaction to this gravitropic stimulus, 5-day old seedlings were transferred on plates containing either 1 % sucrose (Figure 22 A, B) or neither sucrose nor vitamins (Figure 22 C, D). The plates were turned by 90 ° (Figure 22). The results for the controls and the wildtype PINs can be compared to Figure 14.

Consistent with the results obtained for gravitropic growth, PIN1-2-1 reacted to the gravitropic stimulus indistinguishably from Col-0. PIN2-1-2 bent slower (2 ± 1 ° x h^{-1}) compared to Col-0 (7 ± 1 ° x h^{-1}) in the first 4 h, but reached the same levels after 10 h (Figure 22 A). The bending rate of PIN2-1-2 between 4 and 9 h (8 ± 2 ° x h^{-1}) was increased in comparison to Col-0 (5 ± 2 ° x h^{-1}) and PIN1-2-1 (6 ± 1 ° x h^{-1}). On plates without sucrose and vitamins, root bending was reduced for all genotypes (Figure 22 C). During the first 3 h, PIN1-2-1 was comparable to Col-0 (4 ± 1 ° x h^{-1}), but then the bending rate of Col-0 increased. Root bending of PIN2-1-2 was similar to Col-0 and PIN1-2-1 for the first 4 h, then bending slowed down but reached the same levels as PIN1-2-1 after 10 h. The differences described were not significantly different from Col-0.

In the gravitropic growth assay, PIN2-3-2 and PIN3-2-3 rescued the *pin2* phenotype to the same level. Consistently, their reaction to the gravitropic stimulus was similar. On plates containing sucrose, PIN3-2-3 bent slightly faster compared to PIN2-3-2, but not as fast as PIN1-2-1 did (Figure 22 B). The bending rates of 5-7 $\pm$ 1 ° x h^{-1} were indistinguishable within the first 3 h for Col-0, PIN2-3-2 and PIN3-2-3. Although bending rates increased after 3 h for Col-0 and PIN3-2-3, the bending rate of PIN2-3-2 stayed lower for an additional hour. The root bending rates of the genotypes indicated were constant between 4 and 10 h ($5\text{-}6 \pm 1$ ° x h^{-1}). Interestingly, the differences between the genotypes were more pronounced on plates without sugar and vitamins (Figure 22 D). After 2 h, the bending rate of Col-0 increased for 2 h and flattened again, whereas the rate for PIN3-2-3 was constant until both genotypes reached the same bending angle after 6 h. The bending rate of PIN2-3-2 was initially slower (4 ± 1 ° x h^{-1}) compared to Col-0 (9 ± 1 ° x h^{-1}) within the first 6 h and the root angle did not reach the wildtype level after 16 h. On plates without sucrose and vitamins, the bending rate of all genotypes (except the *pin2* mutant that did not bend at all) decreased after 6 h, whereas on plates containing sugar, the bending rates were relatively constant.

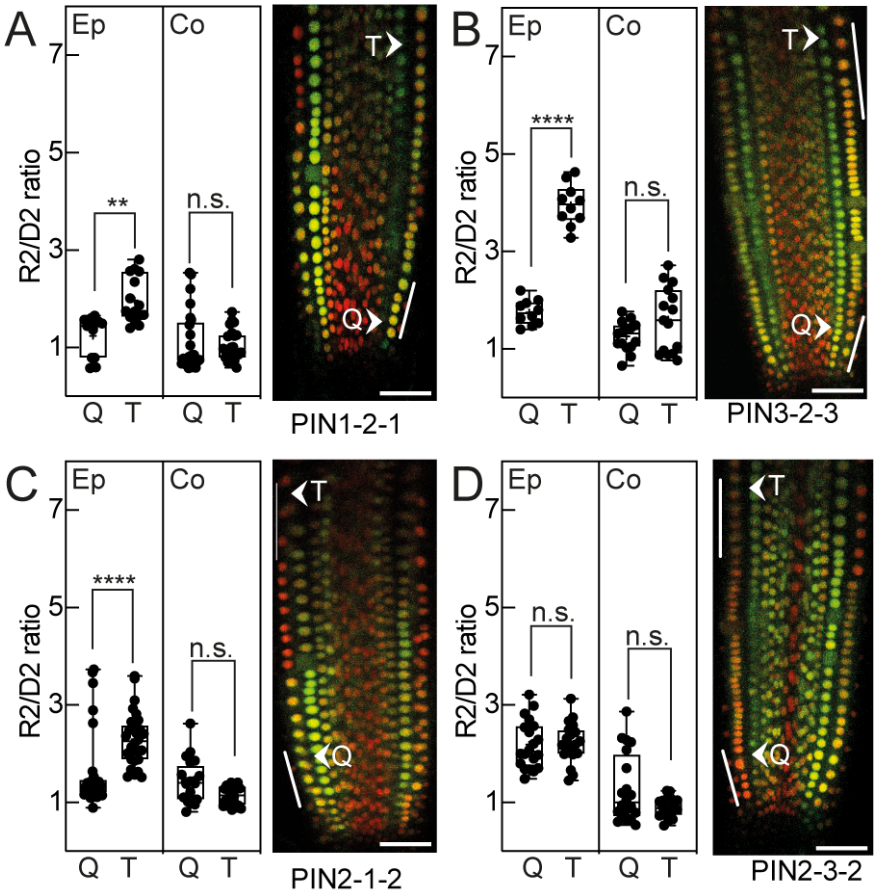

Figure 23 – IAA levels of PIN chimeras in the root tip. Ratio of mDII to DII signal in epidermis (Ep) and cortex (Co) for *pin2;P*$_{PIN2}$*:PIN1-2-1* (A), *pin2;P*$_{PIN2}$*:PIN3-2-3* (B), *pin2;P*$_{PIN2}$*:PIN2-1-2* (C) and *pin2;P*$_{PIN2}$*:PIN2-3-2* (D). First five epidermal cells after anticlinal division of the epidermal/LRC initial cell (Q) and five cells at the transition zone as specified by cell elongation (T) were measured for individual roots (n = 15-30 for epidermis and n = 15-25 for cortex). Cells analyzed are indicated by white lines. Pictures show overlay of DII (green) and mDII (red) signal. Scale bar represents 40 µm. Box plots show the 25th and 75th percentiles, whiskers mark the minimum and maximum values. The line in the box represents the median. Whole data set analyzed by one-way ANOVA, followed by Tukey's posthoc test (PIN1-2-1: ** p-value 0.0077, n.s. not significant p-value 0.9991. PIN3-2-3: **** p-value <0.0001, n.s. p-value 0.4814. PIN2-1-2: **** p-value <0.0001, n.s. p-value 0.4792. PIN2-3-2: n.s. p-value >0.9999 (Ep), n.s. p-value 0.1736 (Co)).

The PIN chimeras were different in their ability to rescue the *pin2* phenotype, as well as in their reaction to a gravitropic stimulus. The auxin sensor R2D2 was used to identify if differences in the auxin levels of epidermis and cortex could give an explanation (Figure 23).

Five epidermal cells, resp. cortical cells, after anticlinal division of the epidermal/LRC initial cell (Q) and five cells at the transition zone as specified by cell elongation (T) were measured for individual roots. The findings for the wildtype and mutant situation, as well as the ancestor PINs, were shown and described in Figure 12 B–F.

The R2/D2 ratio in the epidermis at the meristematic position Q was around 1 and therefore in the same range for PIN1-2-1, PIN3-2-3 and PIN2-1-2. This was comparable to Col-0 and PIN1 (Figure 23 B, D). The ratio was slightly increased for PIN2-3-2 to similar levels as in *pin2*, *pin2;P*$_{PIN2}$*:PIN2*

and *pin2;*P_{PIN2}*:PIN3* roots (Figure 23 C, E, F). The ratio of cells at the transition zone (T) was significantly increased for PIN1-2-1, PIN3-2-3 and PIN2-1-2. This was similar to Col-0 and PIN2. The auxin levels in the epidermis of *pin2;*P_{PIN2}*:PIN3-2-3* roots increased stronger compared to all other genotypes. There was no change between the R2/D2 ratio of Q and T in *pin2;*P_{PIN2}*:PIN2-3-2* roots in the epidermis. This was similar to *pin2, pin2;*P_{PIN2}*:PIN1* and *pin2;*P_{PIN2}*:PIN3* roots.

The auxin levels in the cortex were not significantly different for any PIN chimeras between the two positions in the root, as it was found for Col-0, PIN1, PIN2 and PIN3. The overall R2/D2 levels in the cortex were low and in the similar range as Col-0, PIN1 and PIN3.

The chimeras PIN1-2-1, PIN3-2-3 and PIN2-1-2 had the same tendency as Col-0 and PIN2 with a significant increase of auxin levels over root length in the epidermis and no change in the cortex. Only the PIN2-3-2 chimera showed no difference in the epidermis and the cortex, comparable to PIN1 and PIN3 roots.

3.2.5 TM domain parts of PIN2 and PIN3 can be swapped

The transport studies of PIN2 and PIN3 showed that the two transporters differed by a factor of 7 in their IAA transport rates (PIN2 + PINOID = 3.0 ± 0.6 % x min^{-1} vs. PIN3 + PINOID = 20.8 ± 0.6 % x min^{-1}, Table 8). The potential to rescue the *pin2* phenotype was relatively low for PIN3 and could be increased by exchanging the loop domain of PIN3 against the PIN2 loop domain (Figure 21). Inversely, by bringing the PIN3 loop in the PIN2 TM domain context, the potential to rescue the phenotype was reduced. Both chimeras, PIN2-3-2 and PIN3-2-3, showed a significant dependency on the activating kinase. To better understand the influence of individual protein domains, additional chimeras between PIN2 and PIN3 were generated. Either the first 5 TM helices M1-M5 or the second 5 TM helices M6-M10 of PIN2 and PIN3 were exchanged against each other. This created the PIN chimeras PIN2-2-3, PIN2-3-3, PIN3-2-2 and PIN3-3-2.

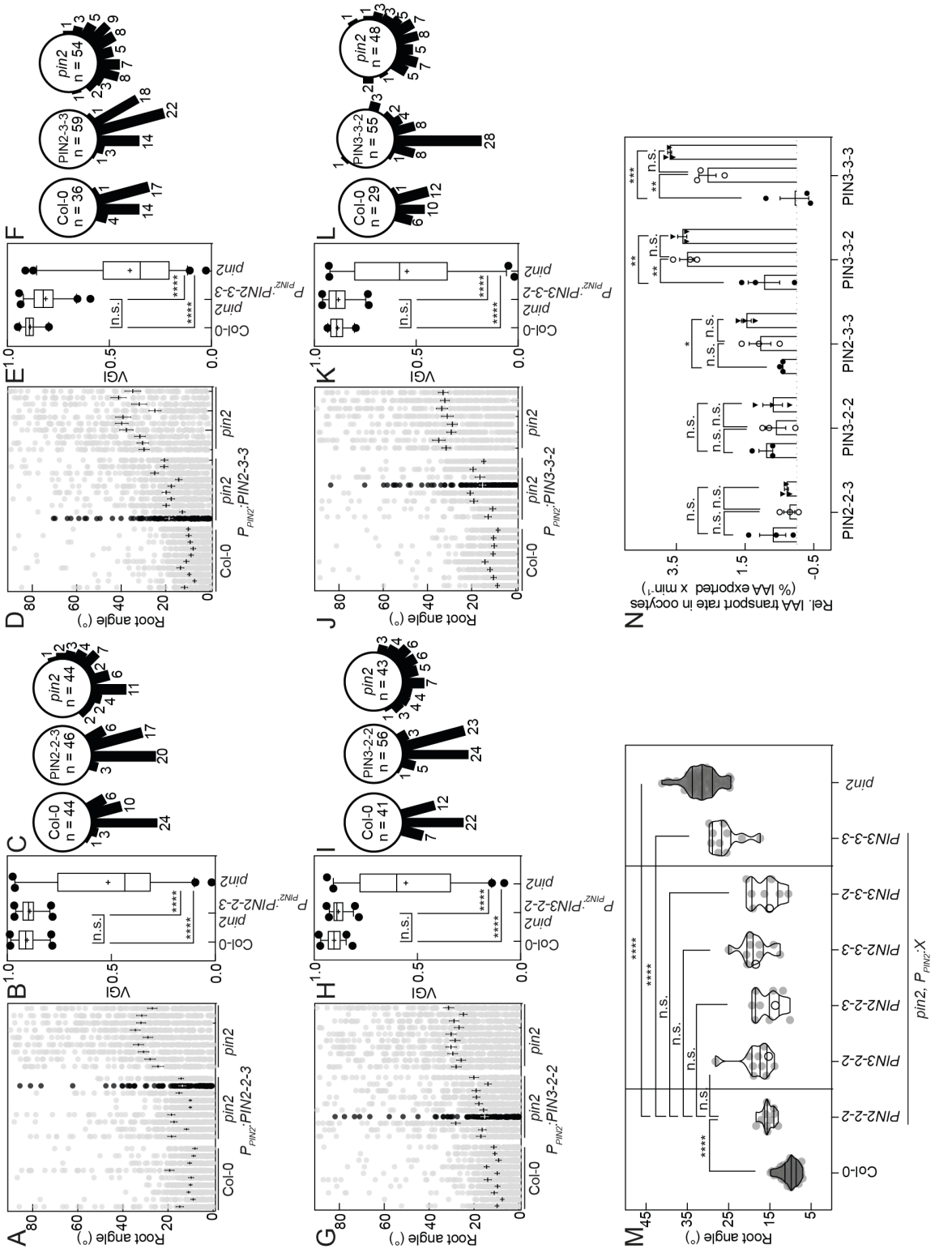
A
B
C
D
E
F
G
H
I
J
K
L
M
N
Root angle (°)
VGI
Col-0
pin2
P_PIN2:PIN2-2-3
P_PIN2:PIN2-3-3
P_PIN2:PIN3-2-2
P_PIN2:PIN3-2
P_PIN2:PIN3-3-2
Col-0 n = 44
PIN2-2-3 n = 46
pin2 n = 44
Col-0 n = 36
PIN2-3-3 n = 59
pin2 n = 54
Col-0 n = 41
PIN3-2-2 n = 56
pin2 n = 43
Col-0 n = 29
PIN3-3-2 n = 55
pin2 n = 48
Rel. IAA transport rate in oocytes
(% IAA exported x min-1)
PIN2-2-3
PIN3-2-2
PIN2-3-3
PIN3-3-2
PIN3-3-3
pin2, P_PIN2:X

Figure 24 – Potential of triple PIN chimeras to rescue the *pin2* phenotype and their IAA transport properties. PIN2-2-3 (A-C), PIN2-3-3 (D-F), PIN3-2-2 (G-I) and PIN3-3-2 (J-L) were expressed from a *PIN2* promoter fragment in the *pin2* mutant. (A, D, G, J) Root angle of independent segregating T2 lines (n = 9 in A, n = 10 in D, n = 10 in G, n = 8 in J) between root tip and gravity vector of *pin2;*P_{PIN2}*:PIN2-2-3*, *pin2;*P_{PIN2}*:PIN2-3-3*, *pin2;*P_{PIN2}*:PIN3-2-2* and *pin2;*P_{PIN2}*:PIN3-3-2* (n = 108-118 for PIN2-2-3, n = 92-105 for PIN2-3-3, n = 93-120 for PIN3-2-2, n = 93-119 for PIN3-3-2) in comparison to wildtype (n = 89-120 in A, n = 96-110 in D, n = 105-116 in G, n = 91-115 in J) and mutant (n = 86-108 in A, n = 53-89 in D, n = 93-106 in G, n = 82-116 in J). Data points are individual seedlings. The mean and SE are indicated. The representative line is shown by black dots. (B, E, H, K) VGI of the representative homozygous T3 line of *pin2;*P_{PIN2}*:PIN2-2-3*, *pin2;*P_{PIN2}*:PIN2-3-3*, *pin2;*P_{PIN2}*:PIN3-2-2* and *pin2;*P_{PIN2}*:PIN3-3-2* (n = 45 for PIN2-2-3, n = 57 for PIN2-3-3, n = 55 for PIN3-2-2, n = 50 PIN3-3-2) in comparison to wildtype (n = 42 in B, n = 35 in E, n = 41 in H, n = 28 in K) and mutant (n = 44 in B, n = 54 in E, n = 43 in H, n = 48 in K). Box plots range from 25th to 75th percentiles, whiskers mark the 5th and 95th percentiles and median is indicated. Points below and above the whiskers are drawn as individual points. The mean is indicated by (+). Groups were compared by one-way ANOVA followed by Tukey's posthoc test. n.s. not significant p-value 0.9221 (PIN2-2-3), 0.0511 (PIN2-3-3), 0.7531 (PIN3-2-2) and 0.9953 (PIN3-3-2), **** p-value <0.0001. (C, F, I, L) Root angles between root tip and gravity vector of the homozygous T3 line of *pin2;*P_{PIN2}*:PIN2-2-3*, *pin2;*P_{PIN2}*:PIN2-3-3*, *pin2;*P_{PIN2}*:PIN3-2-2* and *pin2;*P_{PIN2}*:PIN3-3-2* in comparison to wildtype and mutant. Numbers are individual seedlings. (M) Root angle of the indicated PIN or PIN chimeras expressed from a *PIN2* promoter fragment in the *pin2* mutant background. Frequency distribution of the mean of individual segregating T2 lines shown in (A, D, G, J) in comparison to wildtype (n = 57 in total) and mutant (n = 57 in total). Each data point shows the mean of one independent line. The white dot represents the mean of the representative line of each genotype. Domain-donating PIN2 and PIN3 are included for comparison with PIN chimeras and are shown in Figure 10. The line in the plot marks the median. The lower and upper lines mark the 25th and 75th percentiles. Groups were analyzed by one-way ANOVA, followed by Dunnett's test with P_{PIN2}:PIN2 as control group. n.s. not significant p-value >0.9999 (vs. PIN2-2-3) and 0.1091 (vs. PIN2-3-3) and 0.9974 (vs. PIN3-3-2). **** p-value <0.0001. (N) Relative IAA transport rates for indicated PIN chimeras in comparison to PIN3. All PINs were expressed in Xenopus oocytes either alone (●) or co-expressed with D6PK (○) or PINOID (▼). Data points show transport rates (n = 3 for all PINs). Mean and SE are indicated. Groups (PIN vs. PIN + D6PK vs. PIN + PINOID) were analyzed by one-way ANOVA, followed by Tukey's posthoc test (n.s. not significant. PIN2-2-3 vs. PIN2-2-3 + D6PK p-value 0.3855, PIN2-2-3 vs. PIN2-2-3 + PINOID p-value 0.5055, PIN2-2-3 + D6PK vs. PIN2-2-3 + PINOID p-value 0.9666; PIN3-2-2 vs. PIN3-2-2 + D6PK p-value 0.7349, PIN3-2-2 vs. PIN3-2-2 + PINOID p-value 0.8569, PIN3-2-2 + D6PK vs. PIN3-2-2 + PINOID p-value 0.9711; PIN2-3-3 vs. PIN2-3-3 + D6PK p-value 0.1480, * PIN2-3-3 vs. PIN2-3-3 + PINOID p-value 0.0263, PIN2-3-3 + D6PK vs. PIN2-3-3 + PINOID p-value 0.4009; ** PIN3-3-2 vs. PIN3-3-2 + D6PK p-value 0.0045, ** PIN3-3-2 vs. PIN3-3-2 + PINOID p-value 0.0034, PIN3-3-2 + D6PK vs. PIN3-3-2 + PINOID p-value 0.9480).

These chimeras were expressed from a *PIN2* promoter fragment in the *pin2* mutant and scored analogously to all other tested PINs and PIN chimeras (Figure 24 A, D, G, J). For better comparison, the results were plotted in comparison to wildtype PIN2 and PIN3 (Figure 24 M). All four PIN chimeras rescued the mutant to the same levels as PIN2 (data shown in Figure 10). One representative T2 line was used to generate a homozygous T3 line. The VGI of each genotype was compared to Col-0 and the *pin2* mutant (Figure 24 B, E, H, K). All four PIN chimeras were indistinguishable from Col-0. This was also illustrated by the root angles of the homozygous seedlings (Figure 24 C, F, I, L).

To see whether the kinase preference of the PIN2-3-2 and PIN3-2-3 chimeras could be resolved in the triple chimeras, they were tested in the oocyte assay at $[IAA]_{in}$ = 1 µM. The triple chimeras consisting of two thirds PIN2 did not transport IAA or were outside of the detection limit of the assay, indicating that by replacing one PIN2 domain the chimeras lost their ability to be activated by a kinase or the chimera was not able to form a functional transporter unit. By exchanging the first five

helices of PIN3 against PIN2, the transport rates were drastically reduced. This was not the case if the helices M6-M10 were exchanged, suggesting a more important role of the helices M1-M5 for the transporter's speed. The transport rates of PIN3-3-2 were still as high as for PIN3. Interestingly, the increased activation upon PINOID co-expression was visible in the PIN2-3-3 chimera, but absent in the PIN3-3-2 chimera.

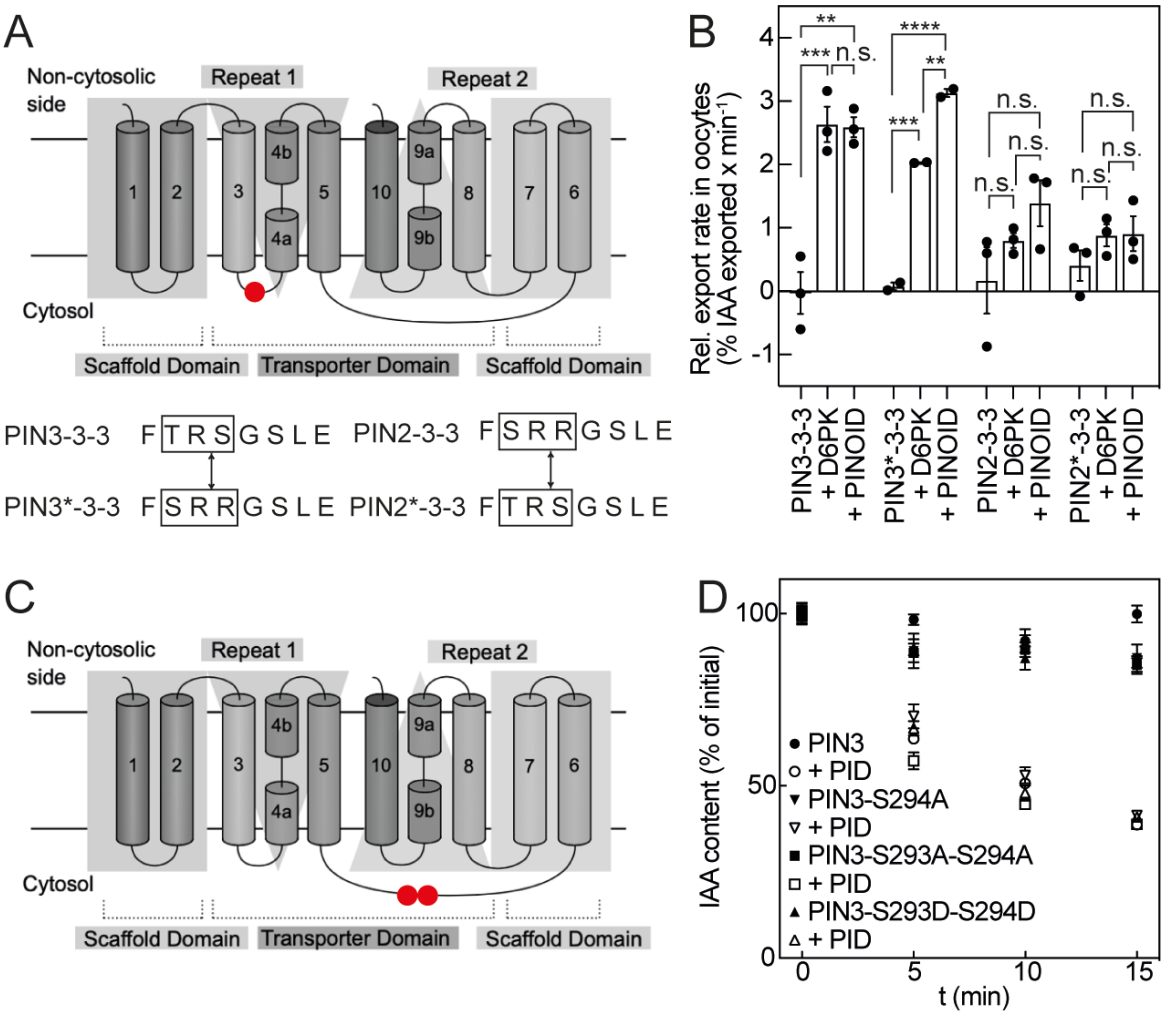

Figure 25 – IAA transport properties of mutated PIN variants. (A) Amino acid swap between PIN2 and PIN3 in the loop domain between TM helix M3 and M4a (red dot). Amino acids 93-95 of PIN3 (TRS) were exchanged with amino acids 93-95 of PIN2 (SRR) to create PIN3*. The same positions were exchanged in PIN2-3-3 to create PIN2*-3-3. (B) Relative IAA export rates of PIN3* and PIN2*-3-3 in comparison to PIN3 and PIN2-3-3. All PINs were expressed in Xenopus oocytes either alone or co-expressed with D6PK or PINOID. Data points show transport rates (n = 2 for PIN3* /+ D6PK /+ PINOID, n = 3 for PIN3 /+ D6PK /+ PINOID, PIN2-3-3 /+ D6PK /+ PINOID and PIN2*-3-3 /+ D6PK /+ PINOID). Mean and SE are indicated. Groups (PIN vs. PIN + D6PK vs. PIN + PINOID) were analyzed by one-way ANOVA, followed by Tukey's posthoc test. PIN3 vs. PIN3 + D6PK *** p-value 0.0010, PIN3 vs. PIN3 + PINOID ** p-value 0.0011, PIN3 + D6PK vs. PIN3 + PINOID n.s. not significant p-value 0.9930. PIN3* vs. PIN3* + D6PK *** p-value 0.0002, PIN3* vs. PIN3* + PINOID **** p-value <0.0001, PIN3* + D6PK vs. PIN3* + PINOID ** p-value 0.0013. PIN2-3-3 vs. PIN2-3-3 + D6PK n.s. p-value 0.5012, PIN2-3-3 vs. PIN2-3-3 + PINOID n.s. p-value 0.1321, PIN2-3-3 + D6PK vs. PIN2-3-3 + PINOID n.s. p-value 0.5433. PIN2*-3-3 vs. PIN2*-3-3 + D6PK n.s. p-value 0.3773, PIN2*-3-3 vs. PIN2*-3-3 + PINOID n.s. p-value 0.3448, PIN2*-3-3 + D6PK vs. PIN2*-3-3 + PINOID n.s. p-value 0.9967. (C) Point mutations of S293 and S294 in the loop domain of PIN3 (red dots). Phospho-dead (StoA) or phospho-mimick (StoD) variants were tested for their IAA transport properties. (D) Representative time-course experiment for PIN3, PIN3-S294A, PIN3-S293A-S294A and PIN3-S293D-S294D. PINs were expressed alone (black symbols) or co-expressed with PINOID (white symbols) in oocytes. Time points are mean and SE of n = 8-10 oocytes.

In order to see if the decrease in transport rates between PIN3 and PIN2-3-3 could be broken down to specific amino acid positions, the sequences of the first five helices were compared. An interesting amino acid in the short loop between helix M3 and M4a was identified (Figure 25 A). At position 95 in PIN2, the positively charged amino acid Arg is found and the uncharged polar amino acid Ser in PIN3. A sequence alignment with all PINs from Arabidopsis revealed that this position is not conserved in any PIN (Ung *et al.*, 2022). Because the amino acid is accessible for the kinases and might be necessary for PIN-kinase interaction, the positions 93–95 (TRS vs. SRR) were exchanged against each other as indicated in PIN3 and PIN2-3-3, creating the point mutations PIN3* and PIN2*-3-3. The mutated PIN variants were tested in the oocyte transport assay.

In this data set, PIN3 showed strong transport activation by D6PK or PINOID as expected, but the kinase preference for PINOID that was reported before, was not visible in the three replicates (Figure 25 B, Figure 7 H). The PIN3* mutant transported IAA upon co-expression of D6PK or PINOID and showed a significantly higher transport rate with PINOID compared to D6PK. Overall, the transport rates of PIN3 and PIN3* were comparable, suggesting that the amino acid exchange did not alter the transporter's activity.

The PIN2-3-3 chimera showed a moderate transport activation with co-expressed D6PK or PINOID. The transport rates were higher with PINOID than with D6PK. By mutating the indicated positions to TRS (from SRR) in PIN2*-3-3, only the activation by PINOID was reduced to the same levels as the activation by D6PK. The D6PK-mediated activation was not altered.

Personal communication by Dr. Ive de Smet (Ghent University/VIB, Belgium) and the phospho-proteomics screen (Figure 9 F) suggested the positions Ser293 and Ser294 in the loop domain of PIN3 as potentially interesting phosphorylation sites. Phospho-dead variants PIN3-S294A and PIN3-S293A-S294A, as well as the phospho-mimicking variant PIN3-S293D-S294D were created. All PIN3 variants were tested in the oocyte assay with respect to their transport properties upon co-

expression of PINOID (Figure 25 C, D). They were identical to PIN3 without mutations, with IAA transport rates of 0.1-1.0 % x min^{-1} for PIN without kinase and 3.9 % x min^{-1} for PIN + PINOID, suggesting that S293 and S294 were no important phospho-sites for the transporter's activity.

3.2.6 Adoption of canonical PIN features by providing a canonical loop domain to the noncanonical PIN8

Noncanonical PINs can be provided with cell-biological features of canonical PINs by inserting the loop domain of a canonical PIN into the TM domain context of noncanonical PINs, as shown for PIN5 (Ganguly *et al*., 2014). PIN8 is closer related to canonical PINs from an evolutionary point (Bennett *et al.*, 2014) and Martina Kolb (TUM) created PIN chimeras of PIN8, PIN2 and PIN3 (Kolb, 2015). She inserted the PIN2 or the PIN3 loop into the short amino acid stretch that connects TM helices M5 and M6 of PIN8. Transport studies in Xenopus oocytes revealed PIN8 as a constitutively active IAA transporter (Ung *et al.*, 2022). PIN8-mediated transport is insensitive to kinase co-expression. The PIN8 chimeras became kinase-sensitive by providing the PIN2 or PIN3 loop domain. The PIN2 loop could not block the constitutive transport component of PIN8 and co-expression of D6PK did not further activate the transporter, but the transport rate was increased upon co-expression of PINOID. The PIN8-3-8 chimera did not transport IAA without kinase and transport was activated by D6PK or PINOID. In order to investigate if the insertion of the PIN1 loop blocks the intrinsic PIN8 transport component and if the transporter becomes kinase-regulatable by D6PK, the PIN8-1-8 chimera was included. The transport data are published in Janacek *et al.*, 2023, under review.

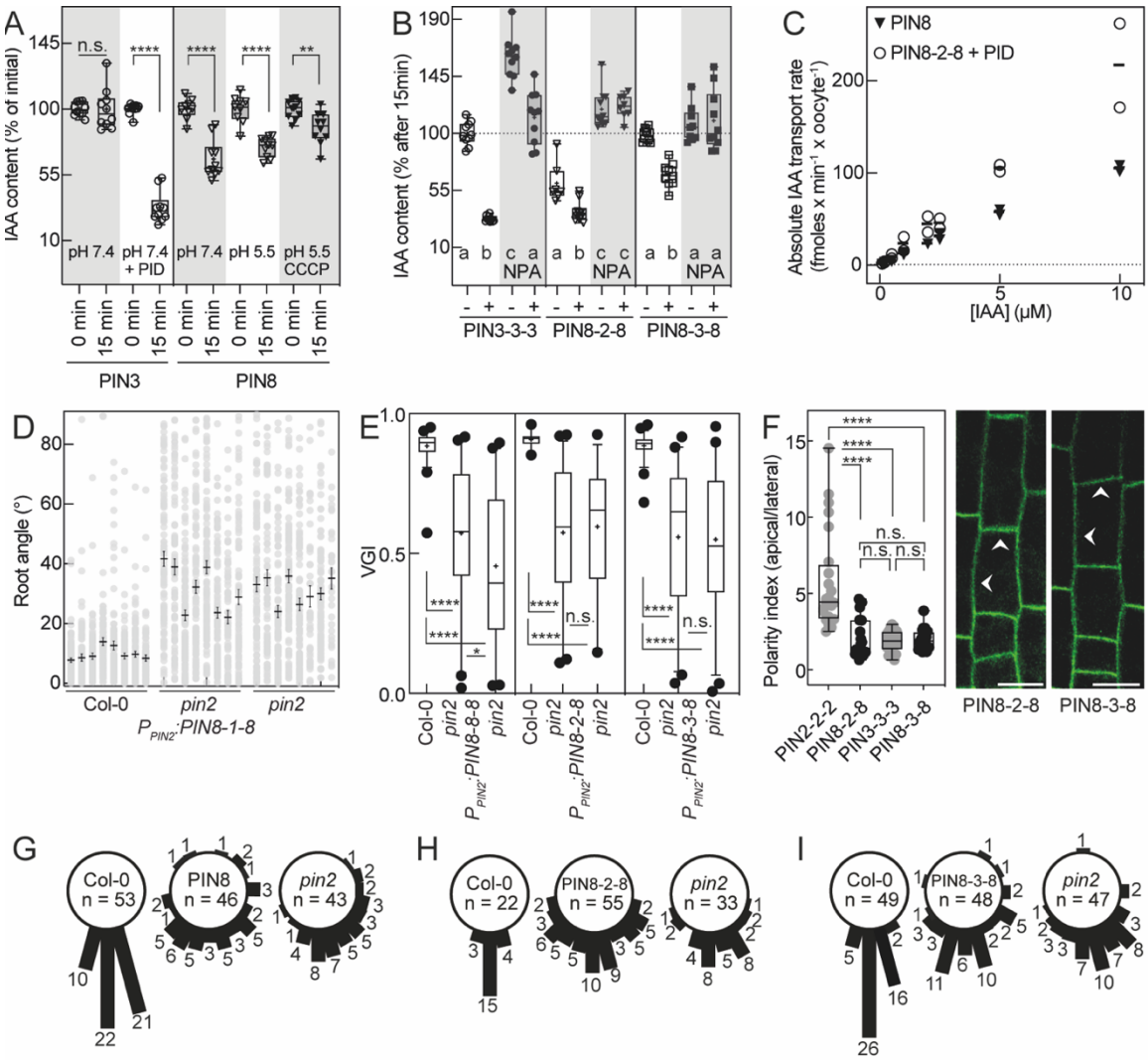
A
IAA content (% of initial)
n.s.
****
****
****
**
pH 7.4
pH 7.4 + PID
pH 7.4
pH 5.5
pH 5.5 CCCP
0 min
15 min
PIN3
PIN8
B
IAA content (% after 15min)
a b c a a b c c a b a a
NPA
PIN3-3-3
PIN8-2-8
PIN8-3-8
C
PIN8
PIN8-2-8 + PID
Absolute IAA transport rate (fmoles x min-1 x oocyte-1)
[IAA] (µM)
D
Root angle (°)
Col-0
pin2
pin2
PPIN2:PIN8-1-8
E
VGI
Col-0
pin2
PPIN2:PIN8-8-8
pin2
PPIN2:PIN8-2-8
PPIN2:PIN8-3-8
n.s.
F
Polarity index (apical/lateral)
PIN2-2-2
PIN8-2-8
PIN3-3-3
PIN8-3-8
PIN8-2-8
PIN8-3-8
G
Col-0 n = 53
PIN8 n = 46
pin2 n = 43
H
Col-0 n = 22
PIN8-2-8 n = 55
pin2 n = 33
I
Col-0 n = 49
PIN8-3-8 n = 48
pin2 n = 47

Figure 26 – IAA transport properties and ability to rescue the *pin2* phenotype and localization of PIN8 and the chimeras. (A) PIN3 (circles) alone or with PINOID and PIN8 (triangles) were expressed in oocytes. IAA efflux properties were tested at pH 7.4 for PIN3 and at pH 7.4 and 5.5 for PIN8. Uncoupler CCCP was tested on PIN8-mediated efflux at pH 5.5. The IAA content after 15 min was compared to the initial IAA content by unpaired two-tailed t-test (PIN3: n.s. not significant p-value >0.9999, **** p-value <0.0001. PIN8: ** p-value 0.0049, **** p-value <0.0001). Each data point is one oocyte (n = 9-10). Box plots range from 25th to 75th percentiles, whiskers mark the minimum and maximum values and the median is indicated. The mean is indicated by (+). (B) PIN3 (circles), PIN8-2-8 (triangles) and PIN8-3-8 (squares) alone (-) or with PINOID (+) were expressed in oocytes. Oocytes were injected with radioactive IAA (white symbols) or radioactive IAA + NPA (black symbols). The IAA content after 15 min of PIN3 was set to 100 % and the IAA content of the indicated samples at the endpoint of the experiment were compared to this. Data points resemble individual oocytes (n = 7-10). Box plots ranges from 25th to 75th percentiles, whiskers mark the minimum and maximum values and the median is indicated. The mean is indicated by (+). Each PIN group (PIN3, PIN8-2-8, PIN8-3-8) was compared by one-way ANOVA followed by Tukey's posthoc test. Statistical groups are indicated by letters. (C) Transport rates as function of $[IAA]_{in}$. Data are mean and SE of n = 2. (D) Root angle of independent segregating T2 lines (n = 8) between root tip and gravity vector of *pin2;*P_{PIN2}*:PIN8-1-8* (n = 76-116) in comparison to wildtype (n =89-103) and mutant (n =41-103). Data points are individual seedlings. The mean and SE are indicated. (E) VGI of the homozygous T3 line of *pin2;*P_{PIN2}*:PIN8*, *pin2;*P_{PIN2}*:PIN8-2-8*, and *pin2;*P_{PIN2}*:PIN8-3-8* (n = 46 for PIN8, n = 55 for PIN8-2-8, n = 48 for PIN8-3-8) in comparison to wildtype (n = 53 for PIN8, n = 22 for PIN8-2-8, n = 49 for PIN8-3-8) and mutant (n = 43 for PIN8, n = 33 for PIN8-2-8, n = 47 for PIN8-3-8). Box plots range from 25th to 75th percentiles, whiskers mark the 5th and 95th percentiles and the median is indicated. Points below and above the whiskers are drawn as individual points. The mean is indicated by (+). Groups were compared by one-way ANOVA followed by Tukey's posthoc test. n.s. not significant p-value 0.8804 (PIN8-2-8), 0.9751 (PIN8-3-8), * p-value 0.0225, **** p-value <0.0001. (F) Polarity index of eGFP-tagged PIN8-2-8, PIN8-3-8 expressed from a *PIN2* promoter fragment in epidermal cells in the *pin2* mutant. Loop domain donors PIN2 and PIN3 were included for comparison as presented in Figure 12. Mean intensities of ROIs at the apical and the lateral side of the cells were used to calculate the ratios. The arrows mark GFP signal. Scale bar represents 20 µm. Box plots range from 25th to 75th percentiles, whiskers mark the minimum and maximum values and the median is indicated. Groups were compared by a one-way ANOVA, followed by Tukey's posthoc test. **** p-value <0.0001, n.s. not significant p-value 0.9749 (PIN8-2-8 vs. PIN3), 0.9953 (PIN8-2-8 vs. PIN8-3-8), 0.9978 (PIN8-3-8 vs. PIN3). n = 24 cells per genotype. (G-I) Root angles between root tip and gravity vector of the representative homozygous T3 line of *pin2;*P_{PIN2}*:PIN8*, *pin2;*P_{PIN2}*:PIN8-2-8* and *pin2;*P_{PIN2}*:PIN8-3-8* in comparison to wildtype and mutant. Numbers are individual seedlings.

In order to see if PIN8-mediated IAA transport shows indications for a proton-coupled mechanism, the oocyte transport assay was performed at pH 7.4 and pH 5.5 (Figure 26 A). If the transport mechanism was dependent on protons, the transport rate should increase at lower pH values and decrease if the proton gradient over the membrane is reduced. Upon co-expression of PINOID, in oocytes expressing PIN3 the IAA content was reduced to 33 % of the initial IAA content after 15 min. PIN8-expressing oocytes contained 66 % of initial IAA at pH 7.4 and 74 % at pH 5.5. To dissipate the proton gradient across the membrane, the decoupler CCCP was co-injected with IAA at a pH_{Ext} of 5.5. After 15 min, 87 % of the initial IAA content were present in PIN8-expressing oocytes at pH 5.5. For all conditions, the IAA content after 15 min was significantly reduced compared to the initial content, suggesting that the transport mechanism is independent of the proton gradient as transport driving force.

The transport studies conducted by Martina Kolb (Kolb, 2015) suggested that the PIN8-2-8 chimera, like PIN8, transports IAA constitutively. PIN8-3-8, however, did not show this property. Therefore, the effect of the auxin transport inhibitor NPA (Abas et al., 2021) was tested on PIN8-2-8 and PIN8-3-8 mediated IAA transport (Figure 26 B).

IAA levels at the end of the experiment were presented relative to the IAA content of PIN3 at the end of the 15 min experiment. The data showed that PIN8-2-8, like PIN8 exhibited constitutive NPA-sensitive IAA transport. Expression of PIN3 + PINOID reduced the initial IAA content to 33 %. What looked like an increased IAA content in Figure 26 B was a methodological artefact (see Chapter 2.3.1). PIN8-2-8 showed constitutively active transport after 15 min with an IAA content of 61 %, that was increased by PINOID co-expression and resulted in an IAA content of 38 %. Co-injection of IAA and NPA into PIN8-2-8 and PIN8-2-8 + PINOID expressing oocytes shut down the IAA transport. By providing the PIN3 loop, PIN8-3-8 lost its active transport component. Co-expression of PINOID was needed to activate the IAA transport. After 15 min, 67 % of the initial IAA content were detectable. The injection of NPA blocked the PIN8-3-8-mediated transport completely. The data indicated that all PIN8 chimeras behave like wildtype PIN8 in terms of transport inhibition by NPA and that the NPA binding site lays within the TM domains, what was proven by the cryo-EM structure of PIN8 (Ung *et al.*, 2022).

PIN8 is, besides PIN6, one of the two PIN from Arabidopsis that shows constitutive transport. The kinetic studies performed on SSM.SURFER revealed that PIN8-mediated transport can be described by a Michaelis-Menten equation with K_m = 356 ± 136 µM and K_d = 39.9 ± 14.9 µM in presence of NPA with PIN8 reconstituted in liposomes (Ung *et al.*, 2022).

The SURFER data are problematic because the limit of detection falls in the range of the physiological IAA concentrations. The oocyte transport assay can be used at low concentration with higher sensitivity compared to the SURFER. PIN8-mediated IAA transport was tested as a function of IAA concentration in a concentration range between 0.1-10 µM IAA. PIN8-mediated IAA transport showed a linear relationship to the IAA concentration with a transport rate of 10.6 ± 0.3 fmoles x min^{-1} x $oocyte^{-1}$ (Figure 26 C). This was three times faster as PIN1 + D6PK (3.1 ± 0.1 fmoles x min^{-1} x $oocyte^{-1}$) and twice as fast as PIN1 + PINOID (5.4 ± 0.8 fmoles x min^{-1} x $oocyte^{-1}$), see Table 8.

In order to analyze if the relationship between transport rate and IAA concentration is linear or within the apparently linear range of a Michaelis-Menten kinetic, the defaults settings of GraphPad Prism to compare both models statistically were used. It was found that the preferred model for PIN8 was indeed the Michaelis-Menten equation with a K_m of 48.9 µM and a 95 % confidence interval from 28.4 to 134.5 µM. This fitted well with the K_d value of PIN8 in liposomes established later in Ung *et al*. The preferred model for PIN3 + D6PK was also the Michaelis-Menten equation with a K_m of 143.3 µM, three times lower than the K_m of PIN8 for IAA, but rather low confidence. Interestingly this value is in good agreement with the K_d of PIN3 = 160.4 µM observed in a recent study (Su *et al.*, 2022). For the other combinations of PIN1, PIN2 and PIN3 with D6PK or PINOID, the comparison revealed a linear correlation as preferred model, which is likely due to the much lower

transport rates of these transporters compared to PIN3 and/or larger variability of the underlying data, as co-expression of PINOID reduced the affinity of PIN3 towards IAA further and increased the transport rate. This suggests that the affinity for IAA in canonical PINs can be modulated by the activating kinase, most likely by interaction with the loop domain.

In experiments performed at $[IAA]_{in}$ = 1 µM, PIN8-2-8 + PINOID showed similar transport properties to PIN3 + PINOID. PIN8-2-8-mediated IAA transport was tested as a function of IAA concentration in a concentration range between 0.1–10 µM. Like the domain donors PIN8 and PIN2, transport of PIN8-2-8 + PINOID showed a linear relationship to the IAA concentration, but no K_m value could be fitted. The transport rate was 21.6 ± 1.4 fmoles x min^{-1} x $oocyte^{-1}$ and therefore as high as PIN3 + PINOID. This suggests that providing a noncanonical PIN with a canonical PIN loop domain transfers canonical transport characteristics, like the regulation by kinases and the different kinetic properties of the transporter.

In order to check the potential of the PIN8-1-8 chimera to complement, it was expressed from a *PIN2* promoter fragment in the *pin2* mutant. As described before, the root angle between the root tip and the gravity vector was used as read-out (Figure 26 D). None of the lines investigated rescued the agravitropic root of the *pin2* mutant. One representative T2 line of PIN8, PIN8-2-8 and PIN8-3-8 generated by Martina Kolb was used to establish homozygous T3 lines. The VGI of *pin2;*P_{PIN2}*:PIN8* seedlings was significantly increased compared to the *pin2* mutant, but did not reach wildtype levels (Figure 26 E). In this data set, the VGI of the *pin2* mutant was relatively high. The VGIs of *pin2;*P_{PIN2}*:PIN8-2-8* and *pin2;*P_{PIN2}*:PIN8-3-8* were comparable to *pin2;*P_{PIN2}*:PIN8* seedlings. By analyzing the root angle of the homozygous seedlings, it became also clear that the three PINs did not reduce the *pin2* mutants' variability of the root angle (Figure 26 G, H, I). The eGFP-tagged PIN8-2-8-eGFP and PIN8-3-8-eGFP chimeras localized non-polarly. The signal was solely detected at the apical and lateral side of the PM and not in internal membranes. This suggests that the positional information for the PIN to localize at the PM was provided by the canonical PIN loop domains. Martina Kolb and me could not succeed in generating *pin2;*P_{PIN2}*:PIN8-eGFP* transformant lines.

The analyses of canonical PIN chimeras in the biochemical transport assay and in the physiological root assay showed that the characteristics of the loop domain go beyond the idea of a regulatory switch and localization navigator of PINs. It became obvious that the PIN TM domains and the loop domain mediate the IAA transport together and should not be interpreted separately from each other. Although, the non-canonical PIN8 could be equipped with canonical PIN features (transport properties and localization) by providing a loop domain, the biochemical properties were not sufficient to give physiological relevance.

The results presented here showed that the transport characteristics of PINs are neither solely embedded in the TM domains nor in the loop domain. The protein domains are very likely to interact with each other.

3.3 Impact of AGC kinases on PIN-mediated transport

AGCVIII kinases from *Arabidopsis thaliana* are important in plant developmental processes, because they directly impact PIN-mediated IAA transport. The phenotypes of some family members, like D6PK and PINOID, resemble the *pin1* mutant phenotype, so it was hypothesized and successfully shown that the kinases act in the same pathway as the PINs (Gälweiler *et al.*, 1998; Zourelidou *et al.*, 2014). The phosphorylation of PINs by AGCVIII kinases is necessary to activate the transport. Although the impact of some members on PINs and their cell-biological features have been extensively studied, not all kinases are able to activate PIN-mediated transport to the same level (Zourelidou *et al.*, 2014; Marhava *et al.*, 2018). The reasons are not yet clear and further investigations are needed. The impact of kinases on PIN-mediated IAA transport can conveniently be studied in the reductionist oocyte transport assay. Several kinases from the AGCVIII family or the MAP kinase family and potential regulators of kinases were tested upon their impact on PIN1, PIN2 and PIN3.

3.3.1 D6PK-LIKE1, D6PK-LIKE2 and D6PK-LIKE3

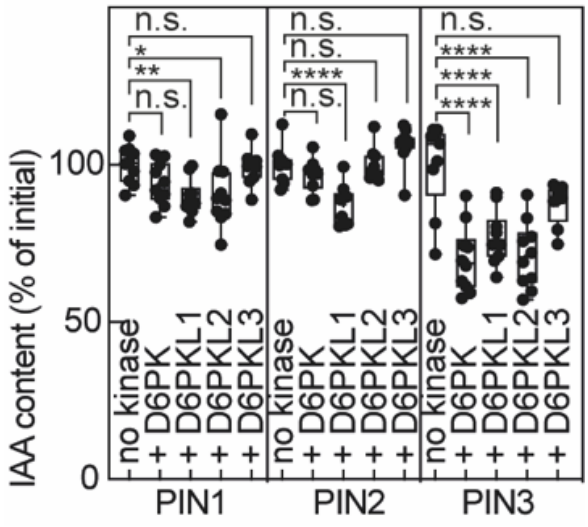

Figure 27 – IAA transport activation by D6PK-LIKE1, D6PK-LIKE2 and D6PK-LIKE3. PIN1, PIN2 and PIN3 were expressed in oocytes alone or co-expressed with D6PK, D6PK-LIKE1, D6PK-LIKE2 or D6PK-LIKE3. The IAA content after 30 min for PIN1 and PIN2, and after 15 min for PIN3, without co-expressed kinase was set to 100 % and the IAA content of PIN + kinase was compared to that by one-way ANOVA followed by Dunnett's test with PIN without kinase as control group (PIN1: + D6PK, n.s., not significant, p-value 0.2209. + D6PK-LIKE1, ** p-value 0.0089. + D6PK-LIKE2, * p-value 0.0237. + D6PK-LIKE3 n.s. p-value 0.9985; PIN2: + D6PK, n.s. p-value 0.5092. + D6PK-LIKE1, **** p-value <0.0001. + D6PK-LIKE2, n.s. p-value >0.9999. + D6PK-LIKE3 n.s. p-value 0.0800; PIN3: + D6PK, **** p-value <0.0001. + D6PK-LIKE1, **** p-value <0.0001. + D6PK-LIKE2, **** p-value <0.0001. + D6PK-LIKE3 n.s. p-value 0.0581). Each data point is one oocyte (n = 8-10). Box plots range from 25th to 75th percentiles, whiskers mark the minimum and maximum values and the median is indicated.

D6PK-LIKE1, D6PK-LIKE2 and D6PK-LIKE3 are closely related to the intensively studied AGC1 kinase D6PK. They act most likely redundantly *in planta* and higher-order mutants of D6PK and D6PK-LIKEs are required to generate Arabidopsis mutants with pronounced phenotypes (Zourelidou *et al.*, 2009). Especially D6PK-LIKE1 is present in the whole plant body compared to all AGC1 kinases, followed by D6PK-LIKE2 (Mergner *et al.*, 2020). In order to test the effect of the D6PK-LIKEs on PIN-mediated transport, D6PK and the three D6PK-LIKEs were tested on PIN1, PIN2 and PIN3 in the oocyte assay (Figure 27). D6PK-mediated activation of PIN1 and PIN2 was small and not statistically significant in this data set. The activation of PIN3 was strong. More data for D6PK on PIN1, PIN2 and PIN3 is presented in Figure 7. D6PK-LIKE1 activated PIN3-mediated IAA transport to comparable levels as D6PK did. The activation of PIN1 was slightly stronger compared to D6PK and significantly different to PIN1 without kinase. The activation of PIN1 by D6PK-LIKE2 was comparable to D6PK-LIKE1. On PIN2, D6PK-LIKE1 had the strongest impact of all D6PK-LIKEs. PIN2 showed no IAA transport upon D6PK-LIKE2 co-expression. The combination of PIN3 and D6PK-LIKE2 was as strong as PIN3 and D6PK. Interestingly, D6PK-LIKE3 co-expression had very little effect on the three PINs. PIN1 and PIN2 were not activated at all and the activation of PIN3 was reduced. That suggests that the four D6PK kinases act differently on PIN-mediated IAA transport, although they are very closely related and supposed to act redundantly *in planta*.

3.3.2 PAX, variants of PAX and PDK1 as regulator of PAX

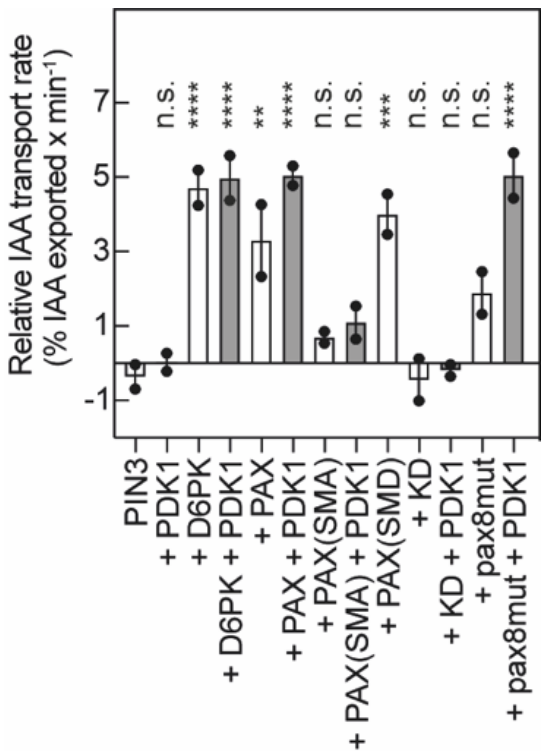

Figure 28 – Impact of PDK1 and PAX variants on PIN3-mediated IAA transport. Relative transport rates of PIN3 upon activation by D6PK or PAX variants (white bars), co-expressed with PDK1 as regulator of PAX (gray bars). PAX(SMA) is a non-activatable variant of PAX with a mutation in the activation loop. PAX(SMD) is a constitutively active variant. KD is the kinase-dead variant of PAX with a mutation in the ATP cleavage site. Pax8mut is a variant with phospho-dead mutations of ten residues. Data points are transport rates of n = 2 for all indicated constructs. The mean and SE are indicated. Groups were analyzed by one-way ANOVA, followed by Dunnett's test against PIN3 without kinase as control. + PDK1: n.s., not significant, p-value 0.9971. + D6PK: **** p-value <0.0001. + D6PK + PDK1: **** p-value <0.0001. + PAX: ** p-value 0.0017. + PAX + PDK1: **** p-value <0.0001. + PAX(SMA): n.s. p-value .0.6731 + PAX(SMA) + PDK1: n.s. p-value 0.3404. + PAX(SMD): *** p-value 0.0003. + KD: n.s. p-value 0.9999. + KD + PDK1: n.s. p-value 0.9997. + pax8mut: n.s. p-value 0.0547. + pax8mut + PDK1: **** p-value <0.0001.

The AGC kinases activate PIN-mediated IAA transport differently, exemplified by the AGC1 kinase D6PK and the AGC3 kinase PINOID (Figure 7). Within the AGC1 clade, the difference was more pronounced for the kinases PAX and D6PK (Marhava *et al.*, 2018). The kinase availability at the PM can be modulated by factors like BRX inhibiting the kinase through binding, or other kinases that are needed to get the full kinase activity. One proposed regulator of PAX is PDK1 (Xiao and Offringa, 2020). The direct effect of PDK1 on PIN3 was tested. Further, it was investigated how PDK1 modulates D6PK or different PAX variants to activate PIN3-mediated IAA transport (Figure 28, constructs provided by A. E. Lanassa Bassukas, TUM). PDK1 was not able to activate PIN3. It had no effect on D6PK-mediated IAA transport, but could increase PAX-mediated activation of transport. A phospho-dead PAX mutant with a S to A mutation (PAX(SMA)) in the kinase activation loop could not activate IAA transport and this could not be overcome by PDK1 co-expression. However, the phospho-mimic PAX variant with a S to D mutation (PAX(SMD)) at the same position activated PIN3 similar to PAX. As expected, the kinase dead variant of PAX (KD) with a mutation in the ATP cleavage site could not activate transport, also upon PDK1 co-expression. A PAX variant with ten phospho-dead mutations to Ala (pax8mut, mutated at S15, S68, S131, S137, S138, T227, S269, S316, S735 and S737) showed reduced activation of transport compared to PAX, but the transport rate was increased to PAX levels by co-expression of PDK1.

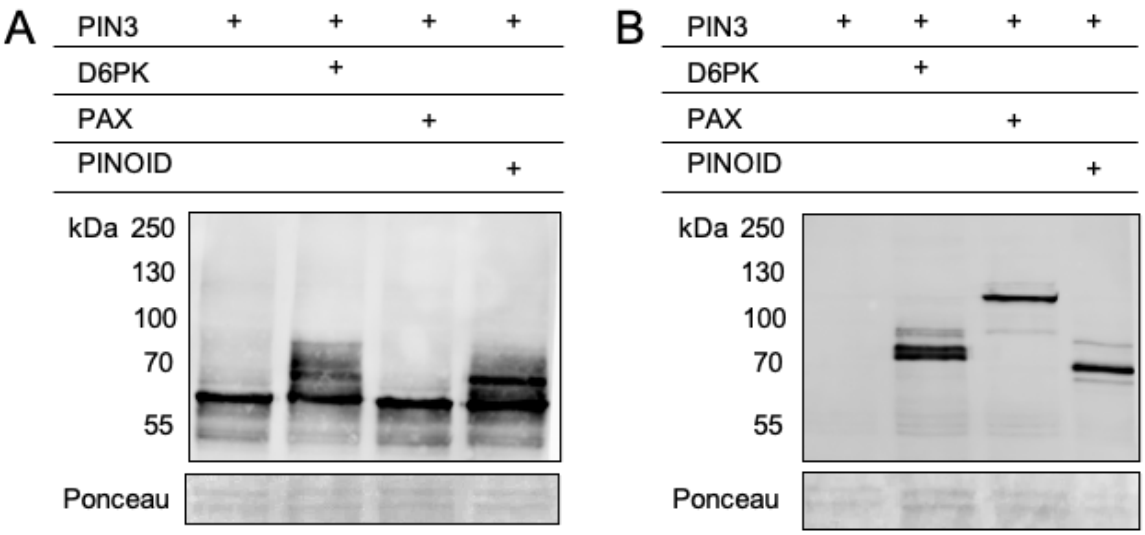

Figure 29 – Immunoblot analysis of PIN3 and its activating kinases. PIN3 was expressed in oocytes either alone or co-expressed with YFP-D6PK, YFP-PAX or YFP-PINOID. (A) The membrane fraction of oocytes was used to detect PIN3 (69 kDa) by anti-PIN3 antibody in oocytes expressing PIN3 or PIN3 and indicated kinases. Loading is shown by a section of the Ponceau-stained membrane. (B) The kinases were detected in the membrane fraction of oocytes expressing the indicated proteins by an anti-GFP antibody. The PIN3 sample was included as control. YFP-D6PK: 82 kDa. YFP-PAX: 112 kDa. YFP-PINOID: 76 kDa. Equal loading is shown by a section of the Ponceau-stained membrane.

In order to check if the kinases D6PK, PAX and PINOID were expressed to same levels in oocytes, the kinases were tagged with eYFP. The membrane fraction of oocytes expressing the indicated protein(s) were analyzed in an immunoblot (Figure 29).

Differences in the overall phosphorylation of PIN3 caused by the kinases were detectable (Figure 29 A). PIN3 alone or together with YFP-D6PK, YFP-PINOID or YFP-PAX were expressed in oocytes. PIN3 was detected in the membrane fraction of oocytes and revealed, that YFP-D6PK and YFP-PINOID strongly phosphorylated the PIN3 loop domain. The phosphorylation by YFP-PAX was not visible on the immunoblot membrane. From phospho-proteomics analyses performed by A. E. Lanassa Bassukas (TUM) and Dr. Julia Mergner (MRI/BayBioMS), it is known that PAX phosphorylates PIN3 *in planta*. All three kinases were detected at the expected protein size to similar levels in the membrane fraction of oocytes (Figure 29 B) and in the cytosolic fraction (immunoblot not shown). The missing phospho-smear of PIN3 suggests that PAX interacts differently with the transporter compared to D6PK or PINOID.

3.3.3 AGC1.7

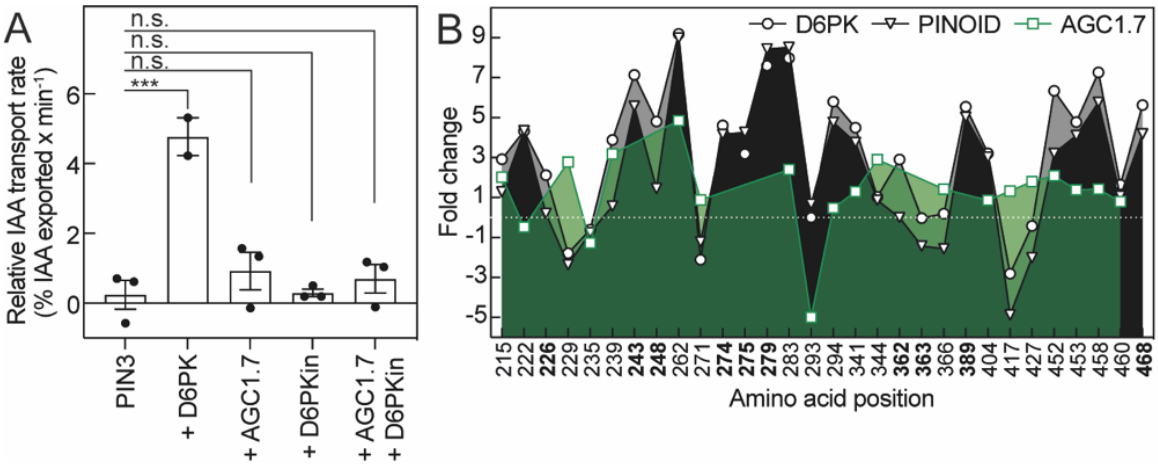

Figure 30 – PIN3-mediated transport activation by AGC1.7 and phosphorylation sites in PIN3. (A) Relative IAA transport rates of PIN3 expressed in oocytes alone or co-expressed with D6PK, AGC1.7, an inactive D6PK variant or AGC1.7 and inactive D6PK together. Data points are transport rates of n = 2-3. The mean and SE are indicated. The groups were compared by one-way ANOVA, followed by Dunnett's test against PIN3 without kinase as control. + D6PK: *** p-value 0.0002. + AGC1.7: n.s., not significant, p-value 0.6079. + D6PKin: n.s. p-value 0.9999. + AGC1.7 + D6PKin: n.s. p-value 0.8455. (B) Phosphorylated sites in PIN3 by D6PK (○), PINOID (▽) or AGC1.7 (□) in comparison to PIN3 without kinase after phospho-peptide enrichment by IMAC. Data for D6PK and PINOID are shown for comparison and explained in Figure 9 F. The bold amino acid positions were only detected upon D6PK or PINOID expression and were not found in the analysis for AGC1.7.

AGC1.7 is known to phosphorylate the PIN1 loop in *in vitro* kinase assays (unpublished data by Ass. Prof. Dr. Hiromasa Shikata, NIBB, Okazaki, Japan), and could activate PIN1-mediated IAA efflux from Xenopus oocytes to very small levels (Martina Kolb, TUM).

Members of the same clade of AGC kinases activated the IAA transport very differently, i.e. D6PK very strong activation, PAX intermediate activation. In order to check if AGC1.7 could activate PIN3-mediated IAA transport, PIN3 and the indicated kinases were expressed in Xenopus oocytes. To check whether the PIN phosphorylation and the interaction of PIN and kinase can be separated in such a scenario, an inactive variant of D6PK (D6PKin) was used in the transport assay (Figure 30 A) (Zourelidou *et al.*, 2014). The hypothesis was that AGC1.7 phosphorylates PIN3 as a requirement for transport but could not interact with the primed PIN to mediate transport. If the interaction of a kinase with the PIN is necessary to transport, the inactive D6PK could have interacted with the primed PIN instead.

PIN3 was activated to expected levels by D6PK and not activated by the inactive D6PK. The co-expression of AGC1.7 did not significantly activate the IAA transport. By co-expressing the inactive D6PK and AGC1.7 together with PIN3, the findings were similar to the PIN3 + AGC1.7 scenario. This suggests that phosphorylation and interaction could not be separated in this experimental setup and the hypothesis was rejected.

A phospho-proteomic analysis of PIN3 with AGC1.7 in comparison to D6PK and the AGC3 kinase PINOID revealed, that most of the phosphorylated positions were detectable with all three kinases (20 of 30 phospho-sites). The position Thr229 was more phosphorylated by AGC1.7 compared to PIN3 without kinase, whereas in presence of DP6PK and PINOID, this site was less phosphorylated than PIN3 without kinase. Only the position Ser293 was less phosphorylated in PIN3 upon AGC1.7 expression and almost not phosphorylated by D6PK and PINOID. The overall phosphorylation from position 341 to 460 was more constant with AGC1.7 than with D6PK or PINOID. The position 417 that was significantly less phosphorylated with D6PK and PINOID (Figure 9) suggested an oocyte-specific kinase that can phosphorylate this site in absence of D6PK or PINOID, or a sterical hindrance of this phospho-site either by direct interaction of PIN loop and kinase or by steric effects on the PIN loop structure by phosphorylation events at other positions. In oocytes expressing PIN3 + AGC1.7, this site was stronger phosphorylated compared to PIN3 without kinase. Suggesting that this position can be phosphorylated by AGC kinases and that the PIN-kinase-interaction is different with AGC1.7 compared to D6PK or PINOID. The differences in the phosphorylation pattern seemed to be more pronounced in the second half of the PIN loop domain.

3.3.4 AGC1.8, AGC1.9, KIPK and chimeras of AGC1.8 and KIPK

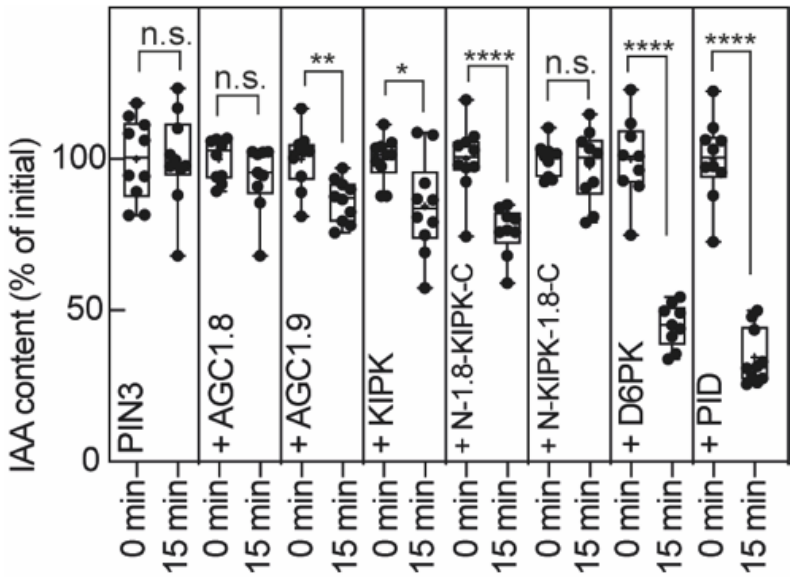

Figure 31 – IAA transport activation by AGC1.8 and KIPK kinase chimeras. The N-terminus of KIPK was replaced by the N-terminus of AGC1.8 and vice versa, creating the kinase chimeras N-1.8-KIPK-C and N-KIPK-1.8-C. PIN3 was expressed in oocytes either alone or co-expressed with AGC1.8, AGC1.9, KIPK, N-1.8-KIPK-C, N-KIPK-1.8-C, D6PK or PINOID. The initial IAA content was set to 100 % and the IAA content after 15 min was compared to it by two-tailed t-test (PIN3: n.s., not significant, p-value >0.999, + AGC1.8: n.s. p-value 0.1561, + AGC1.9: ** p-value 0.0020, + KIPK: * p-value 0.0119, + N-1.8-KIPK-C: **** p-value <0.0001, + N-KIPK-1.8-C: n.s. p-value 0.5772, + D6PK: **** p-value <0.0001, + PINOID: **** p-value <0.0001). Each data point is one oocyte (n = 9-10). Box plots show the 25th and 75th percentiles, whiskers mark the minimum and maximum values. The line in the box represents the median.

In order to investigate why the kinases activated PIN transport differently, kinase chimeras of KIPK and AGC1.8 were tested. The N-terminus was exchanged against each other and tested on PIN3-mediated transport (constructs provided by Dr. Yao Xiao, TUM). Additionally, the kinase AGC1.9 that is closely related to KIPK was tested (Figure 31). The IAA content after 15 min was compared to the initial IAA content that was set to 100 %.

PIN3 without kinase did not transport IAA. The co-expression of AGC1.8 did not activate transport. AGC1.9 could activate the transporter significantly and to similar levels as KIPK. Interestingly, the kinase chimeras behave like the kinase domain donor: N-1.8-KIPK-C activated the transporter and N-KIPK-1.8-C did not. None of the investigated kinases could activate PIN3 to the same levels as D6PK or PINOID. This suggests that kinase chimeras are functional activators of PIN-mediated IAA transport. The kinase domain seemed to be biochemically important, whereas the N-terminus might have a more important physiological role *in planta*.

3.3.5 MAP kinases

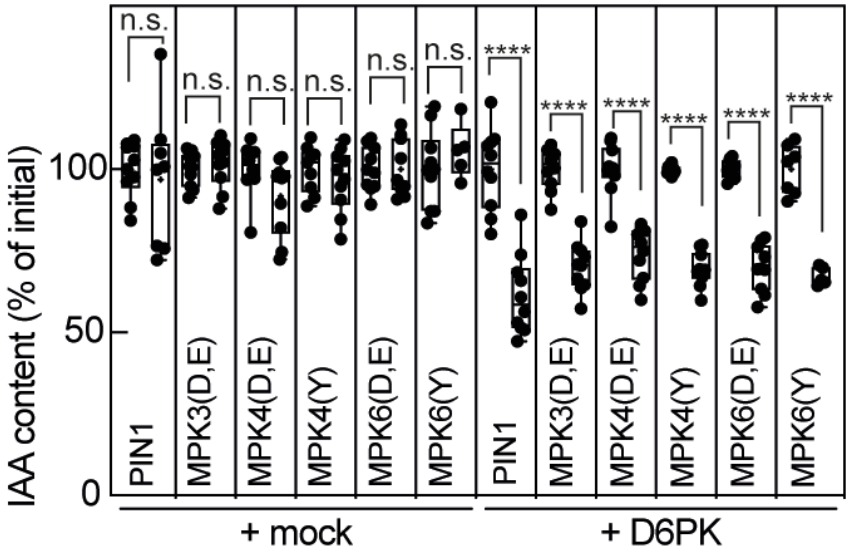

Figure 32 – IAA transport activation by MAP kinases. PIN1 was expressed alone or co-expressed with MPK3, MPK4 or MPK6 in oocytes. The MAP kinases were also co-expressed with PIN1 and D6PK. MAP kinases were constitutively active variants. MPK3(D,E): MPK3 D193G E197A. MPK4(D,E): MPK4 D198G E202A. MPK4(Y): MPK4 Y124C. MPK6(D,E): MPK6 D218G E222A. MPK6(Y): MPK6 Y144C. The first box represents the IAA content at the beginning of the experiment and was set to 100 %. The second box is the IAA content after 30 min. Each data point is one oocyte (n = 5-10). Box plots show the 25th and 75th percentiles, whiskers mark the minimum and maximum values. The line in the box represents the median. Groups were compared by two-tailed t-test. PIN1: n.s., not significant, p-value 0.6699. PIN1 + MPK3(D,E): n.s. p-value 0.5661. PIN1 + MPK4(D,E) n.s. p-value 0.0791. PIN1 + MPK4(Y): n.s. p-value 0.4218. PIN1 + MPK6(D,E): n.s. p-value 0.9955. PIN1 + MPK6(Y): n.s. p-value 0.3645. PIN1 + D6PK: **** p-value <0.0001. PIN1 + D6PK + MPK3(D,E): **** p-value <0.0001. PIN1 + D6PK + MPK4(D,E): **** p-value <0.0001. PIN1 + D6PK + MPK4(Y): **** p-value <0.0001. PIN1 + D6PK + MPK6(D,E): **** p-value <0.0001. PIN1 + D6PK + MPK6 (Y): **** p-value <0.0001.

Strong genetic evidence showed that MPKs alter PIN1 localization *in planta* (Dory *et al.*, 2018). Three target sites in canonical PINs were proposed to be the targets of MPKs. The direct impact of MPK3, MPK4 and MPK6 on PIN1-mediated IAA transport was tested. Also, the hypothesis that the MPKs were regulators of D6PK, comparable to PDK1 on PAX, were tested. For the transport assay, two constitutively active variants of MPK3, MPK4 and MPK6 were used (generated by Benedikt Pfeilschifter, now FAU). None of the MPKs could activate PIN1. Efflux was activated only by D6PK. The D6PK-activated PIN1-mediated transport was not impacted by any co-expressed MPK. This suggests that MPKs cannot activate PIN-mediated transport and do not regulate the AGC kinases upstream of PINs in a way that PIN transport would be affected.

3.3.6 WAG1 and CRK5

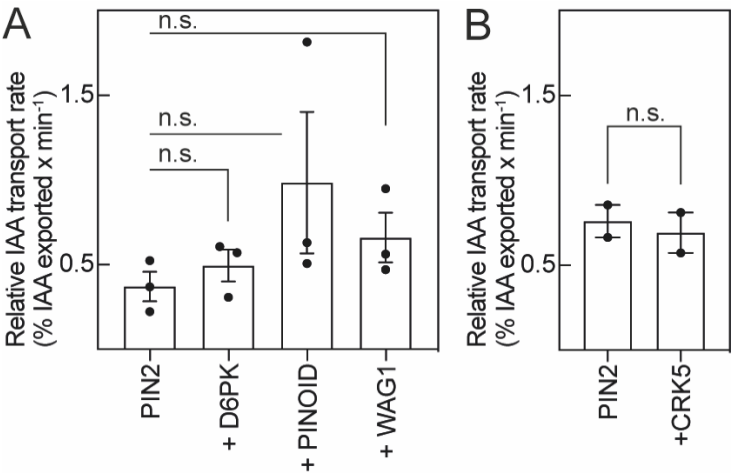

Figure 33 – Impact of WAG1 and CRK5 on PIN2-mediated IAA transport. (A) Relative IAA transport rates of PIN2 co-expressed with D6PK, PINOID or WAG1. Data points are n= 3. Mean and SE are indicated. Groups were compared by one-way ANOVA, followed by Dunnett's test against PIN2 without kinase as control. n.s., not significant. + D6PK: p-value 0.9637. + PINOID: p-value 0.2162. + WAG1: p-value 0.7154. (B) Relative IAA transport rates of PIN2 co-expressed with CRK5. Data points are n = 2. Mean and SE are indicated. Groups were compared by two-tailed t-test (n.s. p-value 0.7001).

Various cell-biological experiments showed that the PINOID-related kinase WAG1 and CRK5, a member of the Ca2+/Calmodulin-dependent kinase-related protein family, are important for the proper localization of PIN2 (Rigo *et al.*, 2013; Glanc *et al.*, 2018).

WAG1 and CRK5 were tested on their ability to activate the PIN2-mediated IAA transport (Figure 33). The IAA transport rate of WAG1-activated PIN2 was slightly but not significantly increased compared to D6PK, but not as high as activation by PINOID (Figure 33 A). CRK5 was not able to activate transport (Figure 33 B). This suggests that WAG1 and CRK5 are more important in a physiological context, then to activate IAA transport.

4 Discussion

Over the last four decades, cell biological studies of PINs as the main auxin efflux transporters generated extensive knowledge about their localization, their polarity control, their trafficking behavior and their reaction upon environmental cues. In 2022, major progress in the field was made by solving the molecular structures of PIN1, PIN3 and PIN8 (Su *et al.*, 2022; Ung *et al.*, 2022; Yang *et al.*, 2022). To this date, the transport properties of canonical PINs were barely investiaged. The understanding of auxin fluxes in plants requires knowledge about the transport properties of the canonical PINs and the impact of the activating kinases.

In order to connect the physiology and the structure of PINs, the transport characteristics of the canonical PINs were investigated using oocyte transport assays in this thesis. Additionally, the impact of the PIN transport properties on gravitropic root growth and on root bending kinetics were investigated. The protein abundance and the phosphorylation pattern of PIN1, PIN2 and PIN3 in Xenopus oocytes were analyzed by mass spectrometry. To understand how individual protein domains contribute to the transport, PIN chimeras were created in a domain swapping approach. Further, the ability of other kinase families than the AGCVIII family to activate PIN-mediated IAA transport was investigated.

4.1 The transport characteristics of PINs vary

4.1.1 PINs possess different transport properties

In 2014, activation of PIN-mediated IAA transport by AGCVIII kinases was demonstrated for the first time (Zourelidou *et al.*, 2014). In the study, oocytes from *Xenopus laevis* were used as heterologous expression system and differences in the transport rates of PIN1 and PIN3 at one cytosolic IAA concentration were presented, but not followed up further. The different transport rates of PIN1 and PIN3 could be reproduced in this thesis and measurements at increasing internal IAA concentrations in oocytes showed that PIN3-mediated transport was strongly enhanced compared to PIN1- and PIN2-mediated transport (Figure 7).

Phospho-MS/MS analyses of membrane and cytosol fractions from oocytes revealed the same protein levels and the same phosphorylation status of PINs expressed in oocytes, independent of D6PK or PINOID co-expression (Figure 9). Although the overall proteomics approach was untargeted, the protein levels could be compared due to one peptide shared by the three PINs (Figure 9). In line with the published Arabidopsis proteome, almost all possible residues in the PIN loop domains were phosphorylated upon co-expression of a kinase (Mergner *et al.*, 2020). Basal phosphorylation of the PINs by oocyte-specific kinases in samples without co-expressed AGCVIII

kinase was detected. This was not sufficient to activate PIN-mediated transport. In order to transport, a AGCVIII kinase was required which indicates certain specificity for transport activation (Figure 7, Figure 9).

Basal PIN phosphorylation was also detected in Flag-tagged PIN1 protein that was purified for a mass spectrometry analysis from HEK294F cells (Yang *et al.*, 2022). The transporter was expressed alone or co-expressed with D6PK. Phosphorylation sites in PIN1 without D6PK were detected (10 residues compared to 11 residues in this thesis), but only three of them were found in both analyses (S221, S252, S253). For PIN1 + D6PK, the study detected 14 phospho-sites, compared to 24 sites in this thesis, with 11 of the 14 sites found in both studies. For PIN2, more residues (15 of 32 residues) were phosphorylated in oocytes than *in planta*, which can result from differences in peptide detection between the two studies or was influenced by the overexpression situation in oocytes (Table 10) (Mergner *et al.*, 2020).

The kinetic studies in oocytes did not allow to test the PIN transport at $[IAA]_{in} > 10$ µM (Figure 8). Using SSM in proteoliposomes yielded a correlation between peak current response and substrate concentration that could be described by a Michaelis-Menten model for PIN8 at [IAA] > 10 µM (Ung *et al.*, 2022). From NPA binding studies with PIN8 proteoliposomes, it was concluded that most of the PIN8 proteins incorporate with the same orientation, i.e. the cytosolic side faces outward (Ung *et al.*, 2022). This suggests that the binding constant (K_d value) of PIN8 is the kinetic variable for IAA binding to the transporter and does not describe any other step in the transport process, like the transition of the occluded state to the outward-facing state (Ung *et al.*, 2022). Due to the extended time scale of oocyte experiments (up to 30 min for PIN1), the fitted K_m value describes the average kinetic constant of the whole transport process, which makes it impossible to compare the two methods.

The K_m value of PIN3 activated by D6PK observed here was in the same range as the K_d value determined by a surface plasmon resonance (SPR) analysis (Su *et al.*, 2022). In the SPR experiments, the PIN3 protein was immobilized on a sensor chip which implies that the K_d value reflects the average kinetic constant as both sides of the transporter are accessible. This is comparable to the kinetic constant from oocytes where the increased time scale leads to the averaged constant, and supports the reliability of kinetic data obtained from the oocyte assay. For the other combinations of PIN1, PIN2 and PIN3 with D6PK or PINOID in oocytes, the comparison revealed a linear correlation as preferred model, which is likely due to the much lower transport rates of these transporters compared to PIN3 and/or larger variability of the underlying data.

The kinetic studies in oocytes revealed that the PIN transport rate is linearly related to the cytosolic IAA concentration at physiological IAA concentrations, with PIN1 and PIN2 being more similar to each other than PIN3 in terms of their transport properties. A clear kinase effect on the transport rate of PIN-mediated IAA transport was detected, which is discussed later in more detail (Chapter 4.1.3).

The linear relationship between transport rate and substrate concentration leads to the conclusion that only the abundance of activated PIN proteins in the PM determines net IAA efflux at physiological concentrations. Computational modeling of root growth used to focus mainly on the localization of PINs and assumed the same transport rates and expression strengths of PINs (Grieneisen *et al.*, 2007). A study, which investigated cytokinin impact on root growth, discovered that models taking the PIN abundance into consideration fit better to the experimentally reported steady state situation than models with equal PIN levels (Ruzicka *et al.*, 2009; Di Mambro *et al.*, 2017). The discovery that the transport rates of canonical PINs differ, if same protein levels are assumed, will lead to improved computational modeling on plant growth (Janacek *et al.*, 2023, under review).

4.1.2 The loop domain contributes to transport

The cytosolic PIN loop domain was recognized as regulatory domain for proper protein sorting and trafficking in the cell (Cheng and Wang, 2022). Several residues were identified as important phosphorylation sites for these processes and also for activation of PIN-mediated transport (Zourelidou *et al.*, 2014; Barbosa *et al.*, 2018). To date, mainly the influence of the loop domain on the cell biology of PINs was investigated (Zhang *et al.*, 2020a; Zhang *et al.*, 2020b). In order to learn about the impact of the TM domains and the loop domain on auxin transport, a domain swapping approach between the canonical PIN1, PIN2 and PIN3 was performed (Figure 16). The resulting PIN chimeras were tested for their functionality and transport characteristics in oocyte transport assays and *in planta*.

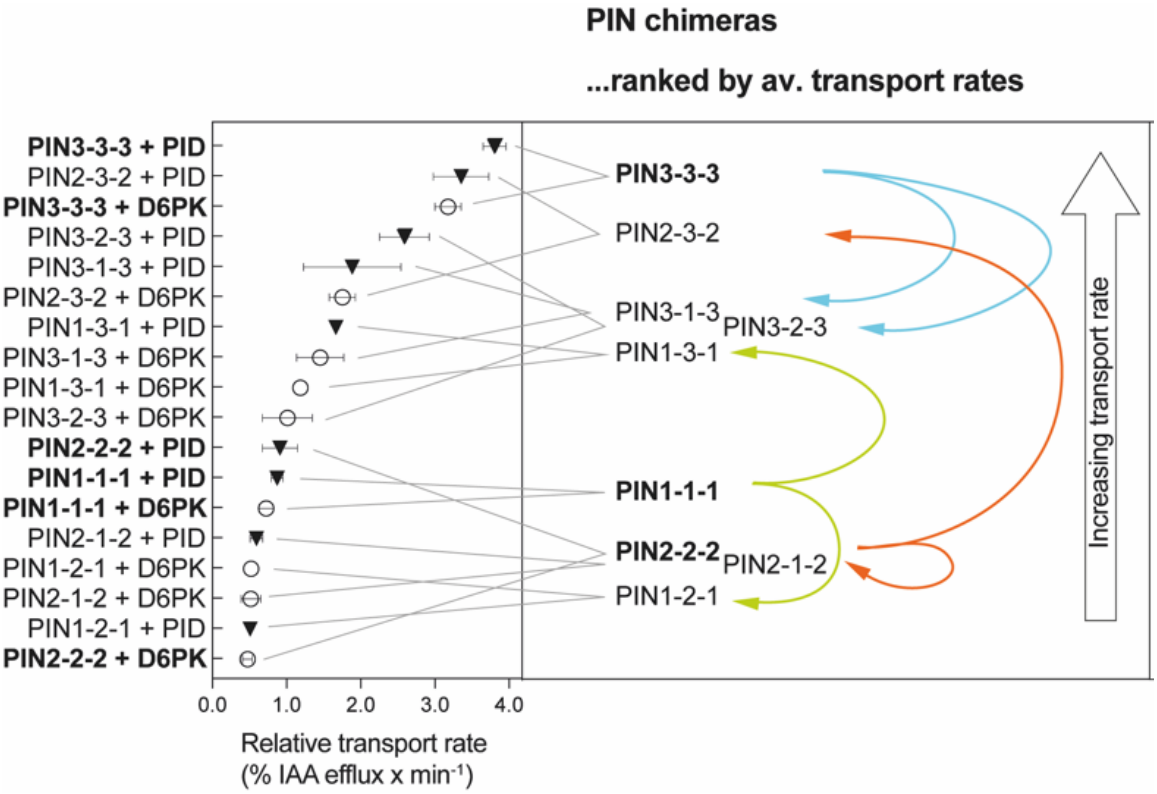

Figure 34 – Relative transport rates of PIN chimeras. Average transport rates of PIN chimeras upon activation by D6PK or PINOID (PID), with SEM indicated. Transport rates for both kinases were averaged and PINs were sorted according to their transport rates. Arrows show position of PIN chimeras relative to their TM domain donor PIN (green: PIN1, red: PIN2, blue: PIN3).

Canonical PIN chimeras

From the kinetic studies of the canonical PINs and the transport data of a PIN3 version without loop, it was concluded that the loop domain is necessary for the protein function, that the loop domain is by default inhibitory and that phosphorylation overcomes this inhibition (Figure 7, Figure 17). In the plant, it cannot be distinguished which kinase activated the transporter. In order to simulate the *in planta* situation, the transport rates for PIN or PIN chimeras activated by D6PK or PINOID were averaged and ranked according to their relative transport rate (Figure 34). By combining the protein domains of a PIN with a high transport rate (PIN3) and the domains of a PIN with a lower transport rate (PIN1 or PIN2), the IAA transport by PINs could be modified. It was not only possible to decrease the transport rate by providing a PIN1 or PIN2 loop to the TM domains of PIN3, but also to increase the transport rates of PIN1 or PIN2 by providing the PIN3 loop domain. This suggests that the TM domains of canonical PINs are *per se* able to transport IAA at similar rates, and that the loop domain regulates the transporter's velocity by restricting degrees of freedom. This regulation is beyond the activation control by phosphorylation as shown by the phospho-proteomics analyses (Figure 9), and suggests an interaction/interplay of the loop domain and the TM domains. An

intramolecular domain-domain coevolution was also hypothesized by genetic studies of various PIN chimeras and is discussed later (Chapter 4.2) (Zhang *et al.*, 2020a).

As established by the kinetic and *in planta* analyses, the idea of PIN1 and PIN2 being more similar to each other than PIN3, is also supported by the transport studies of the PIN1/PIN2 chimeras. Both chimeras PIN1-2-1 and PIN2-1-2 had transport rates in a similar range as PIN1 and PIN2 (Figure 7, Figure 18, Figure 19).

In line with these data, the transport rate of PIN3 was drastically reduced if the loop domain was of PIN1 or PIN2 origin. Both "slow" PINs, PIN1 and PIN2, showed increased transport rates if provided with the PIN3 loop domain.

Noncanonical PIN chimeras

Although the combinations of canonical TM domains and loop domains seemed to follow a logic, this was different for chimeras between the noncanonical PIN8 and the loop domains of PIN1, PIN2 or PIN3 (Figure 26 and Janacek *et al.*, 2023, under review). PIN8 transports IAA independently of AGCVIII kinase co-expression, and the transport rate is linearly related to the cytosolic IAA concentration in the physiological range (Figure 26) (Ung *et al.*, 2022). When PIN8 was provided with any canonical loop domain, the PIN chimeras adopted some canonical features, like transport regulation by kinases or localization to the PM (Figure 26 and Janacek *et al.*, 2023, under review).

However, it became clear that the loop domains influence IAA transport differently. The chimeras PIN8-1-8 and PIN8-2-8 showed a constitutive transport component without co-expressed kinase that was significantly different to the transport rate of PIN1 or PIN2 without kinase (unpaired t-test PIN1 vs. PIN8-1-8 * p-value 0.0376; unpaired t-test PIN2 vs. PIN8-2-8 **** p-value <0.0001) (Janacek *et al.*, 2023, under review). In the PIN8-3-8 chimera, as in PIN3, no transport was detected without co-expression of a kinase (Figure 26). The chimeras were sensitive to transport inhibition by NPA, this further proved the constitutive transport component of PIN8-2-8 (Figure 26).

This suggests that the PIN1 and PIN2 loop domain were unable to block the transporter, whereas the PIN3 loop domain completely shuts down transport. The co-expression of D6PK resulted in an increased transport rate in all three chimeras, but the transport rate was higher when PINOID was co-expressed. This is in line with the differences observed in transport activation for canonical PINs (Figure 7 and Chapter 4.1.3).

Like in PIN8-3-8, providing a PIN1 or PIN2 loop domain to PIN8 increased the transport rates in PIN8-1-8 and PIN8-2-8, although all donor PINs show rather low transport themselves (Janacek *et al.*, 2023, under review). Transport studies of PIN8-2-8 + PINOID at increasing $[IAA]_{in}$ in oocytes revealed transport rates higher than PIN8 and comparable to activated PIN3 (Figure 7, Figure 26). Providing a PIN3 loop to PIN8 resulted in transport rates smaller than PIN3 and more similar to activated PIN8-2-8 (Figure 26).

Model for IAA transport by canonical PINs

The transport properties of the canonical and noncanonical PIN chimeras suggest that the TM domains of "slow" PINs like PIN1, PIN2 or PIN8 can mechanically move like the "fast" PIN3 and that the loop domain strongly modifies the transport properties by modulating the mobility of the transporter or the affinity for IAA.

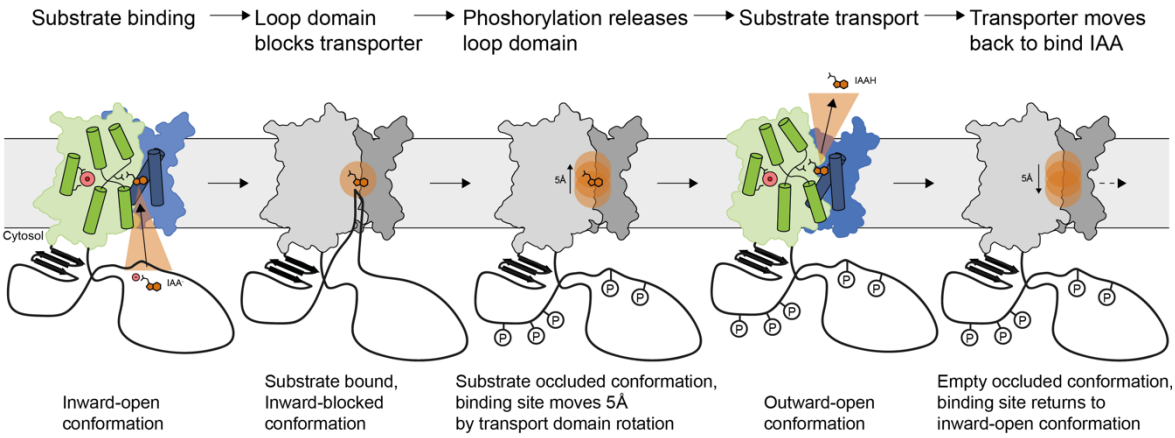

Figure 35 – Model for IAA transport by canonical PINs. After IAA has bound to the inward-open conformation, the loop domain inserts itself into the binding domain and blocks the PIN in the inward-facing conformation. Phosphorylation of the loop by specific AGCVIII kinases leads to the release of the loop domain. The transporter transitions to the outward-facing conformation where IAA is released to the apoplast. The empty occluded conformation moves back to the inward-open conformation. Blue: scaffold domain. Green: transporter domain. Modified from (Ung et al., 2022).

In the cryo-EM structure of inward-facing IAA-bound PIN3 (PDB: 7XXB), Prof. Dr. B. P. Pedersen and team identified densities that can be modeled and a peptide chain in auxin binding pocket (Su *et al.*, 2022). Based on this observation and mechanisms in related protein families, it is speculated that parts of the loop domain interact with the TM domains and block the PIN in the inward-facing conformation after IAA binding (Figure 35) (Selim *et al.*, 2018; Fang *et al.*, 2021). Phosphorylation of critical residues by AGCVIII kinases lead to the release of the loop from the binding pocket and allows the transporter to transition to the outward-facing conformation, where IAA is released to the apoplast. The empty occluded conformation returns to the inward-open conformation and IAA can bind again.

This model is suitable to explain why constitutive IAA transport is observed in PIN8-1-8 and PIN8-2-8 chimeras. If the loop domain fails to interact properly with the TM domains or the interaction is less stable, the transporter can move and change its conformation which would be independent of the phosphorylation event. In light of the results on canonical PIN transport, it also explains why the noncanonical PIN chimeras became regulatable by kinases, i.e. phosphorylation is required to overcome the blocked conformation.

It becomes clear that the loop domains change their properties depending on the TM domain context. The PIN1 and PIN2 loop can prevent conformational changes in all canonical PIN chimeras, i.e. no constitutive transport without kinase, but fail to do this in a noncanonical setting. The PIN2 loop slows down the TM domains of PIN3, but increases the transport if paired with PIN8. It is difficult to explain how PIN-mediated transport becomes faster by adding a loop domain. One idea is that the loop domain adds degrees of freedom to the transporter which would allow faster movement or it reduces the affinity for IAA which would promote faster IAA release.

Regulatory mechanism in a related transporter family

PINs adopt the same protein fold and membrane orientation as $HCO3^-/Na^+$ symporters (Ung *et al.*, 2022). For the bicarbonate transporter SbtA from cyanobacteria, a regulatory mechanism comparable to the hypothesized regulation of PINs was described. The transporter forms a complex with the inorganic carbon sensor protein SbtB (Selim *et al.*, 2018). SbtB regulates the transport activity of SbtA through inserting its T-loop into the cytoplasmic cavity and therefore blocking the substrate release when cytosolic AMP concentrations are high, i.e. low inorganic carbon concentrations (Fang *et al.*, 2021). The T-loop is released through conformational changes after cAMP-binding to SbtB, which accumulates at elevated levels of inorganic carbon. Although the regulation of the SbtA-SbtB complex is independent of phosphorylation, this shows that other members of the BART superfamily are indeed regulated by mechanisms that come into consideration for PINs.

Unpublished data of phosphatase and kinase inhibitor treatments on PIN-mediated transport in oocytes suggests that an initial phosphorylation of the loop domain is necessary for transport activation, but that the transport cycle continues until the PIN is eventually de-phosphorylated (Ass. Prof. Dr. Hiromasa Shikata, NIBB, Okazaki, Japan).

How more complex chimeras could help

One first hint towards understanding the interaction of the loop domain and the TM domains comes from triple chimeras of PIN2 and PIN3 (Figure 24). The transport was reduced when the first TM domain (helices M1-M5) was exchanged against the domain of PIN2. No change was observed when the second TM domain was modified. This suggests that the first TM domain impacts the transport properties more than the second TM domain. This result is unexpected, because the TM domains of PIN2 and PIN3 are highly conserved and the identified critical residues for auxin binding, in the support site and the crossover motif are identical in both PINs (Ung *et al.*, 2022). Site-specific mutations of five residues at the interface of M5 in the transporter domain and the β-strands in the loop domain decreased the transport activity of PIN3 in HEK293T cells (Su *et al.*, 2022). All five sites are conserved between PIN2 and PIN3, which suggests that the interaction of the loop domain and the TM domain cannot be limited to these residues and is more complex.

Higher-order PIN chimeras are required to narrow down possible interaction points. As a follow up experiment, proteins with swapped scaffold and transporter domains, i.e. M1/M2/M6/M7 of PIN2, M3-M5/M8-10 of PIN3 and v.v. should be tested for their transport properties.

4.1.3 The kinase impacts PIN-mediated transport

Transport of IAA by canonical PINs is regulated by AGCVIII kinases. Comprehensive studies on transport activation in oocytes and with phospho-site specific antibodies in Arabidopsis revealed that specific serine residues in the loop domain must be phosphorylated at the PM to activate IAA transport (Zourelidou *et al.*, 2014; Weller *et al.*, 2017). To date, only members of the subclades AGC1 and AGC3 were shown to activate PINs (Zourelidou *et al.*, 2014). Neither AGC2 nor AGC4 nor the AGC kinase PDK1 as master regulator of AGCVIII kinases were able to activate transport (Figure 4, Figure 28). In this thesis, mainly PIN-mediated transport activated by D6PK and PINOID was studied.

Transport studies in oocytes at increasing $[IAA]_{in}$ showed that canonical PINs are insensitive to elevated IAA levels and require co-expression of a kinase for transport activation (Figure 7). For all canonical PINs and PIN chimeras studied in this thesis, the transport rate was higher when PINOID was co-expressed. A phospho-proteomics screen revealed that the phosphorylation status, as a hypothesized read-out for transport activity, of the PINs is independent of the co-expressed kinase (Figure 9). An earlier study used *in vitro* phosphorylated PIN loop domains purified from SDS-PAGE gels and synthetic peptides to identify D6PK-specific phosphosites that were reported as crucial sites for PIN activation (Zourelidou *et al.*, 2014). The use of membrane fractions from oocytes in this thesis allowed to analyze the PIN protein in its entirety. In contrast to the *in vitro* analysis in Zourelidou *et al.* where the whole loop domain was covered in the proteomics screen, small parts of the loop domain were not detected in this thesis. This could either result from differences in the experimental settings or opens the question if these loop regions might serve as interaction points between PIN and kinase. It is conceivable that PINs and kinases form heterodimers, e.g. between different PINs in the same cell, PINs with the kinase or one PIN with different kinases. As the protein levels and phosphorylation patterns of one PIN with any kinase are the same, the different transport rates must be the result of structural interactions of PIN and kinase that are beyond the phosphorylation event for transport activation. If only phosphorylation would be required, the transport rates should be independent of the kinase identity. Phospho-MS analysis of PIN3 + AGC1.7 showed that the critical residues were phosphorylated but the transporter was not activated, which strengthens the previous statement (Figure 30).

The intermolecular PIN-kinase interaction adds an additional layer of regulation to PIN-mediated transport. It suggests that the affinity for IAA in canonical PINs can be modulated by the activating kinase. Co-expression of PINOID reduces the affinity of the PIN towards IAA and leads to an increased transport rate, because affinity and capacity are often inversely correlated. The interaction

of both proteins would either modify the IAA transport ability of the PIN by modulating/covering the auxin binding pocket sterically or leads to an energetically preferred structure of the loop domain which also impacts the transporters motion. The data shows that phosphorylation of the loop domain is necessary for transport, but not sufficient to explain IAA transport by canonical PINs (Weller, 2017).
In the future, interaction studies of PINs and kinases, e.g. by SPR, could reveal if the PIN-kinase interaction is beyond the phosphorylation event and if interactions between the different kinases and PINs vary. Further, it would be interesting to investigate the phosphorylation of the transport-related phospho-sites in terms of cooperativity. This could point to the temporal resolution of overcoming the inhibited PIN state, the supposed interaction with the kinase and finally the interplay of the protein domains during the transport process (Figure 35).

Despite the robust reproducibility *in vitro*, it is questionable if the observations discussed above are physiologically relevant. As a next step, a suitable *in planta* experiment to proof the impact of kinases on PIN-mediated transport should be developed. To activate the transporter, PIN and kinase must be expressed in the same cell and must localize to the same cell side. With the help of single-cell expression data from Arabidopsis, it should be possible to state which AGCVIII kinase can potentially interact with which PIN. Immunostaining experiments in the root revealed that D6PK co-localizes with PIN1 and PIN4 in cells of the root tip, but not with PIN2 in epidermal cells (Zourelidou *et al.*, 2009). With more data on co-localization of PIN and kinase, together with data on the respective transport properties, it would be possible to build models how PIN-kinase combinations would impact auxin flow. But even if localization and impact on transport were solved, the kinases could form heterodimers in the cell. The kinase chimeras of KIPK and AGC1.8 tested on PIN3-mediated transport showed that it is possible to swap kinase domains to gain new regulatory functions (Figure 31).
Although the situation *in planta* is complex, the PIN transport assay in oocytes is suitable to generate knowledge about AGCVIII kinases. The PINs can function as indirect read-out of the kinase activity, as shown for PAX and its variants (Figure 28) (Marhava *et al.*, 2018). The oocyte assay increases the complexity over the very reduced settings in *in vitro* kinase assays but has less variables than an *in planta* experiment.

The physiological impact of several other kinase families on PINs – like the CRKs, the MAP kinases or the CAMEL-CANAR module – appears to be limited to cell-biological properties (Rigo *et al.*, 2013; Dory *et al.*, 2018; Hajny *et al.*, 2020). The developmental problems related to impaired auxin flux in plants results from defects in PIN localization and trafficking. No activation of transport could be detected for any mentioned kinase (Figure 32, Figure 33). Until now, only members of the AGCVIII kinase family have been reported to regulate auxin transport on the fast time scale of

transport activation (Figure 4). All other kinase families impacted the auxin efflux through the slower regulation of transporter localization. It will be interesting to see if new kinase families can be identified that regulate solely the transporter activity or both regulatory processes.

4.2 PIN biochemistry impacts root growth

Tightly controlled auxin flow through the plant body is important for proper plant growth and the reaction to environmental stimuli. PIN-mediated auxin efflux is the main factor in PAT and underlies different regulatory mechanisms. Besides the regulation of (polar) localization, the transport activity depends directly on AGCVIII kinases. Efflux assays in oocytes revealed that canonical PINs differ in their transport rates (Chapter 4.1.1), that the loop domain contributes to the transport properties (Chapter 4.1.2) and that the transport underlies a kinase specificity (Chapter 4.1.3).
To investigate if the different transport properties impact the physiological situation, the agravitropic *pin2* mutant was used. The unique expression profile of *PIN2* in epidermal and cortical cells of the root, as well as the specific dual localization to the apical cell side in the epidermis and the basal side in the cortex, and the agravitropic root phenotype make it an ideal mutant. Under the assumption, that PIN proteins expressed from the same promoter have similar stability in the cell and follow identical protein sorting pathways, i.e. protein levels in the PM are comparable, the PINs and chimeras were expressed from the *PIN2* promoter. It was investigated if the gravitropic root growth can be restored, if the PINs and PIN chimeras localize similarly to PIN2, if different transport rates change the time-depending process of root bending after gravitropic stimulus and how steady-state auxin levels in the root are impacted.

4.2.1 Gravitropic root growth

The transport data of PIN1 and PIN2, with the results from the domain swapping approach, suggested that PIN1 and PIN2 share similar transport characteristics (Chapter 4.1). Strong synergistic interactions between PIN1 and PIN2 were shown by immunostaining experiments in the root, where the ectopic expression of *PIN1* in the *PIN2* expression domain of *pin2* mutant was detected and strong root growth defects in the *pin1 pin2* double mutant were reported (Blilou *et al.*, 2005; Vieten *et al.*, 2005; Thomas *et al.*, 2023). The authors suggested that the ectopic activity of the remaining PINs mask the defects of *pin* mutants (Blilou *et al.*, 2005).
In detailed analyses on fast root gravitropism and on intramolecular domain co-evolution of Arabidopsis PINs, different PINs were expressed from a *PIN2* promoter fragment in the *pin2* mutant and analyzed as in this thesis (Zhang *et al.*, 2019; Zhang *et al.*, 2020a). The authors found that only PIN2 can fully rescue the agravitropic root, similar to this thesis. The *pin2*;P_{PIN2}*:PIN1* and *pin2*;P_{PIN2}*:PIN1-eGFP* expressing lines did not rescue the phenotype, with a VGI in the same range

as the *pin2* mutant. This is in contrast to the findings reported here, where seedlings expressing one of the constructs partially rescued the root phenotype (Figure 10, Figure 11). The PIN1 and PIN1-GFP plasmids in both papers were constructed similarly to the plasmids in this thesis and it remains unclear what led to the different results.

In Zhang *et al.* 2019, the authors analyzed the VGI of *pin2;*P_{PIN2}*:PIN3* lines, which was in good agreement with the results obtained in this thesis (Figure 10). The authors detected a significant difference of the VGI of *pin2;*P_{PIN2}*:PIN3* roots to the VGI of wildtype seedlings, but did not test for a statistical difference to the *pin2* mutant. The statistical analysis of Figure 10 revealed that the *pin2;*P_{PIN2}*:PIN3* seedlings form an own statistical group and are significantly different to Col-0 roots and *pin2* mutant roots, i.e. *pin2;*P_{PIN2}*:PIN3* seedlings partially rescue the agravitropic root.

Rescue was increased when a PIN with similar transport properties to PIN2 was expressed in the root. The same held true for the vice versa situation where PIN2 was comparable to PIN1 during root development in *pin1;*P_{PIN1}*:PIN2* seedlings (Zhang *et al.*, 2020b). This suggests that the different transport properties impact auxin distribution in the root and therefore the gravitropic root growth. It was hypothesized that the auxin flow through the epidermis is enhanced through expression of a "fast" PIN, which impairs the gravitropic growth.

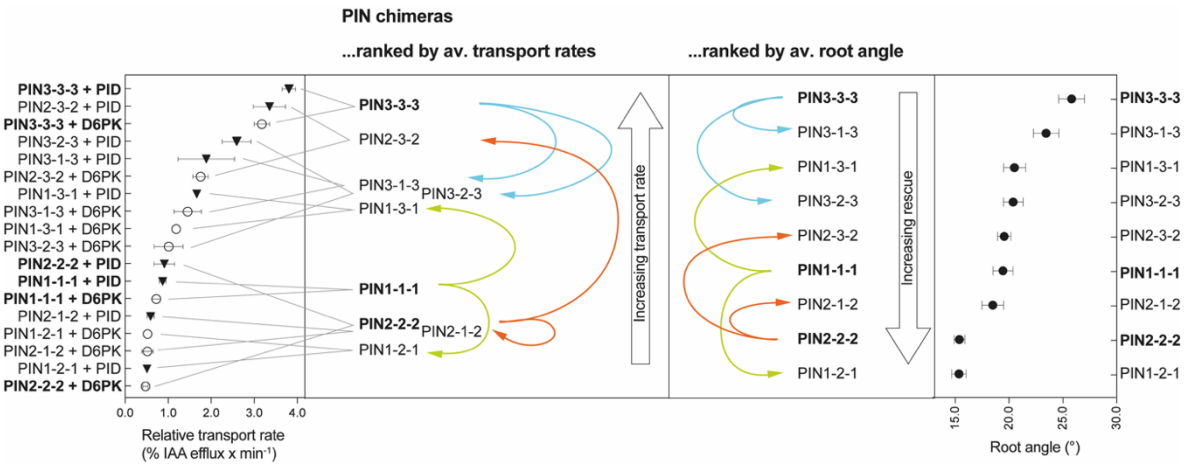

Figure 36 – PIN chimeras ranked by IAA transport rates and root angle. Left: Average transport rates of PIN chimeras upon activation by D6PK or PINOID (PID), with SEM indicated. Transport rates for both kinases were averaged and PINs were sorted according. Right: Average root angle of individual lines expressing *pin2;*P_{PIN2}*:PIN-X*, with SEM. PIN chimeras were ranked according to their ability to rescue the agravitropic *pin2* root. Colored arrows show the relationship of PIN chimeras and the TM domain donor PIN (bold letters). For further information, see Results chapter.

This observation is supported by the transport data and *in planta* data of the canonical PIN chimeras (Chapter 3.2 and Figure 36). The modular combination of TM domains and loop domains resulted in PIN chimeras with modified transport rates (Figure 36). All canonical PIN chimeras rescued the agravitropic *pin2* mutant root at least partially. The PIN1-2-1 chimera rescued the phenotype fully, which was supported by the data in Zhang *et al.*, 2020a. In their study, the authors created PIN chimeras between canonical PIN1 and PIN2, as well as chimeras of PIN2, the semicanonical PIN6 and the noncanonical PIN5 (Zhang *et al.*, 2020a). The authors report that in order to rescue the agravitropic root phenotype, both TM domains must be of same origin (both canonical or noncanonical) and suggest that the TM domains and the loop domain co-evolved intramolecularly. Only chimeras with matching TM domains (independent of PIN identity) and a PIN2 loop domain could reverse the phenotype, i.e. the PIN2-1-2 chimera did not (Zhang *et al.*, 2020a).

Unfortunately, no *pin2;*P_{PIN2}*:PIN2-1-2-eGFP* expressing seedlings could be generated in this thesis. Based on the transport data and the ability of *pin2;*P_{PIN2}*:PIN2-1-2* roots to rescue, it is tempting to hypothesize that PIN2-1-2 localization was not impaired and the chimera was functional in this thesis (Figure 19). Further, the data on PIN chimeras with a PIN1 or PIN3 loop domain suggest that the chimeras partially reverse the phenotype (Figure 18, Figure 20).

Especially the ability of *pin2;*P_{PIN2}*:PIN1-3-1* and *pin2;*P_{PIN2}*:PIN3-1-3* lines to rescue better than *pin2;*P_{PIN2}*:PIN3* lines, suggested that the rescue of the agravitropic root was independent of the PIN's identity, and more related to the transport rate if localization to the PM was given. PIN chimeras with slower transport rates rescued the root phenotype better than PIN chimeras with faster transport rates. The IAA transport rates and the degree of rescue correlated decently with a correlation coefficient of $r = 0.8$. This suggests that transport rates are suited to describe auxin distribution in the root.

However, the direct link between transport rate and degree of rescue did not hold true for noncanonical PIN chimeras (Janacek *et al.*, 2023, under review). Although "canonical features'" of transport regulation and localization could be provided to PIN8 by inserting a loop domain, the chimeras PIN8-1-8, PIN8-2-8 and PIN8-3-8 did not rescue the *pin2* mutant (Figure 26). In early studies on the impact of the loop domain on intracellular trafficking, the noncanonical PIN5 and PIN8 were introduced into *pin2* (*eir2-1*) mutant plants (Ganguly *et al.*, 2014). Both proteins failed to rescue the agravitropic root, although they localized to the PM. Also providing the PIN2 loop to PIN5 (PIN5-2-5) did not lead to polar localization or rescue in this study. Opposing results to this were obtained in the later study on co-evolution of PIN domains (Zhang *et al.*, 2020a). In this study, the PIN5-2-5 chimera showed polar localization to the apical side in epidermal cells and partially rescued the agravitropic root (VGI of 0.8, compared to VGI of 0.95 for *pin2;*P_{PIN2}*:PIN2* lines). The same was observed for the semicanonical PIN6 with PIN2 loop domain (PIN6-2-6), although *pin2;*P_{PIN2}*:PIN6* lines showed no rescue (Zhang *et al.*, 2020a). Preliminary transport studies in oocyte efflux assays were inconclusive about the ability of PIN5-2-5 and PIN6-2-6 to transport IAA (Kolb, 2015). Together with the finding that important residues for PIN-mediated auxin transport are not conserved

in PIN5 (Ung *et al.*, 2022), this suggests that regulation of canonical PINs *in planta* is different from semi- or noncanonical PINs, probably through interactions of loop and TM domains.

The *in planta* data on canonical PINs strengthen the hypothesis, that the transport properties of PINs impact the physiology and are at least as suitable to explain most cell-biological observations as the localization of the transporter. However, the situation in a living system is more complex and differences reported from a heterologous system might be compensated by unknown mechanisms in the plant. The analysis of the noncanonical PIN chimeras showed that not only the ability to transport IAA and the localization to the PM are mandatory for gravitropic root growth (Figure 26), but that additional unknown layers of regulation play a role.

4.2.2 Localization of PINs

The localization of PINs in the PM determines the direction of auxin export from the cell. This is considered a crucial factor in PAT and directly impacts gravitropic root growth. The localization of PIN2 in root epidermal cells is very specifically limited to the apical side of the cell, as shown by GFP-fusions and immunolocalization studies (Figure 12) (Müller *et al.*, 1998; Abas *et al.*, 2006; Wisniewska *et al.*, 2006; Lofke *et al.*, 2015; Zhang *et al.*, 2019; Zhang *et al.*, 2020a). It was shown that the GFP position in the loop domain is decisive if the PIN1 protein localizes apically or basally in epidermal cells (Wisniewska *et al.*, 2006). Insertion of GFP into the first half of the loop domain resulted in basal localization in the epidermis and no rescue of the gravitropic defects in the *pin2* mutant. If GFP was placed in the second half of the loop, PIN1-GFP localized apically in epidermal cells and gravitropic bending was restored. In this thesis, eGFP was inserted at the second half of the loop which should not influence the localization in the epidermis. The eGFP-tagged PINs served as tool to investigate if and how the PINs and chimeras localize apically and polarly in epidermal cells. This is important if the differences observed for the transport properties impact gravitropic root growth. The tagged PINs were expressed from a *PIN2* promoter in the *pin2* mutant and the seedlings were analyzed as described before.

The signal of PIN1-eGFP in the root epidermis was mainly detected at the apical side of epidermal cells, with an increased lateral diffusion towards the cell sides (Figure 12). Less polar localization of PIN1-GFP in epidermal cells was also observed in a study exploring the effects of cytokinin on PIN PM abundancy (Marhavy *et al.*, 2011). In experiments identical to this thesis, epidermal root cells were shown as representative cells, where PIN1-GFP localized solely basally and the signal was strictly polar (Zhang *et al.*, 2020a). However, measuring the polarity index identified apical (~40%), basal (~35%) or nonpolar (~25%) localization of PIN1-GFP. The seedlings of the *pin2;*P_{PIN2}*:PIN1-GFP* line in the paper showed agravitropic root growth, which resulted in a low VGI. As discussed above, this contrasts with the data obtained in this thesis (Chapter 3.1.3). The exact position of the

GFP in the loop domain was not indicated by the authors, which makes it difficult to compare their results with the data in this thesis (Wisniewska *et al.*, 2006; Zhang *et al.*, 2020a).

The localization of PIN3-eGFP was comparable to PIN1-GFP (Figure 12). In root hair cells, overexpressed PIN1-GFP and PIN3-GFP were clearly apolarly distributed in the PM, but the signal of PIN2-GFP was limited to one cell side (Lee and Cho, 2006; Ganguly *et al.*, 2010). It supports the finding that PIN1 and PIN3 localize similarly to each other, but differently to PIN2, i.e. less polar. This suggests that the differences of *pin2;*P_{PIN2}*:PIN1* and *pin2;*P_{PIN2}*:PIN3* lines in gravitropic root growth result from different transport rates and not from differently impaired localization/polarity (Figure 7, Figure 12 and Chapter 4.1). It would be interesting to check if crucial residues for transport activity in *pin2;*P_{PIN2}*:PIN1* and/or *pin2;*P_{PIN2}*:PIN3* roots are phosphorylated solely at the apical cell side or also at the lateral sides (Weller *et al.*, 2017). Phosphorylation at the apical cell side provides the needed directionality of the auxin flux in the epidermis, but laterally phosphorylated PIN would diminish the auxin stream at the same time, i.e. impacting root growth. This could be investigated by using phosphosite-specific antibodies in immunostaining experiments (Weller *et al.*, 2017).

To explore the influence of the loop domain on the localization of PINs, the PIN chimeras were tagged with eGFP. All canonical chimeras localized to the PM, but those with the PIN2 loop domain or PIN2 TM domains showed a higher degree of polarity (Figure 21). If the average root angles of segregating *pin2;*P_{PIN2}*:PIN-X* lines were plotted against the average polarity index of each PIN, the correlation was high with a correlation coefficient of $r = 0.7$. The correlation is as good as the correlation of root angles vs. transport rates (Chapter 4.1). This suggests that localization and transport rates serve equally well and are both required to explain PIN-mediated PAT.

The observation that the TM domains impact the localization was also made by other authors (Zhang *et al.*, 2020a). In their study, chimeras with PIN2 loop localized to the apical side of epidermal cells, but the identity of the TM domains was crucial for the degree of polarity. If the first and second TM domain originated from the same PIN, providing a PIN2 loop resulted in polar apical localization.

Defects in polarity control were observed in noncanonical PINs and their chimeras (Ganguly *et al.*, 2014; Zhang *et al.*, 2020a). PIN5, PIN6 and PIN8 localized (at least partially) to the PM, but in a nonpolar fashion. Their localization was comparable to the canonical PIN1, PIN3 and their chimeras PIN1-3-1 or PIN3-1-3 (Figure 12, Figure 18, Figure 20).

When equipped with a loop domain, the polarity of PIN5-2-5 and PIN8-2-8 did not change, but providing the PIN2 loop to PIN6 (PIN6-2-6) resulted in fully apical and polar localization in epidermal cells (Figure 26 and Janacek *et al.*, 2023, under review) (Ganguly *et al.*, 2014; Zhang *et al.*, 2020a).

Although the noncanonical chimeras localized apolarly and were able to transport IAA at comparable rates, PIN8-2-8 and PIN8-3-8 could not rescue the mutant phenotype, even though PIN6-2-6 did (Figure 26) (Zhang *et al.*, 2020a). This supports the idea of additional yet unknown regulatory mechanisms *in planta* to detect small differences between the PINs. It suggests that PINs with

proposed function at the PM (all canonical PINs and the semi-canonical PIN6) are more tolerant to intramolecular protein modification, e.g. domain swaps, than PINs with no intended function at the PM (PIN5 and PIN8).

4.2.3 Root bending

The less polar localization of PIN1 and PIN3 in contrast to PIN2 might explain why the agravitropic root of *pin2* mutant seedlings was only partially rescued in *pin2;P_{PIN2}:PIN1* and *pin2;P_{PIN2}:PIN3* lines (Figure 10). However, rescue was significantly higher in *pin2;P_{PIN2}:PIN1* seedlings, compared to *pin2;P_{PIN2}:PIN3* seedlings. To answer the question if the different transport rates influence the dynamics of root bending, the response of 5-day old roots to a gravitropic stimulus was monitored over time (Figure 14, Figure 22). Two studies showed that *P_{PIN2}:PIN2* or the GFP-tagged version expressed in a *pin2* mutant fully bring back the ability to react to changes in gravity (Abas *et al.*, 2006; Baster *et al.*, 2013). To date, temporal root bending was only monitored in the light of PIN3 relocalization in *pid wag1 wag2* mutants, but not between different PINs in the *pin2* mutant (Grones *et al.*, 2018).

Root bending in presence of sucrose

On vertical agar plates containing sucrose, the response of *pin2;P_{PIN2}:PIN3* roots was significantly delayed in comparison to wildtype, *pin2;P_{PIN2}:PIN1* or *pin2;P_{PIN2}:PIN2* roots (Figure 14). This is in line with the observation in the gravitropism assay where *pin2;P_{PIN2}:PIN1* and *pin2;P_{PIN2}:PIN2* lines were more similar to each other than *pin2;P_{PIN2}:PIN3* lines (Figure 10). The roots of *pin2;P_{PIN2}:PIN1-2-1* seedlings behave identically to *pin2;P_{PIN2}:PIN2* roots, whereas *pin2;P_{PIN2}:PIN2-1-2* roots were delayed until 10 h post stimulus (Figure 22). This is in line with the observation of increased gravitropism of *pin2;P_{PIN2}:PIN1-2-1* seedlings than *pin2;P_{PIN2}:PIN2-1-2* seedlings (Figure 18, Figure 19).

The roots of *pin2;P_{PIN2}:PIN2-3-2* and *pin2;P_{PIN2}:PIN3-2-3* seedlings were slightly delayed compared to wildtype roots (Figure 22). The data suggest that providing the PIN2 loop domain to either PIN1 or PIN3 improves bending after a stimulus, although the difference to chimeras with PIN2 TM domains were minor and all PIN2-domain containing chimeras showed proper root bending. Unexpectedly, roots of the *pin2* mutant (SALK_042899.22.25) tended to bend upwards on sugar-containing medium, which was not observed for the *eir1-1* mutant (Figure 14, Figure 22 and Dr. Matouš Glanc, former CMB Gent, pers. correspondence, (Abas *et al.*, 2006)).

Glucose is known to impact gravitropic root growth through increased deviation from the gravity vector (Mishra *et al.*, 2009). PIN2-GFP accumulation in the root tip was enhanced upon glucose treatment, which resulted in stronger basipetal auxin transport. Sucrose in the medium led to randomized root growth of the *eir1-4* mutant (García-González *et al.*, 2021). This effect was compensated by illumination of the roots. In a recent paper which identified a new allelic *pin2* mutant

(*pin2-2*), the *pin2* mutant was described as nutrient-sensitive (Thomas *et al.*, 2023). The authors detected that the environmental conditions (nutrient availability) can reverse the mutant root phenotype. Strong impact of sugar on the agravitropic root of *eir1-1*, *eir1-4*, *pin2-2* and *SALK_122916* mutants was reported (Prof. Dr. Benjamin Péret, CNRS, Montpellier, France, pers. correspondence). They suggest that numerous factors impact the strength of the phenotype and that various growth conditions in laboratories led to different conclusions on the protein over time. Therefore, the assay was also performed on plates neither supplemented with sucrose nor vitamins, which is discussed below.

Root bending in absence of sucrose

In order to diminish the impact of the nutritional status on root bending, the assay was performed on plates without sucrose and vitamin supplementation. The overall root bending was reduced, with wildtype roots reaching ~55 ° instead of ~90 ° after 16 h post stimulus, which is likely due to the unfavorable growth conditions (Figure 14, Figure 22). The growth rate on plates without sugar was strongly decreased, which led to smaller differences in root bending and therefore less precise angle analysis.

In contrast to the results obtained from the bending assay with sucrose, *pin2;*P_{PIN2}*:PIN1* roots showed delayed bending and *pin2;*P_{PIN2}*:PIN3* roots reacted quicker to the stimulus (Figure 22). For the PIN chimeras, results were comparable to root bending on sucrose, although the bending rate was reduced. Chimeras with PIN2 loop bended faster than the chimeras with PIN2 TM domains (Figure 22). The *pin2;*P_{PIN2}*:PIN2-3-2* roots bended comparably to *pin2;*P_{PIN2}*:PIN3* roots, but did not reach wildtype levels after 16 h. This implies that root bending of chimeras with transport rates in the range of PIN2 were more similar to wildtype than chimeras with elevated transport rates. However, the increased bending of *pin2;*P_{PIN2}*:PIN3* roots cannot be explained by this and an explanation remains pending.

The *pin2* mutant displayed slight gravitropic bending of 0-15 °, which was comparable to published data (Abas *et al.*, 2006; Baster *et al.*, 2013). Based on the strong difference between conditions with or without sucrose and vitamins, it is concluded that the *pin2* mutant is highly sensitive to the environmental situation, as reported recently (Thomas *et al.*, 2023). Wildtype seedlings were less affected by the environmental settings. Expression of PIN chimeras improved gravitropic bending of the *pin2* mutant and differences between the chimeras could be observed. Although the results from the bending assay showed some variability, it underlines the data obtained from the transport studies and the observations from gravitropic growth (Chapter 3.1 and 3.2), i.e. differences in transport properties are as suitable as the transporter localization to explain root growth.

Conclusion

To bend upon a gravitropic stimulus, the auxin levels must be elevated on the lower root side compared to the upper root side (Chapter 1.2.2). Modeling of root bending in dependence on PIN2 revealed that the auxin concentrations between the upper and lower root side must be tightly controlled and that the PIN2 proportion on the upper root side plays an important role to balance the steepness of this auxin gradient (Retzer *et al.*, 2019). Upon brassinolide treatment, the PIN2 levels at the upper root side did not decrease which resulted in a steeper auxin gradient across the root sides and root overbending. It seems reasonable to hypothesize that the different transport rates of the PINs and the chimeras could lead to a disruption of IAA gradient formation across the root, which would impact the root bending.

Although root bending on plates with sugar was more pronounced, faster and was in line with the transport data, sucrose in the medium presents an unphysiological situation to the root. It was shown that sucrose stimulates IAA biosynthesis and IAA response in the root, as well as influences root traits, like root length, root growth direction and the VGI (Mishra *et al.*, 2009; Sairanen *et al.*, 2012). The root bending in this thesis was monitored completely in the dark, upon five days in the light. Newly introduced experimental setups, like the D-root system, aim to reduce artificial growth situations, i.e. shading of the root to exclude the effect of light (García-González *et al.*, 2021; García-González *et al.*, 2022). In order to improve the experimental design in this thesis, the root bending assays could be performed with illuminated shoot, but shaded roots (García-González *et al.*, 2021).

4.2.4 Auxin levels in the root tip

Studies on the transport properties of canonical PINs and their chimeras revealed different transport rates of PINs. Those correlated well with the ability to rescue the agravitropic root of the *pin2* mutant, and were also in line with results obtained from root bending assays. In order to understand how the steady-state auxin levels in epidermis and cortex are altered by the different transport properties of PINs, the auxin sensor R2D2 was introduced into Col-0, the *pin2* mutant and *pin2;*P_{PIN2}*:PIN-X* expressing lines (Figure 12, Figure 23). The R2D2 signal in this thesis was measured at two different regions in the root, whereby one region was specified by cell elongation (25-30 cells from the cell after anticlinal division of the epidermal/LRC initial cell in Col-0 roots).

In wildtype, the auxin level in the epidermis increased towards the transition zone and stayed similar in cortical cells. This was reversed in the *pin2* mutant. The *pin2;*P_{PIN2}*:PIN2* expressing line mimicked the wildtype and in roots of *pin2;*P_{PIN2}*:PIN1* and *pin2;*P_{PIN2}*:PIN3* seedling the auxin levels in epidermis and cortex were not significantly different, representing a partial rescue of the *pin2* mutant situation (Figure 12). In lines expressing *pin2;*P_{PIN2}*:PIN1-2-1*, *pin2;*P_{PIN2}*:PIN2-1-2* or *pin2;*P_{PIN2}*:PIN3-2-3*, the auxin levels were comparable to Col-0 (Figure 23). Only in *pin2;*P_{PIN2}*:PIN2-3-2* roots, the auxin levels in epidermis and cortex did not increase, comparable to *pin2;*P_{PIN2}*:PIN1* and *pin2;*P_{PIN2}*:PIN3* roots. This is in good agreement with the results from the root

bending assay (without supplemented sucrose), where *pin2;*P_{PIN2}*:PIN2-3-2* and *pin2;*P_{PIN2}*:PIN3* lines provided comparable results. It further shows that not a single PIN2 domain is the deciding factor for rescue of the phenotype and it supports the idea that the 'right' transport rate in epidermis and cortex is crucial for proper root gravitropic growth, with PIN2-3-2 showing a higher transport rate than PIN3-2-3.

Analyses of the root auxin levels by auxin sensors in other contexts revealed that the relative auxin levels depend drastically on the monitored cell file (Brunoud *et al.*, 2012; Di Mambro *et al.*, 2017). The studies reported a steep increase in auxin levels in the epidermis and a flat rise in the cortex with increased distance from the QC. In Di Mambro *et al*., an auxin minimum at the transition zone was reported. The auxin minimum was not detected in this thesis, although the authors described it at ~30 cells from the QC for epidermis and cortex, i.e. the same region as analyzed in this thesis. In contrast, the auxin levels were increased at this position in comparison to the first five cells after anticlinal division of the epidermal/LRC initial cell.

A study on apoplast acidification investigated the role of auxin in root cell elongation (Barbez *et al.*, 2017). By using the R2D2 sensor, the authors detected an increase in auxin levels at the onset of elongation in epidermal cells. The auxin levels in this thesis and in Barbez *et al*. were quantified similarly and a five-fold change in R2/D2 intensity ratio was reported for the 25th cell from the QC, which is in the same range as described in this thesis.

In a later study, plasmodesmata were reported to contribute significantly to a proper root-tip auxin distribution (Mellor *et al.*, 2020). The authors used the DII-VENUS sensor in Col-0 and *pin2* mutant background to match the root auxin levels with their model predictions. Similar to the studies mentioned earlier, the authors detected a steep concentration gradient in the epidermis and less auxin with a smaller gradient in the cortex, which is consistent with the relative auxin levels reported in this thesis. The DII-VENUS signal in the *pin2* mutant revealed overall lower levels of auxin in the outer layers of the root compared to wildtype. In the epidermal cell file, the signal was uniform, i.e. no auxin gradient. In the cortex of *pin2* mutants, the auxin level was comparable to the epidermis. In contrast to the R2D2 ratios in this thesis, the differences between cells in close distance to the QC and cells at the transition zone were small.

In summary, the auxin levels observed in this thesis match well with existing literature, but highlight again that auxin levels are highly dynamic and susceptive to the surroundings and experimental settings. Manipulating the auxin transport in epidermis and cortex through PIN chimeras with different transport properties and by comparing them to wildtype and mutant, resulted in a comprehensive analysis of the canonical PIN chimeras.

4.3 Concluding remarks

This thesis aimed to shed light on the transport properties of PINs as main contributors to PAT. New regulatory levels were discovered that result from intramolecular interactions of PIN protein domains and intermolecular interactions of PIN and activating kinase. The results obtained in this thesis open new questions that concern the intramolecular interactions, the intermolecular interactions and their physiological implementation.

The observation that the loop domain impacts the transport properties and modulates the TM domain context suggests intramolecular interactions between the loop and the TM domains. In order to understand how the loop adjusts, the interacting parts of loop and TM domains should be mapped. In the cryo-EM structure of PIN1 and PIN3, a small part of the loop was resolved and observed to form β-sheets which interact with the TM helices (Su *et al.*, 2022; Yang *et al.*, 2022). Deleting/mutating parts of the loop and testing the PIN functionality in the transport assay, could separate which parts are involved in initial activation control and/or regulation of transport rates. Further, based on the structures of PIN1, PIN3 and PIN8, the electrostatic surfaces could be compared to check if interactions of surface residues and substrate could lead to slower/faster substrate binding/release. In summary, further experiments should aim to resolve the molecular properties of PIN1/PIN2 and PIN3 that explain the unexpected differences in transport rates that cannot be explained by the structures at the moment.

The regulation of PINs by AGCVIII kinases clearly goes beyond the phosphorylation-dependent activation and suggest further intermolecular interactions. The interplay of PIN domains with the kinase(s) should be investigated, in order to understand why the transport rate depends on the activating kinase. It should be answered which part(s) of the loop/TM domains are the interaction sites, how long/stable the PIN-kinase interaction is and if kinases differ in these parameters. The canonical PIN3 was successfully tested for IAA transport in SPR assays and a similar approach could be used to test interactions with different kinases (Su *et al.*, 2022). These experiments could give insight into transporter control by binding of kinase to PIN and could answer why not all AGCVIII kinases can activate PIN-mediated transport.

The physiological relevance of the different PIN transport properties *in planta* is evident based on the results reported, but a conclusive answer cannot be provided. Further experiments should aim to separate the effects of AGCVIII kinases on PINs, i.e. regulation of transport and regulation of localization. In the first step, it would be necessary to control the protein levels in the PM. This would allow to understand if slower PIN transport rates are compensated by increased protein levels in the membrane in order to obtain the same net efflux.

References

Abas, L., Benjamins, R., Malenica, N., Paciorek, T., Wisniewska, J., Moulinier-Anzola, J.C., Sieberer, T., Friml, J., and Luschnig, C. (2006). Intracellular trafficking and proteolysis of the Arabidopsis auxin-efflux facilitator PIN2 are involved in root gravitropism. Nat Cell Biol 8, 249-256.

Abas, L., Kolb, M., Stadlmann, J., Janacek, D.P., Lukic, K., Schwechheimer, C., Sazanov, L.A., Mach, L., Friml, J., and Hammes, U.Z. (2021). Naphthylphthalamic acid associates with and inhibits PIN auxin transporters. Proc Natl Acad Sci U S A 118.

Barbez, E., Dunser, K., Gaidora, A., Lendl, T., and Busch, W. (2017). Auxin steers root cell expansion via apoplastic pH regulation in Arabidopsis thaliana. Proc Natl Acad Sci U S A 114, E4884-E4893.

Barbosa, I.C., Zourelidou, M., Willige, B.C., Weller, B., and Schwechheimer, C. (2014). D6 PROTEIN KINASE activates auxin transport-dependent growth and PIN-FORMED phosphorylation at the plasma membrane. Dev Cell 29, 674-685.

Barbosa, I.C., Shikata, H., Zourelidou, M., Heilmann, M., Heilmann, I., and Schwechheimer, C. (2016). Phospholipid composition and a polybasic motif determine D6 PROTEIN KINASE polar association with the plasma membrane and tropic responses. Development 143, 4687-4700.

Barbosa, I.C.R., Hammes, U.Z., and Schwechheimer, C. (2018). Activation and Polarity Control of PIN-FORMED Auxin Transporters by Phosphorylation. Trends Plant Sci 23, 523-538.

Bassukas, A.E.L., Xiao, Y., and Schwechheimer, C. (2022). Phosphorylation control of PIN auxin transporters. Curr Opin Plant Biol 65, 102146.

Baster, P., Robert, S., Kleine-Vehn, J., Vanneste, S., Kania, U., Grunewald, W., De Rybel, B., Beeckman, T., and Friml, J. (2013). SCF(TIR1/AFB)-auxin signalling regulates PIN vacuolar trafficking and auxin fluxes during root gravitropism. EMBO J 32, 260-274.

Benjamins, R., and Scheres, B. (2008). Auxin: the looping star in plant development. Annu Rev Plant Biol 59, 443-465.

Benjamins, R., Ampudia, C.S., Hooykaas, P.J., and Offringa, R. (2003). PINOID-mediated signaling involves calcium-binding proteins. Plant Physiol 132, 1623-1630.

Benjamins, R., Quint, A., Weijers, D., Hooykaas, P., and Offringa, R. (2001). The PINOID protein kinase regulates organ development in Arabidopsis by enhancing polar auxin transport. Development 128, 4057-4067.

Bennett, M.J., Marchant, A., Green, H.G., May, S.T., Ward, S.P., Millner, P.A., Walker, A.R., Schulz, B., and Feldmann, K.A. (1996). Arabidopsis AUX1 Gene: A Permease-Like Regulator of Root Gravitropism. Science 273, 948-950.

Bennett, S.R.M., Alvarez, J., Bossinger, G., and Smyth, D.R. (1995). Morphogenesis in pinoid mutants of Arabidopsis thaliana. Plant J 8, 505-520.

Bennett, T., Brockington, S.F., Rothfels, C., Graham, S.W., Stevenson, D., Kutchan, T., Rolf, M., Thomas, P., Wong, G.K., Leyser, O., Glover, B.J., and Harrison, C.J. (2014). Paralogous radiations of PIN proteins with multiple origins of noncanonical PIN structure. Mol Biol Evol 31, 2042-2060.

Beziat, C., Barbez, E., Feraru, M.I., Lucyshyn, D., and Kleine-Vehn, J. (2017). Light triggers PILS-dependent reduction in nuclear auxin signalling for growth transition. Nat Plants 3, 17105.

Blakeslee, J.J., Bandyopadhyay, A., Lee, O.R., Mravec, J., Titapiwatanakun, B., Sauer, M., Makam, S.N., Cheng, Y., Bouchard, R., Adamec, J., Geisler, M., Nagashima, A., Sakai, T., Martinoia, E., Friml, J., Peer, W.A., and Murphy, A.S. (2007). Interactions among PIN-FORMED and P-glycoprotein auxin transporters in Arabidopsis. Plant Cell 19, 131-147.

Blilou, I., Xu, J., Wildwater, M., Willemsen, V., Paponov, I., Friml, J., Heidstra, R., Aida, M., Palme, K., and Scheres, B. (2005). The PIN auxin efflux facilitator network controls growth and patterning in Arabidopsis roots. Nature 433, 39-44.

Brunoud, G., Wells, D.M., Oliva, M., Larrieu, A., Mirabet, V., Burrow, A.H., Beeckman, T., Kepinski, S., Traas, J., Bennett, M.J., and Vernoux, T. (2012). A novel sensor to map auxin response and distribution at high spatio-temporal resolution. Nature 482, 103-106.

Cande, W.Z., and Ray, P.M. (1976). Nature of cell-to-cell transfer of auxin in polar transport. Planta 129, 43-52.

Cazzonelli, C.I., Vanstraelen, M., Simon, S., Yin, K., Carron-Arthur, A., Nisar, N., Tarle, G., Cuttriss, A.J., Searle, I.R., Benkova, E., Mathesius, U., Masle, J., Friml, J., and Pogson, B.J. (2013). Role of the Arabidopsis PIN6 auxin transporter in auxin homeostasis and auxin-mediated development. PLoS One 8, e70069.

Chen, R., Hilson, P., Sedbrook, J., Rosen, E., Caspar, T., and Masson, P.H. (1998). The arabidopsis thaliana AGRAVITROPIC 1 gene encodes a component of the polar-auxin-transport efflux carrier. Proc Natl Acad Sci U S A 95, 15112-15117.

Cheng, S., and Wang, Y. (2022). Subcellular trafficking and post-translational modification regulate PIN polarity in plants. Front Plant Sci 13, 923293.

Christensen, S.K., Dagenais, N., Chory, J., and Weigel, D. (2000). Regulation of Auxin Response by the Protein Kinase PINOID. Cell 100, 469-478.

Cseplo, A., Zsigmond, L., Andrasi, N., Baba, A.I., Labhane, N.M., Peto, A., Kolbert, Z., Kovacs, H.E., Steinbach, G., Szabados, L., Feher, A., and Rigo, G. (2021). The AtCRK5 Protein Kinase Is Required to Maintain the ROS NO Balance Affecting the PIN2-Mediated Root Gravitropic Response in Arabidopsis. Int J Mol Sci 22.

Dal Bosco, C., Dovzhenko, A., and Palme, K. (2012). Intracellular auxin transport in pollen: PIN8, PIN5 and PILS5. Plant Signal Behav 7, 1504-1505.

Darwin, C., and Darwin, F. (1880). Sensitiveness of plants to light: it‘s transmitted effect. The power of movement in plants (John Murray, London).

De Smet, I., Voss, U., Lau, S., Wilson, M., Shao, N., Timme, R.E., Swarup, R., Kerr, I., Hodgman, C., Bock, R., Bennett, M., Jurgens, G., and Beeckman, T. (2011). Unraveling the evolution of auxin signaling. Plant Physiol 155, 209-221.

Dhonukshe, P., Huang, F., Galvan-Ampudia, C.S., Mahonen, A.P., Kleine-Vehn, J., Xu, J., Quint, A., Prasad, K., Friml, J., Scheres, B., and Offringa, R. (2010). Plasma membrane-bound AGC3 kinases phosphorylate PIN auxin carriers at TPRXS(N/S) motifs to direct apical PIN recycling. Development 142, 2386-2387.

Di Mambro, R., Svolacchia, N., Dello Ioio, R., Pierdonati, E., Salvi, E., Pedrazzini, E., Vitale, A., Perilli, S., Sozzani, R., Benfey, P.N., Busch, W., Costantino, P., and Sabatini, S. (2019). The Lateral Root Cap Acts as an Auxin Sink that Controls Meristem Size. Curr Biol 29, 1199-1205 e1194.

Di Mambro, R., De Ruvo, M., Pacifici, E., Salvi, E., Sozzani, R., Benfey, P.N., Busch, W., Novak, O., Ljung, K., Di Paola, L., Maree, A.F.M., Costantino, P., Grieneisen, V.A., and Sabatini, S. (2017). Auxin minimum triggers the developmental switch from cell division to cell differentiation in the Arabidopsis root. Proc Natl Acad Sci U S A 114, E7641-E7649.

Dindas, J., Scherzer, S., Roelfsema, M.R.G., von Meyer, K., Muller, H.M., Al-Rasheid, K.A.S., Palme, K., Dietrich, P., Becker, D., Bennett, M.J., and Hedrich, R. (2018). AUX1-mediated root hair auxin influx governs SCF(TIR1/AFB)-type Ca(2+) signaling. Nat Commun 9, 1174.

Ding, Z., Wang, B., Moreno, I., Duplakova, N., Simon, S., Carraro, N., Reemmer, J., Pencik, A., Chen, X., Tejos, R., Skupa, P., Pollmann, S., Mravec, J., Petrasek, J., Zazimalova, E., Honys, D., Rolcik, J., Murphy, A., Orellana, A., Geisler, M., and Friml, J. (2012). ER-localized auxin transporter PIN8 regulates auxin homeostasis and male gametophyte development in Arabidopsis. Nat Commun 3, 941.

Ditengou, F.A., Gomes, D., Nziengui, H., Kochersperger, P., Lasok, H., Medeiros, V., Paponov, I.A., Nagy, S.K., Nadai, T.V., Meszaros, T., Barnabas, B., Ditengou, B.I., Rapp, K., Qi, L., Li, X., Becker, C., Li, C., Doczi, R., and Palme, K. (2018). Characterization of auxin transporter PIN6 plasma membrane targeting reveals a function for PIN6 in plant bolting. New Phytol 217, 1610-1624.

Dory, M., Hatzimasoura, E., Kallai, B.M., Nagy, S.K., Jager, K., Darula, Z., Nadai, T.V., Meszaros, T., Lopez-Juez, E., Barnabas, B., Palme, K., Bogre, L., Ditengou, F.A., and Doczi, R. (2018).

Coevolving MAPK and PID phosphosites indicate an ancient environmental control of PIN auxin transporters in land plants. FEBS Lett 592, 89-102.
Esmon, C.A., Tinsley, A.G., Ljung, K., Sandberg, G., Hearne, L.B., and Liscum, E. (2006). A gradient of auxin and auxin-dependent transcription precedes tropic growth responses. Proceedings of the National Academy of Sciences 103, 236-241.
Fang, S., Huang, X., Zhang, X., Zhang, M., Hao, Y., Guo, H., Liu, L.N., Yu, F., and Zhang, P. (2021). Molecular mechanism underlying transport and allosteric inhibition of bicarbonate transporter SbtA. Proc Natl Acad Sci U S A 118.
Fastner, A., Absmanner, B., and Hammes, U.Z. (2017). Use of Xenopus laevis Oocytes to Study Auxin Transport. Methods Mol Biol 1497, 259-270.
Feraru, E., Feraru, M.I., Moulinier-Anzola, J., Schwihla, M., Ferreira Da Silva Santos, J., Sun, L., Waidmann, S., Korbei, B., and Kleine-Vehn, J. (2022). PILS proteins provide a homeostatic feedback on auxin signaling output. Development 149.
Friml, J., Wisniewska, J., Benkova, E., Mendgen, K., and Palme, K. (2002a). Lateral relocation of auxin efflux regulator PIN3 mediates tropism in Arabidopsis. Nature 415, 806-809.
Friml, J., Benkova, E., Mayer, U., Palme, K., and Muster, G. (2003). Automated whole mount localisation techniques for plant seedlings. Plant J 34, 115-124.
Friml, J., Benková, E., Blilou, I., Wisniewska, J., Hamann, T., Ljung, K., Woody, S., Sandberg, G., Scheres, B., Jürgens, G., and Palme, K. (2002b). AtPIN4 Mediates Sink-Driven Auxin Gradients and Root Patterning in Arabidopsis. Cell 108, 661-673.
Friml, J., Yang, X., Michniewicz, M., Weijers, D., Quint, A., Tietz, O., Benjamins, R., Ouwerkerk, P.B., Ljung, K., Sandberg, G., Hooykaas, P.J., Palme, K., and Offringa, R. (2004). A PINOID-dependent binary switch in apical-basal PIN polar targeting directs auxin efflux. Science 306, 862-865.
Furutani, M., Nakano, Y., and Tasaka, M. (2014). MAB4-induced auxin sink generates local auxin gradients in Arabidopsis organ formation. Proc Natl Acad Sci U S A 111, 1198-1203.
Furutani, M., Sakamoto, N., Yoshida, S., Kajiwara, T., Robert, H.S., Friml, J., and Tasaka, M. (2011). Polar-localized NPH3-like proteins regulate polarity and endocytosis of PIN-FORMED auxin efflux carriers. Development 138, 2069-2078.
Galvan-Ampudia, C.S., and Offringa, R. (2007). Plant evolution: AGC kinases tell the auxin tale. Trends Plant Sci 12, 541-547.
Gälweiler, L., Guan, C., Muller, A., Wisman, E., Mendgen, K., Yephremov, A., and Palme, K. (1998). Regulation of polar auxin transport by AtPIN1 in Arabidopsis vascular tissue. Science 282, 2226-2230.
Ganguly, A., Lee, S.H., and Cho, H.T. (2012). Functional identification of the phosphorylation sites of Arabidopsis PIN-FORMED3 for its subcellular localization and biological role. Plant J 71, 810-823.
Ganguly, A., Park, M., Kesawat, M.S., and Cho, H.T. (2014). Functional Analysis of the Hydrophilic Loop in Intracellular Trafficking of Arabidopsis PIN-FORMED Proteins. Plant Cell 26, 1570-1585.
Ganguly, A., Lee, S.H., Cho, M., Lee, O.R., Yoo, H., and Cho, H.T. (2010). Differential auxin-transporting activities of PIN-FORMED proteins in Arabidopsis root hair cells. Plant Physiol 153, 1046-1061.
García-González, J., Lacek, J., and Retzer, K. (2021). Dissecting Hierarchies between Light, Sugar and Auxin Action Underpinning Root and Root Hair Growth. Plants (Basel) 10.
García-González, J., Lacek, J., Weckwerth, W., and Retzer, K. (2022). Throttling Growth Speed: Evaluation of aux1-7 Root Growth Profile by Combining D-Root system and Root Penetration Assay. Plants 11.
Geisler, M., Blakeslee, J.J., Bouchard, R., Lee, O.R., Vincenzetti, V., Bandyopadhyay, A., Titapiwatanakun, B., Peer, W.A., Bailly, A., Richards, E.L., Ejendal, K.F., Smith, A.P., Baroux, C., Grossniklaus, U., Muller, A., Hrycyna, C.A., Dudler, R., Murphy, A.S., and Martinoia, E. (2005). Cellular efflux of auxin catalyzed by the Arabidopsis MDR/PGP transporter AtPGP1. Plant J 44, 179-194.
George, E.F., Hall, M.A., and Klerk, G.-J.D. (2007). Plant Propagation by Tissue Culture.

Glanc, M., Fendrych, M., and Friml, J. (2018). Mechanistic framework for cell-intrinsic re-establishment of PIN2 polarity after cell division. Nat Plants 4, 1082-1088.

Glanc, M., Van Gelderen, K., Hoermayer, L., Tan, S., Naramoto, S., Zhang, X., Domjan, D., Vcelarova, L., Hauschild, R., Johnson, A., de Koning, E., van Dop, M., Rademacher, E., Janson, S., Wei, X., Molnar, G., Fendrych, M., De Rybel, B., Offringa, R., and Friml, J. (2021). AGC kinases and MAB4/MEL proteins maintain PIN polarity by limiting lateral diffusion in plant cells. Curr Biol.

Goldsmith, M.H., Cataldo, D.A., Karn, J., Brenneman, T., and Trip, P. (1974). The rapid non-polar transport of auxin in the phloem of intact Coleus plants. Planta 116, 301-317.

Goto, N., Starke, M., and Kranz, A.R. (1987). Effect of gibberellins on flower development of the pin-formed mutant of Arabidopsis thaliana.

Grabov, A., Ashley, M.K., Rigas, S., Hatzopoulos, P., Dolan, L., and Vicente-Agullo, F. (2005). Morphometric analysis of root shape. New Phytol 165, 641-651.

Grebe, M., Friml, J., Swarup, R., Ljung, K., Sandberg, G., Terlou, M., Palme, K., Bennett, M.J., and Scheres, B. (2002). Cell Polarity Signaling in Arabidopsis Involves a BFA-Sensitive Auxin Influx Pathway. Curr Biol 12, 329-334.

Grieneisen, V.A., Xu, J., Maree, A.F., Hogeweg, P., and Scheres, B. (2007). Auxin transport is sufficient to generate a maximum and gradient guiding root growth. Nature 449, 1008-1013.

Grones, P., Abas, M., Hajny, J., Jones, A., Waidmann, S., Kleine-Vehn, J., and Friml, J. (2018). PID/WAG-mediated phosphorylation of the Arabidopsis PIN3 auxin transporter mediates polarity switches during gravitropism. Sci Rep 8, 10279.

Gütter, S. (2014). Charakterisierung der Effluxeigenschaften des Aminosäuretransporters UmamiT2 aus Lotus japonicus sowie der Auxintransporter PIN4 & 7 aus Arabidopsis thaliana (University of Regensburg).

Haga, K., and Sakai, T. (2012). PIN auxin efflux carriers are necessary for pulse-induced but not continuous light-induced phototropism in Arabidopsis. Plant Physiol 160, 763-776.

Hajny, J., Prat, T., Rydza, N., Rodriguez, L., Tan, S., Verstraeten, I., Domjan, D., Mazur, E., Smakowska-Luzan, E., Smet, W., Mor, E., Nolf, J., Yang, B., Grunewald, W., Molnar, G., Belkhadir, Y., De Rybel, B., and Friml, J. (2020). Receptor kinase module targets PIN-dependent auxin transport during canalization. Science 370, 550-557.

Hammes, U.Z., Murphy, A.S., and Schwechheimer, C. (2021). Auxin Transporters-A Biochemical View. Cold Spring Harb Perspect Biol.

Hao, P., Xia, J., Liu, J., Di Donato, M., Pakula, K., Bailly, A., Jasinski, M., and Geisler, M. (2020). Auxin-transporting ABC transporters are defined by a conserved D/E-P motif regulated by a prolylisomerase. J Biol Chem 295, 13094-13105.

Haughn, G.W., and Somerville, C.R. (1988). Genetic control of morphogenesis inArabidopsis. Dev Genet 9, 73-89.

Heisler, M.G., Ohno, C., Das, P., Sieber, P., Reddy, G.V., Long, J.A., and Meyerowitz, E.M. (2005). Patterns of auxin transport and gene expression during primordium development revealed by live imaging of the Arabidopsis inflorescence meristem. Curr Biol 15, 1899-1911.

Hellens, R.P., Edwards, E.A., Leyland, N.R., Bean, S., and Mullineaux, P.M. (2000). pGreen: a versatile and flexible binary Ti vector for Agrobacterium-mediated plant transformation. Plant Mol Biol 42, 819-832.

Hertel, R., and Leopold, A.C. (1963). Versuche zur Analyse des Auxintransports in der Koleoptile vonZea mays L. Planta 59, 535-562.

Hertel, R., Lomax, T.L., and Briggs, W.R. (1983). Auxin transport in membrane vesicles from Cucurbita pepo L. Planta 157, 193-201.

Himschoot, E., Pleskot, R., Van Damme, D., and Vanneste, S. (2017). The ins and outs of Ca(2+) in plant endomembrane trafficking. Curr Opin Plant Biol 40, 131-137.

Hrtyan, M., Slikova, E., Hejatko, J., and Ruzicka, K. (2015). RNA processing in auxin and cytokinin pathways. J Exp Bot 66, 4897-4912.

Hu, N.J., Iwata, S., Cameron, A.D., and Drew, D. (2011). Crystal structure of a bacterial homologue of the bile acid sodium symporter ASBT. Nature 478, 408-411.

Huang, F., Zago, M.K., Abas, L., van Marion, A., Galvan-Ampudia, C.S., and Offringa, R. (2010). Phosphorylation of conserved PIN motifs directs Arabidopsis PIN1 polarity and auxin transport. Plant Cell 22, 1129-1142.

Hunte, C., Screpanti, E., Venturi, M., Rimon, A., Padan, E., and Michel, H. (2005). Structure of a Na+/H+ antiporter and insights into mechanism of action and regulation by pH. Nature 435, 1197-1202.

Ischebeck, T., Werner, S., Krishnamoorthy, P., Lerche, J., Meijon, M., Stenzel, I., Lofke, C., Wiessner, T., Im, Y.J., Perera, I.Y., Iven, T., Feussner, I., Busch, W., Boss, W.F., Teichmann, T., Hause, B., Persson, S., and Heilmann, I. (2013). Phosphatidylinositol 4,5-bisphosphate influences PIN polarization by controlling clathrin-mediated membrane trafficking in Arabidopsis. Plant Cell 25, 4894-4911.

Ishida, T., Thitamadee, S., and Hashimoto, T. (2007). Twisted growth and organization of cortical microtubules. J Plant Res 120, 61-70.

Jacobs, M., and Gilbert, S.F. (1983). Basal localization of the presumptive auxin transport carrier in pea stem cells. Science 220, 1297-1300.

Janacek, D.P. (2017). PIN-FORMED PROTEINs: Characterization of transport properties & regulation by domain swapping (University of Regensburg).

Jenness, M.K., Carraro, N., Pritchard, C.A., and Murphy, A.S. (2019). The Arabidopsis ATP-BINDING CASSETTE Transporter ABCB21 Regulates Auxin Levels in Cotyledons, the Root Pericycle, and Leaves. Front Plant Sci 10, 806.

Jia, W., Li, B., Li, S., Liang, Y., Wu, X., Ma, M., Wang, J., Gao, J., Cai, Y., Zhang, Y., Wang, Y., Li, J., and Wang, Y. (2016). Mitogen-Activated Protein Kinase Cascade MKK7-MPK6 Plays Important Roles in Plant Development and Regulates Shoot Branching by Phosphorylating PIN1 in Arabidopsis. PLoS Biol 14, e1002550.

Kamimoto, Y., Terasaka, K., Hamamoto, M., Takanashi, K., Fukuda, S., Shitan, N., Sugiyama, A., Suzuki, H., Shibata, D., Wang, B., Pollmann, S., Geisler, M., and Yazaki, K. (2012). Arabidopsis ABCB21 is a facultative auxin importer/exporter regulated by cytoplasmic auxin concentration. Plant Cell Physiol 53, 2090-2100.

Kashkan, I., Hrtyan, M., Retzer, K., Humpolickova, J., Jayasree, A., Filepova, R., Vondrakova, Z., Simon, S., Rombaut, D., Jacobs, T.B., Frilander, M.J., Hejatko, J., Friml, J., Petrasek, J., and Ruzicka, K. (2022). Mutually opposing activity of PIN7 splicing isoforms is required for auxin-mediated tropic responses in Arabidopsis thaliana. New Phytol 233, 329-343.

Katekar, G.F., and Geissler, A.E. (1977). Auxin Transport Inhibitors: III. Chemical Requirements of a Class of Auxin Transport Inhibitors. Plant Physiol 60, 826-829.

Kleine-Vehn, J., Huang, F., Naramoto, S., Zhang, J., Michniewicz, M., Offringa, R., and Friml, J. (2009). PIN auxin efflux carrier polarity is regulated by PINOID kinase-mediated recruitment into GNOM-independent trafficking in Arabidopsis. Plant Cell 21, 3839-3849.

Kleine-Vehn, J., Wabnik, K., Martiniere, A., Langowski, L., Willig, K., Naramoto, S., Leitner, J., Tanaka, H., Jakobs, S., Robert, S., Luschnig, C., Govaerts, W., Hell, S.W., Runions, J., and Friml, J. (2011). Recycling, clustering, and endocytosis jointly maintain PIN auxin carrier polarity at the plasma membrane. Mol Syst Biol 7, 540.

Kögl, F., Erxleben, H., and Haagen-Smit, A. (1934). Über die Isolierung der Auxine a und b aus pflanzlichen Materialien. 9. Mitteilung über pflanzliche Wachstumsstoffe.

Kolb, M. (2015). Characterization of the putative auxin efflux transporters PIN5, PIN6 and PIN8 - A domain-swapping approach (University of Regensburg).

Koncz, C., and Schell, J. (1986). The promoter of TL-DNA gene 5 controls the tissue-specific expression of chimaeric genes carried by a novel type of Agrobacterium binary vector. Molecular and General Genetics MGG 204, 383-396.

Konings, H. (1967). On the Mechanism of the Transverse Distribution of Auxin in Geotropically Exposed Pea Roots. Acta Botanica Neerlandica 16, 161-176.

Krecek, P., Skupa, P., Libus, J., Naramoto, S., Tejos, R., Friml, J., and Zazimalova, E. (2009). The PIN-FORMED (PIN) protein family of auxin transporters. Genome Biol 10, 249.

Krouk, G., Lacombe, B., Bielach, A., Perrine-Walker, F., Malinska, K., Mounier, E., Hoyerova, K., Tillard, P., Leon, S., Ljung, K., Zazimalova, E., Benkova, E., Nacry, P., and Gojon, A.

(2010). Nitrate-regulated auxin transport by NRT1.1 defines a mechanism for nutrient sensing in plants. Dev Cell 18, 927-937.

Kubes, M., Yang, H., Richter, G.L., Cheng, Y., Mlodzinska, E., Wang, X., Blakeslee, J.J., Carraro, N., Petrasek, J., Zazimalova, E., Hoyerova, K., Peer, W.A., and Murphy, A.S. (2012). The Arabidopsis concentration-dependent influx/efflux transporter ABCB4 regulates cellular auxin levels in the root epidermis. Plant J 69, 640-654.

Lampropoulos, A., Sutikovic, Z., Wenzl, C., Maegele, I., Lohmann, J.U., and Forner, J. (2013). GreenGate---a novel, versatile, and efficient cloning system for plant transgenesis. PLoS One 8, e83043.

Lee, C., Kang, H.J., von Ballmoos, C., Newstead, S., Uzdavinys, P., Dotson, D.L., Iwata, S., Beckstein, O., Cameron, A.D., and Drew, D. (2013). A two-domain elevator mechanism for sodium/proton antiport. Nature 501, 573-577.

Lee, H., Ganguly, A., Lee, R.D., Park, M., and Cho, H.T. (2019). Intracellularly Localized PIN-FORMED8 Promotes Lateral Root Emergence in Arabidopsis. Front Plant Sci 10, 1808.

Lee, S.H., and Cho, H.T. (2006). PINOID positively regulates auxin efflux in Arabidopsis root hair cells and tobacco cells. Plant Cell 18, 1604-1616.

Leitz, G., Kang, B.H., Schoenwaelder, M.E., and Staehelin, L.A. (2009). Statolith sedimentation kinetics and force transduction to the cortical endoplasmic reticulum in gravity-sensing Arabidopsis columella cells. Plant Cell 21, 843-860.

Li, Y., Wang, Y., Tan, S., Li, Z., Yuan, Z., Glanc, M., Domjan, D., Wang, K., Xuan, W., Guo, Y., Gong, Z., Friml, J., and Zhang, J. (2020). Root Growth Adaptation is Mediated by PYLs ABA Receptor-PP2A Protein Phosphatase Complex. Adv Sci (Weinh) 7, 1901455.

Liao, C.Y., Smet, W., Brunoud, G., Yoshida, S., Vernoux, T., and Weijers, D. (2015). Reporters for sensitive and quantitative measurement of auxin response. Nat Methods 12, 207-210, 202 p following 210.

Liu, X.Y., Hou, W.T., Wang, L., Li, B., Chen, Y., Chen, Y., Jiang, Y.L., and Zhou, C.Z. (2021). Structures of cyanobacterial bicarbonate transporter SbtA and its complex with PII-like SbtB. Cell Discov 7, 63.

Lofke, C., Scheuring, D., Dunser, K., Scholler, M., Luschnig, C., and Kleine-Vehn, J. (2015). Tricho- and atrichoblast cell files show distinct PIN2 auxin efflux carrier exploitations and are jointly required for defined auxin-dependent root organ growth. J Exp Bot 66, 5103-5112.

Lomax, T.L., Mehlhorn, R.J., and Briggs, W.R. (1985). Active auxin uptake by zucchini membrane vesicles: quantitation using ESR volume and delta pH determinations. Proc Natl Acad Sci U S A 82, 6541-6545.

Lomax, T.L., Muday, G.K., and Rubery, P.H. (1995). Auxin Transport. In Plant Hormones: Physiology, Biochemistry and Molecular Biology, P.J. Davies, ed (Dordrecht: Springer Netherlands), pp. 509-530.

Ludewig, U., von Wiren, N., and Frommer, W.B. (2002). Uniport of NH4+ by the root hair plasma membrane ammonium transporter LeAMT1;1. J Biol Chem 277, 13548-13555.

Luschnig, C., Gaxiola, R.A., Grisafi, P., and Fink, G.R. (1998). EIR1, a root-specific protein involved in auxin transport, is required for gravitropism in Arabidopsis thaliana. Genes Dev 12, 2175-2187.

Mano, H., and Hasebe, M. (2021). Rapid movements in plants. J Plant Res 134, 3-17.

Marchant, A., Bhalerao, R., Casimiro, I., Eklof, J., Casero, P.J., Bennett, M., and Sandberg, G. (2002). AUX1 promotes lateral root formation by facilitating indole-3-acetic acid distribution between sink and source tissues in the Arabidopsis seedling. Plant Cell 14, 589-597.

Marhava, P., Bassukas, A.E.L., Zourelidou, M., Kolb, M., Moret, B., Fastner, A., Schulze, W.X., Cattaneo, P., Hammes, U.Z., Schwechheimer, C., and Hardtke, C.S. (2018). A molecular rheostat adjusts auxin flux to promote root protophloem differentiation. Nature 558, 297-300.

Marhava, P., Aliaga Fandino, A.C., Koh, S.W.H., Jelinkova, A., Kolb, M., Janacek, D.P., Breda, A.S., Cattaneo, P., Hammes, U.Z., Petrasek, J., and Hardtke, C.S. (2020). Plasma Membrane Domain Patterning and Self-Reinforcing Polarity in Arabidopsis. Dev Cell 52, 223-235 e225.

Marhavy, P., Bielach, A., Abas, L., Abuzeineh, A., Duclercq, J., Tanaka, H., Parezova, M., Petrasek, J., Friml, J., Kleine-Vehn, J., and Benkova, E. (2011). Cytokinin modulates endocytic trafficking of PIN1 auxin efflux carrier to control plant organogenesis. Dev Cell 21, 796-804.

Mellor, N.L., Voss, U., Janes, G., Bennett, M.J., Wells, D.M., and Band, L.R. (2020). Auxin fluxes through plasmodesmata modify root-tip auxin distribution. Development 147.

Mergner, J., Frejno, M., List, M., Papacek, M., Chen, X., Chaudhary, A., Samaras, P., Richter, S., Shikata, H., Messerer, M., Lang, D., Altmann, S., Cyprys, P., Zolg, D.P., Mathieson, T., Bantscheff, M., Hazarika, R.R., Schmidt, T., Dawid, C., Dunkel, A., Hofmann, T., Sprunck, S., Falter-Braun, P., Johannes, F., Mayer, K.F.X., Jurgens, G., Wilhelm, M., Baumbach, J., Grill, E., Schneitz, K., Schwechheimer, C., and Kuster, B. (2020). Mass-spectrometry-based draft of the Arabidopsis proteome. Nature 579, 409-414.

Michniewicz, M., Ho, C.H., Enders, T.A., Floro, E., Damodaran, S., Gunther, L.K., Powers, S.K., Frick, E.M., Topp, C.N., Frommer, W.B., and Strader, L.C. (2019). TRANSPORTER OF IBA1 Links Auxin and Cytokinin to Influence Root Architecture. Dev Cell 50, 599-609 e594.

Michniewicz, M., Zago, M.K., Abas, L., Weijers, D., Schweighofer, A., Meskiene, I., Heisler, M.G., Ohno, C., Zhang, J., Huang, F., Schwab, R., Weigel, D., Meyerowitz, E.M., Luschnig, C., Offringa, R., and Friml, J. (2007). Antagonistic regulation of PIN phosphorylation by PP2A and PINOID directs auxin flux. Cell 130, 1044-1056.

Migliaccio, F., Tassone, P., and Fortunati, A. (2013). Circumnutation as an autonomous root movement in plants. Am J Bot 100, 4-13.

Mishra, B.S., Singh, M., Aggrawal, P., and Laxmi, A. (2009). Glucose and auxin signaling interaction in controlling Arabidopsis thaliana seedlings root growth and development. PLoS One 4, e4502.

Morgan, D.G., and Söding, H. (1958). ÜBER DIE WIRKUNGSWEISE VON PHTHALSÄUREMONO-α-NAPHTHYLAMID (PNA) AUF DAS WACHSTUM DER HAFERKOLEOPTILE. Planta 52, 235-249.

Mravec, J., Skupa, P., Bailly, A., Hoyerova, K., Krecek, P., Bielach, A., Petrasek, J., Zhang, J., Gaykova, V., Stierhof, Y.D., Dobrev, P.I., Schwarzerova, K., Rolcik, J., Seifertova, D., Luschnig, C., Benkova, E., Zazimalova, E., Geisler, M., and Friml, J. (2009). Subcellular homeostasis of phytohormone auxin is mediated by the ER-localized PIN5 transporter. Nature 459, 1136-1140.

Müller, A., Guan, C., Galweiler, L., Tanzler, P., Huijser, P., Marchant, A., Parry, G., Bennett, M., Wisman, E., and Palme, K. (1998). AtPIN2 defines a locus of Arabidopsis for root gravitropism control. EMBO J 17, 6903-6911.

Okada, K., Ueda, J., Komaki, M.K., Bell, C.J., and Shimura, Y. (1991). Requirement of the Auxin Polar Transport System in Early Stages of Arabidopsis Floral Bud Formation. Plant Cell 3, 677-684.

Ottenschlager, I., Wolff, P., Wolverton, C., Bhalerao, R.P., Sandberg, G., Ishikawa, H., Evans, M., and Palme, K. (2003). Gravity-regulated differential auxin transport from columella to lateral root cap cells. Proc Natl Acad Sci U S A 100, 2987-2991.

Paulino, C., Wohlert, D., Kapotova, E., Yildiz, O., and Kuhlbrandt, W. (2014). Structure and transport mechanism of the sodium/proton antiporter MjNhaP1. eLife 3, e03583.

Peret, B., Swarup, K., Ferguson, A., Seth, M., Yang, Y., Dhondt, S., James, N., Casimiro, I., Perry, P., Syed, A., Yang, H., Reemmer, J., Venison, E., Howells, C., Perez-Amador, M.A., Yun, J., Alonso, J., Beemster, G.T., Laplaze, L., Murphy, A., Bennett, M.J., Nielsen, E., and Swarup, R. (2012). AUX/LAX genes encode a family of auxin influx transporters that perform distinct functions during Arabidopsis development. Plant Cell 24, 2874-2885.

Petersson, S.V., Johansson, A.I., Kowalczyk, M., Makoveychuk, A., Wang, J.Y., Moritz, T., Grebe, M., Benfey, P.N., Sandberg, G., and Ljung, K. (2009). An auxin gradient and maximum in the Arabidopsis root apex shown by high-resolution cell-specific analysis of IAA distribution and synthesis. Plant Cell 21, 1659-1668.

Petricka, J.J., Winter, C.M., and Benfey, P.N. (2012). Control of Arabidopsis root development. Annu Rev Plant Biol 63, 563-590.

Piconese, S., Tronelli, G., Pippia, P., and Migliaccio, F. (2003). Chiral and non-chiral nutations in Arabidopsis roots grown on the random positioning machine. J Exp Bot 54, 1909-1918.

Ranocha, P., Dima, O., Nagy, R., Felten, J., Corratge-Faillie, C., Novak, O., Morreel, K., Lacombe, B., Martinez, Y., Pfrunder, S., Jin, X., Renou, J.P., Thibaud, J.B., Ljung, K., Fischer, U., Martinoia, E., Boerjan, W., and Goffner, D. (2013). Arabidopsis WAT1 is a vacuolar auxin transport facilitator required for auxin homoeostasis. Nat Commun 4, 2625.

Rashotte, A.M., DeLong, A., and Muday, G.K. (2001). Genetic and chemical reductions in protein phosphatase activity alter auxin transport, gravity response, and lateral root growth. Plant Cell 13, 1683-1697.

Raven, J.A. (1975). TRANSPORT OF INDOLEACETIC ACID IN PLANT CELLS IN RELATION TO pH AND ELECTRICAL POTENTIAL GRADIENTS, AND ITS SIGNIFICANCE FOR POLAR IAA TRANSPORT. New Phytol 74, 163-172.

Reinhardt, D., Pesce, E.R., Stieger, P., Mandel, T., Baltensperger, K., Bennett, M., Traas, J., Friml, J., and Kuhlemeier, C. (2003). Regulation of phyllotaxis by polar auxin transport. Nature 426, 255-260.

Retzer, K., Akhmanova, M., Konstantinova, N., Malinska, K., Leitner, J., Petrasek, J., and Luschnig, C. (2019). Brassinosteroid signaling delimits root gravitropism via sorting of the Arabidopsis PIN2 auxin transporter. Nat Commun 10, 5516.

Rigo, G., Ayaydin, F., Tietz, O., Zsigmond, L., Kovacs, H., Pay, A., Salchert, K., Darula, Z., Medzihradszky, K.F., Szabados, L., Palme, K., Koncz, C., and Cseplo, A. (2013). Inactivation of plasma membrane-localized CDPK-RELATED KINASE5 decelerates PIN2 exocytosis and root gravitropic response in Arabidopsis. Plant Cell 25, 1592-1608.

Rizzieri, R., Mahadevan, L., Vaziri, A., and Donald, A. (2006). Superficial wrinkles in stretched, drying gelatin films. Langmuir 22, 3622-3626.

Rubery, P.H., and Sheldrake, A.R. (1974). Carrier-mediated auxin transport. Planta 118, 101-121.

Ruiz Rosquete, M., Waidmann, S., and Kleine-Vehn, J. (2018). PIN7 Auxin Carrier Has a Preferential Role in Terminating Radial Root Expansion in Arabidopsis thaliana. Int J Mol Sci 19.

Rutherford, R., and Masson, P.H. (1996). Arabidopsis thaliana sku mutant seedlings show exaggerated surface-dependent alteration in root growth vector. Plant Physiol 111, 987-998.

Ruzicka, K., Simaskova, M., Duclercq, J., Petrasek, J., Zazimalova, E., Simon, S., Friml, J., Van Montagu, M.C., and Benkova, E. (2009). Cytokinin regulates root meristem activity via modulation of the polar auxin transport. Proc Natl Acad Sci U S A 106, 4284-4289.

Ruzicka, K., Strader, L.C., Bailly, A., Yang, H., Blakeslee, J., Langowski, L., Nejedla, E., Fujita, H., Itoh, H., Syono, K., Hejatko, J., Gray, W.M., Martinoia, E., Geisler, M., Bartel, B., Murphy, A.S., and Friml, J. (2010). Arabidopsis PIS1 encodes the ABCG37 transporter of auxinic compounds including the auxin precursor indole-3-butyric acid. Proc Natl Acad Sci U S A 107, 10749-10753.

Sairanen, I., Novak, O., Pencik, A., Ikeda, Y., Jones, B., Sandberg, G., and Ljung, K. (2012). Soluble carbohydrates regulate auxin biosynthesis via PIF proteins in Arabidopsis. Plant Cell 24, 4907-4916.

Salkowski, E. (1885). Ueber das verhalten der skatolcarbonsäure im organismus.

Sambrook, J., Fritsch, E., and Maniatis, T. (1989). Molecular Cloning, a Laboratory Manual. Cold Spring Harbor, New York: Cold Spring Harbor Laboratory Press.

Santner, A.A., and Watson, J.C. (2006). The WAG1 and WAG2 protein kinases negatively regulate root waving in Arabidopsis. Plant J 45, 752-764.

Scholz, S., Plessmann, J., Enugutti, B., Huttl, R., Wassmer, K., and Schneitz, K. (2019). The AGC protein kinase UNICORN controls planar growth by attenuating PDK1 in Arabidopsis thaliana. Plos Genet 15, e1007927.

Selim, K.A., Haase, F., Hartmann, M.D., Hagemann, M., and Forchhammer, K. (2018). P(II)-like signaling protein SbtB links cAMP sensing with cyanobacterial inorganic carbon response. Proc Natl Acad Sci U S A 115, E4861-E4869.

Sheldrake, A.R. (2021). The production of auxin by dying cells. J Exp Bot.

Simon, M.L., Platre, M.P., Marques-Bueno, M.M., Armengot, L., Stanislas, T., Bayle, V., Caillaud, M.C., and Jaillais, Y. (2016). A PtdIns(4)P-driven electrostatic field controls cell membrane identity and signalling in plants. Nat Plants 2, 16089.

Staves, M.P., Wayne, R., and Leopold, A.C. (1997). The effect of the external medium on the gravitropic curvature of rice (Oryza sativa,
Poaceae) roots. Am J Bot 84, 1522-1529.

Su, N., Zhu, A., Tao, X., Ding, Z.J., Chang, S., Ye, F., Zhang, Y., Zhao, C., Chen, Q., Wang, J., Zhou, C.Y., Guo, Y., Jiao, S., Zhang, S., Wen, H., Ma, L., Ye, S., Zheng, S.J., Yang, F., Wu, S., and Guo, J. (2022). Structures and mechanisms of the Arabidopsis auxin transporter PIN3. Nature 609, 616-621.

Su, S.H., Keith, M.A., and Masson, P.H. (2020). Gravity Signaling in Flowering Plant Roots. Plants (Basel) 9.

Swarup, K., Benkova, E., Swarup, R., Casimiro, I., Peret, B., Yang, Y., Parry, G., Nielsen, E., De Smet, I., Vanneste, S., Levesque, M.P., Carrier, D., James, N., Calvo, V., Ljung, K., Kramer, E., Roberts, R., Graham, N., Marillonnet, S., Patel, K., Jones, J.D., Taylor, C.G., Schachtman, D.P., May, S., Sandberg, G., Benfey, P., Friml, J., Kerr, I., Beeckman, T., Laplaze, L., and Bennett, M.J. (2008). The auxin influx carrier LAX3 promotes lateral root emergence. Nat Cell Biol 10, 946-954.

Swarup, R., and Bhosale, R. (2019). Developmental Roles of AUX1/LAX Auxin Influx Carriers in Plants. Front Plant Sci 10, 1306.

Swarup, R., Friml, J., Marchant, A., Ljung, K., Sandberg, G., Palme, K., and Bennett, M. (2001). Localization of the auxin permease AUX1 suggests two functionally distinct hormone transport pathways operate in the Arabidopsis root apex. Genes Dev 15, 2648-2653.

Swarup, R., Kramer, E.M., Perry, P., Knox, K., Leyser, H.M., Haseloff, J., Beemster, G.T., Bhalerao, R., and Bennett, M.J. (2005). Root gravitropism requires lateral root cap and epidermal cells for transport and response to a mobile auxin signal. Nat Cell Biol 7, 1057-1065.

Swarup, R., Kargul, J., Marchant, A., Zadik, D., Rahman, A., Mills, R., Yemm, A., May, S., Williams, L., Millner, P., Tsurumi, S., Moore, I., Napier, R., Kerr, I.D., and Bennett, M.J. (2004). Structure-function analysis of the presumptive Arabidopsis auxin permease AUX1. Plant Cell 16, 3069-3083.

Takehisa, H., Sato, Y., Igarashi, M., Abiko, T., Antonio, B.A., Kamatsuki, K., Minami, H., Namiki, N., Inukai, Y., Nakazono, M., and Nagamura, Y. (2012). Genome-wide transcriptome dissection of the rice root system: implications for developmental and physiological functions. Plant J 69, 126-140.

Tan, S., Zhang, X., Kong, W., Yang, X.L., Molnar, G., Vondrakova, Z., Filepova, R., Petrasek, J., Friml, J., and Xue, H.W. (2020). The lipid code-dependent phosphoswitch PDK1-D6PK activates PIN-mediated auxin efflux in Arabidopsis. Nat Plants 6, 556-569.

Taylor, I., Lehner, K., McCaskey, E., Nirmal, N., Ozkan-Aydin, Y., Murray-Cooper, M., Jain, R., Hawkes, E.W., Ronald, P.C., Goldman, D.I., and Benfey, P.N. (2021). Mechanism and function of root circumnutation. Proc Natl Acad Sci U S A 118.

Teale, W., and Palme, K. (2018). Naphthylphthalamic acid and the mechanism of polar auxin transport. J Exp Bot 69, 303-312.

Terasaka, K., Blakeslee, J.J., Titapiwatanakun, B., Peer, W.A., Bandyopadhyay, A., Makam, S.N., Lee, O.R., Richards, E.L., Murphy, A.S., Sato, F., and Yazaki, K. (2005). PGP4, an ATP binding cassette P-glycoprotein, catalyzes auxin transport in Arabidopsis thaliana roots. Plant Cell 17, 2922-2939.

Thomas, M., Soriano, A., O'Connor, C., Crabos, A., Nacry, P., Thompson, M., Hrabak, E., Divol, F., and Peret, B. (2023). pin2 mutant agravitropic root phenotype is conditional and nutrient-sensitive. Plant Sci 329, 111606.

Thompson, M.V., and Holbrook, N.M. (2004). Root-gel interactions and the root waving behavior of Arabidopsis. Plant Physiol 135, 1822-1837.

Titapiwatanakun, B., Blakeslee, J.J., Bandyopadhyay, A., Yang, H., Mravec, J., Sauer, M., Cheng, Y., Adamec, J., Nagashima, A., Geisler, M., Sakai, T., Friml, J., Peer, W.A., and Murphy, A.S. (2009). ABCB19/PGP19 stabilises PIN1 in membrane microdomains in Arabidopsis. Plant J 57, 27-44.

Ulmasov, T., Murfett, J., Hagen, G., and Guilfoyle, T.J. (1997). Aux/IAA proteins repress expression of reporter genes containing natural and highly active synthetic auxin response elements. Plant Cell 9, 1963-1971.

Ung, K.L., Winkler, M., Schulz, L., Kolb, M., Janacek, D.P., Dedic, E., Stokes, D.L., Hammes, U.Z., and Pedersen, B.P. (2022). Structures and mechanism of the plant PIN-FORMED auxin transporter. Nature 609, 605-610.

Vieten, A., Vanneste, S., Wisniewska, J., Benkova, E., Benjamins, R., Beeckman, T., Luschnig, C., and Friml, J. (2005). Functional redundancy of PIN proteins is accompanied by auxin-dependent cross-regulation of PIN expression. Development 132, 4521-4531.

Wang, P., Shen, L., Guo, J., Jing, W., Qu, Y., Li, W., Bi, R., Xuan, W., Zhang, Q., and Zhang, W. (2019). Phosphatidic Acid Directly Regulates PINOID-Dependent Phosphorylation and Activation of the PIN-FORMED2 Auxin Efflux Transporter in Response to Salt Stress. Plant Cell 31, 250-271.

Wang, Y., Liu, C., Yang, D., Yu, H., and Liou, Y.C. (2010). Pin1At encoding a peptidyl-prolyl cis/trans isomerase regulates flowering time in Arabidopsis. Mol Cell 37, 112-122.

Watanabe, S., Takahashi, N., Kanno, Y., Suzuki, H., Aoi, Y., Takeda-Kamiya, N., Toyooka, K., Kasahara, H., Hayashi, K.-i., Umeda, M., and Seo, M. (2020). TheArabidopsisNRT1/PTR FAMILY protein NPF7.3/NRT1.5 is an indole-3-butyric acid transporter involved in root gravitropism. Proceedings of the National Academy of Sciences 117, 31500-31509.

Weller, B. (2017). Auxin transport regulation through dynamic efflux carrier phosphorylation (Technical University of Munich).

Weller, B., Zourelidou, M., Frank, L., Barbosa, I.C., Fastner, A., Richter, S., Jurgens, G., Hammes, U.Z., and Schwechheimer, C. (2017). Dynamic PIN-FORMED auxin efflux carrier phosphorylation at the plasma membrane controls auxin efflux-dependent growth. Proc Natl Acad Sci U S A 114, E887-E896.

Went, F. (1926). On growth-accelerating substances in the coleoptile of Avena sativa. In Proc Kon Akad Wetensch Amsterdam, pp. 10-19.

Went, F.W. (1974). Reflections and Speculations. Annual Review of Plant Physiology 25, 1-27.

Willige, B.C., Isono, E., Richter, R., Zourelidou, M., and Schwechheimer, C. (2011). Gibberellin regulates PIN-FORMED abundance and is required for auxin transport-dependent growth and development in Arabidopsis thaliana. Plant Cell 23, 2184-2195.

Willige, B.C., Ahlers, S., Zourelidou, M., Barbosa, I.C., Demarsy, E., Trevisan, M., Davis, P.A., Roelfsema, M.R., Hangarter, R., Fankhauser, C., and Schwechheimer, C. (2013). D6PK AGCVIII kinases are required for auxin transport and phototropic hypocotyl bending in Arabidopsis. Plant Cell 25, 1674-1688.

Wisniewska, J., Xu, J., Seifertova, D., Brewer, P.B., Ruzicka, K., Blilou, I., Rouquie, D., Benkova, E., Scheres, B., and Friml, J. (2006). Polar PIN localization directs auxin flow in plants. Science 312, 883.

Wohlert, D., Kuhlbrandt, W., and Yildiz, O. (2014). Structure and substrate ion binding in the sodium/proton antiporter PaNhaP. eLife 3, e03579.

Wolverton, C., Ishikawa, H., and Evans, M.L. (2002a). The kinetics of root gravitropism: dual motors and sensors. J Plant Growth Regul 21, 102-112.

Wolverton, C., Mullen, J.L., Ishikawa, H., and Evans, M.L. (2002b). Root gravitropism in response to a signal originating outside of the cap. Planta 215, 153-157.

Xi, W., Gong, X., Yang, Q., Yu, H., and Liou, Y.C. (2016). Pin1At regulates PIN1 polar localization and root gravitropism. Nat Commun 7, 10430.

Xiao, Y., and Offringa, R. (2020). PDK1 regulates auxin transport and Arabidopsis vascular development through AGC1 kinase PAX. Nat Plants 6, 544-555.

Yang, Y., Hammes, U.Z., Taylor, C.G., Schachtman, D.P., and Nielsen, E. (2006). High-affinity auxin transport by the AUX1 influx carrier protein. Curr Biol 16, 1123-1127.

Yang, Z., Xia, J., Hong, J., Zhang, C., Wei, H., Ying, W., Sun, C., Sun, L., Mao, Y., Gao, Y., Tan, S., Friml, J., Li, D., Liu, X., and Sun, L. (2022). Structural insights into auxin recognition and efflux by Arabidopsis PIN1. Nature 609, 611-615.

Zegzouti, H., Anthony, R.G., Jahchan, N., Bogre, L., and Christensen, S.K. (2006a). Phosphorylation and activation of PINOID by the phospholipid signaling kinase 3-phosphoinositide-

dependent protein kinase 1 (PDK1) in Arabidopsis. Proc Natl Acad Sci U S A 103, 6404-6409.

Zegzouti, H., Li, W., Lorenz, T.C., Xie, M., Payne, C.T., Smith, K., Glenny, S., Payne, G.S., and Christensen, S.K. (2006b). Structural and functional insights into the regulation of Arabidopsis AGC VIIIa kinases. J Biol Chem 281, 35520-35530.

Zhang, J., Vanneste, S., Brewer, P.B., Michniewicz, M., Grones, P., Kleine-Vehn, J., Lofke, C., Teichmann, T., Bielach, A., Cannoot, B., Hoyerova, K., Chen, X., Xue, H.W., Benkova, E., Zazimalova, E., and Friml, J. (2011). Inositol trisphosphate-induced Ca2+ signaling modulates auxin transport and PIN polarity. Dev Cell 20, 855-866.

Zhang, Y., Hartinger, C., Wang, X., and Friml, J. (2020a). Directional auxin fluxes in plants by intramolecular domain-domain coevolution of PIN auxin transporters. New Phytol 227, 1406-1416.

Zhang, Y., Xiao, G., Wang, X., Zhang, X., and Friml, J. (2019). Evolution of fast root gravitropism in seed plants. Nat Commun 10, 3480.

Zhang, Y., Rodriguez, L., Li, L., Zhang, X., and Friml, J. (2020b). Functional innovations of PIN auxin transporters mark crucial evolutionary transitions during rise of flowering plants. Sci Adv 6.

Zhang, Z., van Ophem, D., Chelakkot, R., Lazarovitch, N., and Regev, I. (2022). A mechano-sensing mechanism for waving in plant roots. Sci Rep 12, 9635.

Zhao, H., Duan, K.X., Ma, B., Yin, C.C., Hu, Y., Tao, J.J., Huang, Y.H., Cao, W.Q., Chen, H., Yang, C., Zhang, Z.G., He, S.J., Zhang, W.K., Wan, X.Y., Lu, T.G., Chen, S.Y., and Zhang, J.S. (2020). Histidine kinase MHZ1/OsHK1 interacts with ethylene receptors to regulate root growth in rice. Nat Commun 11, 518.

Zourelidou, M., Muller, I., Willige, B.C., Nill, C., Jikumaru, Y., Li, H., and Schwechheimer, C. (2009). The polarly localized D6 PROTEIN KINASE is required for efficient auxin transport in Arabidopsis thaliana. Development 136, 627-636.

Zourelidou, M., Absmanner, B., Weller, B., Barbosa, I.C., Willige, B.C., Fastner, A., Streit, V., Port, S.A., Colcombet, J., de la Fuente van Bentem, S., Hirt, H., Kuster, B., Schulze, W.X., Hammes, U.Z., and Schwechheimer, C. (2014). Auxin efflux by PIN-FORMED proteins is activated by two different protein kinases, D6 PROTEIN KINASE and PINOID. eLife 3.

Acknowledgements

Allen voran möchte ich mich bei PD Dr. Ulrich Z. Hammes bedanken, der meine Doktorarbeit angeleitet hat und mir dieses spannende Thema schon in Regensburg überlassen hat. Du hast mich jederzeit gefordert und gefördert, in allen fachlichen und persönlichen Bereichen. Danke für dein Vertrauen und deine Unterstützung.
Ich bedanke mich bei Prof. Dr. Claus Schwechheimer, an dessen Lehrstuhl ich meine Arbeit anfertigen durfte und der mit viel fachlichem Input mein Projekt vorangebracht hat.
Danke an Prof. Kay H. Schneitz, der sich bereit erklärt hat als Zweitprüfer meine Dissertation zu begutachten. Danke an Prof. Ralph Hückelhoven, der den Vorsitz meines Prüfungskomitees übernommen hat.

Danke an die beste Martina T. Kolb. Danke für unzählige Stunden im Isotopenlabor, viel Gepiepse, viel Science, viele Gespräche, viele Konzerte, viel Lachen & Weinen.
Danke an die liebe Julia Karmann, in deren Nähe ich mich immer wohlgefühlt habe. Danke für dein offenes Ohr, deine Ratschläge und unser kleines Idyll in Ampertshausen.
Zusammen haben wir drei so viel erlebt und ich werde mich immer gerne an diese intensive und verrückte Zeit erinnern ♡
Danke an Angela, für deine tatkräftige Unterstützung und dass du immer für jeden Spaß zu haben bist. Danke an Clara und Lukas, die als nächste Generation unseren Labor-Spirit weiterleben. Danke an Jonathan, Philip und nochmal Lukas, die in ihren Bachelorarbeiten Teilprojekte bearbeitet haben.

Mein großer Dank geht an alle Frosch-Beteiligten: Prof. Dr. Hannelore Daniel, Dr. Britta Spanier, Katrin Petzold und allen voran an Helene Prunkl. Danke Helene, dass du mir die Kunst der Frosch-OP beigebracht hast und stundenlang Oozyten sortiert hast. Du hast damit die Grundlage dieser Arbeit geschaffen.

Danke an alle Mitarbeitenden des Lehrstuhls für Systembiologie der Pflanzen (TUM) und des Lehrstuhls für Zellbiologie und Pflanzenbiochemie (Universität Regensburg). Mein besonderer Dank geht an die guten Seelen der Lehrstühle Veronika Mrosek, Petra Wick und Daniela Elephand-Dill.

Zuletzt bin ich vor allem dankbar für die lieben Menschen aus meinem nicht-universitären Umfeld. Ohne euch wäre es wahrlich schwer gewesen diese Arbeit zu einem guten Abschluss zu bringen. Ich trag euch in meinem Herz.

Naphthylphthalamic acid associates with and inhibits PIN auxin transporters

Lindy Abas[a,1,2], Martina Kolb[b,1], Johannes Stadlmann[c], Dorina P. Janacek[b], Kristina Lukic[d], Claus Schwechheimer[b], Leonid A. Sazanov[d], Lukas Mach[a], Jiří Friml[d], and Ulrich Z. Hammes[b,2]

[a]Department of Applied Genetics and Cell Biology, University of Natural Resources and Life Sciences (BOKU), 1190 Vienna, Austria; [b]Plant Systems Biology, School of Life Sciences Weihenstephan, Technical University of Munich, 85354 Freising, Germany; [c]Department of Chemistry, University of Natural Resources and Life Sciences (BOKU), 1190 Vienna, Austria; and [d]Institute of Science and Technology Austria, 3400 Klosterneuburg, Austria

Edited by Julian I. Schroeder, University of California at San Diego, La Jolla, CA, and approved November 12, 2020 (received for review October 5, 2020)

***N*-1-naphthylphthalamic acid (NPA) is a key inhibitor of directional (polar) transport of the hormone auxin in plants. For decades, it has been a pivotal tool in elucidating the unique polar auxin transport-based processes underlying plant growth and development. Its exact mode of action has long been sought after and is still being debated, with prevailing mechanistic schemes describing only indirect connections between NPA and the main transporters responsible for directional transport, namely PIN auxin exporters. Here we present data supporting a model in which NPA associates with PINs in a more direct manner than hitherto postulated. We show that NPA inhibits PIN activity in a heterologous oocyte system and that expression of NPA-sensitive PINs in plant, yeast, and oocyte membranes leads to specific saturable NPA binding. We thus propose that PINs are a bona fide NPA target. This offers a straightforward molecular basis for NPA inhibition of PIN-dependent auxin transport and a logical parsimonious explanation for the known physiological effects of NPA on plant growth, as well as an alternative hypothesis to interpret past and future results. We also introduce PIN dimerization and describe an effect of NPA on this, suggesting that NPA binding could be exploited to gain insights into structural aspects of PINs related to their transport mechanism.**

auxin transport | NPA | PIN | auxin transport inhibitor | naphthylphthalamic acid

Many aspects of plant growth are controlled by the hormone auxin. A distinct feature of auxin is that its hormonal action requires it to be actively transported between cells and ultimately throughout the whole plant in a controlled directional or polarized manner, a process known as polar auxin transport (PAT). The ability of plants to perform PAT is ascribed to the auxin export activity of PIN transporters (1). Plasma membrane PINs can be restricted to a specific side of cells (2), and when this polarity is maintained in continuous plant cell files, the combined activity of identically localized PINs results in auxin flowing in that direction (3). This lays the vectorial foundations for PAT to create local auxin gradients and plant-wide PAT streams that are critical for auxin action and normal plant growth (4, 5).

Synthetic PAT inhibitors such as *N*-1-naphthylphthalamic acid (NPA) were initially developed as herbicides and then subsequently exploited by researchers to identify and characterize the unique PAT-based mechanisms that drive plant development (6). Having been used for over six decades, the question as to how NPA actually inhibits PAT has been keenly pursued. Several putative modes of action have been proposed, but the topic remains to date not fully or satisfactorily resolved (6).

Early studies established NPA binding with high affinity to membrane-integral components of plant membranes (7–10). With the later discovery of *pin1* mutants bearing their distinct bare inflorescences reminiscent of NPA-treated plants (11), followed by identification of the PIN gene family and gradual confirmation that PINs were NPA-sensitive auxin transporters that mediated PAT (1–5), it was apparent that the physiological and genetic evidence overwhelmingly linked NPA to inhibition of PIN activity (6). However, direct molecular association of NPA with PINs has never been reported (6). Instead, a substantial body of data has accumulated suggesting that the NPA target is not PIN itself, but rather other proteins or complexes that either actively coparticipate in PAT or are indirectly involved in control of PAT components (6, 12). Members of the B-family of ABC transporters, such as ABCB1 and ABCB19, showed high-affinity NPA binding and NPA-sensitive auxin export (1, 12–15), thus leading to proposals that they may either physically interact with PINs, or functionally interact such that their nonpolar auxin export activity contributes to PAT and/or to regulation of PINs (12, 16). In these scenarios, PIN/PAT would be rendered vulnerable to the NPA sensitivity of ABCB. However, these schemes are not yet fully resolved, are not fully consistent with key genetic and physiological data (6), and are particularly obfuscated by ABCB1/19 functioning both interactively and independently from PINs (1, 12, 15–20), with ABCB-PIN interaction occurring in an as-yet-unclarified manner (15, 18).

A further twist in assigning ABCBs as the main NPA target is their regulation by their chaperone TWD1/FKBP42 (14, 16), with TWD1 itself also being an NPA-binding protein (14, 17). NPA interferes with this regulation and affects TWD1-ABCB interaction, but curiously NPA cannot bind stably to the ABCB-TWD1 complex (14, 17). As TWD1 has also been implicated in NPA-sensitive actin-based PIN trafficking (17), this has led to a model proposing that TWD1 could mediate the NPA sensitivities of both ABCB and PINs, thus presenting TWD1 as a modulator of PAT (17, 21). In an analogous scheme in some plant species, CYPA immunophilins such as tomato DGT, which are functionally similar to TWD1/FKBP42, are suggested to replace TWD1 in modulating auxin transporters and transducing NPA effects to PINs (12, 21).

Similar to TWD1, BIG/TIR3 has also been associated with NPA and PIN trafficking (22). Given the undisputed role of trafficking in controlling PIN polarity (5), these reported effects warrant attention, although they are inconsistent with other reports that NPA perturbs neither vesicular trafficking nor actin dynamics in conditions where auxin transport is inhibited (23, 24). Together with trafficking, phosphorylation is another key modulator of PIN polarity as well as activity (5), so it is not surprising to find hypotheses suggesting that NPA could interfere with critical phosphorylation events (6), particularly as PID, a kinase crucial for PIN trafficking and activation, has also been connected to ABCB function and TWD1/ABCB/NPA interactions (25). Others propose that NPA may mimic natural compounds in their capacity as endogenous regulators of PAT, with plant flavonoids being suspected candidates (6, 26). Since flavonoids can compete with or inhibit ATP-binding in mammalian kinases and ABC transporters (27, 28), and as flavonoids can bind to and inhibit PID (25), a phosphorylation-based NPA mode of action would overlap with this hypothesis and poses the question whether NPA acts similarly as an ATP mimic.

With these many potential NPA-affected pathways, there is a need to distinguish between low- and high-affinity NPA targets and possible secondary effects due to prolonged PAT inhibition. Current consensus is that low concentrations of NPA (<10 μM) cause direct inhibition of auxin transporters in PAT (21) and the consequent physiological effects seen in planta (IC_{50} 0.1 to 10 μM) (7, 9, 19, 23, 29). This is associated with high-affinity binding to membranes (K_d 0.01 to 0.1 μM) (7, 8) and the inhibition of PIN/ABCB activity in short-term auxin transport assays (1, 14, 18, 20, 23). In contrast, NPA is thought to affect trafficking (21, 30) and other non-PAT processes (31) when used at higher doses (50 to 200 μM NPA), presumably via binding to its lower-affinity targets, although excessive NPA exposure may also have fast-acting toxic side effects (23). As the in vitro affinity of TWD1 for NPA is surprisingly low (K_d ~100 μM) (17), the TWD1-mediated NPA effects on PIN/PAT are thought to be of the low-affinity type and linked to trafficking perturbations (17, 21). However, as NPA is always externally applied to plants or cells, it is not clear how or where the drug distributes or accumulates, and thus there may be discrepancies between actual and reported/apparent effective concentrations, as might be the case for TWD1 (17). Finally, NPA also binds with low affinity to inhibit APM1, an aminopeptidase implicated in auxin-related plant growth, but as with trafficking effects, this low-affinity NPA interaction is not connected to direct regulation of PAT (31).

Thus, the available data proffer various indirect mechanisms that could lead to NPA inhibition of PIN-mediated PAT, but the proposed schemes have complicating aspects and struggle at times to satisfactorily explain the prime effects of NPA. Here we propose an alternative simpler scenario involving a more direct link between NPA and PINs that would resolve some of these currently outstanding issues. We present evidence from heterologous transport assays, classical in situ membrane binding, and oligomerization studies which collectively suggest that NPA can interact directly in a high-affinity manner with PINs, leading to conformational or structural effects and inhibition of auxin export activity.

Significance

The plant hormone auxin regulates many aspects of plant life and has the unique ability to flow throughout the plant in defined directions, as observed by Darwin over a century ago. The chemical NPA inhibits this directional flow, thereby severely affecting plant growth. In studying the specific effects of NPA, researchers have also uncovered general principles underlying plant development. Exactly how NPA inhibits directional auxin flow is unclear. NPA interacts with proteins that can transport auxin, such as ABCB transporters, and we show here that NPA also associates with and inhibits the major transporters that specialize in directional auxin flow—PINs. This explanation of NPA action will guide future research and may help reveal how PINs perform auxin transport.

Author contributions: L.A., M.K., C.S., L.M., J.F., and U.Z.H. designed research; L.A., M.K., J.S., and D.P.J. performed research; K.L., L.A.S., and J.F. contributed new reagents/analytic tools; L.A., M.K., J.S., and U.Z.H. analyzed data; and L.A. wrote the paper.

The authors declare no competing interest.

This article is a PNAS Direct Submission.

[1]L.A. and M.K. contributed equally to this work.

[2]To whom correspondence may be addressed. Email: melinda.abas@boku.ac.at or ulrich.hammes@wzw.tum.de.

This article contains supporting information online at https://www.pnas.org/lookup/suppl/doi:10.1073/pnas.2020857118/-/DCSupplemental.

Published December 22, 2020.

Results and Discussion

NPA Inhibits PIN-Mediated Auxin Transport in Oocytes. A notable advancement in auxin transport research was the recent establishment of a *Xenopus* oocyte assay to measure export activity of *Arabidopsis thaliana* PINs (32). As with previous assays, it monitors the retention of radiolabeled ^{3}H-indoleacetic acid (IAA). However, the ability to inject ^{3}H-IAA as well as any inhibitory drugs directly into oocytes avoids the vagaries associated with external application and passive preloading of both in previous heterologous assays. More importantly, there is also a unique on/off activity switch for the expressed *At*PINs by virtue of the absence or presence of coexpressed mandatory activating kinases (32). We thus utilized this improved and tractable system to investigate NPA effects on PIN activity.

When coinjected with ^{3}H-IAA into oocytes (NPA_{in}), 10 μM NPA (final internal concentration) abolished ^{3}H-IAA export mediated by kinase-activated *At*PIN1 or *At*PIN3, whereas 1 μM NPA_{in} caused partial inhibition (Fig. 1 *A* and *C*). We also saw NPA_{in} inhibition of *At*PIN6 export activity (*SI Appendix*, Fig. S1*A*), confirming that this noncanonical PIN is NPA-sensitive (33). NPA_{in} inhibition of PIN-dependent ^{3}H-IAA export occurred with either PID or D6PK as the activating kinase (Fig. 1*C*); thus kinase identity was not crucial.

We checked that inhibition of PIN activity was not due to deleterious effects of NPA on general oocyte viability by measuring ^{3}H-IAA or ^{14}C-leucine import by *At*AUX1 and *At*CAT6, respectively. In contrast to PINs, the activity of these other plasma membrane transporters was not compromised by 10 μM NPA_{in} (*SI Appendix*, Fig. S1 *C* and *D*), showing that NPA inhibits neither global transport nor ^{3}H-IAA transport in general. We found no effect of NPA_{in} on ^{3}H-IAA retention in control oocytes expressing inactive PIN without kinase, expressing kinase only, or neither (Fig. 1*C* and *SI Appendix*, Fig. S1 *A* and *E*), confirming that NPA

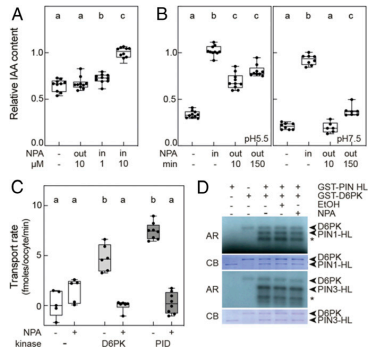

Fig. 1. NPA inhibits PIN-mediated ^{3}H-IAA efflux in oocytes. (*A*) In oocytes, coinjected NPA_{in} fully (10 μM) or partially (1 μM) inhibits ^{3}H-IAA efflux mediated by PIN1 (+YFP:D6PK), whereas external 10 μM NPA_{out} added immediately to the pH-7.5 medium has no effect (ANOVA; $n = 12$; a–c, b–c, $P < 0.001$; a–b, $P = 0.029$). (*B*) In pH-5.5 medium (*Left*), external 10 μM NPA_{out} is effective at inhibiting ^{3}H-IAA efflux mediated by PIN3 (+YFP:D6PK) after a 10-min preincubation whereas external NPA_{out} at pH 7.5 (*Right*) causes only partial inhibition after 2.5 h, compared to full inhibition by coinjected 10 μM NPA_{in} (ANOVA; $n = 10$; $P < 0.0001$ for all subsets). (*C*) Coinjected 10 μM NPA_{in} fully inhibits PIN3-mediated ^{3}H-IAA efflux from oocytes independent of the choice of activating kinase, YFP:D6PK or PID (two-way ANOVA, $n = 5$ to 8; $P < 0.001$ for ±kinase as well as ±NPA subsets). (*D*) In [γ-^{32}P]-*ATP* in vitro kinase assays, 10 μM NPA does not inhibit D6PK autophosphorylation or D6PK phosphorylation of PIN1 (*Upper*) or PIN3 (*Lower*) hydrophilic loops (HL); A single asterisk indicates PIN degradation products. AR, autoradiogram; CB, Coomassie Blue gel.

only affected outward movement of ^{3}H-IAA when mediated by active PINs. As a further control, we ruled out NPA being a direct competitor of IAA transport by performing transport assays with ^{3}H-NPA. We found that ^{3}H-NPA was not transported by PIN1 or PIN3 (with YFP:D6PK) in oocytes (*SI Appendix*, Fig. S1*B*), complementing earlier in planta data that NPA is not polarly transported in maize (7). Collectively, these controls indicate that the effect of NPA on ^{3}H-IAA retention in oocytes can be attributed to inhibition of PIN-mediated export activity.

Whereas previous auxin transport studies have used externally applied NPA by necessity, the oocyte system offers the opportunity to introduce NPA internally or externally, and as this has never been tested, we investigated this. In comparison to internally injected NPA_{in}, adding 10 μM NPA to external medium (NPA_{out}) of pH 7.5 at the start of the assay was ineffective in inhibiting PIN-mediated ^{3}H-IAA export (Fig. 1*A*, NPA_{out}). However, inhibition, was enhanced by either longer preincubation with 10 μM NPA_{out} at pH 7.5 or by changing to a plant-type medium pH of 5.5 (Fig. 1*B*). The more potent immediate effect of NPA_{out} at pH 5.5 and the delayed lesser effect at pH 7.5 suggest that NPA, a weak organic acid, diffuses into oocytes in the uncharged protonated state, with this species being more abundant at the lower pH of 5.5. This is consistent with previous suggestions of passive and pH-dependent uptake into maize coleoptiles (9). More importantly, we show that NPA has to enter cells and bind to an intracellular site to inhibit PIN-mediated ^{3}H-IAA export.

PIN activity in oocytes is kinase-dependent. As the requirement is for active phosphorylation rather than kinase presence per se (32), it was necessary to check if kinase activity was being affected by NPA. PID phosphorylation activity has been reported as NPA-insensitive (25), and here, using in vitro assays, we found that NPA perturbed neither autophosphorylation nor phosphorylation of PIN1 or PIN3 hydrophilic loops by D6PK (Fig. 1*D*). Taken together, as NPA affects neither kinase nor general oocyte transport competence nor background leakage, we conclude that NPA may be targeting PINs themselves at an intracellular site to inhibit PIN-mediated auxin efflux in oocytes.

NPA Binds to Plant Membranes Enriched in NPA-Sensitive PINs. These results prompted us to see if NPA could indeed bind to PINs. Radioligand-binding assays were used to initially establish and characterize high-affinity ^{3}H-NPA binding to plant microsomal membranes (7–10), followed by later reports linking microsomal ^{3}H-NPA–binding profiles to the presence or absence (in mutant lines) of suspected target proteins such as ABCB1/19, TWD1, actin, PID, or BIG/TIR3 (13, 14, 17, 20, 34). Microsomes from *pin1* or *pin2* mutants have been used to argue for the lack of NPA binding by PINs (17, 20), although such interpretation may be unwarranted as single mutants are not devoid of other PIN members. As there are no reports using PIN-enriched samples, we tested this using transient overexpression of *At*PINs in *Nicotiana benthamiana*. To remove nonexpressing cells, we isolated the lower epidermis of infiltrated leaves and used this pure population of transfected cells to prepare membranes highly enriched for the heterologously expressed *At*PINs (*SI Appendix*, Fig. S2*A*). This enabled us to develop a microscale binding assay using minimal amounts of membranes, such that any endogenous NPA binding was at undetectable levels. We also minimized reaction volumes to <10 μL, allowing us to monitor not just binding to membrane pellets but also the corresponding depletions from the supernatant (SN) (*SI Appendix*, Fig. S2*D*). The latter was a more reliable measure as bound ^{3}H-NPA started to dissociate from membranes during washing of pellets. Such rapid dissociation has been reported (7, 8, 10) and agrees with reversible NPA inhibition of PAT in planta (7).

Using competition by excess unlabeled NPA to define specific/saturable binding (8), we found that ^{3}H-NPA bound to membranes expressing *A. thaliana* PIN1, PIN2, PIN3, or PIN6 but not to membranes from mock controls (Fig. 2*A*). Addition of excess IAA or another aromatic acid (benzoic acid [BA]) did not compete with ^{3}H-NPA, showing that the observed binding was specific for NPA and reconfirming that IAA and NPA bind at different sites (7–9). Adding ATP did not hinder binding of ^{3}H-NPA, revealing that NPA cannot mimic the known ability of flavonoids to compete for ATP-binding sites (27, 28). Furthermore, ATP did not enhance ^{3}H-NPA binding in either controls or *At*PIN-expressing membranes, arguing against active ^{3}H-NPA transport into sealed vesicles by ATP-limited transporters (Fig. 2*A*). We could also exclude ^{3}H-NPA transport by PINs, as the added excess IAA would have competed with such transport; this agrees with our oocyte results and confirms that we were detecting binding per se rather than vesicular uptake (8). Binding was reversible, as mentioned above, and saturable by about 100 nM ^{3}H-NPA (*SI Appendix*, Fig. S2*D*), indicating high affinity.

The lack of binding in mock controls (Fig. 2*A*) indicated that overexpressed PINs were required for ^{3}H-NPA binding. We also expressed *Kf*PIN, a functional auxin transporter from the algae *Klebsormidium flaccidum*, but this did not lead to any specific binding of ^{3}H-NPA (*SI Appendix*, Fig. S2 *A* and *B*), which is consistent with *Kf*PIN-mediated auxin export being NPA-insensitive in *Nicotiana* BY2 cells (35). As *Kf*PIN was either exporting auxin by itself or integrating into NPA-insensitive auxin export complexes in the BY2 cells, when interpreted together with the NPA sensitivity of *At*PIN1/3/6-mediated auxin export (1, 33) (Fig. 1 *A* and *C* and *SI Appendix*, Fig. S1*A*), our results show that NPA sensitivity of PINs correlates with their NPA-binding capability, providing additional support for PINs being an NPA-binding component of auxin export.

PIN-Expressing Plant Membranes Are Not Enriched for Other Potential NPA-Binding Proteins. The mock and *Kf*PIN controls suggested that, in the absence of NPA-sensitive PINs, endogenous *N. benthamiana* proteins, membrane lipids or cell walls that were present in the membranes did not detectably contribute to ^{3}H-NPA binding. We were able to exclude any involvement of PIN–cell-wall interactions (5) by using membranes released by enzymatic digestion; these cell-wall–free preparations also bound similar amounts of ^{3}H-NPA (*SI Appendix*, Fig. S2*C*).

To test whether endogenous *N. benthamiana* proteins such as ABCBs or TWD1 were up-regulated in the PIN-overexpressing samples and thus potentially participating or contributing to ^{3}H-NPA binding, we performed quantitative multiplexed mass spectrometry (QMS). Three control and three *At*PIN-expressing samples were labeled with isobaric tags, allowing direct comparison of the relative abundances of endogenous *N. benthamiana* proteins between all six samples. About 3,600 *N. benthamiana* proteins could be quantified (Fig. 2*B*). Based on spectral counts, heterologous *At*PIN1, *At*PIN2, and *At*PIN3 were found to be much more abundant than the only endogenous PIN detected, *Nb*PIN7 (Fig. 2*B* and *SI Appendix*, Table S1). Direct quantitative comparison between *Nb*PIN7 and *At*PIN3 was possible using the relative abundances of shared peptides, revealing that *Nb*PIN7 was at least 20-fold less abundant than *At*PIN3, although this difference is certainly underestimated as interference by technical noise greatly distorts comparison between peptides if they have vastly different relative abundance values, as is the case here (*Materials and Methods*). From immunoblot analysis (*SI Appendix*, Fig. S2*A*), we estimate that *At*PINs were >200-fold more highly expressed in *N. benthamiana* samples when compared to native *At*PIN expression in shoot (36) or to *At*PIN expressed in *N. benthamiana* using native promoter expression (37), providing support that NPA binding could be attributed to an overabundance of *At*PINs.

Global comparison of the relative abundances of 3,687 *N. benthamiana* proteins between controls and PIN samples in QMS revealed no up-regulation of any proteins comparable to the overabundant levels achieved by *At*PINs (Fig. 2 *B* and *C*). Major plasma membrane proteins such as ATPases, aquaporins, and cellulose synthases, as well the auxin transporters AUX/LAX and *Nb*PIN7, were similar between all samples, also indicating equivalent amounts of plasma membranes (Fig. 2 *B* and *C* and *SI Appendix*, Table S1). BIG/TIR3, D6PK-like, and 20 ABC transporters were found, with 6 ABCB-family members including ABCB1 but not ABCB19. *Nb*TWD1/FKBP42 was not detected, which may reflect low abundance in planta, as reported for *At*TWD1 (14, 15). However, five other sequence-related FKBP proteins were detected with *Nb*Pasticcino and *Nb*FKBP62 being most similar to TWD1/FKBP42 (*SI Appendix*, Fig. S2*H*). Nine CYPs were present (*SI Appendix*, Fig. S2*J*), including two orthologs of tomato DGT, annotated here as *Nb*DGT1 and *Nb*DGT2. As *Nb*DGT1/2 are more closely related to tomato DGT (95 to 96% identity) than *A. thaliana* orthologs (*At*ROC1/CYP1; 81% identity to tomato DGT), they may be potential PIN interactors (21). *N. benthamiana* has putative orthologs of *At*APM1 (*SI Appendix*, Fig. S2*I*), but none was detected in the QMS.

For all these endogenous proteins and identified potential NPA-binding or PIN-interacting proteins, we found no up-regulation

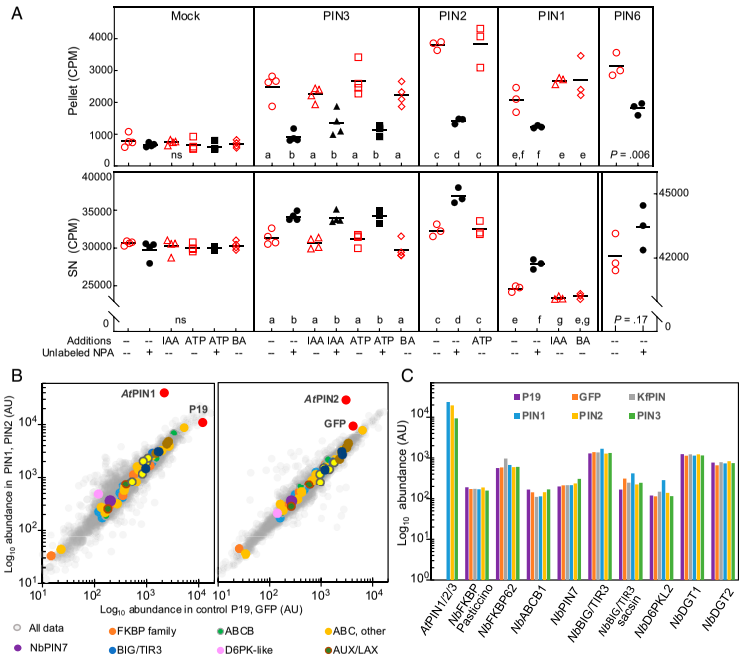

Fig. 2. NPA binds to leaf epidermal membranes overexpressing *At*PINs. (*A*) ^{3}H-NPA binds in a specific&saturable manner to *N. benthamiana* epidermal peel membranes expressing *At*PIN1/2/3/6 but not to membranes from mock controls, with accumulation (open red symbols) in pellet (*Upper*) and depletion from SN (*Lower*) competed by 20 μM unlabeled NPA (filled black symbols). Addition of 20 μM IAA or BA or 3 mM ATP did not compete for binding. Comparisons by *t* test (PIN6, $n = 3$) or ANOVA ($n = 3$ or 4). For pellet: a–b, $P = 0.03$; c–d, $P = 0.001$; e–f, $P = 0.008$. For SN: a–b, $P = 0.004$; c–d, $P = 0.003$; e–f, f–g, $P = 0.001$; e–g, $P = 0.04$. (*B*) Relative abundance values of 3,687 endogenous *N. benthamiana* proteins from QMS analysis (gray cloud; $\log_{10}$ scale; AU, arbitrary units) were compared between controls and PIN-expressing samples (*Left*, P19 vs. PIN1+P19; *Right*, GFP vs. PIN2+GFP). Highlighted *N. benthamiana* proteins are described in the text. Heterologous *At*PIN1/PIN2, GFP, and P19 are shown as red dots; *At*PIN1/PIN2 are plotted against the technical noise in their respective controls (*Materials and Methods*). GFP refers to GFP-KDEL (*SI Appendix*, Fig. S2*F*). (*C*) Relative abundance values of selected *N. benthamiana* proteins from QMS analysis compared across three nonbinding control (P19, GFP, *Kf*PIN) and three overexpressing PIN (*At*PIN1/2/3) samples ($\log_{10}$ scale; AU, arbitrary units). Selected relative abundance values in *B* and *C* are in *SI Appendix*, Table S1.

suggestive of a stoichiometric complex with overexpressed *At*PINs (Fig. 2 *B* and *C* and *SI Appendix*, Table S1). We cannot rule out that transient chaperone interactions were required to confer NPA-binding ability, or that complexes between overexpressed PINs and other unchanging abundant proteins may have occurred. However, as these along with *Nb*PIN7 and *NbABCB1* remained unchanged and showed no detectable binding in any controls (Fig. 2*A* and *SI Appendix*, Fig. S2 *B*–*D*), we conclude that, if present, any endogenous interactors did not contribute to the observed ^{3}H-NPA binding and/or that PINs were the necessary NPA-binding component of any such complexes. The lack of detectable binding by *Nb*ABCB1 or *Nb*PIN7 can be attributed to the minimal amounts of material used and low endogenous abundance compared to the highly overexpressed *At*PINs.

As a precise NPA-binding pocket in *At*TWD1 has been identified by NMR analysis (albeit using an unusually high concentration of 3.1 mM NPA due to methodological constraints) (17), we further checked if the other *N. benthamiana* FKBPs found in QMS could be expected to bind NPA. Sequence alignment with *At*TWD1 revealed similarity in only one of the four clusters involved in binding (*SI Appendix*, Fig. S2 *G* and *H*), implying that these *N. benthamiana* FKBPs are unlikely to bind NPA, particularly at the low concentrations (<0.1 μM) of ^{3}H-NPA used compared to the reported K_d of ∼100 μM for *At*TWD1 (17). We also noted that K79 in the second cluster, identified as the most critical residue for NPA binding (17), is not conserved in *Nb*FKBP42, but is instead E79 (*SI Appendix*, Fig. S2*G*). We found that in other plant species, K79 frequently varies as E79/Q79/A79 within an otherwise conserved region of FKBP42 (*SI Appendix*, Fig. S2*K*). As mutating K79 to L79 abolished NPA binding in *At*TWD1 and conferred NPA insensitivity in vivo (17), it would thus be interesting to see if E79/Q79/A79 variants can bind NPA, particularly A79 which resembles the nonbinding L79 mutation.

Overall, our QMS and sequence analysis did not reveal any endogenous proteins that could potentially account for the observed NPA binding, leaving the enriched heterologous *At*PINs as the most plausible NPA-binding component in this experimental setup.

NPA Binds to Heterologous PIN-Enriched Membranes and Is Independent of Phosphorylation. To further confirm PINs as the NPA-binding component, we repeated the binding assays using *At*PINs expressed in nonplant hosts (*SI Appendix*, Fig. S3 *C*–*E*). Membranes from oocytes (PIN1) as well as yeast (PIN6:GFP) both bound ^{3}H-NPA in a specific/saturable manner whereas nonexpressing controls did not, with excess BA in all samples not competing for binding (Fig. 3 *A* and *B*). This shows that plant-derived components are not required, agreeing with our QMS results that endogenous *N. benthamiana* proteins were not contributing to NPA binding. Furthermore, as PIN-expressing oocyte membranes bound NPA in this in vitro setting, this suggests that the in vivo transport inhibition observed was not due to NPA perturbing transient chaperone or trafficking events in oocytes, as these are not expected to occur in isolated membranes.

In oocyte membranes, NPA binding was independent of PIN1 hydrophilic loop phosphorylation as similar binding occurred with or without D6PK phosphorylation of PIN1 (Fig. 3*A*), which can be detected in PIN1 immunoblots by slower migration and a phosphorylation smear (32, 37) (Fig. 3*C*) and which was stable throughout the binding assay. D6PK itself did not participate in ^{3}H-NPA binding, as it partitioned into the SN and was absent from the membrane fraction used for binding assays (Fig. 3*D*). The *N. benthamiana* ^{3}H-NPA binding results also gave no indication of phosphorylation requirements in that we did not attempt to preserve phosphatase-sensitive phosphorylation during membrane extraction and thus PIN1 and PIN3 in the *N. benthamiana* membranes were no longer phosphorylated (no smear detected in immunoblots) whereas PIN2 had some residual smear (*SI Appendix*, Fig. S2*A*), yet all were able to bind NPA (Fig. 2*A*). We further checked the effect of NPA on in vivo steady-state phosphorylation of PIN in plant cells, where multiple kinases and phosphatases would contribute (37). Using *35S:PIN1* to avoid complications from transcriptional responses, we found no reduction in the PIN1 phosphorylation smear, noting also that PIN stability was unaffected by NPA (Fig. 3*E*). Thus, NPA does not impinge on global PIN phosphorylation status in vivo, agreeing with our in vitro data (Fig. 1*D*), and neither phosphorylation nor

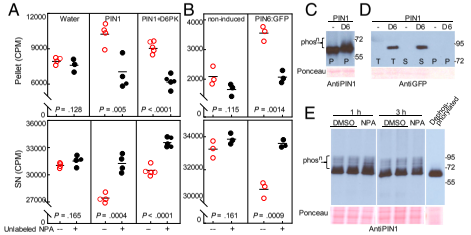

Fig. 3. NPA binds to oocyte and yeast membranes expressing PINs. (*A*) ^{3}H-NPA binds in a specific/saturable manner to membranes from oocytes expressing PIN1 or PIN1+YFP:D6PK but not to membranes from control oocytes (injected with water instead of RNA), with an increase in pellet (red symbols, *Upper*) and depletion in SN (red symbols, *Lower*) compared to samples with 30 μM unlabeled NPA (black symbols) (*t* test, $n = 4$ to 5). All samples contained 30 μM BA. (*B*) ^{3}H-NPA binds in a specific/saturable manner to membranes from yeast expressing PIN6:GFP but not to noninduced control membranes with an increase in pellet (red symbols, *Upper*) and depletion in SN (red symbols, *Lower*) compared to samples with 30 μM unlabeled NPA (black symbols) (*t* test, $n = 3$). All samples contained 15 μM BA. (*C*) Anti-PIN1 immunoblots using membranes from PIN1 + YFP:D6PK (D6) oocytes detect PIN1 traveling as a slower migrating species with a smear, indicative of YFP:D6PK-mediated phosphorylation, which is not seen when PIN1 is expressed alone. (*D*) YFP:D6PK (D6) partitioned into the soluble SN fraction (S) and was not detectable in the oocyte membrane pellet fraction (P) used for binding assays (T, total extract; antiGFP immunoblot). (*E*) In *35S:PIN1* suspension culture cells, 10 μM NPA treatment (1 to 3 h) did not reduce the endogenous PIN1 phosphorylation smear (antiPIN1 immunoblot). Dephosphorylated PIN1 is shown for comparison.

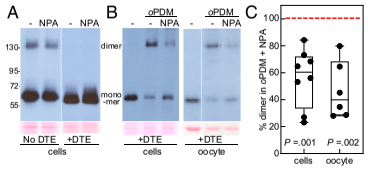

Fig. 4. NPA inhibits *o*PDM cross-linking of PIN1 into dimers. (*A*) Endogenous PIN1 dimers seen in nonreducing SDS/PAGE (No DTE) are unaffected by in vivo NPA treatment of suspension cells (10 μM, 2 h; antiPIN1 immunoblot). (*B*) In membranes from suspension cells or oocytes, PIN1 is cross-linked into DTE-resistant dimers by *o*PDM in vitro, and this is inhibited by NPA (antiPIN1 immunoblot). (*C*) Monomers and cross-linked PIN1 dimers from *o*PDM treatments (± NPA) were quantified from immunoblots and dimer:monomer ratios were calculated. The ratio in *o*PDM+NPA was compared to *o*PDM+DMSO by a one-sample *t* test with the latter used as the test value of 100% as indicated by the dashed red line. NPA reduced the amount of *o*PDM-linked PIN1 dimers in both suspension cells ($n = 8$, 95% CI [26, 62]) and oocytes ($n = 6$, 95% CI [31, 75]).

kinase appear to be required or inhibitory for NPA association with PINs.

In summary, we found that ^{3}H-NPA binding to *N. benthamiana*, oocytes, and yeast membranes correlates with the overexpression of *At*PINs, independent of host, phosphorylation status, or other plant proteins or cell-wall components, collectively supporting a direct association with PINs or a major role for PINs in enhancing NPA binding to PIN-enriched membranes.

NPA Interferes with a PIN Dimer Interface. As we saw NPA binding as well as NPA inhibition of PIN activity in oocytes, we sought a mechanism that might explain or connect these two observations. We found that PINs form disulfide-dependent dimers that are visible in nonreducing sodium dodecyl sulfate/polyacrylamide gel electrophoresis (SDS/PAGE) and which are not affected by NPA (Fig. 4*A*). However, we then treated plant or oocyte membranes with *ortho*-phenylenedimaleimide (*o*PDM), a bifunctional reagent that can covalently cross-link two vicinal free cysteines (Cys). This led to *o*PDM-linked PIN dimers now resistant to reducing agents such as dithioerythritol (DTE) (Fig. 4*B*), and we found that less cross-linking occurred when NPA was present (Fig. 4 *B* and *C*). This effect was seen with both PIN1 and PIN2 from cultured plant cells as well as with PIN1 from oocytes (Fig. 4 *B* and *C* and *SI Appendix*, Fig. S4*A*), indicating a property inherent of PINs and independent of the host membrane. The cross-linking of other proteins in the same sample was not affected by NPA (*SI Appendix*, Fig. S4 *C* and *D*), and we further confirmed that NPA did not affect the chemical reactivity of *o*PDM or Cys (*SI Appendix*, Fig. S4*B*). We also checked other compounds and found that neither auxins (IAA or 1-naphthylacetic acid [NAA]) nor the alternative PAT inhibitor 2,3,5-triiodobenzoic acid (TIBA) could inhibit cross-linking of PINs by *o*PDM (*SI Appendix*, Fig. S4 *D* and *E*).

These data support an inhibitory effect on cross-linking of PINs that was unique for NPA and suggestive of an interaction between NPA and PIN. Possible explanations are that NPA binds near a Cys to sterically hinder the reaction with *o*PDM, or elsewhere to cause a conformational change, or that NPA can prise PIN monomers apart beyond the 9-Å maximum cross-linking span of *o*PDM (38). This observation is reminiscent of NPA disrupting TWD1-ABCB1 interaction (14), although NPA is proposed to bind to soluble domains in TWD1 or ABCB1 (14, 17, 20), whereas all Cys in PIN1/2 are predicted to be in putative transmembrane domains or in short membrane-proximal cytoplasmic loops. Thus, the NPA effect on PINs appears to be different from that of TWD1/ABCB in involving transmembrane domains rather than soluble regions, agreeing with reports describing NPA-binding sites as membrane-integral (10). We note that the predicted cytoplasmic locations for Cys in PIN1/2 are consistent with our oocyte results of an intracellular NPA-binding site.

Since we used intact membranes for both ^{3}H-NPA binding and *o*PDM cross-linking, we cannot rule out that NPA interaction involves the immediate lipid environment of PINs, particularly as PIN activity (Fig. 1) and oligomerization (Fig. 4) are affected and as lipids are known to be important regulators of both in transporters and membrane proteins in general (39, 40). However, as we used three different phyla (plants, animals, fungi) known to have very different membrane lipid composition (39), it seems that PINs themselves are the determining factor in shaping any potential NPA–lipid interaction. Additionally, although ABCBs may stabilize PINs in certain sterol domains in plants and yeast (15), the ability of PINs to function in foreign oocyte membranes is now accepted as evidence that neither ABCB chaperoning nor specialized plant lipid domains are essential for PIN activity (12).

Notwithstanding any lipid involvement, NPA was able to bind to as well as inhibit cross-linking of PINs in oocyte membranes. Thus, a possible explanation for the transport inhibition in oocytes could be an NPA–PIN interaction that leads to conformational or structural perturbations in PINs, providing a potential mechanism for PIN inactivation and inviting consideration of using NPA as a structural or functional activity probe for PINs.

Conclusions

Our data provide an evidential basis to invoke a straightforward mechanistic explanation for NPA inhibition of PINs, in which NPA can bind to PINs independently of other potential NPA-binding proteins. Direct PIN inhibition offers a physiologically relevant model of NPA action and a parsimonious hypothesis to plan and interpret future work, as an alternative to, or combined with, current indirect models. It may also be prudent to reinterpret past work in light of our results to reconsider possible overlooked effects or contributions due to NPA binding by PINs.

The combination of existing models with the one presented here means that NPA could synergistically inhibit both PIN- and ABCB-based major auxin streams. Since it is unlikely to be due to chance that a synthetic compound binds diverse targets (ABCB, PIN, TWD1) in a common auxin export pathway, one way to explain this apparent coincidence is the concept that NPA mimics an endogenous counterpart which has evolved to do precisely so. Our results provide hints as to how NPA or an endogenous inhibitor may interact with PINs, namely an intracellular allosteric site distinct from IAA substrate-binding sites, possibly involving membrane-proximal conserved Cys residues and an interface between monomers. Any involvement of the PIN hydrophilic loop is restricted to the ∼100 residues shared between canonical PIN1/2/3 and the shorter loop of PIN6. Furthermore, binding is independent of the many phosphorylation sites contained therein and does not require loop kinases. Further investigations into these and other aspects of NPA–PIN interactions are warranted with the collateral benefit of gaining much needed structural and mechanistic insights into PINs.

Materials and Methods

Oocyte Transport. Oocytes were injected with ^{3}H-IAA or ^{3}H-NPA (American Radiolabeled Chemicals) (32). NPA was coinjected with ^{3}H-IAA (1 or 10 μM final internal concentration; NPA_{in}) or added into the medium (10 μM final external; NPA_{out}) at 0, 10, or 150 min before injecting ^{3}H-IAA. Results are presented as "relative IAA content" (^{3}H-IAA cpm in oocytes at 30 vs. 0 min) or as transport rates from linear regression of a cpm vs. time plot, translated to fmol based on the specific activity of ^{3}H-IAA. External medium was Barth's solution (32) with 10 mM Hepes, pH 7.5 or 5.5. For AUX1/^{3}H-IAA (41) and CAT6/^{14}C-leucine (ARC) (42) assays, oocytes were injected with 10 μM NPA_{in}, and results are presented as cpm in oocytes at the end of assays.

Phosphorylation and Dimers. In vitro [γ-^{32}P]-*ATP* phosphorylation assays were performed with ±10 μM NPA (32). For global phosphorylation or endogenous dimer analysis, *35S:PIN1* suspension cells were treated with 10 μM NPA or dimethylsulfoxide (DMSO) (1 to 4 h in 0.5x Murashige–Skoog medium [MSM]), and membranes were extracted (36, 37).

***N. benthamiana* Membranes.** *At*PIN1/2/3/6 or *Kf*PIN (in pMDC7 or pK7WG2D) were agroinfiltrated together with P19 (43) into *N. benthamiana* leaves. Mock controls received empty vectors and/or P19. Leaves with pMDC7 were induced (24 h, 2 μM β-estradiol/0.2x MSM). The lower epidermis was peeled off, and membranes were extracted by homogenization (36) or released by digestion (1 h, 4 °C, 0.07% cellulase/0.03% macerozyme in 50 mM Tris–HCl, pH 7.4/5 mM ethylenediaminetetraacetic acid [EDTA]/0.05% casein/2% glycerol [EB] with 1 mM phenylmethylsulfonyl fluoride [PMSF]/1 μg/mL aprotinin/leupeptin/pepstatin/E64 [PI]). Membranes were collected (45,000 x *g*, 30 min, 4 °C), washed (20 mM Tris–HCl, pH 8/5 mM EDTA [TE]), and resuspended in EB + PI.

Yeast Membranes. *At*PIN6 in pDDGFP_LEU2D was transformed into *Saccharomyces cerevisiae* BJ5460. Cultures started in LEU-dropout medium +2% lactate (from OD 0.05 to 0.6) were induced with 2% galactose (20 h, 30 °C) (*SI Appendix*, Fig. S3*D*). Yeast were spheroplasted using Zymolase 20T (Roth), disrupted in TE + PI, and twice spun through 5% glycerol/TE/1 mM PMSF onto a 0.1-mL 50% sucrose cushion (45,000 x *g*, 30 min, 4 °C). Membrane pellets were resuspended in 5% glycerol/TE/1 mM PMSF.

Oocyte Membranes. Oocytes were homogenized (100 mM Tris–HCl, pH 7.5/10 mM EDTA/5 mM EGTA/0.1% casein/10% glycerol/50 mM NaF/20 mM β-glycerol PO_4/10 mM $NaMO_4$/Phosstop/PI), and a crude pellet was collected (45,000 x *g*, 30 min, 4 °C). Yolk proteins (vitellogenins) were removed from this pellet by successive washing with 100 mM $MgCl_2$, 1 M NaCl, and TE (modified from ref. 44) (*SI Appendix*, Fig. S3*A*) and resuspended in EB + PI. Residual vitellogenin was similar in all samples (*SI Appendix*, Fig. S3*B*). Control water-injected and RNA-injected oocytes were prepared from the same batches.

Radioligand Binding Assay. We modified previous assays (7–10) into a microscale assay (<10 μL). Each reaction contained membranes (1 to 3 μL pellet volume) from 15 to 30 mg *N. benthamiana* peel, 12 OD units yeast or two oocytes, in all cases ~100 to 300x the amounts required to obtain a very strong signal in immunoblot analysis of PIN expression levels (*SI Appendix*, Figs. S2*A* and S3 *C* and *E*). For each series, equal aliquots of membranes were pelleted (21,000 x *g*, 30 min, 4 °C) and washed with 20 mM $MgCl_2$, and all traces of supernatant removed. The pellet was carefully resuspended in an exact volume (3 to 6 μL) of binding buffer (RB: 5% glycerol/0.1 mM $MgSO_4$/5 mM KCl and 50 mM $KHPO_4$/$NaHPO_4$, pH 6.5 or 7.5) containing ^{3}H-NPA (~0.05 μCi, 60 Ci/mmol) and 1-μL additions (unlabeled NPA, BA, or IAA (20- to 30-μM final concentrations) or ATP (3-mM final concentration, pH adjusted to 7.4 with two molar equivalents of Tris base) or solvent (DMSO or pH 7.4 Tris–HCl). When ATP was used, 5 mM $MgCl_2$ was included in the whole series. All yeast (15 μM) and oocyte (30 μM) samples contained BA. After 2 to 6 h, samples were spun (21,000 x *g*, 15 min, 4 °C), and a precise volume of SN was removed. Pellets were counted directly (as in refs. 7–9), or washed by quickly transferring to GF/F Whatman filters (as in ref. 10) using 10 μL RB and rapidly washing with 3x 0.7 mL RB/0.1 μM BA in a vacuum manifold. Radioactivity in pellets, filters, and SN was measured by liquid scintillation counting, and results are reported as cpm (61% counting efficiency). A typical reaction contained a 1.5-μL membrane pellet resuspended in 6 μL, from which 5 or 6 μL SN was subsequently removed for washed or unwashed pellets, respectively (*SI Appendix*, Fig. S2*D*). Accurate pipetting was essential for this microscale assay; we used low-binding extrafine-tipped pipette tips (10 μL extralong Surphob Tips, Biozym) and an Eppendorf 10-μL pipette with a metal-tip cone and volume lock. ^{3}H-NPA was used within 2.5 y of purchase.

Cross-linking. Membranes from cells or oocytes were pretreated with 20 to 50 μM NPA, TIBA, NAA, IAA, or DMSO (30 to 60 min; 0.2 M $NaHPO_4$ pH 7.5/10% glycerol or RB), cross-linked (5 to 60 min, 0.2 to 0.5 mM oPDM [Sigma] or DMSO) and quenched (5 mM *N*-ethylmaleimide or 20 mM DTE followed by 60 mM *N*-ethylmaleimide). NPA did not affect the chemical reactivity or stability of oPDM or Cys, tested using Ellman's reagent/DTNB ($Abs_{412\ nm}$) (*SI Appendix*, Fig. S4*B*).

Immunoblotting. Membrane fractions were prepared as above or as in ref. 36. Membranes from <0.1 mg *N. benthamiana* peel, 1/50th oocyte, or 0.1 OD units yeast were blotted (36, 37) and probed with antiPIN1 or antiPIN2 (36), antiPIN3 (45), anti*Kf*PIN (35), antiGFP (Roche) or rabbit antiPIN6 raised against residues 167 to 405 of *At*PIN6. Molecular weight markers and Ponceau-stained blots are shown next to immunoblots. Bands were quantified from images captured using ImageLab/ChemiDocXRS (Biorad).

QMS. Equal amounts of *N. benthamiana* membranes from three controls (P19, GFP-KDEL, *Kf*PIN) and three *At*PIN-expressing samples (PIN1, PIN2+GFP-KDEL, PIN3; all six samples contained P19) were sequentially solubilized with 2% dodecylmaltoside, 0.4% SDS, and 0.5% sodium deoxycholate (*SI Appendix*, Fig. S2 *E* and *F*), precipitated with CHCl$_3$/MeOH, solubilized with a graded ethanol series, labeled using isobaric TMTsixplex as per the manufacturer's instructions (Thermo Fisher Scientific) and combined for QMS (46). We used the *N. benthamiana* NbDE proteome database (47). Sequences were analyzed in MEGA-X using multiple alignment by ClustalW or MUSCLE with manual curation. For heterologous proteins (*At*PIN, GFP-KDEL), the apparent relative abundance values in the other nonexpressing samples are technical noise from the overtly overexpressing sample(s) due to precursor ion impurity and coisolation. We confirmed this using an alternate SPS3 data-acquisition regime, where noise values for PIN1 were reduced from 5–11% (*SI Appendix*, Table S1) to 0–0.6% in SPS3 and for PIN2 from 9–17% to 0.6–1.5%. Similarly, direct quantitative comparison using shared peptides between *At*PIN and *Nb*PIN7 was unreliable as the extreme differences in relative abundances caused technical noise in the nonexpressing samples. Fig. 2*C* uses relative abundance values normalized using global average relative abundance from 3,687 *N. benthamiana* proteins detected in each sample (*SI Appendix*, Table S1).

Statistics. Data were analyzed in Microsoft Excel 2016, IBM SPSS Statistics v24, or GraphPad Prism8. Unpaired *t* tests (two-tailed *P* values) were used, except for Fig. 3*C* (one-sample *t* test). One-way ANOVA was used unless otherwise stated and was not significant (ns) if $P > 0.05$. Post-hoc analysis was by Holm–Sidak, Dunn, or Tukey's tests; lowercase letters indicate homogeneous subsets. For ^{3}H-NPA–binding data, bars show means.

Data Availability. All study data are included in the article and supporting information.

ACKNOWLEDGMENTS. This work was supported by Austrian Science Fund Grant FWF P21533-B20 (to L.A.); German Research Foundation Grant DFG HA3468/6-1 (to U.Z.H.); and European Research Council Grant 742985 (to J.F.). We thank Herta Steinkellner and Alexandra Castilho for *N. benthamiana* plants, Fabian Nagelreiter for statistical advice, Lanassa Bassukas for help with [γ-^{32}P]-*ATP* assays, and Josef Penninger for providing access to mass spectrometry instruments at the Vienna BioCenter Core Facilities. We thank PNAS reviewers for the many comments and suggestions that helped to improve this manuscript.

1. J. Petrášek *et al.*, PIN proteins perform a rate-limiting function in cellular auxin efflux. *Science* **312**, 914–918 (2006).
2. L. Gälweiler *et al.*, Regulation of polar auxin transport by AtPIN1 in Arabidopsis vascular tissue. *Science* **282**, 2226–2230 (1998).
3. J. Wiśniewska *et al.*, Polar PIN localization directs auxin flow in plants. *Science* **312**, 883 (2006).
4. E. Benková *et al.*, Local, efflux-dependent auxin gradients as a common module for plant organ formation. *Cell* **115**, 591–602 (2003).
5. M. Adamowski, J. Friml, PIN-dependent auxin transport: Action, regulation, and evolution. *Plant Cell* **27**, 20–32 (2015).
6. W. Teale, K. Palme, Naphthylphthalamic acid and the mechanism of polar auxin transport. *J. Exp. Bot.* **69**, 303–312 (2018).
7. K. S. Thomson, R. Hertel, S. Müller, J. E. Tavares, 1-N-naphthylphthalamic acid and 2,3,5-triiodobenzoic acid : In-vitro binding to particulate cell fractions and action on auxin transport in corn coleoptiles. *Planta* **109**, 337–352 (1973).
8. M. R. Sussman, G. Gardner, Solubilization of the receptor for N-1-naphthylphthalamic acid. *Plant Physiol.* **66**, 1074–1078 (1980).
9. M. R. Sussman, M. H. M. Goldsmith, The action of specific inhibitors of auxin transport on uptake of auxin and binding of N-1-naphthylphthalamic acid to a membrane site in maize coleoptiles. *Planta* **152**, 13–18 (1981).
10. P. Bernasconi, B. C. Patel, J. D. Reagan, M. V. Subramanian, The N-1-Naphthylphthalamic acid-binding protein is an integral membrane protein. *Plant Physiol.* **111**, 427–432 (1996).
11. K. Okada, J. Ueda, M. K. Komaki, C. J. Bell, Y. Shimura, Requirement of the auxin polar transport system in early stages of Arabidopsis floral bud formation. *Plant Cell* **3**, 677–684 (1991).
12. M. Geisler, B. Aryal, M. di Donato, P. Hao, A critical view on ABC transporters and their interacting partners in auxin transport. *Plant Cell Physiol.* **58**, 1601–1614 (2017).
13. B. Noh, A. S. Murphy, E. P. Spalding, Multidrug resistance-like genes of Arabidopsis required for auxin transport and auxin-mediated development. *Plant Cell* **13**, 2441–2454 (2001).
14. A. Bailly *et al.*, Modulation of P-glycoproteins by auxin transport inhibitors is mediated by interaction with immunophilins. *J. Biol. Chem.* **283**, 21817–21826 (2008).
15. B. Titapiwatanakun *et al.*, ABCB19/PGP19 stabilises PIN1 in membrane microdomains in Arabidopsis. *Plant J.* **57**, 27–44 (2009).
16. G. Wu, M. S. Otegui, E. P. Spalding, The ER-localized TWD1 immunophilin is necessary for localization of multidrug resistance-like proteins required for polar auxin transport in Arabidopsis roots. *Plant Cell* **22**, 3295–3304 (2010).
17. J. Zhu *et al.*, TWISTED DWARF1 mediates the action of auxin transport inhibitors on actin cytoskeleton dynamics. *Plant Cell* **28**, 930–948 (2016).
18. J. J. Blakeslee *et al.*, Interactions among PIN-FORMED and P-glycoprotein auxin transporters in Arabidopsis. *Plant Cell* **19**, 131–147 (2007).
19. J. Mravec *et al.*, Interaction of PIN and PGP transport mechanisms in auxin distribution-dependent development. *Development* **135**, 3345–3354 (2008).
20. J.-Y. Kim *et al.*, Identification of an ABCB/P-glycoprotein-specific inhibitor of auxin transport by chemical genomics. *J. Biol. Chem.* **285**, 23309–23317 (2010).
21. M. Geisler, A. Bailly, M. Ivanchenko, Master and servant: Regulation of auxin transporters by FKBPs and cyclophilins. *Plant Sci.* **245**, 1–10 (2016).
22. T. Paciorek *et al.*, Auxin inhibits endocytosis and promotes its own efflux from cells. *Nature* **435**, 1251–1256 (2005).
23. J. Petrášek *et al.*, Do phytotropins inhibit auxin efflux by impairing vesicle traffic? *Plant Physiol.* **131**, 254–263 (2003).
24. P. Dhonukshe *et al.*, Auxin transport inhibitors impair vesicle motility and actin cytoskeleton dynamics in diverse eukaryotes. *Proc. Natl. Acad. Sci. U.S.A.* **105**, 4489–4494 (2008).
25. S. Henrichs *et al.*, Regulation of ABCB1/PGP1-catalysed auxin transport by linker phosphorylation. *EMBO J.* **31**, 2965–2980 (2012).
26. D. E. Brown *et al.*, Flavonoids act as negative regulators of auxin transport in vivo in Arabidopsis. *Plant Physiol.* **126**, 524–535 (2001).
27. G. Conseil *et al.*, Flavonoids: A class of modulators with bifunctional interactions at vicinal ATP- and steroid-binding sites on mouse P-glycoprotein. *Proc. Natl. Acad. Sci. U.S.A.* **95**, 9831–9836 (1998).
28. C. Gu *et al.*, Inhibition of inositol polyphosphate kinases by quercetin and related flavonoids: A structure-activity analysis. *J. Med. Chem.* **62**, 1443–1454 (2019).
29. H. Fujita, K. Syōno, PIS1, a negative regulator of the action of auxin transport inhibitors in Arabidopsis thaliana. *Plant J.* **12**, 583–595 (1997).
30. N. Geldner, J. Friml, Y.-D. Stierhof, G. Jürgens, K. Palme, Auxin transport inhibitors block PIN1 cycling and vesicle trafficking. *Nature* **413**, 425–428 (2001).
31. W. A. Peer *et al.*, Mutation of the membrane-associated M1 protease APM1 results in distinct embryonic and seedling developmental defects in Arabidopsis. *Plant Cell* **21**, 1693–1721 (2009).
32. M. Zourelidou *et al.*, Auxin efflux by PIN-FORMED proteins is activated by two different protein kinases, D6 PROTEIN KINASE and PINOID. *Elife* **3**, e02860 (2014).
33. S. Simon *et al.*, PIN6 auxin transporter at endoplasmic reticulum and plasma membrane mediates auxin homeostasis and organogenesis in Arabidopsis. *New Phytol.* **211**, 65–74 (2016).
34. M. Ruegger *et al.*, Reduced naphthylphthalamic acid binding in the *tir3* mutant of Arabidopsis is associated with a reduction in polar auxin transport and diverse morphological defects. *Plant Cell* **9**, 745–757 (1997).
35. R. Skokan *et al.*, PIN-driven auxin transport emerged early in streptophyte evolution. *Nat. Plants* **5**, 1114–1119 (2019).
36. L. Abas, C. Luschnig, Maximum yields of microsomal-type membranes from small amounts of plant material without requiring ultracentrifugation. *Anal. Biochem.* **401**, 217–227 (2010).
37. S. Tan *et al.*, Salicylic acid targets protein phosphatase 2A to attenuate growth in plants. *Curr. Biol.* **30**, 381–395.e8 (2020).
38. N. S. Green, E. Reisler, K. N. Houk, Quantitative evaluation of the lengths of homobifunctional protein cross-linking reagents used as molecular rulers. *Protein Sci.* **10**, 1293–1304 (2001).
39. M. Opekarová, W. Tanner, Specific lipid requirements of membrane proteins: A putative bottleneck in heterologous expression. *Biochim. Biophys. Acta* **1610**, 11–22 (2003).
40. K. Gupta *et al.*, The role of interfacial lipids in stabilizing membrane protein oligomers. *Nature* **541**, 421–424 (2017).
41. Y. Yang, U. Z. Hammes, C. G. Taylor, D. P. Schachtman, E. Nielsen, High-affinity auxin transport by the AUX1 influx carrier protein. *Curr. Biol.* **16**, 1123–1127 (2006).
42. U. Z. Hammes, E. Nielsen, L. A. Honaas, C. G. Taylor, D. P. Schachtman, AtCAT6, a sink-tissue-localized transporter for essential amino acids in Arabidopsis. *Plant J.* **48**, 414–426 (2006).
43. F. Garabagi, E. Gilbert, A. Loos, M. D. McLean, J. C. Hall, Utility of the P19 suppressor of gene-silencing protein for production of therapeutic antibodies in *Nicotiana* expression hosts. *Plant Biotechnol. J.* **10**, 1118–1128 (2012).
44. M. J. Bergeron *et al.*, Frog oocytes to unveil the structure and supramolecular organization of human transport proteins. *PLoS One* **6**, e21901 (2011).
45. M. M. Marqués-Bueno, J. Moreno-Romero, L. Abas, R. De Michele, M. C. Martinez, A dominant negative mutant of protein kinase CK2 exhibits altered auxin responses in Arabidopsis. *Plant J.* **67**, 169–180 (2011).
46. L. Zhang, J. E. Elias, "Relative protein quantification using tandem mass tag mass spectrometry" in *Proteomics. Methods in Molecular Biology*, L. Comai, J. Katz, P. Mallick, Eds. (Humana Press, New York, 2017), vol. 1550, pp. 185–198.
47. J. Kourelis *et al.*, A homology-guided, genome-based proteome for improved proteomics in the alloploid *Nicotiana benthamiana*. *BMC Genomics* **20**, 722 (2019).

PLANT BIOLOGY

Downloaded at Stazbibliotheken on December 20, 2020

LETTER

https://doi.org/10.1038/s41586-018-0186-z

A molecular rheostat adjusts auxin flux to promote root protophloem differentiation

P. Marhava[1,5], A. E. L. Bassukas[2,5], M. Zourelidou[2], M. Kolb[2,3], B. Moret[1], A. Fastner[3], W. X. Schulze[4], P. Cattaneo[1], U. Z. Hammes[2,3], C. Schwechheimer[2]* & C. S. Hardtke[1]*

Auxin influences plant development through several distinct concentration-dependent effects[1]. In the *Arabidopsis* root tip, polar auxin transport by PIN-FORMED (PIN) proteins creates a local auxin accumulation that is required for the maintenance of the stem-cell niche[2–4]. Proximally, stem-cell daughter cells divide repeatedly before they eventually differentiate. This developmental gradient is accompanied by a gradual decrease in auxin levels as cells divide, and subsequently by a gradual increase as the cells differentiate[5,6]. However, the timing of differentiation is not uniform across cell files. For instance, developing protophloem sieve elements (PPSEs) differentiate as neighbouring cells still divide. Here we show that PPSE differentiation involves local steepening of the post-meristematic auxin gradient. BREVIS RADIX (BRX) and PROTEIN KINASE ASSOCIATED WITH BRX (PAX) are interacting plasma-membrane-associated, polarly localized proteins that co-localize with PIN proteins at the rootward end of developing PPSEs. Both *brx* and *pax* mutants display impaired PPSE differentiation. Similar to other AGC-family kinases, PAX activates PIN-mediated auxin efflux, whereas BRX strongly dampens this stimulation. Efficient BRX plasma-membrane localization depends on PAX, but auxin negatively regulates BRX plasma-membrane association and promotes PAX activity. Thus, our data support a model in which BRX and PAX are elements of a molecular rheostat that modulates auxin flux through developing PPSEs, thereby timing PPSE differentiation.

Auxin is a concentration-dependent permissive–restrictive signal in plant cell proliferation and differentiation–elongation that directly impinges on adaptive processes and growth rates[1,2]. Local auxin accumulations are important cues for organ organization. For example, high auxin concentration specifies the stem-cell niche in the *Arabidopsis* root tip[2–4]. Proximally, auxin concentration decreases gradually as stem-cell daughters repeatedly divide before they eventually differentiate. Notably, differentiation is accompanied by a renewed rise in auxin levels[5,6]. The underlying auxin distribution is generated by plasma-membrane-integral PINs, which are auxin efflux carriers with a coordinated asymmetric cellular localization that gives rise to directional polar auxin transport[2–4]. In root vasculature, PINs generally localize to the rootward end of cells, transporting auxin towards the root tip[3]. PINs are regulated by auxin, predominantly post-translationally[7–9]. Moreover, the AGC-family kinases D6 PROTEIN KINASE (D6PK) and PINOID (PID) activate auxin efflux through PIN phosphorylation[10–12].

The proximo-distal auxin profile in root meristems intersects with differential auxin activity in the radial dimension. For example, developing PPSEs (Extended Data Fig. 1a, b) display higher auxin accumulation than surrounding cells[6] (Extended Data Fig. 2a–d) and differentiate, whereas neighbouring cells still remain meristematic[6,13,14] (Extended Data Fig. 2e). To explore whether PPSE differentiation depends on auxin activity, we manipulated the auxin response by expressing a constitutively active variant of an auxin-response factor, MONOPTEROS (MP^{Δ})[15], under the control of PPSE-specific *COTYLEDON VASCULAR PATTERN 2* (*CVP2*) promoter[13,16]. *CVP2::MP*$^{\Delta}$ accelerated PPSE differentiation, indicating that auxin responses critically determine the differentiation process (Extended Data Fig. 2f, g).

How differential auxin activity is achieved in PPSEs remained unclear. BRX is plasma-membrane-associated, polarly localized and specifically expressed in developing PPSEs[13,17]. In *brx* mutants, PPSEs frequently fail to differentiate[13]. These cells lack the characteristic cell-wall changes and appear as gaps in the PPSE differentiation zone[13,16,18] (Extended Data Fig. 2h). A similar phenotype is observed in *octopus* (*ops*) mutants[13,17], which are affected in a parallel genetic pathway required for PPSE differentiation[19]. Whereas OPS localizes to the shootward end of PPSEs, BRX co-localizes with PINs at the rootward end[2,6,13,18]. Auxin negatively regulates BRX protein abundance and plasma-membrane association, but induces *BRX* transcription[18,20]. Thus, BRX is a candidate for mediating auxin effects in PPSE differentiation. In *brx* PPSEs, auxin accumulation as compared to neighbouring cells was markedly lower and more variable than in the wild type (Extended Data Fig. 2i, j). Although *CVP2::MP*$^{\Delta}$ expression in *brx* did not reduce the proportion of PPSE strands with gaps (Extended Data Fig. 2k), it significantly stimulated root growth (Extended Data Fig. 2l) and reduced gap size (Extended Data Fig. 2m). Such partial rescue was not observed with another PPSE-specific promoter that was inactive in gap cells (Extended Data Fig. 2k–n). Moreover, impaired PPSE differentiation was observed after pharmacological inhibition of auxin biosynthesis (Extended Data Fig. 2o, p), and *brx* protophloem defects were aggravated by genetic interference with auxin uptake (Extended Data Fig. 2q). These observations support the hypothesis that finely tuned auxin activity contributes to PPSE differentiation.

BRX protein is expressed only at low levels and in few cells, complicating cell-biological and biochemical investigations of BRX in its native context. However, a recently established trans-differentiation assay for sieve element formation[21] (Extended Data Fig. 3a, b) enabled us to perform proteomics analyses in a native cell type and identify specific BRX interactors by immunoprecipitation (Extended Data Fig. 3c, d). Among them, we retrieved D6PK and several D6PK-LIKE (D6PKL) kinases as well as PINs, but by far the most abundant was a D6PK/D6PKL-related kinase (AT2G44830)[22], which we named PROTEIN KINASE ASSOCIATED WITH BRX (PAX).

To examine a potential role of AGC kinases in PPSE differentiation, we analysed *d6pk/d6pkl* as well as *pax* mutants. *D6PK/D6PKL* genes display substantial genetic redundancy and, consistent with normal PIN phosphorylation in their roots[10,11,23], *d6pk0123* quadruple mutants had only a mild, possibly enhanced root-growth phenotype (Extended Data Fig. 4a). By contrast, *pax* loss-of-function mutants displayed reduced primary root growth (Fig. 1a), which was accompanied by PPSE differentiation defects (Fig. 1b–e). No phenotype was observed in a mutant of the closest *PAX* homologue, the uncharacterized *PAX-LIKE (PAXL)* kinase (AT5G40030)[22], and *paxl* mutation only mildly enhanced the *pax* phenotype (Fig. 1b). A PAX–CITRINE fusion protein expressed under its native promoter complemented the PPSE differentiation phenotype of *pax* mutants (Extended Data Fig. 4b) and revealed PAX expression in developing protophloem, as well as weaker expression in the xylem axis (Fig. 2a). PAX displayed rootward cellular polarity (Fig. 2b) and co-localized with BRX (Fig. 2c). Exclusive expression of *PAX–CITRINE* in developing PPSEs, under the *BRX* promoter, fully rescued the *pax* protophloem phenotype (Extended Data Fig. 4c, d). As previously observed in *brx*, the *pax* PPSE differentiation defects were accompanied by impaired phloem sap delivery into the meristem[16] (Extended Data Fig. 4e). In summary, *pax* mutants represent a (hypomorphic) phenocopy of *brx* mutants.

The *brx* phenotype was not enhanced in *brx pax* double mutants (Extended Data Fig. 4f), suggesting that *brx* is genetically epistatic to *pax*. In turn, the *pax* phenotype was not significantly enhanced by *d6pk/d6pkl* mutations (Extended Data Fig. 4g). However, similar to D6PK or PID, PAX (and PAXL) activated auxin efflux when co-expressed with PINs in *Xenopus laevis* oocytes[12] (Fig. 2d, Extended Data Fig. 4h). However, PAX was the weakest activator in this assay. Moreover, similar to D6PKL proteins, ADP-ribosylation factor–guanine-exchange factor (ARF–GEF) inhibition by brefeldin A (BFA) triggered rapid dissociation of PAX from the plasma membrane (Fig. 3a, Extended Data Fig. 4i). BRX is also BFA-sensitive[18], yet in direct comparison, BFA-induced BRX plasma-membrane dissociation was slower than for PAX (Fig. 3a, Extended Data Fig. 4j, k). Consistently, BFA treatment also triggered PPSE differentiation defects in a dosage-dependent manner (Extended Data Fig. 4l, m). Moreover, BRX abundance, but not PIN abundance, was severely reduced in *pax* PPSEs (Fig. 3b–g). By contrast, PAX abundance or localization did not substantially depend on BRX (Extended Data Fig. 4n). In protoplasts, BRX localized evenly at the plasma membrane, whereas PAX accumulated in large patches[24] (Extended Data Fig. 4o). Their co-expression recruited BRX into PAX patches. However, a cytoplasmic PAX variant[24] did not disrupt the even plasma-membrane distribution of BRX. These results suggest that PAX is required for efficient BRX plasma-membrane recruitment.

Auxin activity is systemically reduced throughout *brx* root meristems[16]. We thus sought to monitor PIN activity in *brx* or *pax*. We focused our analysis on the dominant PIN in developing PPSEs, PIN1 (Extended Data Fig. 5a). Corroborating the PIN1–green fluorescent protein (GFP) results, PIN1 abundance and localization in both the protophloem and the meristem were not affined in *pax* or *brx* mutants (Extended

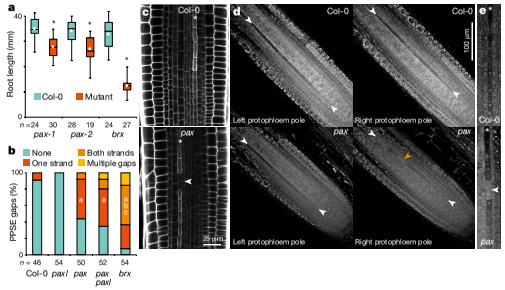

Fig. 1 | Phenotypic characterization of *pax* mutants. a, Root length of seven-day-old mutant and wild-type *A. thaliana* L. Heynh reference accession Columbia-0 (Col-0) seedlings. *pax-1* and *pax-2* are two independent *PAX* loss-of-function alleles. All data that are displayed subsequently were generated using *pax-1*. Box plots throughout show the second and third quartiles, maximum, minimum and mean (white dot). Statistically significant differences are indicated (two-sided Student's *t*-test; *$P < 0.0008$). **b**, Quantification of protophloem strands with gap cells, 6-day-old seedlings. Statistically significant differences are indicated (Fisher's exact test, two-sided, all *P* values < 0.001; a, significantly different to Col-0; b, significantly different to *pax*; c, significantly different to *pax paxl*). **c**, Confocal microscopy of propidium iodide (PI)-stained root meristems. Asterisks indicate PPSE strands and the arrowhead indicates a gap cell in the *pax* protophloem. **d**, Confocal microscopy of Col-0 and *pax* root meristems (ClearSee fixation with PI staining), showing both protophloem poles. Note PPSE cell files (white arrowheads) that start with meristematic cells and end with mature empty sieve elements. In one *pax* pole, PPSE differentiation is perturbed (gap cells, orange arrowhead). **e**, Expanded view, highlighting a gap cell in a *pax* PPSE cell file (arrowhead). *n*, number of independent biological replicates.

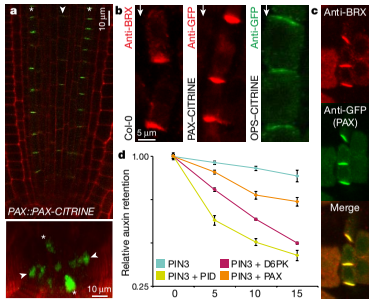

Fig. 2 | Expression analysis of PAX protein. a, Top, Confocal microscopy of the PAX–CITRINE fusion protein (green fluorescence) expressed under its native promoter in the meristem (longitudinal plane). Bottom, optical cross section. Asterisks indicate PPSE cell files and arrowheads indicate the xylem axis. **b**, Detection of endogenous BRX (red) using anti-BRX antibody staining, or PAX–CITRINE (red) or OPS–CITRINE (green) using anti-GFP antibody staining, in protophloem of fixed meristems (squashed after fixation). Arrows point rootward. **c**, Simultaneous detection of PAX–CITRINE (green) and BRX (red) by immunostaining, demonstrating co-localization. **d**, Auxin transport assays, average retention of radio-labelled auxin in *X. laevis* oocytes expressing the indicated heterologous plant proteins ($n = 10$ per time point; error bars, s.e.m.).

[1]Department of Plant Molecular Biology, University of Lausanne, Lausanne, Switzerland. [2]Plant Systems Biology, Technical University of Munich, Freising, Germany. [3]Department of Cell Biology and Plant Biochemistry, Regensburg University, Regensburg, Germany. [4]Department of Plant Systems Biology, University of Hohenheim, Stuttgart, Germany. [5]These authors contributed equally: P. Marhava, A. E. L. Bassukas. *e-mail: claus.schwechheimer@wzw.tum.de; christian.hardtke@unil.ch

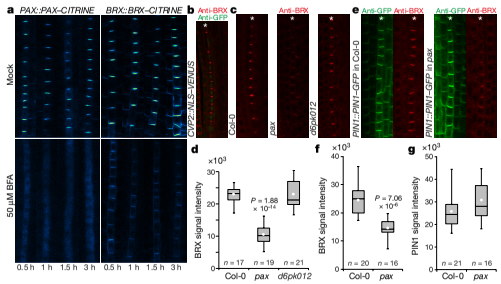

Fig. 3 | PAX-dependence of efficient BRX plasma-membrane association. a, Plasma-membrane dissociation of PAX–CITRINE and BRX–CITRINE in response to BFA treatment. **b**, Simultaneous detection of nuclear NLS–VENUS protein (green) expressed under the control of PPSE-specific *CVP2* promoter and BRX (red) by antibody staining. Asterisks in all microscopy images indicate the PPSE cell file. **c**, Detection of BRX (red) by antibody staining. **d**, BRX signal intensity quantification (anti-BRX antibody detection) in PPSEs (mean from approximately ten cells per root, arbitrary units). **e**, Simultaneous immunolocalization of PIN1–GFP (anti-GFP, green) expressed under its native promoter and BRX (anti-BRX, red) by antibody staining in Col-0 and *pax*. **f**, **g**, BRX signal intensity quantification (**f**, anti-BRX antibody detection) and PIN1–GFP signal intensity (**g**, anti-GFP antibody detection) in PPSEs (means from approximately ten cells per root, arbitrary units). **d**–**g**, Statistically significant differences from Col-0 are indicated, two-sided Student's *t*-test.

Data Fig. 5b). To survey PIN1 activity, we performed immunostaining with antibodies against PIN1 phosphosites that are critical for PIN1 activation[11,12]. Phosphoserine S231 (J231) signal was significantly reduced in *pax* PPSEs, whereas phosphoserine S271 (J271) was not affected (Extended Data Fig. 5c–e). By contrast, both phosphoserines were barely detectable in *brx* meristems (Extended Data Fig. 5c, f). Reduced PIN1 phosphorylation was also observed in *ops* (Extended Data Fig. 5f), suggesting that meristem-wide reduced PIN1 activity is a secondary systemic consequence of severely disturbed PPSE differentiation, similar to other traits[16]. Yet, *brx* or *pax* protophloem defects were aggravated in the presence of a *pin1* mutation (Extended Data Fig. 5g–i). In *brx pin1* double mutants, protophloem was frequently barely distinguishable, or even absent (approximately 20% of seedlings) (Extended Data Fig. 5i), underlining the importance of properly regulated auxin transport for PPSE differentiation.

The systemic ramifications of discontinuous protophloem on meristem development can be considered to be a post-catastrophic scenario that is triggered and enhanced by repeated PPSE differentiation failure, and is difficult to recover from once phloem sap (and thus auxin) delivery is impaired[16]. This complicates efforts to untangle cause and

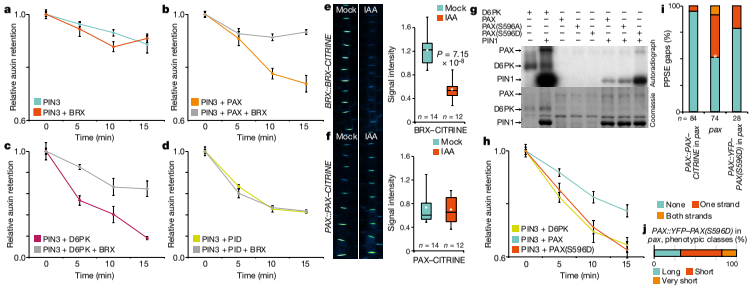

Fig. 4 | Regulatory input of auxin on PAX and BRX activity. a–**d**, Auxin transport assays in *X. laevis* oocytes expressing the indicated heterologous plant proteins ($n = 10$ per time point; error bars, s.e.m.). **e**–**f**, Response of BRX (**e**) or PAX (**f**) fusion protein to 5 μM auxin (IAA) treatment (3 h), with quantification (arbitrary units; means from approximately ten cells per root). The statistically significant difference is indicated, two-sided Student's *t*-test. **g**, Radioactive in vitro kinase assays with GST fusion proteins of D6PK, PAX or the PAX(S596A) and PAX(S596D) point mutants, with the PIN1 cytosolic loop as substrate (top), and corresponding loading controls (bottom). **h**, Auxin transport assays in *X. laevis* oocytes expressing the indicated heterologous plant proteins ($n = 10$ per time point; error bars: s.e.m.). **i**, Quantification of gap-cell frequency in PPSE strands. For *PAX::YFP–PAX(S596D)*, only long root seedlings (see **j**) were scored. *pax* alone was significantly different from *PAX::PAX–CITRINE* in *pax* (two-sided Fisher's exact test, $*P < 0.0001$). *PAX::YFP–PAX(S596D)* was not significantly different from *PAX::PAX–CITRINE* in *pax* or from *pax* alone. **j**, Quantification of root phenotype classes in a *PAX::YFP–PAX(S596D)* line ($n = 50$).

effect in the cellular action of regulators from the multicellular context. For example, it remained unclear whether *pax* mutants display PPSE differentiation defects because of inefficient BRX plasma membrane recruitment, or whether *brx* mutants display PPSE differentiation defects because of a failure to control PAX activity. To investigate whether BRX interaction with AGC kinases affects auxin transport, we tested the effect of BRX co-expression on kinase-mediated PIN activation in oocytes. In these experiments, BRX substantially inhibited stimulation of auxin efflux by PAX or D6PK (Fig. 4a–c, Extended Data Fig. 5j, k). Because this inhibition was not observed in assays with the more distantly related PID (Fig. 4d), our findings suggest that BRX action affects a subset of related AGC kinases, and that its inhibitory effect is determined by kinase identity.

The observation that BRX inhibits auxin efflux appeared particularly interesting in light of its known auxin-induced plasma-membrane dissociation[18] (Fig. 4e, Extended Data Fig. 6a, b). By contrast, neither PAX abundance nor localization were affected by auxin (Fig. 4f). However, phosphoproteomics indicated auxin-induced phosphorylation of phosphoserine S596 in the PAX activation loop (Extended Data Fig. 6c), which correlated with simultaneously increased PIN1 phosphorylation (Extended Data Fig. 6d). In vitro, recombinant PAX phosphorylated PIN1 with comparably low efficiency, and S596 was dispensable for kinase activation (Fig. 4g, Extended Data Fig. 6e). A PAX(S596D) phosphomimic variant, however, was considerably more active than wild-type PAX and displayed increased phosphorylation activity towards PIN1 (Fig. 4g, Extended Data Fig. 6e). Matching this biochemical observation, PAX(S596D) also stimulated auxin efflux considerably more in oocytes, to a level approximately equal to D6PK (Fig. 4h, Extended Data Fig. 6f). However, unlike wild-type PAX, the PAX(S596D) variant at best partially rescued the *pax* mutant (Fig. 4i, Extended Data Fig. 6g). Moreover, PAX(S596D) frequently triggered a gain-of-function phenotype of even shorter, often barely developing roots (Fig. 4j). Consistent with the D6PK-like activity of PAX(S596D), D6PK expressed from the *PAX* promoter could not rescue the *pax* phenotype (Extended Data Fig. 6h, i). These findings suggest that fine-tuning of PAX activity is a feature of properly integrated PPSE development.

In a parsimonious interpretation of our results, PAX and BRX act together as a molecular rheostat to modulate auxin efflux dynamically (Extended Data Fig. 7). In this scenario, PAX recruits BRX to the plasma membrane, which inhibits PIN-mediated auxin efflux at lower auxin levels. Because of this inhibition, cellular auxin increases until BRX eventually becomes displaced from the plasma membrane. Concomitantly, PAX is activated and stimulates auxin efflux. Reinforced through auxin-induced *BRX* transcription[6,18] (Extended Data Fig. 6j, k), this interplay could reach a dynamic steady-state equilibrium, which would impair higher local auxin activity in the multicellular context to properly time PPSE differentiation.

Online content

Any Methods, including any statements of data availability and Nature Research reporting summaries, along with any additional references and Source Data files, are available in the online version of the paper at https://doi.org/10.1038/s41586-018-0186-z.

Received: 14 September 2017; Accepted: 24 April 2018;
Published online: 06 June 2018

1. Benjamins, R. & Scheres, B. Auxin: the looping star in plant development. *Annu. Rev. Plant Biol.* **59**, 443–465 (2008).
2. Blilou, I. et al. The PIN auxin efflux facilitator network controls growth and patterning in *Arabidopsis* roots. *Nature* **433**, 39–44 (2005).
3. Grieneisen, V. A., Xu, J., Marée, A. F., Hogeweg, P. & Scheres, B. Auxin transport is sufficient to generate a maximum and gradient guiding root growth. *Nature* **449**, 1008–1013 (2007).
4. Sabatini, S. et al. An auxin-dependent distal organizer of pattern and polarity in the *Arabidopsis* root. *Cell* **99**, 463–472 (1999).
5. Brunoud, G. et al. A novel sensor to map auxin response and distribution at high spatio-temporal resolution. *Nature* **482**, 103–106 (2012).
6. Santuari, L. et al. Positional information by differential endocytosis splits auxin response to drive *Arabidopsis* root meristem growth. *Curr. Biol.* **21**, 1918–1923 (2011).
7. Sauer, M. et al. Canalization of auxin flow by Aux/IAA-ARF-dependent feedback regulation of PIN polarity. *Genes Dev.* **20**, 2902–2911 (2006).
8. Geldner, N., Friml, J., Stierhof, Y. D., Jürgens, G. & Palme, K. Auxin transport inhibitors block PIN1 cycling and vesicle trafficking. *Nature* **413**, 425–428 (2001).
9. Paciorek, T. et al. Auxin inhibits endocytosis and promotes its own efflux from cells. *Nature* **435**, 1251–1256 (2005).
10. Barbosa, I. C., Zourelidou, M., Willige, B. C., Weller, B. & Schwechheimer, C. D6 PROTEIN KINASE activates auxin transport-dependent growth and PIN-FORMED phosphorylation at the plasma membrane. *Dev Cell* **29**, 674–685 (2014).
11. Weller, B. et al. Dynamic PIN-FORMED auxin efflux carrier phosphorylation at the plasma membrane controls auxin efflux-dependent growth. *Proc. Natl Acad. Sci. USA* **114**, E887–E896 (2017).
12. Zourelidou, M. et al. Auxin efflux by PIN-FORMED proteins is activated by two different protein kinases, D6 PROTEIN KINASE and PINOID. *eLife* **3**, e02860 (2014).
13. Rodriguez-Villalon, A. et al. Molecular genetic framework for protophloem formation. *Proc. Natl Acad. Sci. USA* **111**, 11551–11556 (2014).
14. Furuta, K. M. et al. *Arabidopsis* NAC45/86 direct sieve element morphogenesis culminating in enucleation. *Science* **345**, 933–937 (2014).
15. Ckurshumova, W., Smirnova, T., Marcos, D., Zayed, Y. & Berleth, T. Irrepressible *MONOPTEROS/ARF5* promotes *de novo* shoot formation. *New Phytol.* **204**, 556–566 (2014).
16. Rodriguez-Villalon, A., Gujas, B., van Wijk, R., Munnik, T. & Hardtke, C. S. Primary root protophloem differentiation requires balanced phosphatidylinositol-4,5-biphosphate levels and systemically affects root branching. *Development* **142**, 1437–1446 (2015).
17. Truernit, E., Bauby, H., Belcram, K., Barthélémy, J. & Palauqui, J. C. OCTOPUS, a polarly localised membrane-associated protein, regulates phloem differentiation entry in *Arabidopsis thaliana*. *Development* **139**, 1306–1315 (2012).
18. Scacchi, E. et al. Dynamic, auxin-responsive plasma membrane-to-nucleus movement of *Arabidopsis* BRX. *Development* **136**, 2059–2067 (2009).
19. Breda, A. S., Hazak, O. & Hardtke, C. S. Phosphosite charge rather than shootward localization determines OCTOPUS activity in root protophloem. *Proc. Natl Acad. Sci. USA* **114**, E5721–E5730 (2017).
20. Mouchel, C. F., Osmont, K. S. & Hardtke, C. S. BRX mediates feedback between brassinosteroid levels and auxin signalling in root growth. *Nature* **443**, 458–461 (2006).
21. Kondo, Y. et al. Vascular cell induction culture system using *Arabidopsis* leaves (VISUAL) reveals the sequential differentiation of sieve element-like cells. *Plant Cell* **28**, 1250–1262 (2016).
22. Galván-Ampudia, C. S. & Offringa, R. Plant evolution: AGC kinases tell the auxin tale. *Trends Plant Sci.* **12**, 541–547 (2007).
23. Willige, B. C. et al. D6PK AGCVIII kinases are required for auxin transport and phototropic hypocotyl bending in *Arabidopsis*. *Plant Cell* **25**, 1674–1688 (2013).
24. Barbosa, I. C. et al. Phospholipid composition and a polybasic motif determine D6 PROTEIN KINASE polar association with the plasma membrane and tropic responses. *Development* **143**, 4687–4700 (2016).

Acknowledgements We thank the University of Lausanne Protein Analysis Facility for mass spectrometry services, the Swiss National Science Foundation for Grant 31003A_166394 (C.S.H.), the German-Israeli Foundation for I-236-203.17-2014 (C.S.) and the Deutsche Forschungsgemeinschaft for SCHW 751/12-2 (C.S.), HA 3468/6-1 and SFB924 (U.Z.H.).

Reviewer information *Nature* thanks A. P. Mahonen, D. Weijers and the other anonymous reviewer(s) for their contribution to the peer review of this work.

Author contributions P.M., A.E.L.B., M.Z., M.K., B.M., A.F., W.X.S. and P.C. performed experiments and analysed data. P.M., A.E.L.B., M.Z., W.X.S., U.Z.H., C.S. and C.S.H. designed experiments. P.M., A.E.L.B., U.Z.H., C.S. and C.S.H. wrote the manuscript.

Competing interests The authors declare no competing interests.

Additional information
Extended data is available for this paper at https://doi.org/10.1038/s41586-018-0186-z.
Supplementary information is available for this paper at https://doi.org/10.1038/s41586-018-0186-z.
Reprints and permissions information is available at http://www.nature.com/reprints.
Correspondence and requests for materials should be addressed to C.S. and C.S.H.
Publisher's note: Springer Nature remains neutral with regard to jurisdictional claims in published maps and institutional affiliations.

METHODS

No statistical methods were used to predetermine sample size. The experiments were not randomized and investigators were not blinded to allocation during experiments and outcome assessment. Experiments were repeated two to four times. All attempts at replication were successful.

Plant materials and growth conditions. The wild-type *Arabidopsis* line used in this study was the *A. thaliana* L. Heynh reference accession Columbia-0 (Col-0), which was also the genetic background for the mutants and transgenic lines. For plant tissue culture, seeds were surface-sterilized, stratified for 2 days in the dark at 4 °C, and germinated in vertically placed Petri dishes on 0.9% agar and 0.5 × Murashige and Skoog (1/2 MS) medium (Duchefa) with 0.3% sucrose at 22 °C under continuous light. The mutant *pax-1* and *pax-2* alleles (T-DNA insertion lines SAIL_688_B04 and GABI_274F04, respectively) were identified from available collections and obtained from the Nottingham *Arabidopsis* Stock Centre. The following transgenic and mutant lines have been described elsewhere: *BRX::BRX–CITRINE*[13], *PIN1::PIN1–GFP*[23], *PIN3::PIN3–GFP*[26], *PIN7::PIN7–GFP*[27], *CVP2::NLS–VENUS*[16], *35S::DII-NLS–VENUS* and *35S::mDII-NLS–VENUS*[5], *brx-2*[13], *ops-2*[17], *pin1-613*[28], *aux1-7*[29], *d6pk*, *d6pkl1*, *d6pkl2*, *d6pkl3*, as well as their *d6pk012* triple and *d6pk0123* quadruple mutants[12]. Primers used for genotyping are summarized in Extended Data Table 1.

Constructs and generation of transgenic lines. Transgenes for plant transformation were created in suitable binary vectors and produced using standard molecular biology procedures and/or the NEBuilder HiFi DNA Assembly Reaction Protocol. The *35S::mDII-VENUS* and *35S::DII-VENUS* lines in Col-0 and *brx-2* backgrounds have previously been described[6]. For the *CVP2::MP*$^{\Delta}$ or *CLE45::MP*$^{\Delta}$ constructs, a 2.6-kb genomic promoter fragment upstream of the initiation codon of the *CVP2* gene[16] or a 2.0-kb genomic promoter fragment upstream of the initiation codon of the *CLAVATA3/EMBRYO SURROUNDING REGION 45 (CLE45)* gene[16] was amplified, combined with amino acids 1–794 of the *MP* open reading frame[35] and introduced into the pCAMBIA1305.1 binary vector. To generate the translational *PAX::PAX–CITRINE* fusion, the *PAX* promoter region (4.5-kb upstream of the ATG start codon) was amplified and cloned into pDONR P4P1R as well as a genomic fragment of the *PAX* transcript region without a STOP codon into pDONR 221. The entry clones together with CITRINE in pDONR P2RP3 were cloned into the destination vector pH7m34GW by the multisite Gateway recombination system. To create *UBQ10::PAX–CITRINE*, the entry clones containing the *UBQ10* promoter in pDONR P4P1R, the *PAX* coding sequence without a STOP codon in pDONR 221, and the CITRINE coding sequence in pDONR P2RP3 were combined into binary vector pH7m34GW. The binary constructs were introduced into *Agrobacterium tumefaciens* strain GV3101^{pMP90} and transformed into the pertinent *Arabidopsis* genotypes using the floral dip method. For recombinant expression of the glutathione-S-transferase N-terminally tagged fusion proteins GST–PAX, GST–PAX(S596D) and GST–PAX(S596A), a Gateway-compatible attB-flanked PCR product of *PAX* coding sequence was amplified from cDNA and cloned into the Gateway-compatible donor vector pDONR 201 (Invitrogen). The mutagenesis leading to PAX(S596D) phosphomimetic or PAX(S596A) phosphomutant variants in the activation loop of the *PAX* coding sequence was achieved using site-directed mutation PCR on a pDONR 201 entry clone carrying the *PAX* coding sequence insert. The resulting pDONR 201 entry clones served as substrate to recombine the *PAX* coding sequences into the pDEST15 (Life Technologies) destination vector that was ultimately used for recombinant protein expression. The expression vectors pDEST15 containing GST–D6PK and GST–PIN1 cytosolic loop have previously been described[12]. Primers used for cloning are summarized in Extended Data Table 1.

Microscopy. To visualize reporter genes and staining signals, fluorescence for CITRINE (excitation 514 nm, emission 529 nm), VENUS (excitation 515 nm, emission 528 nm), propidium iodide (PI) (excitation 536 nm, emission 617 nm), Alexa Fluor 488 (excitation 498 nm, emission 520 nm) and Alexa Fluor 546 (excitation 556 nm, emission 573 nm) were detected in seedlings examined under Zeiss LSM 700 or 710 inverted confocal scanning microscopes. Pictures were taken with 20× or 40× water/oil immersion objectives. PI staining of seven-day-old seedlings was used for quantification of protophloem cell size. For presentation, composite images had to be assembled in various instances. Sequential scanning was used for co-localization studies to avoid any interference between fluorescence channels. For image analyses, ImageJ (NIH; https://rsb.info.nih.gov/ij), Zeiss Zen (black edition) and Imaris software were used. If necessary, images were processed using the 'sharpen' tool for clearer visualization of cellular organization. For signal quantifications, all samples were analysed in the same area of the root meristem, and the average signal intensity per transgenic line was calculated as the mean of means. Statistical significance was evaluated with Student's *t* test.

Pharmacological and hormonal treatments. For treatments, 5–7-day-old seedlings were either grown on, or transferred either onto solid or into liquid 1/2 MS medium with or without the chemicals and incubated for the indicated time. Drugs and hormones used were as follows: BFA (dissolved in DMSO), IAA (dissolved in DMSO), L-kynurenine (dissolved in DMSO), PI (1 mg ml^{-1} in water, diluted 1:25).

VISUAL assay and proteomics. The VISUAL protocol[21] was performed as previously described[19] with subsequent BRX–CITRINE or YFP pull down. In brief, cotyledons of six-day-old transgenic *Arabidopsis* seedlings were cultured for 3 days in induction medium and subsequently ground in extraction buffer. Supernatants (4 mg of total protein extract in two technical replicates) were incubated with anti-GFP beads (GFP-Trap_MA, Chromotek). Beads were magnetically separated and protein was eluted in 2× SDS sample buffer, loaded on an SDS–PAGE gel for electrophoresis, and subsequently analysed by liquid chromatography with tandem mass spectrometry.

Protein immunolocalization. Whole mount immunolocalization on five-day-old seedlings was performed as described previously[7]. The primary antibody dilutions were: 1:600 for anti-GFP mouse (Roche), 1:500 for anti-BRX rabbit (this study), 1:100 for anti-PIN1 S1-P rabbit[11], 1:300 for anti-PIN1 S4-P rabbit[11] and 1:100 for anti-PIN1 goat (Santa Cruz Biotechnology). The secondary antibody dilutions were: 1:600 for Alexa Fluor 488 anti-mouse (Molecular Probes) and 1:600 for Alexa Fluor 546 anti-rabbit (Molecular Probes). The anti-BRX antibody was obtained by custom antibody production directed against the keyhole-limpet hemocyanin (KLH)-conjugated BRX peptide GGSSNYGPGSYHGGC with affinity purification (Agrisera).

Oocyte experiments. Auxin transport assays in *X. laevis* oocytes were carried out as described[12,30]. The oocytes were obtained from the animal facility of the Technical University of Munich, Department of Nutritional Physiology. The animals were kept in accordance with local guidelines and regulations. To monitor expression levels, post-assay immunoblots were performed with anti-PIN1 sheep and anti-PIN3 sheep primary antibodies (Nottingham *Arabidopsis* Stock Centre, used at 1:5,000 dilution), and anti-GFP rabbit (custom antibody[31], 1:2,000 dilution). The secondary antibodies were anti-sheep from donkey (1:5,000, Santa Cruz Biotechnology) and anti-rabbit from goat (1:10,000, Santa Cruz Biotechnology).

Protoplast transformation. Protoplasts were isolated from *Arabidopsis* suspension-cultured cells (Col-0) five to seven days after subculturing by incubation of 2 g of cell culture with 1% Cellulase R-10 (SERVA) and 0.25% Macerozyme R-10 (SERVA). Typically, protoplasts were transformed with 20 μg of plasmid DNA using polyethylene glycol-mediated transformation and analysed after 16 to 20 h of incubation as described[24].

In vitro kinase assay. The in vitro kinase assay was performed using recombinant glutathione-S-transferase N-terminally tagged fusion proteins GST–PIN1[12] CL (cytosolic loop), GST–D6PK[12], GST–BRX[18], GST–PAX, GST–PAX(S596D) and GST–PAX(S596A), expressed in the *Escherichia coli* strain BL21(DE3) and purified using Glutathione Sepharose 4B (GE Healthcare). The kinase reactions were performed by incubating the purified GST-fusion proteins for 60 min at 28 °C in the kinase reaction buffer (25 mM Tris HCl pH 7.5, 5 mM $MgCl_2$, 0.2 mM EDTA, 1× cOmplete protease inhibitor cocktail (Roche)), supplemented with 10 μCi [γ-^{32}P] ATP (370 Mbq, specific activity 185 Tbq, Hartmann Analytics). The reactions were stopped by boiling the protein samples mixed with 5× concentrated Laemmli buffer for 10 min. Subsequently, the protein mixtures were separated by SDS–PAGE. After samples had been run, the SDS–PAGE gel was vacuum-dried and used for autoradiography. The same gel was later rehydrated and stained with Commassie Brilliant Blue to serve as a loading control.

Reporting summary. Further information on experimental design is available in the Nature Research Reporting Summary linked to this paper.

Data availability. The datasets displayed in the current study are available from the corresponding authors upon reasonable request. For gel source images, see Supplementary Fig. 1.

25. Benková, E. et al. Local, efflux-dependent auxin gradients as a common module for plant organ formation. *Cell* **115**, 591–602 (2003).
26. Zádníková, P. et al. Role of PIN-mediated auxin efflux in apical hook development of *Arabidopsis thaliana*. *Development* **137**, 607–617 (2010).
27. Friml, J. et al. Efflux-dependent auxin gradients establish the apical–basal axis of *Arabidopsis*. *Nature* **426**, 147–153 (2003).
28. Bennett, T. et al. The *Arabidopsis* MAX pathway controls shoot branching by regulating auxin transport. *Curr. Biol.* **16**, 553–563 (2006).
29. Marchant, A. et al. AUX1 promotes lateral root formation by facilitating indole-3-acetic acid distribution between sink and source tissues in the *Arabidopsis* seedling. *Plant Cell* **14**, 589–597 (2002).
30. Fastner, A., Absmanner, B. & Hammes, U. Z. Use of *Xenopus laevis* oocytes to study auxin transport. *Methods Mol. Biol.* **1497**, 259–270 (2017).
31. Absmanner, B., Stadler, R. & Hammes, U. Z. Phloem development in nematode-induced feeding sites: the implications of auxin and cytokinin. *Front. Plant Sci.* **4**, 241 (2013).

Alleviating the barrier of adventitious roots formation in recalcitrant mature tissue by slow release of a synthetic auxin

Ohad Roth[1], Sela Yechezkel[2], Ori Serero[2,3], Avi Eliyahu[2,3], Inna Vints[1], Pan Tzeela[2,3], Alberto Carignano[4], Dorina P. Janacek[5], Verena Peters[6], Amit Kessel[7], Vikas Dwivedi[2], Mira Carmeli-Weissberg[2], Felix Shaya[2], Adi Faigenboim-Doron[2], Joseph Riov[3], Eric Klavins[4], Corinna Dawid[6], Ulrich Z. Hammes[5], Nir Ben-Tal[7], Richard Napier[8], Einat Sadot[2*], Roy Weinstain[1*]

[1] School of Plant Sciences and Food Security, Faculty of Life Sciences, Tel Aviv University, Tel Aviv, Israel
[2] The Institute of Plant Sciences, The Volcani Center, Ministry of Agriculture and Rural Development, Israel
[3] The Robert H. Smith Institute of Plant Sciences and Genetics in Agriculture, The Robert H. Smith Faculty of Agriculture, Food and Environment, The Hebrew University of Jerusalem, Rehovot, Israel
[4] Department of Electrical and Computer Engineering, University of Washington, Seattle, United States
[5] Chair of Plant Systems Biology, Technical University of Munich, Freising, Germany
[6] Chair of Food Chemistry and Molecular and Sensory Science, Technical University of Munich, Freising, Germany
[7] Department of Biochemistry and Molecular Biology, School of Neurobiology, Biochemistry & Biophysics, Faculty of Life Sciences, Tel Aviv University, Tel Aviv, Israel
[8] School of Life Sciences, University of Warwick, Coventry, UK
* Correspondence should be addressed to E.S. (email: vhesadot@volcani.agri.gov.il) or to R.W. (email: royweinstain@tauex.tau.ac.il)

Abstract

Clonal propagation of plants by induction of adventitious roots (ARs) from stem cuttings is a requisite step in breeding programs. Nevertheless, a major barrier exists for propagating valuable plants that naturally have low capacity to form ARs. Due to the central role of auxin in organogenesis, indole-3-butyric acid (IBA) is often utilized, yet many recalcitrant plants do not form ARs in response to such treatment. We describe the synthesis and screening of a focused library of synthetic auxin conjugates in *Eucalyptus grandis* cuttings, highlighting 4-chlorophenoxyacetic acid-L-tryptophan-OMe as a competent enhancer of adventitious rooting in a number of recalcitrant woody plants. Comprehensive metabolic and functional analyses revealed that this activity is engendered by prolonged auxin signaling due to initial fast uptake and slow release and clearance of the free auxin 4-chlorophenoxyacetic acid. This work highlights the utility of a slow-release strategy for bioactive compounds and provides an exemplar for further rational development of more effective plant-growth regulators for agriculture.

bioRxiv preprint doi: https://doi.org/10.1101/2023.03.13.532257; this version posted March 13, 2023. The copyright holder for this preprint (which was not certified by peer review) is the author/funder, who has granted bioRxiv a license to display the preprint in perpetuity. It is made available under aCC-BY-NC-ND 4.0 International license.

Introduction

Adventitious roots (ARs) are defined as roots that regenerate from non-root tissues, in contrast to lateral roots (LR) that are post-embryonic roots formed from root tissue[1]. Clonal (vegetative) propagation of plants by induction of ARs from stem cuttings is a requisite step in selection and breeding programs as well as in routine agricultural practices and has tremendous economic importance[2]. Clonal propagation is also a cornerstone in forestry, the ornamental plant industry, and the development of elite rootstocks to provide resistance to pests, diseases and changing environmental conditions[2]. Despite its significant economic and agricultural importance, a major barrier still exists for propagating clones of many valuable plants that naturally have low capacity (and often, none) to form ARs or that lose this ability during maturation[3–5].

AR development is a heritable, quantitative genetic trait that shows high plasticity and is controlled by multiple intrinsic and environmental factors[6,7]. In particular, it was shown to be controlled by a complex network of plant hormones crosstalk, in which auxin signaling plays a central role in each step of the process[8–12]. In some plant species, lower endogenous indole 3-acetic acid (IAA) levels in difficult-to-root mature cuttings compared to easy-to-root juvenile ones, e.g., *Eucalyptus grandis* (*E. grandis*) and *Pisum sativum (P. sativum*), have been reported[13,14], as well as absence of IAA maxima in the cambium zone of difficult-to-root pine cuttings[15]; the cambium being the tissue from which ARs typically form[16] and where IAA maxima are often observed[17,18]. However, other plant species show comparable endogenous auxin levels in juvenile and mature shoots or even higher in the mature difficult-to-root ones[19,20] yet the ability to form AR is significantly impaired in mature shoots, with or without exogenous auxin application. Thus, the accepted presumption to date is that auxin responsiveness (as derived from auxin metabolism, transport and perception) has changed in mature cuttings, not any more able to convey the correct signaling pathways to support AR formation. Indeed, stronger auxin response (*DR5:GUS*) was reported in young vs. mature cuttings of *P. sativum* upon similar exogenous auxin treatments[13] and differential expression profiles of auxin-regulated genes were observed in easy- vs. difficult-to-root poplar[21], pine[15,22,23] and *Eucalyptus* species[14,24–27] along AR induction.

Although IAA is the most prevalent endogenous auxin in plants, and the first to be used for induction of AR formation[28], indole 3-butyric acid (IBA) and 1-naphthalaneacetic acid (NAA) have been found to be more efficient and for the past 60 years are the major components in most commercial rooting formulas[2,29]. Initially, the increased efficacy of IBA and NAA was attributed to their higher light-resistance, but more recent studies point to their differential metabolism and transport (compared to IAA) as the potential source for their efficacy[30–32]. Over the years, efforts

have been made to increase the effectiveness of IBA by different approaches, including its conjugation to various molecules[33–36]. Nevertheless, many recalcitrant plants respond poorly to exogenous application of these compounds[37,38], and their vegetative propagation remains a significant challenge.

The above observations have prompted us to hypothesize that synthetic auxins might represent an underexplored chemical space of bioactive compounds that could assist in overcoming the loss of rooting capability in difficult-to-root plants. Synthetic auxins constitute a large set of small organic molecules with structural resemblance to IAA and that mimic the effects of the endogenous IAA by promoting the interaction between the auxin receptors TRANSPORT INHIBITOR RESPONSE1 (TIR1)/AUXIN-SIGNALING F-BOX (AFB) and Aux/IAA[39]. Despite this central similarity, differences in metabolism[40], transport[41,42] and perception specificity[43–45] have been observed between IAA and several synthetic auxins (and among themselves), that presumably lead to different expression profiles of auxin responsive genes and/or sets of auxin-related phenotypes[45,46]. A number of synthetic auxins have been previously shown to promote rooting[47] (e.g. 2,4-dichlorophenoxyacetic acid (2,4-D) and 2,4,5-trichlorophenoxyacetic acid (2,4,5-T), however, with the exception of NAA, their high auxin activity limits their practical use due to high phytotoxicity, or promotion of callus instead of roots[48]. We envisioned that the inherent phytotoxicity and growth-inhibitory effect of synthetic auxins could be mitigated by their slow release *in planta*, maintaining a low yet functional level of the bioactive molecule over a prolonged time, thus opening the door to utilizations beyond their traditional role as herbicides[49]. Moreover, lengthy auxin treatments were reported to improve AR induction[50–53], which could further enhance the effectiveness of a slow-release approach.

To test this hypothesis, we synthesized a rationally-designed, focused library of four synthetic auxins conjugated to different residues, under the presumption that the conjugates will be hydrolyzed *in planta* (either enzymatically or chemically) to release the parent synthetic auxin. The conjugates were evaluated on difficult-to-root cuttings obtained from mature parts of *E. grandis* trees (Fig. 1a). A leading compound was found to enhance basal regeneration rates by 2-3-fold when applied to cuttings from diverse woody species. The dynamics underlying the compound activity is described herein.

bioRxiv preprint doi: https://doi.org/10.1101/2023.03.13.532257; this version posted March 13, 2023. The copyright holder for this preprint (which was not certified by peer review) is the author/funder, who has granted bioRxiv a license to display the preprint in perpetuity. It is made available under aCC-BY-NC-ND 4.0 International license.

Results

Design, synthesis, and screening of synthetic auxins conjugates

To develop a suitable chemical library, the synthetic auxins 4-chlorophenoxyacetic acid (4-CPA) (**1**), 2-methyl-4-chlorophenoxyacetic acid (MCPA) (**2**), 2-(2,4-dichlorophenoxy) propionic acid (2-DP) (**3**), and NAA (**4**) were chosen for conjugation. The first three belong to the phenoxy acid family[54] and feature a relatively strong, medium, and weak auxin activity, respectively, as determined by root elongation inhibition of *Prosopis juliflora*[55]. NAA belongs to the aromatic acetate family[56] and is often used in commercial rooting enhancement mixtures[2]. Each of the synthetic auxins (**1**–**4**) was conjugated through its carboxylic acid, a required moiety for the hormone biological activity[57–59], with a series of amine residues or methanol, forming a set of 39 conjugates (**1**–**4a**–**q,** Supplementary Fig. 1). The rooting enhancement capability of the conjugates and the free auxins (43 compounds in total) was evaluated using cuttings from mature *E. grandis* trees, which regenerate roots at low efficiency following 1 min submergence treatment with K-IBA, the potassium salt of IBA and the agricultural "gold standard" rooting enhancer[6]. The conjugates (100 µM) were applied by submerging the cutting base for 1 min or by spraying the cutting apical part, either as a standalone treatment or in combination with a 6,000 ppm K-IBA (24.9 mM) submergence treatment. The cuttings were then incubated in a rooting table for approximately 1 month before examination. In total, 20–90 cuttings were tested per conjugate-based treatment and ~500 cuttings per K-IBA control treatment. At the chosen screening concentration (100 µM), none of the compounds outperformed K-IBA as a standalone treatment, however applications based on the combination of compounds **1a**, **1j**, **1o**, **1p** or **1q** with K-IBA showed significantly higher rooting rates (Supplementary Fig. 2). Of these compounds, **1q**, a conjugate of 4-CPA to L-tryptophan methyl ester (L-Trp-OMe, Fig. 1b), had the strongest effect, with nearly 40% root regeneration for either spray or submergence treatments when combined with K-IBA, compared to 17% for K-IBA alone (Supplementary Fig. 2). Of note, the corresponding free synthetic auxins at a similar concentration had no positive effect when combined with K-IBA. Likewise, increasing the amount of K-IBA applied as a single treatment from 6,000 up to 12,000 ppm did not improve rooting rates (Supplementary Fig. 3), ruling out mere increase in auxin levels as underlying the effect observed when conjugates were added. Due to its hydrophobicity, applying higher concentrations of **1q** in a water-based solution was found to be challenging. As an alternative, we combined spray and submergence treatments, each at three different concentrations (20, 50 and 100 µM), in addition to 6,000 ppm K-IBA, in order

to increase the applied concentration of **1q**. Strikingly, this dual application method resulted in AR induction efficiencies of 66% and 77% in response to **1q** at 20 and 50 µM, respectively (Fig. 1c), ~3-folds higher than K-IBA alone. This effect was accompanied by the formation of comparable number, however significantly longer, roots per rooted cutting compared to K-IBA (Fig. 1d,e). To conclude, we find that a simple and short application of a synthetic auxin-based conjugate significantly augmented the saturated effect of K-IBA on de-novo root regeneration, which is a critical practice for the agricultural industry.

Distinct bioavailability of 4-CPA underlies the activity of 1q

We speculated that **1q** exerts its bioactivity via a two-step process, in which **1q** is first hydrolyzed to its carboxylic acid form (**1r**), followed by removal of the amino acid that leads to release of bioactive 4-CPA (Fig. 2a). To rule out the possibility that **1q** itself can interact with the auxin perception machinery, and thus directly modulate AR formation, its ability to affect the TIR1-Aux/IAA7 auxin-perception complex formation was evaluated *in vitro* via surface plasmon resonance (SPR) measurements. The results show that neither **1q** nor **1r** have any measurable auxin or anti-auxin activity (Fig. 2b and Supplementary Fig. 4, respectively). Thus, the activity of **1q** seems to depend on its ability to release a bioactive 4-CPA. To understand the fate of **1q** *in planta*, cuttings of *E. grandis* were submerged and sprayed with either 4-CPA or **1q** (in addition to K-IBA submergence), and the small-molecules content of the cutting bases were analyzed periodically via HPLC-MS/MS for up to 8 days following treatment. Figure 2c shows the metabolic derivatives of **1q** following its application, and Figure 2d shows the levels of 4-CPA measured following **1q** or free 4-CPA application. The first time point, 1 h post-application, illuminates one of the features of **1q**; the esterification of the carboxylic acid leads to a more hydrophobic molecule (logD at pH = 7.0: 0.06 vs. 3.17), resulting in a 10-fold higher uptake of **1q** (Fig 2c) compared to free 4-CPA (Fig. 2d) (515.5 ± 24.4 vs. 53.2 ± 5.6 pg/mg fresh weight (FW)). This time point also demonstrates the rapid de-esterification of **1q** *in planta*, with ~13% **1r** out of the measured **1q**-derived forms, and a negligible amount of 4-CPA, pointing to the amide bond cleavage as the rate-limiting step in 4-CPA release. Indeed, 6 h after application, **1q** levels decreased by ~82% (to 90.9 ± 4.1 pg/mg FW) while comparable **1r** and 4-CPA levels were detected (48.5 ± 0.8 and 38.2 ± 1.1 pg/mg FW, respectively). This observation suggests that initially, a significant portion of **1q** is not available for immediate de-esterification. In the subsequent ~48 h, **1q** level remained relatively constant whilst a clear conversion of **1r** to 4-CPA was detected. Interestingly, despite the higher

bioRxiv preprint doi: https://doi.org/10.1101/2023.03.13.532257; this version posted March 13, 2023. The copyright holder for this preprint (which was not certified by peer review) is the author/funder, who has granted bioRxiv a license to display the preprint in perpetuity. It is made available under aCC-BY-NC-ND 4.0 International license.

uptake of **1q** compared to free 4-CPA, the maximal level of 4-CPA was comparable in both treatments (53.2 ± 4.0 and 72.0 ± 2.0 pg/mg FW for 4-CPA or **1q**, respectively) (Fig. 2d). However, the timing of their formation was strikingly different; while 4-CPA level peaked 1 h post-application for the free 4-CPA (Fig. 2d), it only peaked after 24 h for **1q** (Fig. 2c). In addition, clearance rates were very different; 4-CPA retained an approximate physiologically relevant level of an auxin (>10 pg/mg FW, as measured for IAA in *E. grandis* cuttings, Supplementary Fig. 5) for only 2 days when applied directly but persisted for >6 days when applied in the form of **1q** (Fig. 2c,d). The above observations suggest that **1q** application could support prolonged auxin signaling *in planta*. To further evaluate this point, we turned to *Arabidopsis thaliana* (*Arabidopsis*), first seeking to establish the activity of **1q** in this model plant and then to correlate it with auxin signaling. In line with the results in *E. grandis*, a brief (1.5 h) shoot application of **1q**, but not of 4-CPA or IBA (10 µM), resulted in a substantial increase in AR formation of intact etiolated *Arabidopsis* seedlings (Fig. 2e). In accord, applying the same treatment to *Arabidopsis DR5:Luciferase* line, encoding for a high turnover auxin reporter suitable for long-term imaging[60], led to stronger and more prolonged auxin signaling in response to **1q** compared to 4-CPA (Fig. 2f). Importantly, these observations also demonstrate that K-IBA treatment is not necessarily a prerequisite for the activity of **1q**. Collectively, the results of the above experiments suggest that **1q** serves as a reservoir for continuous auxin release that promotes AR induction and development.

Weak receptor-binding and altered cellular stability and mobility shape 4-CPA activity

In addition to the characteristics of the conjugate, which engender higher uptake and slow auxin release, intrinsic properties of the released synthetic auxin might shape the cellular responses to **1q** and were therefore examined. SPR measurements showed that 4-CPA is a ~2-orders of magnitude weaker binder of TIR1 than IAA (Fig. 2b). A comparable weaker auxin activity was found *in vivo*, using qualitative (lacZ-based, TIR1+Aux/IAA7, Supplementary Fig. 6a) and quantitative (degron-YFP based, TIR1+Aux/IAA9 and AFB2+Aux/IAA9) yeast-2-hybrid (Y2H) assays (Supplementary Fig. 6b). Initial weak auxin activity was also found in root growth inhibition and *DR5:Venus* response assays in *Arabidopsis* (Fig. 3a,b). Several synthetic auxins were shown to evoke unique expression profiles of auxin responsive genes compared to IAA[46], which could underlie the AR promotion activity observed for **1q**. An extended analysis of 4-CPA binding performances by a systematic evaluation of 11 Aux/IAA and both TIR1 and AFB2 receptors (with the appropriate EC_{50} for each, calculated from the curves shown in

Supplementary Fig. 6b), did not reveal a specific degradation pattern in response to 4-CPA (Fig. 3c and Supplementary Fig. 6c). Thus, based on the *Arabidopsis* auxin perception mechanism, a differential signaling response to 4-CPA as a result of unique binding is unlikely. Nevertheless, while *Arabidopsis* root growth recovers quickly from IAA inhibition, it is entirely arrested in response to 4-CPA (Fig. 3a), suggesting differences in transport and/or catabolism between the two molecules. A shoot-to-root movement assay in *Arabidopsis* implied that 4-CPA is a mobile auxin (Supplementary Fig. 7). However, although 4-CPA was found to utilize the native IAA importer AUXIN-RESISTANT1 (AUX1) (Fig. 3d,e), a solid-supported membrane (SSP)-based electrophysiology assay testing the transport activity of PIN-FORMED8 (PIN8), an adopted model for PINs activity[61], demonstrated that unlike IAA (and the analogue 2,4-D[61]), 4-CPA did not induce a significant current response at the concentration tested (20 µM) (Fig. 3f). These observations suggest that 4-CPA is only partially subjected to the canonical polar auxin transport mechanism. Unlike 4-CPA, AUX1-expressing oocytes did not accumulate **1r** upon 30 min incubation (Supplementary Fig. 8a), and comparable levels of **1q** (and its derivative **1r**) were found in both AUX1-expressing and non-expressing oocytes (Supplementary Fig. 8b). To evaluate the contribution of 4-CPA movement to AR formation following **1q** treatment, we examined the *aux/lax* quadruple mutant[62], and found it insensitive to AR induction by **1q** (brief shoot application, Supplementary Fig. 9). Together, these experiments suggest that cell-to-cell movement of 4-CPA, but not of its precursors, is crucial for effective AR induction in response to a brief treatment of **1q**. To address the hypothesis that 4-CPA differs from IAA not only in transport but also in catabolism, we adopted the *gh3* octuple mutant, in which IAA inactivation via conjugation to amino acids is deficient[63]. The activity of enzymes from this family was recently shown to be the first step in auxin catabolism[64]. By measuring root growth after 6 days of treatment with IAA or 4-CPA at 10 nM (conditions showing similar effect on growth of Col-0 roots, Fig. 3a,g) we found the *gh3* plants to be hyper-sensitive to IAA, but not to 4-CPA (Fig. 3g). These results are in line with previous conjugation rates measured for 2,4-D vs. IAA[40], and favors the assumption that 4-CPA is not an efficient substrate for the main IAA-inactivation pathway in *Arabidopsis*. Collectively, this body of evidence suggests that 4-CPA weak binding to the auxin receptors is compensated by enhanced cellular persistence. Thus, the prolonged auxin signaling following **1q** application is achieved not only due to the slow release of 4-CPA, but also as a consequence of 4-CPA bypassing key auxin homeostasis regulators.

4-CPA release is enzymatically regulated in plants

The rapid de-esterification of **1q** in *E. grandis* implies that 4-CPA release rate is largely determined by its amide bond hydrolysis (Fig. 2c). To investigate the mechanism of this step, we synthesized 4-CPA conjugated to D-Trp-OMe, forming the enantiomer of **1q** (**1s**, Fig. 4a). Since enantiomers possess similar chemical and physical properties, differences in their hydrolysis rate (or activity) *in planta* could be attributed to enzymatic regulation. HPLC-MS/MS analysis of apical and basal parts of *E. grandis* cuttings 24 h after application of **1q** or **1s** showed that 4-CPA accumulates only in response to **1q** treatment (Fig. 4a). Furthermore, in a root elongation assay using *Arabidopsis* seedlings, **1q** was found to engender ~100-fold stronger inhibitory response than **1s** (Supplementary Fig. 10). From these results, a major role for enzymatic cleavage in 4-CPA release can be inferred. Members of the metallopeptidases family; IAA-Leu-RESISTANT1 (ILR1)/ILR1-like (ILLs) are known to hydrolase amides of indole-based compounds[65–68], raising the possibility of a similar amido-hydrolase activity towards **1q** and/or **1r**. To test this hypothesis, we adopted the *Arabidopsis* triple mutant *ilr1 ill2 iar3*, which shows a compromised response to a range of IAA-amino acid conjugates[64,69]. The *ilr1 ill2 iar3* triple mutant was insensitive to **1q** in root elongation (continuous incubation, measured after 3 days, Fig. 4b) and in AR induction in etiolated seedlings (brief shoot application, Fig. 4c) assays. To validate these results, the appropriate GST-recombinant *Arabidopsis* enzymes were tested *in vitro* for their activity against **1q** and **1r**, or against IAA-alanine (IAA-Ala), an established substrate[67] serving to verify the enzymes activity in the assay. While all three enzymes hydrolyzed IAA-Ala (Supplementary Fig. 11b), only ILR1 and ILL2 efficiently hydrolyzed **1r**, and none hydrolyzed the parent **1q** (Fig. 4d). Of note, a marginal but detectable activity of ILR1 and ILL2 was also detected against the D-enantiomer of **1r** (**1t**, Supplementary Fig. 11d), which might explain the minor bioactivity observed for its parent compound **1s** in *Arabidopsis* (Supplementary Fig. 11c). In an attempt to better understand their specificities, we turned to the three-dimensional structures of the three enzymes, using the available X-ray crystal structure of ILL2[70], and AlphaFold[71] predictions for ILR1 and IAR3. We found the ligand-binding pockets of the two active enzymes, ILR1 and ILL2, to contain a deep hydrophobic niche, in contrast to the pocket of IAR3, which is elongated, shallow and contains a smaller hydrophobic patch (Supplementary Fig. 12). In agreement, molecular docking calculations (Glide, Schrödinger, 2021-4) positioned the non-polar indole of **1r** inside the deep hydrophobic niche of the active enzymes, while in the non-active IAR3, neither the indole nor the phenoxy group formed sufficient non-polar interactions with the catalytic pocket (Fig. 4d). Further correlating the ligand-pocket non-polar interactions

to substantial enzymatic activity, docking analysis positioned the indole group of IAA-Ala inside the IAR3 pocket, in close interaction with the hydrophobic patch (Supplementary Fig. 13). Having established that ILR1 and ILL2 are responsible for the hydrolysis of **1r**, we nevertheless observed a residual root growth inhibition for *ilr1 ill2 iar3* in response to longer incubation durations with **1q** (Supplementary Fig. 14a), implying participation of additional amidohydrolase (Ah). We speculated that other ILL enzymes might underlie this effect, and generated two quintuple mutant lines; *ilr1 ill2 iar3 ill3 ill5* and *ilr1 ill2 iar3 ill1 ill6* (termed quintuple *3,5* or *1,6* respectively) using CRISPR-Cas9 (Supplementary Fig. 15–18). The *quintuple 3,5* was only slightly less sensitive to a 7-days incubation with **1q** (0.5 μM) compared to the triple mutant, while the *quintuple 1,6* was entirely resistant (Supplementary Fig. 14a). Structural modelling of the four enzymes (ILL1,3,5, and 6) revealed differences in the hydrophobicity and geometry of their ligand binding sites, with ILL1 and ILL6 binding sites being more hydrophobic than those of ILL3 and ILL5 (Supplementary Fig. 14b). Collectively, we established that the second, rate-limiting, step in 4-CPA release is enzymatically regulated, and that members of the ILR1/ILLs family are the major enzymes cleaving **1r** to release 4-CPA *in planta*.

Structural conservation of ILR1 ligand binding pocket contributes to 4-CPA release

Identifying specific members of the ILR1/ILLs family as the main activators of **1q** *in planta* opened the door to rationalizing and predicting its activation in other difficult-to-root cultivars. To this end, we performed a phylogenetic analysis based on 301 ILR1/ILLs proteins from 43 seed-plants (Extended Data - Tables 1 and 2) that suggested two sub-trees (Fig. 5a). The two super-families are composed of two (AhA1-A2) and three (AhB1-3) distinct groups, with members of *Arabidopsis* occupying the AhA1 (ILL3), AhA2 (ILR1), AhB1 (ILL6), and AhB2 (ILL1, ILL2, IAR3 and ILL5) groups (Fig. 5a). We first sought to determine if activation of **1q** is functionally conserved between *Arabidopsis* and *E. grandis*. The *E. grandis* genome contains 11 *ILR1/ILLs* genes, of which we suggest only 9 to be active; based on proteins sequence-length and transcriptome of manually enriched vascular-cambium tissue (Fig. 5b, Extended Data Table 1, Supplementary Fig. 19). We focused on family AhA2 due to its high-confidence topology compared to AhB2 (Fig. 5a and alternative tree in Supplementary Fig. 19), and since the single *E. grandis* protein in the AhB1 group is apparently a pseudogene (*Eucgr.F03795*; expression not detected, and short putative protein sequence of 290 amino acids, Fig. 5b and Extended Data, Table 1). Of the 3 active AhA2 genes, *EgK02589* (the suggested direct ortholog

bioRxiv preprint doi: https://doi.org/10.1101/2023.03.13.532257; this version posted March 13, 2023. The copyright holder for this preprint (which was not certified by peer review) is the author/funder, who has granted bioRxiv a license to display the preprint in perpetuity. It is made available under aCC-BY-NC-ND 4.0 International license.

of ILR1; Fig. 5a) and *EgK02598* (which is clustered at the other orthologous group of Ah2A) were found to be highly expressed in vascular-cambium obtained 24 h after K-IBA treatment (Fig. 5b). The two genes were separately over-expressed in the *Arabidopsis ilr1 ill2 iar3* triple mutant background and their enzymatic activity was inferred from a root-growth complementation assay in the presence of **1q**. Interestingly, while lines overexpressing *EgK02589* restored the sensitivity to **1q** in a root-growth inhibition assay, lines expressing *EgK02598* did not (Fig. 5c). In agreement, structural modeling and docking calculations found the ligand binding pocket of EgK02598 flatter than those of EgK02589 and ILR1, and less favorable for the indole or phenoxy groups of **1r** to form significant non-polar and van der Waals interactions (Fig. 5d). These observations promote the hypothesis that EgK02589 contributes to the hydrolysis of **1q** to release active 4-CPA in the cambium. To broaden this observation, we similarly tested the activity of orthologs of ILR1/EgK02589 from *Populus trichocarpa* (Potri.006G207400, Pt400) and *Prunus persica* (Prupe.7G100000, Pp000), and one ortholog of EgK02598 from *Populus trichocarpa* (Potri.016G074100, Pt100). Again, only Pt400 and Pp000 but not Pt100 restored the response to **1q** (Fig. 5c), a trend that was further supported by structural modeling and docking calculations (Fig. 5d).

Collectively, the above experiments provide evidences that structural conservation of the ligand binding pocket among members of the ILR orthologous group supports **1r** cleavage, demonstrating the potential of structural modeling and docking calculations to predict the activation of **1q** in various plant species.

1q enhances adventitious roots formation in a range of woody species

The experimental evidences for enhanced de-novo root regeneration following **1q** application, together with the conservation of its key activating enzymes in diverse plant species, inspired us to examine the utility of **1q** in alleviating the barrier to rooting of agriculturally and environmentally-important difficult-to-root cultivars. We first examined *Eucalyptus x trabutii*; a very difficult to propogate hybrid of *E. camaldulensis* and *E. botryoides,* that has a relatively high resistance to cold[72] and is important in supporting honeybee nutrition during the Israeli autumn[73]. For this hybrid, a combined application of **1q** and K-IBA dramatically outpreformed K-IBA alone in rooting efficency (45% vs. none, Fig. 6a). Likewise, for the apple (*Malus domestica*) rootstock clone CG41, which supports high yields, dwarfism and resistance to soil diseases but is considered difficult-to-root[74–76], supplementation of **1q** increased rooting rate by ~2-fold compared to K-IBA alone (Fig. 6b). As part of our efforts to support local cultivation of the argan tree (*Argania spinosa*); a species known for its tolerance to extreme environmental

conditions and for its valuable oil, we evaluated several clones: three difficult-to-root clones (C124, C127, and ARS7[77]), of which the first two were directly obtained from the first trees that were planted in Israel as part of a botanical garden in 1931, and an easy-to-root clone, ARS1[77]. Application of **1q** doubled the rooting rates of cuttings from the >90-year-old C127 plant material but did not increase the low rooting efficiencies of C124 (Fig. 6c). For ARS7, again, **1q** doubled the basal root formation response to K-IBA, while for the more permissive ARS1, maximal response was found in both treatments (Fig. 6c). The success of the combined K-IBA + **1q** treatment enabled us to generate several plantations of selected elite clones of argan for further analyzing yield and profitability under different soil and climate conditions around the country (Supplementary Fig. 21). Altogether, these results suggest that woody, mature cuttings, for which poor regeneration rates are attributed to low auxin sensitivity, the saturated effect of IBA can be increased by low levels of **1q** (μM range). The results further suggest that ectopic addition of IBA is not necessarily a prerequisite for the rooting enhancement response to **1q** in mature woody tissues. Indeed, the rooting rates of *Populus alba* cuttings were doubled following application of **1q** as a standalone treatment (Fig. 6d).

Conclusion and outlook

A model of the dynamics and metabolic fate of **1q** *in planta* is presented in Figure 7a. We suggest that following application, **1q** efficiently penetrates into the plant tissues and then into cells due to its neutral charge at a physiological pH and overall hydrophobicity. In the cells, the ester bond is quickly hydrolyzed (either chemically or by abundant cellular esterases) forming **1r**, which is mostly ionized in the cellular pH and therefore trapped inside the cell in the absence of efficient active transport[78]. Alternatively, **1q** could be hydrolyzed extracellularly. This scenario, however, is less likely considering that the highly acidic **1r** (predicted pK_a 3.3) is mostly ionized in the apoplast pH, which will result in low cellular accessibility[78]. In agreement, in long-exposure root elongation assays that mitigate differences in the uptake of small molecules, *Arabidopsis* roots were found to be more sensitive to **1q** than to **1r** (Supplementary Fig. 10). Subsequently, **1r** is cleaved by members of the ILR1/ILLs family, which presumably reside in the endoplasmic reticulum and in the cytosol[66,79], to release 4-CPA intracellularly. Thus, although the measurements in *E. grandis* cutting bases detected comparable maxima levels of 4-CPA following **1q** or free 4-CPA treatments (Fig. 2c,d), we suggest higher intracellular accumulation of 4-CPA in response to **1q**. Practically, the dynamics

bioRxiv preprint doi: https://doi.org/10.1101/2023.03.13.532257; this version posted March 13, 2023. The copyright holder for this preprint (which was not certified by peer review) is the author/funder, who has granted bioRxiv a license to display the preprint in perpetuity. It is made available under aCC-BY-NC-ND 4.0 International license.

and metabolic fate of **1q** *in planta* translate into a slow-release mechanism of a bioactive auxin inside the cells.

While the immediate auxin signaling elicited by 4-CPA is weaker than the one evoked in response to a native auxin, the higher cellular stability of 4-CPA supports an amplified and more sustained signaling over time. We provide biochemical evidence that 4-CPA is not a favorable substrate to the PIN8 transporter, and genetic evidence for its low affinity to the IAA conjugating enzymes GH3s[80]. Since transport and conjugation are two of the main feedback responses to auxin[81,82], we suggest that evading these homeostasis regulators further contributes to prolonged auxin signaling. We also provide data suggesting that 4-CPA is able to move basipetally, and that AUX1 is required for its rooting enhancement effect. This in turn suggests that 4-CPA is a subject of an uncharacterized efflux transporter, which may support the compound basipetal movement, presumably through the phloem bulk flow, following apical application. Whether apical response to 4-CPA contributes indirectly to AR formation remains an open question. The delivery model we describe offers an advantage over the traditional application of free auxins (e.g., IBA, NAA, etc.) that are typically mostly ionized in the apoplast and may require active transport for efficient uptake. Together, our observations suggest that the short dual application of IBA and **1q** enables a fast and strong auxin response (K-IBA applied at mM concentrations) followed by a prolonged and sustaining signaling (**1q** applied at μM) (Fig. 7b).

Using a two-phases of auxin treatment, Ludwig-muller et al. were able to distinguish between induction of callus proliferation and AR establishment[50]. In analogy to our system, a higher-resolution understanding of how the two compounds interact (temporally and spatially) during AR induction and development is of significant mechanistic and practical interest, and may assist in optimizing future applications. Moreover, the flexible molecular design of a synthetic auxin conjugate can be further fine-tuned by modulating either the synthetic auxin or its conjugated amino acid to provide a palette of auxin responses varying in strength and duration that could be tailored to different plant species and even specific clones. Finally, the slow-release approach as applied herein can be incorporated into other agricultural practices in which auxin is applied beyond as herbicides, such as modulating root system complexity or the timing of fruits set, to allow for more optimized responses.

Acknowledgments

We thank the undergraduate students Ariel Verblun and Geffen Yehezkely in R.W. lab for supporting experiments. We also thank Eilon Shani for providing *DR5:Luciferase, DR5:Venus,* and *aux1-7 Arabidopsis* lines, Malcolm Bennett and Ranjan Swarup for providing the *aux/lax* quadruple mutant, Mark Estelle for providing Y2H vectors, Karin Ljung for providing the *gh3* octuple mutant, and Bonnie Bartel for providing the *ilr1-1 ill2-1 iar3-2* triple mutant and vectors expressing GST-recombinant version of ILR1, ILL2, and IAR3. We also thank Itay Mayrose and Keran Halabi for their assistance in constructing ILR1/ILLs phylogenetics. This work was supported by funding from the Chief Scientist of the Ministry of Agriculture and Rural Development, Israel (grant numbers 20-10-0067, 13-37-0005 and 20-01-0270 to R.W. and E.S.), the US-Israel Binational Agricultural Research and Development Fund (BARD, grant number IS-5195-19R to R.W, E.S, and Chris J. Staiger (Purdue University, IN)), and the Yuri Milner 70@70 Fellowship (to O.R.).

References

1. Verstraeten, I., Schotte, S. & Geelen, D. Hypocotyl adventitious root organogenesis differs from lateral root development. *Front. Plant Sci.* **5**, (2014).
2. Hartmann, H. T., Kester, D. E., Davis, F. T., Geneve, R. L., Wilson, S. B., *Hartmann & Kester's Plant Propagation: Principles and Practices* (Pearson, 2017)
3. Poethig, R. S. Phase change and the regulation of shoot morphogenesis in plants. *Science (1979)* **250**, 923–930 (1990).
4. Pijut, P. M., Woeste, K. E. & Michler, C. H. Promotion of adventitious root formation of difficult-to-root hardwood tree species. *Hortic. Rev.* **38**, 213 (2011).
5. Hackett, W. P. Juvenility, maturation, and rejuvenation in woody plants. *Hortic. Rev.* **7**, 109–154 (2011).
6. Bellini, C., Pacurar, D. I. & Perrone, I. Adventitious roots and lateral roots: similarities and differences. *Annu. Rev. Plant Biol.* **65**, 639–666 (2014).
7. Geiss, G., Gutierrez, L. & Bellini, C. Adventitious root formation: new insights and perspectives. *Annual plant reviews* **37**, 127–156 (2009).
8. Pacurar, D. I., Perrone, I. & Bellini, C. Auxin is a central player in the hormone cross-talks that control adventitious rooting. *Physiol. Plant.* **151**, 83–96 (2014).
9. Caboni, E. et al. Biochemical aspects of almond microcuttings related to in vitro rooting ability. *Biol. Plant.* **39**, 91–97 (1997).
10. Lakehal, A. et al. A molecular framework for the control of adventitious rooting by TIR1/AFB2-Aux/IAA-dependent auxin signaling in *Arabidopsis*. *Mol. Plant* **12**, 1499–1514 (2019).

bioRxiv preprint doi: https://doi.org/10.1101/2023.03.13.532257; this version posted March 13, 2023. The copyright holder for this preprint (which was not certified by peer review) is the author/funder, who has granted bioRxiv a license to display the preprint in perpetuity. It is made available under aCC-BY-NC-ND 4.0 International license.

11. Bellamine, J., Penel, C., Greppin, H. & Gaspar, T. Confirmation of the role of auxin and calcium in the late phases of adventitious root formation. *Plant Growth Regul.* **26**, 191–194 (1998).
12. Blažková, A. et al. Auxin metabolism and rooting in young and mature clones of *Sequoia sempervirens*. *Physiol. Plant.* **99**, 73–80 (1997).
13. Rasmussen, A., Hosseini, S. A., Hajirezaei, M.-R., Druege, U. & Geelen, D. Adventitious rooting declines with the vegetative to reproductive switch and involves a changed auxin homeostasis. *J. Exp. Bot.* **66**, 1437–1452 (2015).
14. Abu-Abied, M. et al. Microarray analysis revealed upregulation of nitrate reductase in juvenile cuttings of *Eucalyptus grandis*, which correlated with increased nitric oxide production and adventitious root formation. *Plant J.* **71**, 787–799 (2012).
15. Abarca, D. et al. The GRAS gene family in pine: transcript expression patterns associated with the maturation-related decline of competence to form adventitious roots. *BMC Plant Biol.* **14**, 354 (2014).
16. Fahn, A. *Plant Anatomy*. (Pergamon, 1990)
17. Uggla, C., Moritz, T., Sandberg, G. & Sundberg, B. Auxin as a positional signal in pattern formation in plants. *Proc. Natl. Acad. Sci. U.S.A* **93**, 9282–9286 (1996).
18. Tuominen, H., Puech, L., Fink, S. & Sundberg, B. A radial concentration gradient of indole-3-acetic acid is related to secondary xylem development in hybrid aspen. *Plant Physiol.* **115**, 577–585 (1997).
19. Ballester, A., SAN-JOSÉ, M. C., Vidal, N., Fernández-Lorenzo, J. L. & Vieitez, A. M. Anatomical and biochemical events during in vitro rooting of microcuttings from juvenile and mature phases of chestnut. *Ann. Bot.* **83**, 619–629 (1999).
20. Vidal, N., Arellano, G., San-José, M. C., Vieitez, A. M. & Ballester, A. Developmental stages during the rooting of in-vitro-cultured *Quercus robur* shoots from material of juvenile and mature origin. *Tree Physiol.* **23**, 1247–1254 (2003).
21. Legué, V., Rigal, A. & Bhalerao, R. P. Adventitious root formation in tree species: involvement of transcription factors. *Physiol. Plant.* **151**, 192–198 (2014).
22. Díaz-Sala, C. Direct reprogramming of adult somatic cells toward adventitious root formation in forest tree species: the effect of the juvenile–adult transition. *Front. Plant. Sci.* **5**, (2014).
23. Solé, A. et al. Characterization and expression of a Pinus radiata putative ortholog to the Arabidopsis SHORT-ROOT gene. *Tree Physiol.* **28**, 1629–1639 (2008).
24. Abu-Abied, M. et al. Gene expression profiling in juvenile and mature cuttings of *Eucalyptus grandis* reveals the importance of microtubule remodeling during adventitious root formation. *BMC Genom.* **15**, 826 (2014).
25. de Almeida, M. R. et al. Reference gene selection for quantitative reverse transcription-polymerase chain reaction normalization during in vitro adventitious rooting in *Eucalyptus globulus* Labill. *BMC Mol. Biol.* **11**, 73 (2010).

26. de Almeida, M. R. et al. Comparative transcriptional analysis provides new insights into the molecular basis of adventitious rooting recalcitrance in *Eucalyptus*. *Plant Sci.* **239**, 155–165 (2015).

27. Ruedell, C. M., de Almeida, M. R. & Fett-Neto, A. G. Concerted transcription of auxin and carbohydrate homeostasis-related genes underlies improved adventitious rooting of microcuttings derived from far-red treated *Eucalyptus globulus* Labill mother plants. *Plant Physiol. Biochem.* **97**, 11–19 (2015).

28. Cooper, W. C. Hormones in relation to root formation on stem cuttings. *Plant Physiol.* **10**, 789 (1935).

29. Oinam, G., Yeung, E., Kurepin, L., Haslam, T. & Lopez-Villalobos, A. Adventitious root formation in ornamental plants: I. General overview and recent successes. *Propag. Ornam. Plants* **11**, 78–90 (2011).

30. Epstein, E. & Ludwig-Müller, J. Indole-3-butyric acid in plants: occurrence, synthesis, metabolism and transport. *Physiol. Plant.* **88**, 382–389 (1993).

31. Strader, L. C. & Bartel, B. Transport and metabolism of the endogenous auxin precursor indole-3-butyric acid. *Mol. Plant* **4**, 477–486 (2011).

32. Wiesman, Z., Riov, J. & Epstein, E. Comparison of movement and metabolism of indole-3-acetic acid and indole-3-butyric acid in mung bean cuttings. *Physiol. Plant.* **74**, 556–560 (1988).

33. Felker, P. & Clark, P. R. Rooting of mesquite (*Prosopis*) cuttings. *J. Range Manag.* **34**, 466-468 (1981).

34. Van der Krieken, W. M. et al. Increased induction of adventitious rooting by slow release auxins and elicitors. In *Biology of Root Formation and Development.* 95-104 (Springer, 1997).

35. Mihaljevic, S. & Salopek-Sondi, B. Alanine conjugate of indole-3-butyric acid improves rooting of highbush blueberries. *Plant Soil Environ.* **58**, 236–241 (2012).

36. Haissig, B. E. Influence of aryl esters of indole-3-acetic and indole-3-butyric acids on adventitious root primordium initiation and development. *Physiol. Plant.* **47**, 29–33 (1979).

37. Pizarro, A. & Díaz-Sala, C. Cellular dynamics during maturation-related decline of adventitious root formation in forest tree species. *Physiol. Plant.* **165**, 73–80 (2019).

38. Vilasboa, J., da Costa, C. T. & Fett-Neto, A. G. Rooting of eucalypt cuttings as a problem-solving oriented model in plant biology. *Prog. Biophys. Mol. Biol.* **146**, 85–97 (2019).

39. Quareshy, M., Prusinska, J., Li, J. & Napier, R. A cheminformatics review of auxins as herbicides. *J. Exp. Bot.* **69**, 265–275 (2018).

40. Eyer, L. et al. 2,4-D and IAA amino acid conjugates show distinct metabolism in *Arabidopsis*. *PLoS One* **11**, e0159269 (2016).

41. Yang, Y., Hammes, U. Z., Taylor, C. G., Schachtman, D. P. & Nielsen, E. High-affinity auxin transport by the AUX1 influx carrier protein. *Curr. Biol.* **16**, 1123–1127 (2006).

42. Hoyerova, K. et al. Auxin molecular field maps define AUX1 selectivity: many auxin herbicides are not substrates. *New Phytol.* **217**, 1625–1639 (2018).

bioRxiv preprint doi: https://doi.org/10.1101/2023.03.13.532257; this version posted March 13, 2023. The copyright holder for this preprint (which was not certified by peer review) is the author/funder, who has granted bioRxiv a license to display the preprint in perpetuity. It is made available under aCC-BY-NC-ND 4.0 International license.

43. Calderón Villalobos, L. I. A. et al. A combinatorial TIR1/AFB–Aux/IAA co-receptor system for differential sensing of auxin. *Nat. Chem. Biol.* **8**, 477–485 (2012).

44. Lee, S. et al. Defining binding efficiency and specificity of auxins for SCFTIR1/AFB-Aux/IAA co-receptor complex formation. *ACS Chem. Biol.* **9**, 673–682 (2014).

45. Vain, T. et al. Selective auxin agonists induce specific AUX/IAA protein degradation to modulate plant development. *Proc. Natl. Acad. Sci. U.S.A* **116**, 6463–6472 (2019).

46. Pufky, J., Qiu, Y., Rao, M. v, Hurban, P. & Jones, A. M. The auxin-induced transcriptome for etiolated Arabidopsis seedlings using a structure/function approach. *Funct. Integr. Genom.* **3**, 135–143 (2003).

47. Delargy, J. A. & Wright, C. E. Root formation in cuttings of apple in relation to auxin application and to etiolation. *New Phytol.* **82**, 341–347 (1979).

48. Verstraeten, I., Beeckman, T. & Geelen, D. Adventitious root induction in *Arabidopsis thaliana* as a model for in vitro root organogenesis. in *Plant Organogenesis: Methods and Protocols* 159–175 (Springer, 2013)

49. Grossmann, K. Auxin herbicides: current status of mechanism and mode of action. *Pest Manag. Sci.* **66**, 113–120 (2010).

50. Ludwig-Müller, J., Vertocnik, A. & Town, C. D. Analysis of indole-3-butyric acid-induced adventitious root formation on Arabidopsis stem segments. *J. Exp. Bot.* **56**, 2095–2105 (2005).

51. Blythe, E. K., Sibley, J. L., Tilt, K. M. & Ruter, J. M. Methods of auxin application in cutting propagation: a review of 70 years of scientific discovery and commercial practice. *J. Environ. Hortic.* **25**, 166–185 (2007).

52. Riov, J. et al. Improved method for vegetative propagation of mature *Pinus halepensis* and its hybrids by cuttings. *Isr. J. Plant Sci.* **67**, 5–15 (2020).

53. Eliasson, L. & Areblad, K. Auxin effects on rooting in pea cuttings. *Physiol. Plant.* **61**, 293–297 (1984).

54. Wain, R. L., Wightman, F. & Russell, E. J. The growth-regulating activity of certain ω-substituted alkyl carboxylic acids in relation to their β-oxidation within the plant. *Proc. R. Soc. Lond. B: Biol. Sci.* **142**, 525–536 (1954).

55. Behrens Richard & Howard Morton L. Some factors influencing activity of 12 phenoxy acids on mesquite root inhibition. *Plant Physiol.* **38**, 165–170 (1963).

56. Zimmerman, P. W. Several chemical growth substances which cause initiation of roots and other responses in plants. *Contrib. Boyce Thompson Inst.* **7**, 209–229 (1935).

57. Katekar, G. F. Auxins: on the nature of the receptor site and molecular requirements for auxin activity. *Phytochemistry* **18**, 223–233 (1979).

58. Kepinski, S. & Leyser, O. The *Arabidopsis* F-box protein TIR1 is an auxin receptor. *Nature* **435**, 446–451 (2005).

59. Dharmasiri, N., Dharmasiri, S. & Estelle, M. The F-box protein TIR1 is an auxin receptor. *Nature* **435**, 441–445 (2005).

60. Xuan, W., Opdenacker, D., Vanneste, S. & Beeckman, T. Long-term in vivo imaging of luciferase-based reporter gene expression in Arabidopsis roots. in *Root Development* 177–190 (Springer, 2018).

61. Ung, K. L. et al. Structures and mechanism of the plant PIN-FORMED auxin transporter. *Nature* **609**, 605–610 (2022).

62. Bainbridge, K. et al. Auxin influx carriers stabilize phyllotactic patterning. *Genes. Dev.* **22**, 810–823 (2008).

63. Casanova-Sáez, R. et al. Inactivation of the entire Arabidopsis group II GH3s confers tolerance to salinity and water deficit. *New Phytol.* **235**, 263–275 (2022).

64. Hayashi, K. et al. The main oxidative inactivation pathway of the plant hormone auxin. *Nat. Commun.* **12**, 1–11 (2021).

65. Bartel, B. & Fink, G. R. ILR1, an amidohydrolase that releases active indole-3-acetic acid from conjugates. *Science (1979)* **268**, 1745–1748 (1995).

66. Davies, R. T., Goetz, D. H., Lasswell, J., Anderson, M. N. & Bartel, B. *IAR3* encodes an auxin conjugate hydrolase from Arabidopsis. *Plant Cell* **11**, 365–376 (1999).

67. LeClere, S., Tellez, R., Rampey, R. A., Matsuda, S. P. T. & Bartel, B. Characterization of a family of IAA-amino acid conjugate hydrolases from *Arabidopsis*. *J. Biol. Chem.* **277**, 20446–20452 (2002).

68. Campanella, J. J., Olajide, A. F., Magnus, V. & Ludwig-Muller, J. A novel auxin conjugate hydrolase from wheat with substrate specificity for longer side-chain auxin amide conjugates. *Plant Physiol.* **135**, 2230–2240 (2004).

69. Rampey, R. A. et al. A family of auxin-conjugate hydrolases that contributes to free indole-3-acetic acid levels during Arabidopsis germination. *Plant Physiol.* **135**, 978–988 (2004).

70. Bitto, E. et al. X-ray structure of ILL2, an auxin-conjugate amidohydrolase from *Arabidopsis thaliana*. *Proteins.* **74**, 61–71 (2009).

71. Jumper, J. et al. Highly accurate protein structure prediction with AlphaFold. *Nature* **596**, 583–589 (2021).

72. Valentini, R., Mugnozza, G. S., Giordano, E. & Kuzminsky, E. Influence of cold hardening on water relations of three *Eucalyptus* species. *Tree Physiol.* **6**, 1–10 (1990).

73. Eliyahu, A. et al. Vegetative propagation of elite Eucalyptus clones as food source for honeybees (*Apis mellifera*); adventitious roots versus callus formation. *Isr. J. Plant Sci.* **67**, 83–97 (2020).

74. Robinson, T. L. et al. Performance of Cornell-Geneva rootstocks across North America in multi-location NC-140 rootstock trials. in *Proceedings of the 1st International Symposium on Rootstocks for Deciduous Fruit Tree Species.* 241–245 (2004, ISHS).

75. Marini, R. P. et al. Performance of 'golden delicious' apple on 23 rootstocks at 12 locations: a five-year summary of the 2003 nc-140 dwarf rootstock trial. *J. Am. Pomol. Soc.* **63**, 115 (2009).

bioRxiv preprint doi: https://doi.org/10.1101/2023.03.13.532257; this version posted March 13, 2023. The copyright holder for this preprint (which was not certified by peer review) is the author/funder, who has granted bioRxiv a license to display the preprint in perpetuity. It is made available under aCC-BY-NC-ND 4.0 International license.

76. Marini, R. P. *et al*. Performance of 'Golden Delicious' apple on 23 rootstocks at eight locations: a ten-year summary of the 2003 NC-140 dwarf rootstock trial. *J. Am. Pomol. Soc.* **68**, 54–68 (2014).

77. Tzeela, P. et al. Comparing adventitious root-formation and graft-unification abilities in clones of *Argania spinosa*. *Front. Plant Sci.* **13**, (2022).

78. Ruberv, P. H. & Sheldrake, A. R. Effect of pH and surface charge on cell uptake of auxin. *Nat. New Biol.* **244**, 285–288 (1973).

79. Sanchez Carranza, A. P. et al. Hydrolases of the ILR1-like family of Arabidopsis thaliana modulate auxin response by regulating auxin homeostasis in the endoplasmic reticulum. *Sci. Rep.* **6**, 24212 (2016).

80. Staswick, P. E. et al. Characterization of an Arabidopsis enzyme family that conjugates amino acids to indole-3-acetic acid. *Plant Cell* **17**, 616–627 (2005).

81. Hagen, G. & Guilfoyle, T. Auxin-responsive gene expression: genes, promoters and regulatory factors. *Plant Mol. Biol.* **49**, 373–385 (2002).

82. Wabnik, K., Govaerts, W., Friml, J. & Kleine-Vehn, J. Feedback models for polarized auxin transport: an emerging trend. *Mol BioSyst.* **7**, 2352–2359 (2011).

83. Kessel, A. & Ben-Tal, N. Free energy determinants of peptide association with lipid bilayers. *Curr. Top. Membr.* **52**, 205–253 (2002).

Manuscript Figures

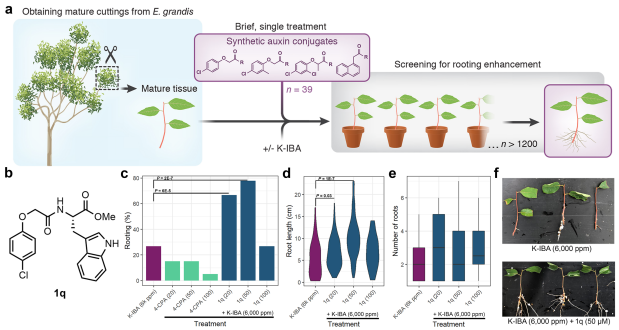

Fig. 1: A chemical screen for rooting enhancers of difficult-to-root cuttings highlighted 4-CPA-Trp-OMe (1q). **a**, Illustration of the chemical screen. **b**, structure of **1q**; the most efficient compound. **c**, Rooting percentages 1 month after application. Fisher's exact test p-values are presented for significantly better applications compared to K-IBA (6,000 ppm) as a single treatment. n = 60, 20, 20, 20, 45, 45, and 45 cuttings per sample, respectively. Compound concentration (in µM) is shown in brackets. **d**, Distributions of root-length in regenerated cuttings. Two-sided Mann-Whitney U test p-values are presented. **e**, Box-plot presenting number of roots per regenerated cutting. None of the applications outperformed K-IBA significantly (Mann-Whitney U test). **f**, Representative pictures of cuttings 35 days from the indicated treatment.

bioRxiv preprint doi: https://doi.org/10.1101/2023.03.13.532257; this version posted March 13, 2023. The copyright holder for this preprint (which was not certified by peer review) is the author/funder, who has granted bioRxiv a license to display the preprint in perpetuity. It is made available under aCC-BY-NC-ND 4.0 International license.

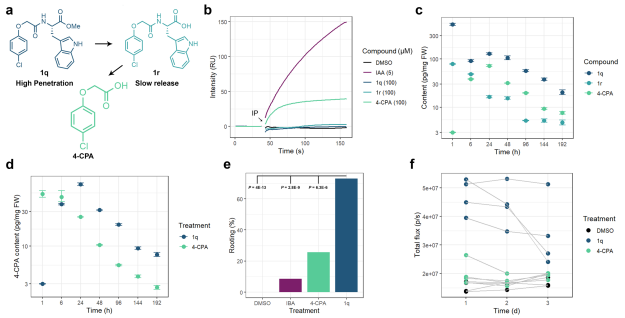

Fig. 2: 1q combines high penetration with slow 4-CPA release to facilitate prolonged auxin signaling. **a**, Schematic representation of 4-CPA release from **1q** *in planta*. **b**, SPR assay testing the intrinsic activity of the indicated compounds or DMSO (1%) *in-vitro* using TIR1 and IAA7 degron. IP stands for injection point of TIR1 mixed with the tested auxin in solution, RU stands for resonance unit. **c**, HPLC-MS quantification of the compounds shown in **a** following application of **1q** (100 µM) + K-IBA (6,000 ppm). Each sample is composed of 3 replicates, extracted from a pool of 20 cutting-bases harvested together. Data presented in logarithmic scale. Error-bars represent standard errors. **d**, HPLC-MS quantification of 4-CPA following **1q** (100 µM) + K-IBA (6,000 ppm) or 4-CPA (100 µM) + K-IBA (6,000 ppm). Each sample consists of 3 replicates except for 4-CPA after 1 h which consists of 2. Samples composition is as specified in **c**. Data presented in logarithmic scale. Error-bars represent standard errors. **e**, Percentages of two-week-seedlings (*Arabidopsis*) that developed adventitious roots in response to the indicated treatments (10 µM for IBA, 4-CPA or **1q**, and 0.1% for DMSO applied specifically to shoots for 1.5 h via a split-dish). Shown are p-values of Fisher's exact test testing the hypothesis that **1q** treatment results with higher rooting percentages. n = 37 ,35, 38, and 37 respectively. **f**, Time-lapse quantification of *DR5:luciferase* activity in *Arabidopsis* seedlings following the indicated treatments (10 µM for 4-CPA or **1q**, 0.1% for DMSO. Shoot specific 1.5 h application). Each dot represents ~20 seedlings (pooled). P = 2.93E-05, repeated measures ANOVA.

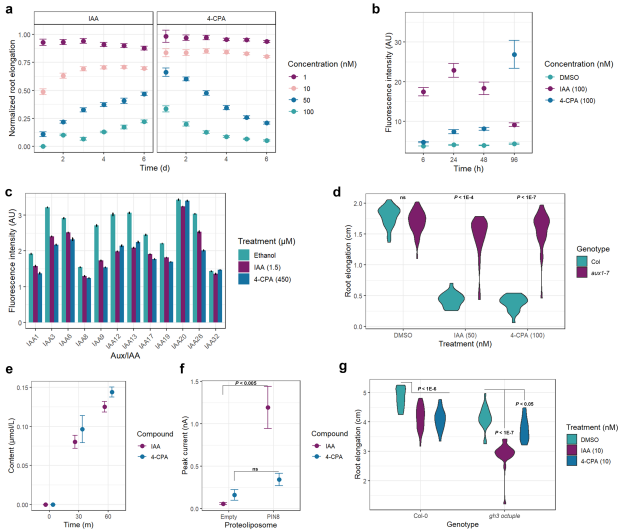

Fig. 3: Bypassing key auxin homeostasis regulators supports 4-CPA long-term signaling. **a**, Normalized root elongation of seedlings incubated with IAA or 4-CPA at the indicated concentrations (0.1% DMSO as control), n = 18–23 plants per sample. **b**, Activity of the auxin reporter *DR5:Venus* in roots. n = 4–6 root tips per sample. **c**, Quantitative Y2H assay using TIR1 and YFP-tagged Aux/IAAs and the indicated auxin or ethanol (0.1%) as mock. n = 3. **d**, Root elongation of *auxl-7* seedlings in response to 3 days treatment. n > 40 for auxins, n > 20 for DMSO (0.1%). Tukey HSD p-values are presented, ns stands for not significant. **e**, HPLC-MS quantification of the indicated auxin in oocyte cells expressing AUX1 transporter. n = 3. **f**, Solid-supported membrane (SSM)-based electrophysiology assay with empty or PIN8-containing proteoliposomes, n = 4. Student's *t*-test p-values are presented. **g**, Root elongation of *gh3* octuple mutant plants in response to a 3-days treatment with the indicated compounds. n = 18–24 plants per sample. Tukey HSD p-values are presented. In all panels error-bars represent standard errors.

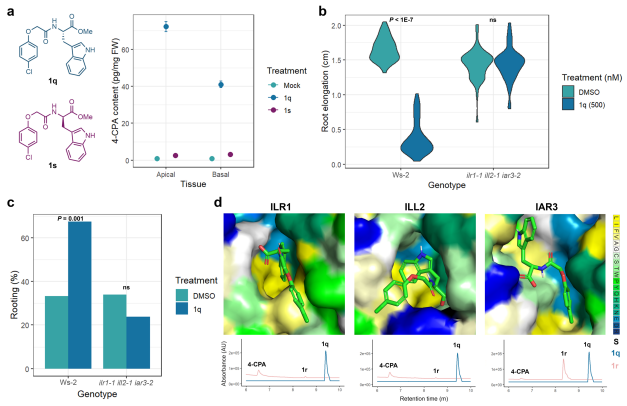

Fig. 4: 1r hydrolysis to 4-CPA is enzymatically regulated in *E. grandis* and *Arabidopsis*. **a**, Structures of the enantiomers **1q** and **1s** (*left*) and HPLC-MS quantification of 4-CPA 24 h after apical or basal application with the indicated enantiomer (100 µM) + K-IBA basal treatment (6k ppm), or DMSO (0.1%) as mock (*right*). Error-bars represent standard errors **b**, Root elongation of *ilr1-1 ill2-1 iar3-2* triple mutant in response to a 3-days treatment with **1q** or DMSO (0.1%). n = 47–54 plants per sample. Tukey HSD p-values are presented, ns stands for not significant. **c**, Percentages of seedlings developed adventitious roots in response to **1q** treatment (10 µM for **1q**, 0.1% for DMSO. Shoot specific 1.5 h application in a split-dish), n = 43–59 plants per sample. P-value of Fisher's exact test testing the hypothesis that **1q** treatment results with higher rooting percentages is shown. ns stands for not significant. **d**, *Top:* Docking calculations of **1r** with ILR1, ILL2 and IAR3. Amino acids are color-coded according to the Kessel/Ben-Tal hydrophobicity scale[83] (ranging from most hydrophobic (yellow) to most hydrophilic (blue)). *Bottom: In-vitro* hydrolytic activity of the enzymes towards **1q** (blue) or **1r** (pink) as monitored by HPLC-MS. **1q** is not cleaved by any of the enzymes while **1r** is cleaved by ILR1 and ILL2 (but not IAR3) to release free 4-CPA.

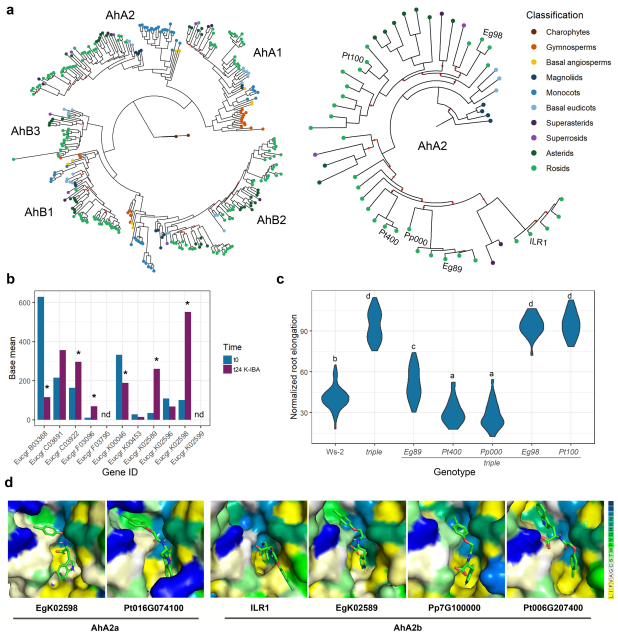

Fig. 5: Structural conservation of ILR1 ligand binding pocket contributes to 4-CPA release. a, *Left:* Phylogenetic analysis of ILR1/ILLs family in seed-plants. Sequences from the charophyte algae *Klebsormidium nitens* were used as an outgroup. *Right:* Sub-tree presenting the phylogeny of core angiosperm-sequences in family AhA2. Annotated are the characterized enzymes; EgK02598 (Eg98), Potri.016G074100 (Pt100), Potri.006G207400 (Pt400), Prupe.7G100000 (Pp000), EgK02589 (Eg89), and ILR1. Branches are annotated in brown or red for bootstrap values lower than 85 or 70, respectively. **b**, Expression profile (shown as base mean; the mean of normalized counts of all samples, normalizing for sequencing depth) of *E. grandis* ILR1/ILLs in samples enriched for cambium tissue of mature cuttings, either immediately after pruning (blue) or 24 h after K-IBA (6,000 ppm) submergence (pink). Asterisks are indicators for significant differential expression according to DESeq2 ($P < 0.01$). nd stands for not detected. **c**, Normalized root elongation in response to 4-days treatment with **1q** (300 nM) or DMSO (0.1%) as mock. n = 78 or 72 for Ws-2 or *ilr1-1 ill2-1 iar3-2* (*triple*), respectively, and 25–45 for over-expression lines. At least 10 T_2 lines for each transgene were characterized, and data was collected from single, homozygous lines. Lower-case letters

indicate significant groups based on Tukey HSD test. **d**, Docking modeling of **1r** with the indicated enzymes. Amino acids are color-coded according to residues hydrophobicity raging from most hydrophobic (yellow) to most hydrophilic (blue)).

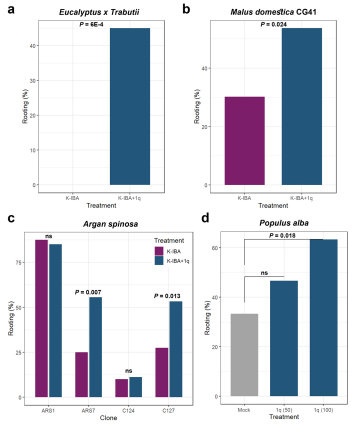

Fig. 6: 1q is a robust rooting enhancer for woody cuttings. a–c, Rooting percentages of mature cuttings obtained from the indicated species and clones applied with dual treatment of K-IBA (6,000 ppm) + **1q** (50 µM). n = 20 (**a**), 41 and 43 (**b**), 36–133 (**c**) cuttings per sample. P-values of Fisher's exact test testing the hypothesis that the dual treatment results with higher rooting percentages compare to K-IBA alone are shown. ns stands for not significant. **d**, Rooting percentages of mature cuttings obtained from *Populus alba* treated with **1q** as a single agent at the indicated concentrations (shown in brackets as µM). n = 30 cuttings per sample. P-value of Fisher's exact test testing the hypothesis that the **1q** treatment results with higher rooting percentages compare to mock (0.1% DMSO) is shown. ns stands for not significant. The duration of all experiments was 1–2 months.

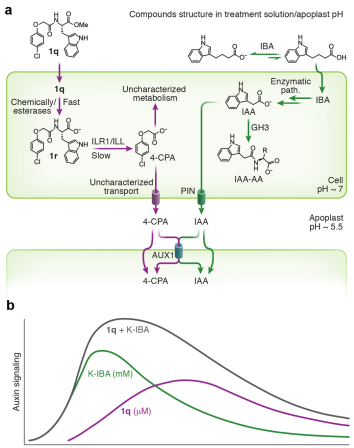

Fig. 7: Model comparing the fate of 1q and K-IBA following their application to woody cuttings. Schematic illustration of **1q** (purple) and K-IBA (green) fate when applied to woody cuttings (**a**) and their ensuing auxin signaling (**b**). Although K-IBA is applied at a very high concentration, its mostly negative charge under physiological conditions limits its accessibility to the plant, and later to cells. Inside the cell, IBA is converted into IAA, a strong yet highly regulated auxin. We suggest that these are the main factors underlying the auxin signaling pattern following a short K-IBA treatment (**b**). In contrast, **1q** is hydrophobic, limiting its concentration in a water-based solution, yet enabling enhanced tissue and cellular uptake. We suggest that efficient auxin delivery by **1q** is also a result of two distinct hydrolytic steps, responsible for a graduate, slow 4-CPA release. Moreover, 4-CPA is largely resistant to auxin feedback regulation, such as conjugation and transport, thus facilitating prolonged auxin signaling compared to IAA (**b**).

BRIEF COMMUNICATION
https://doi.org/10.1038/s41477-019-0542-5
nature plants

PIN-driven auxin transport emerged early in streptophyte evolution

Roman Skokan[1,2,9], Eva Medvecká[3,9], Tom Viaene[4], Stanislav Vosolsobě[1], Marta Zwiewka[3], Karel Müller[2], Petr Skůpa[2], Michal Karady[5,6], Yuzhou Zhang[7], Dorina P. Janacek[8], Ulrich Z. Hammes[8], Karin Ljung[5], Tomasz Nodzyński[3], Jan Petrášek[1,2] and Jiří Friml[7]*

PIN-FORMED (PIN) transporters mediate directional, intercellular movement of the phytohormone auxin in land plants. To elucidate the evolutionary origins of this developmentally crucial mechanism, we analysed the single PIN homologue of a simple green alga *Klebsormidium flaccidum*. *Kf*PIN functions as a plasma membrane-localized auxin exporter in land plants and heterologous models. While its role in algae remains unclear, PIN-driven auxin export is probably an ancient and conserved trait within streptophytes.

Asymmetric distribution of the hormone auxin orchestrates many aspects of plant development. Auxin gradients are largely dependent on its directional (polar), cell-to-cell transport mediated by the asymmetrically distributed, plasma membrane (PM)-localized PIN transmembrane auxin efflux transporters[1]. PINs are omnipresent in the genomes of land plants[2] and are functionally conserved between higher vascular land plants and bryophytes[3]. Land plants evolved from and are embedded in the streptophyte lineage together with freshwater green algae called charophytes[4]. While charophyte full-genome evidence is scarce, it is already clear that they possess and express PIN homologues[5–7]. They produce the major native auxin indole-3-acetic acid (IAA) and some related compounds[8], and polar auxin transport was even shown in the morphologically very complex charophyte *Chara corallina*[9]. However, charophytes are just beginning to emerge as model organisms and the function of their PIN-like proteins has yet been unaddressed. The charophyte genus *Klebsormidium* with its filament-type multicellularity represents a sister lineage to the morphologically more complex streptophytes[4]. *Klebsormidium nitens* has been the first charophyte alga to have its genome sequenced and contains a single PIN homologue[5], and at least one *(KfPIN)* is expressed in *K. flaccidum*[6]. The growth of *K. nitens* has been shown to respond to higher concentrations of exogenously applied auxins[10]. We decided to study the PIN/s of *Klebsormidium* species (particularly *Kf*PIN) to gain insight into the evolutionary origins of the PIN family's role in auxin transport.

To address the properties of the *Kf*PIN protein from *K. flaccidum*, where experimental options are limited, we used several land plant models well suited for studying auxin transport, namely the bryophyte *Physcomitrella patens*, the angiosperm *Arabidopsis thaliana* and the cell culture of *Nicotiana tabacum* cv. Bright-Yellow 2 (BY-2).

Stable expression of *Kf*PIN or of its translational fusion to the green fluorescent protein (GFP) in *P. patens* under the control of a rice actin promoter (*pACT::KfPIN* or *pACT::KfPIN:GFP*) generated a phenotype similar to the one resulting from overexpressing its native or the *A. thaliana* PM-resident PIN proteins[3] and indicative of auxin starvation, such as growth inhibition and reduced gametophore initiation in protonemal cultures (Fig. 1a–c). In *A. thaliana*, CaMV 35S promoter-mediated stable *Kf*PIN expression (*35S::KfPIN*) produced plants with impaired root gravitropism and abnormal leaf vasculature patterning (Fig. 1d–g), phenotypes related to defective PIN-driven auxin transport[11–13]. Finally, oestradiol-induced *Kf*PIN expression in BY-2 cells (*XVE::KfPIN*) produced markedly elongated cells (Fig. 1h,i), a hallmark of auxin starvation following upregulation of characterized angiosperm PIN auxin exporters[14]. Hence, strong *Kf*PIN expression in all of these plant models causes growth reactions indicative of distorted auxin homeostasis, probably via changes in cellular auxin transport.

Next, we tested for auxin transport capability of *Kf*PIN. The transgenic *pACT::KfPIN:GFP* protonemata of *P. patens* showed upregulated secretion of auxin into the culture medium (Fig. 2a). In *A. thaliana*, the PIN ectopic expression in root hairs is inversely proportional to their elongation[15] and the same effect was observed in *35S::KfPIN* lines (Fig. 2b,c). Both of these results are indicative of auxin export activity[3]. The most direct evidence comes from the accumulation and retention assays of ^{3}H-labelled auxins, where BY-2 cells[14] and the oocytes of *Xenopus laevis*[16] are well-established models. When expression was induced in *XVE::KfPIN* BY-2 cells, these showed decreased accumulation of labelled auxins compared to non-induced controls (Fig. 2d,e). No differences were observed in the competition assay with the non-labelled auxin precursor tryptophan or in the accumulation of the inactive auxin analogue benzoic acid (Supplementary Fig. 1). Of note, the *Kf*PIN-mediated auxin efflux in BY-2 cells was less sensitive to inhibition by 1-*N*-naphthylphthalamic acid (Fig. 2d,e). In the non-plant frog model, plant PINs have been shown to export auxin when co-expressed with specific plant protein kinases such as PINOID (PID)[17], and the same was observed for *Kf*PIN in this system (Fig. 2f,g). A BLAST search (Supplementary Table 1) has yielded phototropin as the closest homologue of *A. thaliana* PID in the genome of *K. nitens*, providing little insight into putative native regulation of

[1]Department of Experimental Plant Biology, Faculty of Science, Charles University, Prague, Czech Republic. [2]The Czech Academy of Sciences, Institute of Experimental Botany, Prague, Czech Republic. [3]CEITEC, Masaryk University, Mendel Centre for Genomics and Proteomics of Plants Systems, Brno, Czech Republic. [4]Department of Plant Systems Biology, VIB, and Department of Plant Biotechnology and Bioinformatics, Ghent University, Ghent, Belgium. [5]Department of Forest Genetics and Plant Physiology, Umeå Plant Science Centre, Swedish University of Agricultural Sciences, Umeå, Sweden. [6]Department of Chemical Biology and Genetics, Centre of the Region Haná for Biotechnological and Agricultural Research, Faculty of Science, Palacký University, Olomouc, Czech Republic. [7]IST Austria, Klosterneuburg, Austria. [8]School of Life Sciences Weihenstephan, Technical University of Munich, Freising, Germany. [9]These authors contributed equally: Roman Skokan, Eva Medvecká. *e-mail: jiri.friml@ist.ac.at

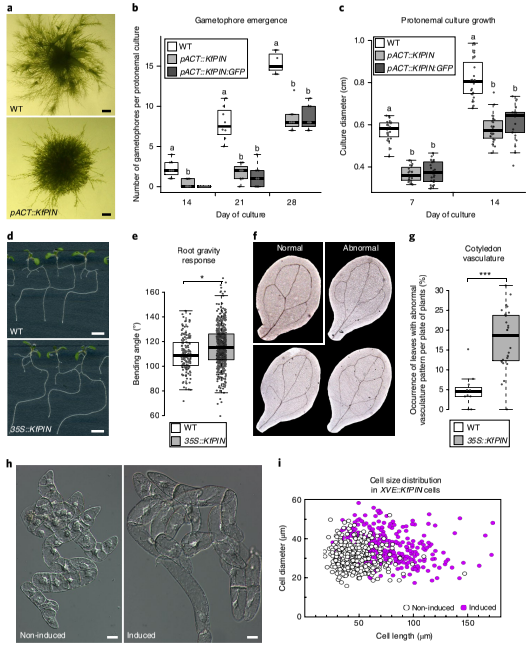

Fig. 1 | *Kf*PIN expression in land plant models provokes phenotypes indicative of modulated auxin transport. a–c, *P. patens*. **a**, WT and *pACT::KfPIN*-expressing 2-week-old protonemal culture; scale bars, 500 µm. **b**, Quantification of gametophore emergence. The decrease in the transgenic lines compared to the WT was determined as significant by a generalized linear model with Poisson distribution (line identity reduced the deviance by 65%). The fitted gametophore emergence rate is 0.043×1.86^{week} and $0.0049 \times 3.21^{week}$ of the WT rate in the *pACT::KfPIN* and *pACT::KfPIN:GFP* lines, respectively; the significance was determined by a likelihood ratio test ($Df = 4$, $P < 2.2 \times 10^{-16}$). $n = 8$ biologically independent thalli of WT and 2 different transgenic lines. **c**, Quantification of the protonemal culture growth rate. The decrease in the transgenic lines compared to the WT was determined as significant by a linear model and tested by the *F*-statistic (line identity reduces the residual variability by 46%, $F = 58.76$, $Df = 4$, $P < 2.2 \times 10^{-16}$). The one-week-old culture size was 65% and 64% the size of the WT in the *pACT::KfPIN* and *pACT::KfPIN:GFP* lines, respectively. $n = 8$ biologically independent thalli of WT and 2 different transgenic lines. **d–g**, *A. thaliana*. **d**, Gravitropic root bending in 8-day-old seedlings of the WT and *35S::KfPIN*-expressing lines; two successive 90° rotations were performed for analysis; scale bars, 5 mm. **e**, *A. thaliana* lines expressing *35S::KfPIN* showing decreased gravitropic response compared to WT (by 5.5° and 10.3° increase of the measured root bending angle after the first and second bends, respectively), as determined by a linear mixed-effect model and tested by a likelihood ratio test (first bend: $\chi^2 = 5.61$, $Df = 1$, $P = 0.0179$; second bend: $\chi^2 = 4.91$, $Df = 1$, $P = 0.0267$); $n = 166$ WT plants and 173, 126 and 263 plants of three independently generated transgenic lines. **f**, Examples of 'normal', the most commonly occurring vein pattern, and 'abnormal', not commonly occurring vein pattern, in 9-day-old *A. thaliana* primary leaves. **g**, Quantification of the presence of abnormal vasculature. There is a 3.82× increased presence of abnormal vasculature in *35S::KfPIN A. thaliana* primary leaves determined by generalized linear mixed-effect models with binomial distribution and tested by a likelihood ratio test ($\chi^2 = 13.539$, $Df = 1$, $P = 0.00023$). The points in the plot represent the proportion of abnormal leaves per plate with $n = 136$ WT and 201, 127 and 57 plants of three independently derived transgenic lines. **h,i**, *N. tabacum* BY-2 cells. **h**, Nomarski differential interference contrast of 2-day-old *XVE::KfPIN* cells, non-induced (left) and induced (right); scale bar, 25 µm. **i**, Cell size (diameter versus length) parameters; representative experiment from three biologically independent experiments (cultures inoculated separately); $n = 2{,}460$ (non-induced) and 2,008 (induced) individual cells in total. Elongation in induced cells increased by 53% as determined by a linear mixed-effect model with logarithmic transformation and tested by a likelihood ratio test ($\chi^2 = 1636.4$, $Df = 1$, $P < 2.2 \times 10^{-16}$). The boxes in all box plots show the 25%, 50% and 75% quartiles, the whiskers show the extreme values within 1.5× the interquartile distance and the individual data points are shown as dots. The asterisks above the plots show the significance level: $^*P < 0.05$, $^{***}P < 0.001$. The letters a and b signify a between-group difference at the $P = 0.05$ level.

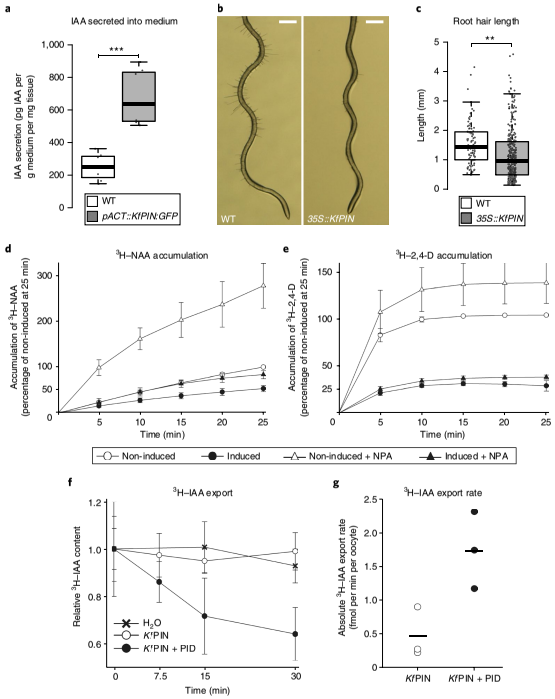

Fig. 2 | *Kf*PIN auxin transport capacity. a, Quantification of auxin secretion into medium in liquid protonemal culture of *P. patens* expressing *pACT::KfPIN:GFP* compared to WT. There is a 2.7× increased secretion in the transgenic line determined by analysis of variance with square-root transformation ($F = 42.23$, $P = 2.943 \times 10^{-5}$); $n = 7$ independently inoculated protonemal cultures, each of WT and transgenic plants. **b**,**c**, *KfPIN* expression inhibits root hair length in *A. thaliana*. **b**, Roots of 8-day-old WT and *35S:KfPIN thaliana* plants; scale bars, 500 µm. **c**, Quantification of root hair length in *35S:KfPIN A. thaliana* reaching 37% of the WT length as determined by a linear mixed-effect model and tested by a likelihood ratio test ($\chi = 20.52$, Df = 1, $P = 5.9 \times 10^{-6}$); the points represent individual root hairs, $n = 80$ WT and 230 transgenic plants (two lines). **d**,**e**, ^{3}H-labelled auxin accumulation in 1-day-old induced or non-induced *XVE:KfPIN* cells of *N. tabacum* BY-2. NPA, 1-*N*-naphthylphthalamic acid (10 µM). $n = 3$ biologically independent experiments (with separately inoculated cultures); each point in the charts represents the mean; the error bars show the s.e.m.; one transgenic line. **d**, ^{3}H-NAA accumulation. **e**, ^{3}H–2,4-D accumulation. **f**,**g**, ^{3}H-labelled auxin (IAA) retention over time in *X. laevis* oocytes expressing either *Kf*PIN or *Kf*PIN and PID protein kinase of *A. thaliana* (*Kf*PIN + PID). **f**, A representative experiment of three independently performed experiments. Each point in the chart represents the mean of 10 oocytes measured; the error bars show the s.e.m. H_2O represents control oocytes injected with water instead of mRNA. **g**, Comparison of the IAA transport rate between oocytes expressing either *Kf*PIN or *Kf*PIN + PID; linear regression. $n = 3$ biologically independent experiments (including the one shown in **f**), each with oocytes from a unique frog. The dash represents the mean; the error bars show the s.e.m. The box plots and significance levels (asterisks above plots) are defined as in the legend of Fig. 1.

*Kf*PIN transport activity by phosphorylation. Altogether, the results listed above strongly suggest a substrate-specific auxin transport function of the *Kf*PIN protein. The above observations are consistent with *Kf*PIN auxin transport action at the PM, leading us to investigate its cellular localization pattern. The *pACT::KfPIN:GFP* transgenic protonemal filaments of *P. patens* showed fluorescence at

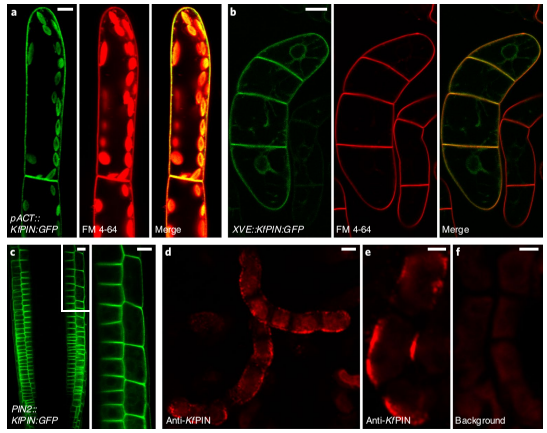

Fig. 3 | *Kf*PIN subcellular localization. a–**f**, Confocal microscopy. **a**, *P. patens pACT::KfPIN:GFP* protonema. Shown are the GFP signal at the PM, FM 4-64 PM staining and a merged image. Intracellular chloroplast autofluorescence is apparent in the green and red channels. **b**, *N. tabacum* BY-2 *XVE::KfPIN:GFP* cells, with induced expression. Shown are the GFP signal at the PM and endoplasmic reticulum, FM 4-64 PM staining and a merged image. **c**, *A. thaliana PIN2::KfPIN:GFP* root. The GFP signal is predominantly at the PM. Shown are images of the whole root (left) and a magnification of the marked area (right). **d**–**f**, *K. flaccidum*. **d**,**e**, Anti-*Kf*PIN indirect immunofluorescence, showing the *Kf*PIN signal at the cell periphery. **f**, A control sample without primary antibodies showing background signal. The relevant fluorescent signal in all transgenic plant lines and immunolocalized algae was observed at least three times independently. Scale bars, 20 µm (**b**), 10 µm (**c**), 5 µm (**a**,**d**,**f**) and 2.5 µm (**e**).

the PM, co-aligning with the marker dye FM 4-64 (Fig. 3a). The intracellular signal apparent in both the red and green channels is a common autofluorescence in protonemal tissue and does not reflect the specific transgene fluorescence[3]. Unlike the native PM-localized *Pp*PINs[3], *Kf*PIN was not localized polarly. Following induction, the same fusion construct transformed into BY-2 cells under the control of an oestradiol-inducible promoter (*XVE::KfPIN:GFP*) resulted in a PM-specific signal, co-aligning with FM 4-64 staining, and a weaker endoplasmic reticulum signal probably resulting from the high expression rate (Fig. 3b). Importantly, the induced *XVE::KfPIN:GFP* BY-2 cells also showed increased ^{3}H-labelled auxin efflux and developed the elongated phenotype indicative of auxin starvation (Supplementary Fig. 1), correlating with the intensity of *Kf*PIN:GFP fluorescence within individual cells (Supplementary Fig. 2), which demonstrates functionality of the GFP-tagged version. Finally, *A. thaliana* plants transformed with the *KfPIN:GFP* translational fusion expressed under the control of the native *At*PIN2 promoter (*PIN2::KfPIN:GFP*) revealed a PM localization pattern in roots, which was apolar (Fig. 3c), unlike that of the native *At*PIN2 protein[18] and in line with the apolar *Kf*PIN:GFP pattern observed in *P. patens* protonema. These results show that *Kf*PIN expressed in land plant models localizes predominantly to the PM.

With the use of land plants, we have obtained ample evidence concerning the auxin transport properties of *Kf*PIN. Therefore, we strove to obtain supporting evidence in *Klebsormidium*. PCR with reverse transcription revealed a stable transcription pattern of the *KfPIN* homologue in *K. nitens* throughout a subculture interval (Supplementary Fig. 3). To detect the native *Kf*PIN protein localization pattern, we performed immunostaining experiments, having designed an anti-*Kf*PIN specific antibody and adjusted the staining protocol[19] for the algal material. In the successfully stained cells, we observed a signal localized to the surface (Fig. 3d,e), whereas none was observed in control experiments without primary antibodies (Fig. 3f) or with primary antibodies against *A. thaliana* PIN1 and PIN2 (Supplementary Fig. 2). Immunostaining against α-tubulin served as a positive control (Supplementary Fig. 2). The same anti-*Kf*PIN antibody also produced a cell surface signal in the roots of *35S::KfPIN A. thaliana* plants, which was absent in wild-type (WT) roots (Supplementary Fig. 2). As *Klebsormidium* is non-transformable, we attempted to find direct evidence for auxin transport between the cells and the environment in WT alga by measuring the accumulation of ^{3}H-labelled auxins as in BY-2. These experiments were, however, technically non-feasible due to the probably prevalent IAA binding to the surface over entry into the cells (Supplementary Fig. 3). However, in our investigation of the biosynthesis of auxin and its release into the culture medium throughout the subculture interval of *K. nitens*, we did detect IAA in both the biomass and culture medium, especially in the advanced stage of culture growth (Supplementary Fig. 4).

Using land plant models, we show that the PIN homologue of *Klebsormidium* is capable of a substrate-specific auxin transport action at the PM, which is typical for the so-called canonical PIN proteins of land plants[20]. Unlike the canonical PINs, however, *Kf*PIN could not localize polarly, which is a crucial mechanism to restrict the direction of auxin flow[1]. The native *Kf*PIN localization pattern we observed in *Klebsormidium* was peripheral and enriched

laterally rather than at the cell-to-cell interface, which would suggest auxin efflux from the cells into the environment. We speculate that this might be the native function, as the morphologically simple filamentous structure of *Klebsormidium*, without polar growth or differentiated cell types during the vegetative phase, provides little justification for the necessity of localized auxin gradients to maintain cell identity or trigger developmental changes as in three-dimensional land plant bodies. This could also be the case in other charophyte algae, where PIN homologues have been identified regardless of morphological complexity, even in unicellular representatives[6]. The hypothetical purpose of the ancestral cell-to-environment auxin efflux might include quorum sensing or detoxification, as a higher auxin concentration inhibits cell division in *Klebsormidium*[10]. When auxin became a significant agent in plant developmental regulation, PIN-mediated auxin transport would also have become more complex, including the evolution of PIN polar localization to control its directionality. Intriguingly, the uniquely complex stoneworts (*Charophyceae*) might represent a case of convergent evolution of the recruitment of PINs to regulate an increasingly sophisticated development: multiple *Chara* species show evidence of independent PIN radiation[7], polar localization of PIN-like proteins[11] and basipetal auxin transport[8], although the last of these has not yet been connected to the native PINs. We conclude that PM-localized auxin transport is an ancient and conserved characteristic within the PIN family and that it emerged early in streptophyte evolution. The fascinating questions regarding the ancient and derived traits of PIN-mediated auxin transport, such as post-translational regulation by protein kinases and its utilization in separate branches of streptophytes, will be addressed as more model organisms, especially from charophyte algae, become sufficiently established in research.

Methods

The Supplementary Methods includes sections entitled 'Plant material and chemicals' and 'Microscopy and statistics', and additional information concerning the sections below.

Molecular biology, transformation and reverse transcription. See Supplementary Methods for the *KfPIN* and *KfPIN:GFP* cloning protocols and the primer sequences. See Supplementary Fig. 5 for the results of the analysis using quantitative PCR with reverse transcription. Total RNA was isolated from *Klebsormidium* ssp. biomass, *P. patens* fresh protonemal tissue, 2-week-old *A. thaliana* or 2-day-old BY-2 by Trizol (LifeTechnologies), purified with an RNeasy kit (Qiagen) and treated with DNAse (DNA-free Kit; Ambion). Iproof (BioRad) or M-MLV Reverse Transcriptase (Promega) was used for reverse transcription.

Phenotype analysis. Phenotype observation and evaluation in *P. patens* were performed as described previously[9]. Gravitropic root bending was observed 24 h after turning 4-day-old *A. thaliana* plants by 90°; the process was repeated once after the first screen. Primary leaves of 9-day-old *A. thaliana* plants were cleared as described previously[12] and categorized as having a 'normal' (four distinct compartments of the same or similar size) or an 'abnormal' (four compartments of markedly different sizes or >4 compartments initiated or finished) vascular pattern. The root hair length was analysed in 8-day-old *A. thaliana* plants. Cell parameters in BY-2 were measured in 2-day-old cells (since inoculation). Image analysis was performed in ImageJ.

Auxin transport and metabolism assays. Auxin accumulation and retention assays in BY-2 and *X. laevis* oocytes were performed as described previously[9,13]. The absolute auxin export rates for three biological replicates in *X. laevis* oocytes were obtained as the slope value after linear regression of the three curves per variable (*Kf*PIN versus *Kf*PIN+PID). PID refers to *A. thaliana* PINOID protein kinase (GenBank NM_129019). For a negative control, oocytes were injected with water instead of messenger RNA. See Supplementary Methods for the analysis of the IAA content in the biomass and culture medium of *K. nitens*, and *P. patens* protonemata.

Immunostaining. *Kf*PIN in *A. thaliana* and *K. flaccidum* (strain UTEX no. 323) was immunolocalized as described previously[10] using the automated InsituPro VSi station slide module (Intavis). Before the procedure, *K. flaccidum* cells were fixed for 1 h in 3.7% paraformaldehyde and placed on superfrost slides. The slides were then rinsed in pure methanol and subsequently in liquid nitrogen to improve the surface adhesion of the cells. See Supplementary Methods for antibodies.

Reporting Summary. Further information on research design is available in the Nature Research Reporting Summary linked to this article.

Data availability

The underlying data of this study are available from the corresponding author upon request.

Received: 18 August 2017; Accepted: 7 October 2019;
Published online: 11 November 2019

References

1. Adamowski, M. & Friml, J. PIN-dependent auxin transport: action, regulation, and evolution. *Plant Cell* **27**, 20–32 (2015).
2. Bennett, T. PIN proteins and the evolution of plant development. *Trends Plant Sci.* **20**, 498–507 (2015).
3. Viaene, T. et al. Directional auxin transport mechanisms in early diverging land plants. *Curr. Biol.* **24**, 2786–2791 (2014).
4. Leliaert, F. et al. Phylogeny and molecular evolution of the green algae. *Crit. Rev. Plant Sci.* **31**, 1–46 (2012).
5. Hori, K. et al. *Klebsormidium flaccidum* genome reveals primary factors for plant terrestrial adaptation. *Nat. Commun.* **5**, 9 (2014).
6. Ju, C. et al. Conservation of ethylene as a plant hormone over 450 million years of evolution. *Nat. Plants* **1**, 14004 (2015).
7. Nishiyama, T. et al. The Chara genome: secondary complexity and implications for plant terrestrialization. *Cell* **174**, 448–464 (2018).
8. Zizkova, E. et al. Control of cytokinin and auxin homeostasis in cyanobacteria and algae. *Ann. Bot.* **119**, 151–166 (2017).
9. Boot, K. J. M., Libbenga, K. R., Hille, S. C., Offringa, R. & van Duijn, B. Polar auxin transport: an early invention. *J. Exp. Bot.* **63**, 4213–4218 (2012).
10. Ohtaka, K., Hori, K., Kanno, Y., Seo, M. & Ohta, H. Primitive auxin response without TIR1 and Aux/IAA in the charophyte alga *Klebsormidium nitens*. *Plant Physiol.* **174**, 1621–1632 (2017).
11. Luschnig, C., Gaxiola, R. A., Grisafi, P. & Fink, G. R. EIR1, a root-specific protein involved in auxin transport, is required for gravitropism in *Arabidopsis thaliana*. *Genes Dev.* **12**, 2175–2187 (1998).
12. Zhang, J. et al. Inositol trisphosphate-induced Ca^{2+} signaling modulates auxin transport and PIN polarity. *Dev. Cell* **20**, 855–866 (2011).
13. Xi, W. Y., Gong, X. M., Yang, Q. Y., Yu, H. & Liou, Y. C. Pin1 At regulates PIN1 polar localization and root gravitropism. *Nat. Commun.* **7**, 10 (2016).
14. Petrasek, J. & Zazimalova, E. Tobacco BY-2 cells: from cellular dynamics to omics. In *Biotechnology in Agriculture and Forestry* Vol. 58 (eds Nagata, T. et al.) 107–115 https://doi.org/10.1007/3-540-32674-X (Springer, 2006).
15. Ganguly, A. et al. Differential auxin-transporting activities of PIN-FORMED proteins in *Arabidopsis* root hair cells. *Plant Physiol.* **153**, 1046–1061 (2010).
16. Fastner, A., Absmanner, B. & Hammes, U. Z. Use of *Xenopus laevis* oocytes to study auxin transport. In *Plant Hormones: Methods and Protocols* 3rd edn, Vol. 1497 (eds Kleine-Vehn, J. & Sauer, M.) 259–270 (Humana, 2017).
17. Zourelidou, M. et al. Auxin efflux by PIN-FORMED proteins is activated by two different protein kinases, D6 PROTEIN KINASE and PINOID. *eLife* **3**, 68 (2014).
18. Muller, A. et al. AtPIN2 defines a locus of *Arabidopsis* for root gravitropism control. *EMBO J.* **17**, 6903–6911 (1998).
19. Paciorek, T., Sauer, M., Balla, J., Wisniewska, J. & Friml, J. Immunocytochemical technique for protein localization in sections of plant tissues. *Nat. Protoc.* **1**, 104–107 (2006).
20. Petrasek, J. et al. PIN proteins perform a rate-limiting function in cellular auxin efflux. *Science* **312**, 914–918 (2006).
21. Zabka, A. et al. PIN2-like proteins may contribute to the regulation of morphogenetic processes during spermatogenesis in *Chara vulgaris*. *Plant Cell Rep.* **35**, 1655–1669 (2016).

Acknowledgements

We thank E. D. Cooper and C. F. Delwiche for sharing the *K. flaccidum* transcriptome sequences before their publication and valuable suggestions; and M. Filová and R. Granbom for technical assistance. This work was financially supported by the Ministry of Education, Youth and Sports of Czech Republic (MEYS CR) under the projects NPU I, MSM/LO1417 (R.S., S. V. and J.P.), CEITEC 2020, LQ1601 (T.N. and M.Z.), CZ.02.1.01/0/0.0/0.0/16_019/0000827 (M.K.) and CZ.02.1.01/0.0/0.0/16_013/0001775 (J.P.), the Czech Science Foundation, projects GA18-26981S (J.F. and M.Z.) and GA17-17966Y (M.Z.), German Research Foundation (DFG) project HA 3468/6-1 (U.Z.H.), the European Union's Horizon 2020 programme (ERC grant agreement 742985) (J.F.) and US NSF Award DEB-1036506. T.N., M.Z. and E.M. acknowledge the CELLIM Core Facility of CEITEC and R.S., P.S. and J.P. acknowledge the imaging facility of IEB CAS, both supported by the Czech-BioImaging large RI project (LM2015062 funded by MEYS CR). T.N., M.Z. and E.M. acknowledge the Plant Sciences Core Facility of CEITEC MU. K.L. and M.K. acknowledge the Knut and Alice Wallenberg Foundation, the Swedish Governmental Agency for Innovation Systems (VINNOVA), the Swedish Research Council (VR) and the Swedish Metabolomics Centre.

Author contributions

J.F., J.P. and R.S. conceptualized the project. R.S., E.M. and T.V. performed and analysed most experiments. T.V. cloned most constructs. Y.Z. cloned the *PIN2:KfPIN:GFP* construct and produced and analysed the *Arabidopsis* line. D.P.J. and U.Z.H. provided data on *Xenopus* oocytes. M.Z. designed the anti-*Kf*PIN-specific antibody. M.K. analysed auxin content in biomass and media. S.V. performed statistical analysis. M.Z., T.N., K.M., K.L., P.S., J.F. and J.P. oversaw the experiments. R.S. wrote the manuscript and J.F. and J.P. oversaw the writing.

Competing interests

The authors declare no competing interests.

Additional information

Supplementary information is available for this paper at https://doi.org/10.1038/s41477-019-0542-5.

Correspondence and requests for materials should be addressed to J.F.

Peer review information *Nature Plants* thanks Bert van Duijn and the other, anonymous, reviewer(s) for their contribution to the peer review of this work.

Reprints and permissions information is available at www.nature.com/reprints.

Publisher's note Springer Nature remains neutral with regard to jurisdictional claims in published maps and institutional affiliations.

Structures and mechanism of the plant PIN-FORMED auxin transporter

https://doi.org/10.1038/s41586-022-04883-y

Received: 4 January 2022

Accepted: 19 May 2022

Published online: 29 June 2022

Open access

Check for updates

Kien Lam Ung[1,4], Mikael Winkler[1,4], Lukas Schulz[2], Martina Kolb[2], Dorina P. Janacek[2], Emil Dedic[1], David L. Stokes[3], Ulrich Z. Hammes[2✉] & Bjørn Panyella Pedersen[1✉]

Auxins are hormones that have central roles and control nearly all aspects of growth and development in plants[1–3]. The proteins in the PIN-FORMED (PIN) family (also known as the auxin efflux carrier family) are key participants in this process and control auxin export from the cytosol to the extracellular space[4–9]. Owing to a lack of structural and biochemical data, the molecular mechanism of PIN-mediated auxin transport is not understood. Here we present biophysical analysis together with three structures of *Arabidopsis thaliana* PIN8: two outward-facing conformations with and without auxin, and one inward-facing conformation bound to the herbicide naphthylphthalamic acid. The structure forms a homodimer, with each monomer divided into a transport and scaffold domain with a clearly defined auxin binding site. Next to the binding site, a proline–proline crossover is a pivot point for structural changes associated with transport, which we show to be independent of proton and ion gradients and probably driven by the negative charge of the auxin. The structures and biochemical data reveal an elevator-type transport mechanism reminiscent of bile acid/sodium symporters, bicarbonate/sodium symporters and sodium/proton antiporters. Our results provide a comprehensive molecular model for auxin recognition and transport by PINs, link and expand on a well-known conceptual framework for transport, and explain a central mechanism of polar auxin transport, a core feature of plant physiology, growth and development.

Auxins are a group of hormones that regulate nearly all growth and developmental processes in plants. Indole-3-acetic acid (IAA; $pK_a = 4.7$) is the most prominent auxin, and is synonymously referred to as 'auxin'. IAA provides a growth signal that orchestrates most complex environmental responses in plants, including phototropism and geotropism[1].

Many of the effects on plant growth depend on the distribution of auxin in the plant body, which is controlled by the process of polar auxin transport[2,3]. This process relies on export of auxin out of cells by PIN transporters[4–9]. The physiological importance of PINs is underlined by often severe *pin* mutant phenotypes, which can be mimicked by auxin efflux inhibitors such as the commercially available herbicide naphthylphthalamic acid[10] (NPA (also known as naptalam); $pK_a = 4.6$).

The PIN protein family is exclusive to the plant kingdom and is classified as part of the large bile/arsenite/riboflavin transporter (BART) superfamily, which also includes transporters of bile acid, arsenite and riboflavin with members distributed across all kingdoms of life[11,12]. PIN proteins are predicted to have ten transmembrane helices comprising two five-transmembrane helix repeats separated by a cytosolic loop. Canonical PINs (PIN1–4 and PIN7 in *A. thaliana*) are characterized by a long (323–355 residue) loop and are mostly located in the plasma membrane, whereas non-canonical PINs (PIN5 and PIN8 and the intermediate PIN6 in *A. thaliana*) possess a much shorter loop and can be found in organellar membranes such as endoplasmic reticulum membranes[13–15] (Extended Data Figs. 1 and 2a). The long loops of canonical PINs have phosphorylation sites that regulate activity; the loops have been shown to be auto-inhibitory, requiring kinase activity to initiate transport[16].

Here we present structural and biophysical characterization of a PIN protein. In particular, cryo-electron microscopy (cryo-EM) has been used to solve structures in an outward-facing state with and without bound IAA as well as in an inward-facing state with bound NPA at resolutions between 2.9 and 3.4 Å. Combined with transport data from mutant protein, these structures suggest a molecular mechanism and model for auxin transport that is broadly applicable to the ubiquitous PIN family.

We chose to study PIN8 from *A. thaliana* after screening various PIN homologues for expression and purification. PIN8 is a non-canonical PIN of 40 kDa in size, with a short cytosolic loop of 43 residues that lacks the phosphorylation motifs seen in the long auto-inhibitory loops of canonical PINs. When expressed in oocytes, PIN8 exhibited robust IAA transport activity similar to that of kinase-activated PIN1. This activity is independent of activating kinases and sensitive to the inhibitor NPA, demonstrating that PIN8 is a constitutively active auxin transporter (Fig. 1a and Extended Data Fig. 2b).

To characterize electrogenic transport of IAA by PIN8, we overexpressed the protein in *Saccharomyces cerevisiae* and, following purification, reconstituted it into proteoliposomes. We measured transport using capacitive coupling using solid supported membrane (SSM) electrophysiology,

[1]Department of Molecular Biology and Genetics, Aarhus University, Aarhus, Denmark. [2]Plant Systems Biology, School of Life Sciences Weihenstephan, Technical University of Munich, Freising, Germany. [3]Skirball Institute of Biomolecular Medicine, Department of Cell Biology, New York University School of Medicine, New York, NY, USA. [4]These authors contributed equally: Kien Lam Ung, Mikael Winkler. ✉e-mail: ulrich.hammes@tum.de; bpp@mbg.au.dk

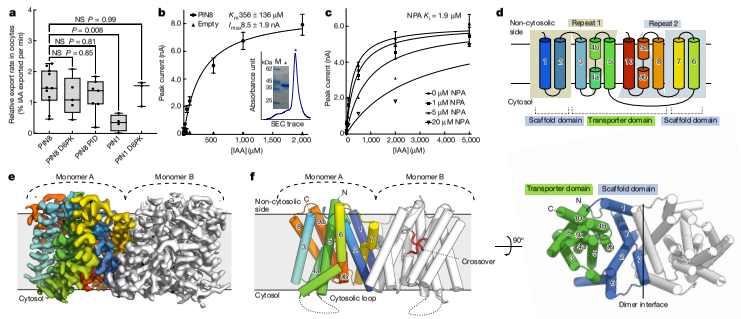

Fig. 1 | Activity and overall structure of PIN8. a, Relative IAA transport rates for PIN8 and PIN1 incubated with PIN-activating kinases D6PK and PID show that PIN8 is constitutively active in oocytes (internal oocyte IAA concentration = 1 µM). The centre line is the median, the box extends from the 25th to 75th percentile and whiskers extend to minimum and maximum values. Points represent biologically independent experiments (PIN8: $n = 11$, PIN8 D6PK: $n = 5$, PIN8 PID: $n = 7$, PIN1: $n = 4$, PIN1 D6PK: $n = 3$). For differences between PIN8 and other groups, a one-way ANOVA followed by Dunnett's multiple comparisons test was performed. PIN8 versus PIN8 D6PK: $P = 0.8508$, PIN8 versus PIN8 PID: $P = 0.8090$, PIN8 versus PIN1: $P = 0.0078$, PIN8 versus PIN1D6PK: $P = 0.9968$. **b**, Peak current response by SSM electrophysiology on PIN8 proteoliposomes. Transport is described by Michaelis–Menten kinetics ($r^2 = 0.98$, $K_m = 356 \pm 136$ µM, maximum current (I_{max}) = 8. 5 ± 1.9 nA; data are mean ± s.e.m.; PIN8: $n = 4$ different proteoliposome preparations, empty: $n = 3$ liposome preparations). Inset, stained SDS–PAGE analysis and size-exclusion chromatography (SEC) trace for the PIN8 purification. **c**, Transport current in the presence of NPA shows inhibition ($K_i = 1.9$ µM (95% confidence interval: 0.9–3.8 µM; $n = 3$ for 0 and 1 µM NPA and $n = 2$ for 5 and 20 µM NPA); data are mean or mean ± s.e.m. ($n > 2$)). **d**, Topology of the PIN8 monomer shows an inverted repeat of five transmembrane helices and the relation between transporter and scaffold domains. **e**, Cryo-EM map of the PIN8 dimer with one monomer coloured according to panel **d**. **f**, Side view of PIN8 with M1–M10 labelled. The central crossover highlighted in red in monomer B. Right, top view from the non-cytosolic side displays the dimer interface and the two domains found in each monomer: the transporter domain (green) and the scaffold domain (blue).

and show that PIN8 has a relatively low apparent affinity for IAA, with a Michaelis constant (K_m; Methods, 'SSM physiology assays') of 356 ± 136 µM ($n = 4$) (Fig. 1b and Extended Data Fig. 2c). We measure the dissociation constant (K_d) of IAA binding to be 39.9 µM (Extended Data Fig. 2d). We observe a modest pH dependence with an optimum at 6.0–7.4 (Extended Data Fig. 2e). As in oocyte assays, transport can be inhibited by NPA, which inhibit with an inhibition constant (K_i) of 1.9 µM, suggesting an affinity one order of magnitude higher than that of IAA (Fig. 1c). We screened a number of additional PIN substrates (Extended Data Fig. 2f) and find that IAA analogues—for example, naphthaleneacetic acid (NAA) or the herbicide 2,4-dichlorophenoxyacetic acid (2,4-D), elicit a current response in PIN8, whereas uncharged auxins as well as some endogenous auxins do not. Comparison of these substrates suggests that shape complementary has a large role in recognition: for example, the larger size of indole-3-butyric acid (IBA) and the reduced ring system of 2-phenylacetic acid (PAA) both result in reduced currents.

We solved three distinct structures of PIN8 using single-particle cryo-EM after reconstitution of the purified protein into peptidisc: an apo form at 2.9 Å resolution, PIN8 with IAA bound at 3.2 Å, and PIN8 with NPA bound at 3.4 Å resolution (Extended Data Figs. 3–5 and Extended Data Table 1). In addition, a structure of the apo form that is indistinguishable from the apo peptidisc structure was produced from a detergent-solubilized preparation at 3.3 Å (Extended Data Table 1). The highest-resolution map of the apo form was used for initial model building, but all maps display excellent density for the entire protein except for 39 residues of the disordered cytosolic loop, which were not modelled (Fig. 1d,e). We could model multiple water molecules and lipids as well as IAA and NPA in the relevant structures.

The apo form of PIN8 displays a symmetric dimer of PIN8 (Fig. 1f) characterized by a twofold rotation axis perpendicular to the membrane plane with a distinct concavity extending into the membrane along this axis from the non-cytosolic side. Within each monomer there are ten transmembrane helices (M1–M10), comprising an inverted repeat of five transmembrane helices[17] (Fig. 1d). In each repeat, the fourth helix is disrupted around a conserved proline residue in the middle of the membrane plane: Pro116 in M4 and Pro325 in M9. These disrupted helices make an X-shaped crossover that marks the auxin binding pocket (Fig. 1f).

The PIN8 monomer is divided into two domains that we name the scaffold domain and the transporter domain (Fig. 1d, f and Extended Data Fig. 6a). The scaffold domain comprises helices M1, M2, M6 and M7 and creates a large interface (1,512 Å^2) to the other monomer in the dimeric complex. This interface is mediated mainly by M2 and M7, and is further stabilized by a lipid in a groove between M1 and the kinked M6 (Extended Data Fig. 6b). We also observe another lipid with an aliphatic tail sticking into a pocket of the transporter domain. We tested a dependence on lipids for activity and found that PIN8 functions similarly in mixed lipid and pure phosphatidylcholine liposomes (Extended Data Fig. 6c). The transporter domain consists of helices M3–M5 and M8–M10 and harbours the central X-shaped crossover (Fig. 1f). The overall fold of the monomer is similar to that of the bile acid/sodium symporters, but the membrane topology is inverted[18] (Extended Data Fig. 7). Next to the crossover, there is a well-defined water-filled binding pocket nestled between the scaffold domain and the transporter domain that is open to the non-cytosolic side of the protein via the concavity (Fig. 1f). By contrast, access to the cytosol is blocked, clearly defining the conformation of the apo-PIN8 dimer as an empty outward-open state.

The substrate-bound form of PIN8, IAA–PIN8, is almost identical to apo-PIN8 (root mean squared deviation of Cα atoms (r.m.s.d.$_{Cα}$) = 0.6 Å)

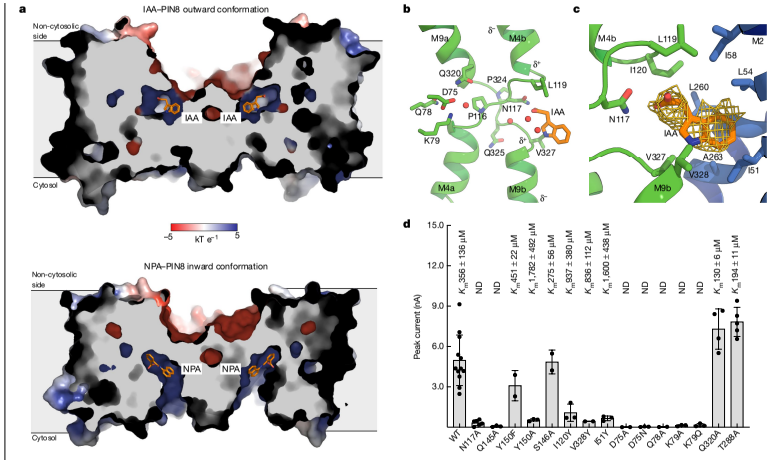

Fig. 2 | Structures with IAA and NPA bound. a, Cut away view of electrostatic surface representation of IAA–PIN8 and NPA–PIN8 show the change in conformation. Whereas the concavity at the non-cytosolic side has negative potential, the binding pocket itself has a positive potential in both cases. **b**, View of the crossover and the position of IAA and the support site with central residues highlighted. **c**, Close-up view of IAA map density and the residues from the scaffold domain interacting with the indole ring. **d**, Peak current response evoked by 500 µM IAA determined by SSM electrophysiology for PIN8 mutants. K_m values (mean ± s.d.) derived from the full measurement (Extended Data Fig. 8a) are shown above the bars; ND indicates that a Michaelis–Menten curve could not be fit. The bars show mean ± s.e.m. ($n > 2$); points represent biologically independent measurements (wild type (WT): $n = 4$ different liposome preparations; mutants: $n = 6$ (N117A), $n = 5$ (T288A), $n = 4$ (Q320A), $n = 3$ (Q145A, D75N, K79A, K79Q, Q78A, I51Y, I120Y and Y150A), $n = 2$ (Y150F, S146A, D75A and V328Y)).

(Fig. 2a). There is a clear density for IAA in the binding pocket, with three surrounding water molecules (Fig. 2b,c). Thus, the IAA–PIN8 structure represents a substrate-bound outward-open state, the expected release state for auxin.

IAA is bound with its carboxylate group oriented towards the crossover; although only two residues are within hydrogen-bonding distance (Asn117 and Gln145), IAA is stabilized by the positive dipole from M4b and M9b helices. The backbone carbonyl of Pro116 creates a polar pocket that is also lined by Tyr150 and Ser146. Here we observe three well-defined water molecules that may reflect partial disassociation of IAA from the binding pocket in the release state. Mutating either Asn117 and Gln145 to alanine abolishes transport, supporting their importance (Fig. 2d). Tyr150 mutants display mixed results: Y150F retains activity, affinity and sensitivity to NPA, whereas removal of the bulky side chain in Y150A results in very low activity and affinity (Extended Data Fig. 8a,b). By contrast, mutation of Ser146 had no effect on activity (Fig. 2d and Extended Data Fig. 8a).

In the transporter domain, the IAA carbon backbone contacts Leu119 (M4b) and Ile120 (M4b) towards the non-cytosolic side, whereas the indole ring contacts Val327 (M9b) and Val328 (M9b) towards the cytosolic side. These four hydrophobic residues are symmetrically located on the crossover immediately after the two key prolines as part of a duplicated and conserved crossover sequence motif (P(N/Q)XΦΦ; where Φ is a hydrophobic residue) (Fig. 2b–d and Extended Data Figs. 1 and 8b). The hydrophobic residues of the crossover motif provide affinity for the auxin substrate. This is supported by the bulky I120Y and V328Y mutants, which both reduce apparent affinity by interfering with substrate binding but still retain NPA sensitivity (Fig. 2d and Extended Data Fig. 8a,b). Together, the interactions between the transporter domain and IAA emphasize that PIN8 selects for IAA on the basis of shape complementarity, as also suggested by the SSM electrophysiology results. In the scaffold domain, the indole ring has additional non-specific hydrophobic interactions with Ile51 (M2), Leu54 (M2) and the pseudo-symmetrically related Leu260 (M7) and Ala263 (M7). Bulky mutations in these hydrophobic residues (such as I51Y) lead to a considerably reduced transport current (Fig. 2d and Extended Data Fig. 8a,b). All the residues defining the binding pocket show high sequence conservation across different plant species and are fully conserved in all *A. thaliana* PIN proteins except PIN5 (Extended Data Figs. 1 and 8c).

The NPA-bound form of PIN8 adopts an inward-open conformation (Fig. 2a). The scaffold domains and dimeric interface is unchanged relative to the outward-open conformation (r.m.s.$d_{C\alpha}$ = 0.9 Å), but the two transporter domains are rotated by approximately 20° to expose the auxin binding site and Asn117 to the cytosolic side. This rotation results in a translation of the binding site by approximately 5 Å (Fig. 3a and Supplementary Video 1). NPA has more extensive interaction with the protein compared with IAA in the outward-open state (Fig. 3b,c and Extended Data Fig. 8c,d). Similar to IAA, the carboxylate group of NPA points towards the crossover, but has several stronger interactions that are not observed in the outward-open state. In addition to interactions seen for IAA, NPA interacts with main chain nitrogen atoms of Val327

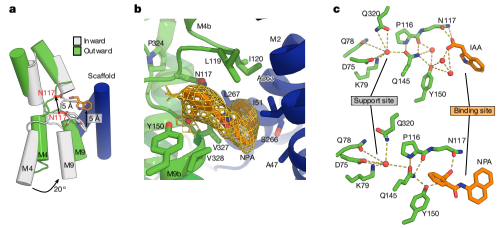

Fig. 3 | Conformational change and the support site. a, Inward and outward structures superposed on the scaffold domain (blue) reveal an elevator-type movement, with the substrate binding site moving 5 Å. **b**, Close-up view of the NPA map density and the residues interacting with it. **c**, The hydrogen-bonding network linking the binding site to the support site through Gln145 in the outward state (top) and inward state (bottom).

and Val328, as well as with Gln145 and Tyr150 in a network that does not involve water. The benzene ring and naphthyl ring of NPA still interact with the two crossover motifs of the transporter domain, similar to IAA. Several new interactions are also observed with the scaffold domain, many of which are mediated by the naphthyl ring of NPA and are probably unique to the larger, more complex NPA molecule (Fig. 3b,c and Extended Data Fig. 8a–d). Inhibition by NPA can thus be explained by two components: (1) stronger binding due to engagement of additional residues from the scaffold domain, and (2) the larger size of NPA that prevents transition to the outward state.

Adjacent to the primary auxin binding site, an accessory 'support site' is apparent on the other side of the crossover between M3, M5 and M9. This support site is linked to the primary auxin binding site via an extensive hydrogen bond network bridged by the central Gln145 and the backbone carbonyl of Pro116. The higher-resolution apo-PIN8 map reveals two peaks in the site, which are modelled as water (Extended Data Fig. 8e). In the lower-resolution IAA–PIN8 and NPA–PIN8 map, the same site contains one single weak peak that is also modelled as water (Fig. 3c and Extended Data Fig. 8c–e). The presence of Na^+ at analogous sites in bile acid/sodium symporters led us to probe ion dependence by comparing PIN8 transport in sodium- and potassium-exclusive buffers. In both cases, PIN8 retains full activity, suggesting that specific counter-transport of ions does not take place (Extended Data Fig. 9a). In all structures, the water molecules in the support site engage in a hydrogen bond network with Asp75 (M3), Gln78 (M3), Lys79 (M3), Gln320 (M9a) and Gln145 (M5) (Fig. 3c). Mutational analysis indicates that all of these residues except Gln320 are absolutely essential for activity (Fig. 2d and Extended Data Fig. 8a). Notably, Asp75 and Lys79 are fully conserved and constitute a proton donor–acceptor pair with potential for proton transport; indeed, this idea is supported by isosteric mutations that remove the charge from either residue (D75N or K79Q) and abolish transport (Fig. 2d and Extended Data Fig. 8a,c,d). The distance from Asp75 to Lys79 is below 3 Å in all structures, consistent with an unprotonated state for Asp75. However, activity of PIN8 in proteoliposomes is not sensitive to proton-motive force decouplers and has minimal pH dependence, suggesting that a proton-motive force is not obligatory for transport (Extended Data Figs. 2e and 9b). Furthermore, export rates in oocytes are also indifferent to external pH (Extended Data Fig. 9c).

Discussion

Plant growth and morphology are largely governed by polar auxin transport as mediated by canonical PINs. Comparison of all the PINs from *A. thaliana* with PIN8 studied here indicates that—with an exception of the unusual non-canonical PIN5—the auxin and support sites are perfectly conserved. This conservation, which also extends to other plant species, indicates that our observations can be generalized[19] (Extended Data Figs. 1, 2a and 8c,d). The low apparent affinity for IAA measured in proteoliposome assays is 5–500-fold lower than the physiological concentrations of auxin in plant tissues[20] (0.1–10 µM). Although we cannot rule out experimental artifacts, this implies that distinct functions of *A. thaliana* PINs arise from differing localization, abundance and auto-inhibition properties rather than direct modulation of substrate affinity[3]. Some studies have suggested that ABCB transporters interact with PINs to generate selectivity in IAA transport[21–23]. Our work suggests that this interaction is not needed for activity in vitro, and is most probably not required in planta.

The PIN family is part of the BART superfamily, which includes the structurally characterized ASBT bile acid/sodium symporters from the BASS family[18]. Although PIN8 and ASBT adopt the same fold, ASBT assumes an inverted orientation and does not appear to dimerize (Extended Data Fig. 7). In addition, at least three other families of proteins adopt this same fold (DALI *Z*-score > 10), namely two Na^+/H^+ antiporter families (CPA1 and CPA2) and the $HCO3^-/Na^+$ symporter family[24–29]. Similar to the bile acid/sodium symporters, these other protein families all share negligible sequence homology with PINs. The $HCO3^-/Na^+$ symporters adopt the same membrane orientation as PIN8, whereas the Na^+/H^+ antiporters share the inverted orientation with the bile acid/sodium symporters, perhaps explaining why the structural link between PINs and these divergent protein families has not been noted previously (Extended Data Fig. 7).

These other protein families are all secondary active transporters that use sodium or protons to drive transport, and all are proposed to function using an elevator mechanism in which the scaffold domain is fixed and the transporter domain pivots about the conserved proline crossover motif. Notably, the site occupied by the driving sodium and protons in these families is located at the same position as the support site in PINs (Extended Data Fig. 7), and it is clear from this work that PIN8 uses the same general proline crossover-based elevator mechanism (Fig. 3a and Supplementary Video 1).

Our data show that the negative charge of the IAA is sufficient for transport (Extended Data Figs. 2e and 9). However, the basic architecture of a support site is present that would allow for ion binding, as well as a conserved and functionally essential Asp75–Lys79 pair that could mediate proton translocation[30]. Most mutations of the support site completely abrogate activity, underlining the essential nature of this region, but neither oocyte nor SSM electrophysiology assays suggest dependence on counter-transport of either sodium or protons to drive auxin export. Our data thus support a uniport mechanism for PINs, although we cannot definitely rule out proton antiport in vivo.

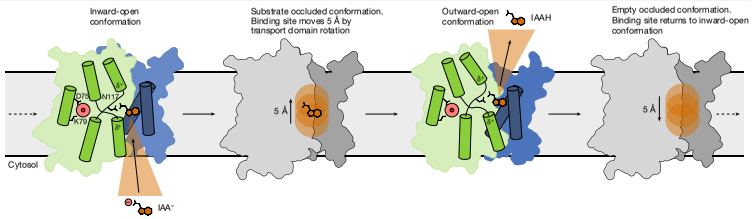

Fig. 4 | Proposed mechanism of auxin export by PIN proteins. In the inward-open conformation (left), IAA enters the binding site with a deprotonated carboxylate. The positive dipole of the M4b and M9b helices helps diffuse the charge. During rotation of the transporter domain, the binding site moves 5 Å towards the non-cytosolic side (second from left). At the non-cytosolic side, IAA is released, probably assisted by a protonation event (second from right). The support site could also become protonated before reverting to the inward-facing conformation (right), but our data indicate that this is not obligatory for function.

On the basis of the data available, we propose the following model for auxin transport by PINs (Fig. 4): The inward-facing conformation allows an ionized auxin molecule to enter the binding site between transport and scaffold domains. The negatively charged carboxylate group is stabilized by the positive dipole of M4b and M9b, while being held in place by Asn117 and interacting with the support site through Gln145. The carbon backbone and indole ring are recognized by the four hydrophobic residues from the two crossover motifs of the scaffold domain. During transition to the outward-facing conformation, the proline crossover rotates 20° and the auxin binding site in the scaffold domain is translated away from the cytosol by 5 Å. Release of IAA in the outward-facing state is facilitated by a pH shift that protonates and neutralizes the carboxylate. After substrate release, the protein reverts back to the inward-open state.

It has been suggested that the oligomeric state of PINs might have a role in regulation, but the large dimer-interaction surface in PIN8 argues against a dynamic equlibrium[31,32]. Nevertheless, it is conceivable that the monomers operate independently and also that PINs could form hetero-oligomers[33].

We have not directly addressed auto-inhibition by the cytosolic loop in canonical PINs, but the connection to other known protein families provides some hints: For HCO_3^-/Na^+ symporters, it has been shown that a loop from a cytosolic regulatory partner locks the protein in an inward conformation by interacting with the binding site[24,29]. By analogy, it seems plausible that the auto-inhibitory loop in canonical PINs operates by a similar mechanism.

In conclusion, we have presented in vitro biochemical characterization of a PIN as well as structures representing two key conformational states in the presence and absence of auxin and the herbicide NPA. The structure with NPA demonstrates competitive inhibition in PIN proteins, and could provide the basis for structure-based development of novel herbicides. We describe the molecular mechanism of auxin transport by PINs that can function independently of monovalent ions or protons, thus expanding our understanding of the crossover elevator mechanism used by proteins from diverse protein superfamilies from all kingdoms of life. This work provides a comprehensive foundation for future studies aiming to elucidate PIN function in polar auxin transport, which is essential for plant growth and development.

Online content

Any methods, additional references, Nature Research reporting summaries, source data, extended data, supplementary information, acknowledgements, peer review information; details of author contributions and competing interests; and statements of data and code availability are available at https://doi.org/10.1038/s41586-022-04883-y.

1. Weijers, D. & Wagner, D. Transcriptional responses to the auxin hormone. *Annu. Rev. Plant Biol.* **67**, 539–574 (2016).
2. Goldsmith, M. H. M. The polar transport of auxin. *Annu. Rev. Plant Physiol.* **28**, 439–478 (1977).
3. Hammes, U. Z., Murphy, A. S. & Schwechheimer, C. Auxin transporters—a biochemical view. *Cold Spring Harb. Perspect. Biol.* **14**, a039875 (2021).
4. Gälweiler, L. et al. Regulation of polar auxin transport by AtPIN1 in *Arabidopsis* vascular tissue. *Science* **282**, 2226–2230 (1998).
5. Chen, R. et al. The *Arabidopsis thaliana AGRAVITROPIC 1* gene encodes a component of the polar-auxin-transport efflux carrier. *Proc. Natl Acad. Sci. USA* **95**, 15112–15117 (1998).
6. Luschnig, C., Gaxiola, R. A., Grisafi, P. & Fink, G. R. EIR1, a root-specific protein involved in auxin transport, is required for gravitropism in *Arabidopsis thaliana*. *Genes Dev.* **12**, 2175–2187 (1998).
7. Petrásek, J. et al. PIN proteins perform a rate-limiting function in cellular auxin efflux. *Science* **312**, 914–918 (2006).
8. Raven, J. A. Transport of indoleacetic acid in plant cells in relation to pH and electrical potential gradients, and its significance for polar IAA transport. *New Phytol.* **74**, 163–172 (1975).
9. Rubery, P. H. & Sheldrake, A. R. Carrier-mediated auxin transport. *Planta* **118**, 101–121 (1974).
10. Okada, K., Ueda, J., Komaki, M. K., Bell, C. J. & Shimura, Y. Requirement of the auxin polar transport system in early stages of *Arabidopsis* floral bud formation. *Plant Cell* **3**, 677–684 (1991).
11. Chen, J. S. et al. Phylogenetic characterization of transport protein superfamilies: superiority of SuperfamilyTree programs over those based on multiple alignments. *J. Mol. Microbiol. Biotechnol.* **21**, 83–96 (2011).
12. Mansour, N. M., Sawhney, M., Tamang, D. G., Vogl, C. & Saier Jr, M. H. The bile/arsenite/riboflavin transporter (BART) superfamily. *FEBS J.* **274**, 612–629 (2007).
13. Ding, Z. et al. ER-localized auxin transporter PIN8 regulates auxin homeostasis and male gametophyte development in *Arabidopsis*. *Nat. Commun.* **3**, 941 (2012).
14. Ditengou, F. A. et al. Characterization of auxin transporter PIN6 plasma membrane targeting reveals a function for PIN6 in plant bolting. *New Phytol.* **217**, 1610–1624 (2018).
15. Mravec, J. et al. Subcellular homeostasis of phytohormone auxin is mediated by the ER-localized PIN5 transporter. *Nature* **459**, 1136–1140 (2009).
16. Zourelidou, M. et al. Auxin efflux by PIN-FORMED proteins is activated by two different protein kinases, D6 PROTEIN KINASE and PINOID. *eLife* **3**, e02860 (2014).
17. Duran, A. M. & Meiler, J. Inverted topologies in membrane proteins: a mini-review. *Comput. Struct. Biotechnol. J.* **8**, e201308004 (2013).
18. Hu, N.-J., Iwata, S., Cameron, A. D. & Drew, D. Crystal structure of a bacterial homologue of the bile acid sodium symporter ASBT. *Nature* **478**, 408–411 (2011).
19. Bennett, T. et al. Paralogous radiations of PIN proteins with multiple origins of noncanonical PIN structure. *Mol. Biol. Evol.* **31**, 2042–2060 (2014).
20. Petersson, S. V. et al. An auxin gradient and maximum in the *Arabidopsis* root apex shown by high-resolution cell-specific analysis of IAA distribution and synthesis. *Plant Cell* **21**, 1659–1668 (2009).
21. Bandyopadhyay, A. et al. Interactions of PIN and PGP auxin transport mechanisms. *Biochem. Soc. Trans.* **35**, 137–141 (2007).
22. Deslauriers, S. D. & Spalding, E. P. Electrophysiological study of *Arabidopsis* ABCB4 and PIN2 auxin transporters: evidence of auxin activation and interaction enhancing auxin selectivity. *Plant Direct* **5**, e361 (2021).
23. Noh, B., Murphy, A. S. & Spalding, E. P. Multidrug resistance-like genes of *Arabidopsis* required for auxin transport and auxin-mediated development. *Plant Cell* **13**, 2441–2454 (2001).

24. Fang, S. et al. Molecular mechanism underlying transport and allosteric inhibition of bicarbonate transporter SbtA. *Proc. Natl Acad. Sci. USA* **118**, e2101633118 (2021).
25. Hunte, C. et al. Structure of a Na^+/H^+ antiporter and insights into mechanism of action and regulation by pH. *Nature* **435**, 1197–1202 (2005).
26. Lee, C. et al. A two-domain elevator mechanism for sodium/proton antiport. *Nature* **501**, 573–577 (2013).
27. Paulino, C., Wöhlert, D., Kapotova, E., Yildiz, Ö. & Kühlbrandt, W. Structure and transport mechanism of the sodium/proton antiporter MjNhaP1. *eLife* **3**, e03583 (2014).
28. Wöhlert, D., Kühlbrandt, W. & Yildiz, O. Structure and substrate ion binding in the sodium/proton antiporter PaNhaP. *eLife* **3**, e03579 (2014).
29. Liu, X.-Y. et al. Structures of cyanobacterial bicarbonate transporter SbtA and its complex with PII-like SbtB. *Cell Discov.* **7**, 63 (2021).
30. Buch-Pedersen, M. J., Pedersen, B. P., Veierskov, B., Nissen, P. & Palmgren, M. G. Protons and how they are transported by proton pumps. *Pflugers Arch.* **457**, 573–579 (2009).
31. Abas, L. et al. Naphthylphthalamic acid associates with and inhibits PIN auxin transporters. *Proc. Natl Acad. Sci. USA* **118**, e2020857118 (2021).
32. Teale, W. D. et al. Flavonol-mediated stabilization of PIN efflux complexes regulates polar auxin transport. *EMBO J.* **40**, e104416 (2021).
33. Pařízková, B., Pernisová, M. & Novák, O. What has been seen cannot be unseen—detecting auxin in vivo. *Int. J. Mol. Sci.* **18**, E2736 (2017).

Methods

Protein purification

A. thaliana protein sequences used in this study are publicly available at Uniprot (https://www.uniprot.org/) with the following accession codes. PIN1: Q9C6B8, PIN2: Q9LU77, PIN3: Q9S7Z8, PIN4: Q8RWZ6, PIN5: Q9FFD0, PIN6: Q9SQH6, PIN7: Q940Y5 and PIN8: Q9LFP6.

PIN genes were cloned into an *S. cerevisiae* overexpression plasmid based on p423_GAL1 and tested for expression and purification properties. The *A. thaliana PIN8* gene (Uniprot: Q9LFP6) was selected and put in frame with a tobacco etch virus (TEV) protease cleavage site and a deca-histidine affinity tag. This construct was used as the template for site-directed mutagenesis using the Quickchange commercial protocol (Agilent) for all point mutants.

Transformed *S. cerevisiae* strain *DSY-5* were grown in 5 l shaking flasks or culture vessels, grown to high cell density and collected after 22 h induction with galactose[34]. Collected cells were washed three times in water and re-suspended in buffer A (0.1 M Tris pH 7.5, 0.6 M NaCl, 1 mM ethylenediamine tetraacetic acid (EDTA), 1.2 mM phenylmethylsulphonyl fluoride). Cells were lysed by bead beating and lysate was clarified by centrifugation at 5,000*g* for 20 min. Membrane fractions were pelleted by ultracentrifugation at 200,000*g* for 2 h and re-suspended in buffer B (0.05 M Tris pH 7.5, 0.5 M NaCl, 20% glycerol) before being frozen in liquid nitrogen.

For protein purification, 3–4 g of membrane was thawed and solubilized for 45 min in a total volume of 50 ml of buffer C (0.05 M Tris pH 7.5, 0.5 M NaCl, 10% glycerol) supplemented with 1% *n*-dodecyl-*β*-d-maltoside (DDM) and 0.1% cholesterol hemisuccinate (CHS). Insoluble material was discarded by centrifugation at 17,000*g* for 30 min following by filtration using a 1.2 µm filter. 20 mM imidazole pH 7.5 was added and the sample loaded on a 1 ml nickel-nitrilotriacetic (Ni-NTA) column. A two-step wash was performed with buffer D (buffer A with 20 mM imidazole, 0.1% DDM, 0.01% CHS) and buffer E (buffer A with 70 mM imidazole, 0.05% DDM, 0.005% CHS).

For SSM electrophysiology assays, the sample was eluted with buffer F (0.05 M Tris pH 7.5, 0.15 M NaCl, 10% glycerol, 0.05% DDM, 0.005% CHS, 500 mM imidazole). The eluate was incubated with TEV protease and dialysed against buffer F supplemented with 0.5 mM EDTA and 0.5 mM tris(2-carboxyethyl)phosphine (TCEP) overnight. The sample was then filtered and re-run on a Ni-NTA column to adsorb the His-tagged proteins consisting of TEV protease, cleaved tag and uncleaved tagged protein. The flow-through fraction, containing tag-free PIN8, was concentrated on a 100 kDa cut-off centricon (Vivaspin) and polished by SEC on a Biorad650 or Superdex200 10/300 column pre-equilibrated with buffer G optimized by a thermostability assay[35] (0.05 M Tris pH 7.5, 0.15 M NaCl, 10% glycerol, 0.05% DDM, 0.005% CHS, 0.5 mM EDTA).

For cryo-EM, peptidisc sample preparation followed general protocols[36,37]. In brief, after the two-step wash, proteins were re-lipidated using buffer I (0.05 M Tris pH 7.5, 0.15 M NaCl, 10% glycerol, 0.03% DDM, 0.003% CHS, 0.06 mg ml^{-1} soybean extract polar lipids (Avanti)). Prior to starting the on-bead peptidisc reconstitution, the column was washed with buffer J (0.05 M Tris pH 7.5, 0.15 M NaCl, 10% glycerol, 0.008% DDM, 0.0008% CHS). Peptidisc reconstitution was initiated by washing the column with detergent-free buffer K (0.05 M Tris pH 7.5, 0.15 M NaCl, 10% glycerol) containing 1 mg ml^{-1} peptidisc (Genscript). An additional washing step with buffer K was performed to eliminate residual free peptidisc prior to elution using buffer K supplemented with 500 mM imidazole. After this the sample was incubated with TEV protease and dialysed against buffer K supplemented with 0.5 mM EDTA and 0.5 mM TCEP.

For the cryo-EM detergent sample, immediately after the re-lipidation step with buffer I, the DDM detergent was exchanged to lauryl maltose neopentyl glycol (LMNG) using buffer L (0.05 M Tris pH 7.5, 0.15 M NaCl, 10% glycerol, 0.006% LMNG, 0.0006% CHS) prior to protein elution using buffer L supplemented with 500 mM imidazole. The sample was then incubated with TEV protease and dialysed against buffer L supplemented with 0.5 mM EDTA and 0.5 mM TCEP. After dialysis, cryo-EM sample purification continued identically to the SURFE^{2}R sample protocol described in 'SSM electrophysiology assays', with the exception that the SEC buffer was replaced with buffer K (peptidisc sample) or buffer L (LMNG sample) without glycerol and supplemented with 0.5 mM EDTA.

SSM electrophysiology assays

For SSM electrophysiology, a SURFE^{2}R N1 from Nanion Technologies was used. In brief, Soy Phospholipid Mixture (38% phosphatidylcholine, 30% phosphatidyl ethanolamine, 18% phosphatidyl inositol, 7% phosphatidic acid and 7% other soy lipids) and 1-palmitoyl-2-oleoyl-*sn*-glycero-3-phosphocholine (POPC) were purchased from Avanti. Liposomes were prepared in Ringer solution without Ca^{2+} (115 mM NaCl, 2.5 mM KCl, 1 mM $NaHCO_3$, 10 mM HEPES pH 7.4, 1 mM $MgCl_2$) and homogenized using a Lipsofast (Avestin Inc) with a 400 nM pore size. Triton X-100 was added to the liposomes to a final concentration of 1% (v/v). Protein was added to liposomes to a calculated liposome:protein ratio (LPR) of 10:1. The detergent was removed using 400 mg ml^{-1} Bio Beads (BioRad) overnight at 4 °C in a rotary shaker. Proteoliposomes were frozen in liquid nitrogen and kept at −80 °C until use.

Sensor coating was performed as described[38]. Proteoliposomes were diluted 1:5 in Ringer solution without Ca^{2+}, sonicated five times and then applied to the sensors by centrifugation (30 min, 3,000*g*, 4 °C). Non-activating buffer was Ringer solution without Ca^{2+} as described unless specified otherwise and activating buffer contained the substrate of interest. To substitute Na^+, K^+-Ringer without $CaCl_2$ (117.5 mM KCl, 10 mM HEPES pH 7.4, 1 mM $MgCl_2$) and to substitute K^+, Na^+-Ringer without $CaCl_2$ (117.5 mM NaCl, 10 mM HEPES pH 7.4, 1 mM $MgCl_2$) were used. Uncouplers: carbonyl cyanide *m*-chlorophenyl hydrazone (CCCP) in ethanol was used at 5 µM and 2,4-dinitrophenol (DNP) in ethanol was used at 100 µM. All other chemicals were purchased from Roth or Sigma. Each experiment was performed on at least two individual sensors. On each sensor each measurement consists of three technical replicates where the mean is calculated.

In most instances, we used a single solution exchange experiment. In this case proteoliposomes, immobilized on the supported membrane are kept in non-activating buffer as specified. At the beginning of the experiment non-activating buffer was exchanged for fresh identical non-activating buffer and after 1 s activating buffer (same buffer containing substrate) was added. After a further 1 s, buffer was again exchanged to non-activating buffer. Current response was recorded throughout the entire 3 s. For competition or inhibition, the respective compound was present in non-activating and activating solution.

Currents in response to substrate in the activating solutions are responses to electrogenic events which occur (1) when a charged molecule is crossing the membrane; (2) when a substrate, which does not necessarily have to be charged, binds to the protein and this binding leads to a conformational change by which charges become displaced in the membrane; (3) currents are shielded or neutralized by the substrate; and (iv) any combination of these possibilities. The peak current in response to substrate application was used to describe the properties of the proteins.

To describe the current response to different substrate concentrations a Michaelis–Menten curve was fit. We use K_m throughout the manuscript, but since the peak current is a mixture of binding and transport signal (that is, pre-steady state and steady state currents), this parameter can also be more appropriately described as EC_{50}. A K_m derived from a biophysical assay will be specific to that experimental setup, and comparison to other types of assay or a physiological condition should be done cautiously. In the case of competitive studies, we explicitly use K_i or K_i, since in these instances the parameters were specifically determined. GraphPad Prism V 9.3 was used for statistical analyses.

Cryo-EM sample preparation

Peak fractions of freshly purified PIN8 were concentrated to 4–10 mg ml^{-1}. C-flat Holey Carbon grids (CF-1.2/1.3, Cu-300 mesh) were glow-discharged for 45 s at 15 mA in a GloQube Plus (Quorum). A drop of 4 µl of sample was applied to the non-carbon side of the grids, and blotted with a Vitrobot Mark IV (ThermoFisher Scientific) operating at 4 °C and 100% humidity and using blot time of 4 s, before plunge-freezing into liquid ethane. The substrate-bound states were obtained by incubating the sample with 15 mM of IAA sodium salt or 2 mM of NPA for 2 h prior to grid freezing.

Image collection and data processing

A Titan Krios G3i microscope (ThermoFisher Scientific) operating at 300 kV and equipped with a BioQuantum Imaging Filter (energy slit width of 20 eV) with a K3 detector (Gatan) was used to collect the movies. The datasets containing the peptidisc samples, were acquired using automated acquisition EPU v2.11.1.11 at nominal 130,000 magnification corresponding to a physical pixel size 0.647 Å. For all datasets, the movies were saved in super-resolution pixel size and binned 2× in EPU back to the nominal pixel size.

On-the-fly gain normalized exposures were imported into cryoSPARC (v3.2.0)[39] and processed in streaming mode for patch motion correction, patch contrast transfer function (CTF) estimation, particle picking and extraction. After several rounds of particle cleaning, an initial preliminary volume map was used to create templates for template picking. From a full dataset of apo-PIN8 with 7,900 movies, template picking provided a total of 2,082,448 particles. After two rounds of 2D classification, the best representative classes were selected manually. These particles served as an input for ab initio model reconstruction. After three rounds of particles sorting by heterogenous refinement using the ab initio 3D template, the remaining 327,193 particles were used for non-uniform refinement with C2 symmetry imposed and resulted in a global 2.9 Å resolution map. In parallel a C1 symmetry refinement job was performed but showed no differences between the two monomers.

To ensure the method of membrane protein stabilization did not influence oligomeric state and overall structure we solved apo PIN8 both in peptidisc (2.9 Å) and in the detergent LMNG (3.3 Å). The respective maps reveal no variation in conformation and we focus on the peptidisc-derived map given its higher resolution. There was also no evidence of monomers or higher oligomeric states in any of the grids screened.

The processing pipeline for the ligand-bound PIN8 was identical to the one from apo-PIN8. In brief, the entire IAA–PIN8 dataset comprised of 15,771 movies and template picking yielded a total of 2,639,895 particles. After several rounds of 2D classification and heterogenous refinement to obtain a final 200,061 particles, a non-uniform refinement with C2 symmetry imposition resulted in a global 3.2 Å resolution map. A full dataset of NPA–PIN8 comprised of 14,500 movies and template picking yielded a total of 3,345,146 particles. After several rounds of 2D classification and heterogenous refinement to obtain a final 77,608 particles, a non-uniform refinement with C2 symmetry imposition resulted in a global 3.4 Å resolution map. As for the apo form, a parallel C1 refinement was performed with no differences evident between the two monomers. Local resolution estimation was performed using cryoSPARC.

Model building and refinement

A PIN8 model prediction was calculated using the RoseTTAFold server[40] and docked into the PIN8 map in Chimera[41]. Two molecules of PIN8 could be readily fitted into the map. The flexible cytoplasmic loop of PIN8 (residues 165 to 205) is not visible in the maps and was excluded from model building in Coot[42]. The final models include residues 1–164 and 206–367 (of 367 residues total). The initial PIN8 dimer model was analysed by molecular dynamics-based geometry fitting to the map using MDFF[43] through Namdinator v2.0 (ref. [44]). Models could be further improved by iterative manual model building in Coot combined with real-space refinement using Phenix, initially with an Amber force-field molecular dynamic refinement[45]. The coordination of lipids and the ligand IAA was prepared using ligand builder eLBOW[46]. In all electron microscopy maps, although the lipid belt surrounding the PIN8 dimer is visible, the electron density only allowed for the tentative modelling of two phosphatidylcholine molecules for ligand-bound PIN8 and four molecules for apo-PIN8. Geometry was validated in MolProbity v4.2 including CaBLAM and Ramachandran-Z analysis[47–49] (Rama-Z). Figures were prepared using PyMOL Molecular Graphics System v1.5.0.4 (Schrödinger). Conservation of residues across species was analysed using ConSurf[50]. Sequence alignments were constructed with PROMALS3D[51]. Alignments were visualized using ALINE v1.0.025[52]. Structural similarity to other protein families were identified using DALI[53]. Phylogenetic analysis was made using NGPhylogeny.fr[54]. In brief, MAFFT was used for multiple sequence alignment (MSA), BMGE was used for MSA pruning and FastME was used for unrooted tree generation. Bootstrap values were calculated from 500 trials.

Oocyte efflux assays

Oocyte efflux experiments were carried out as described[55]. In brief, oocytes were injected with 150 ng transporter cRNA without or with 75 ng kinase cRNA. ^{3}H-IAA (25 Ci mmol^{-1}) was purchased from ARC or RC Tritec. Oocytes were injected with IAA to reach an internal IAA concentration of 1 µM, corresponding to 100%. Residual radioactivity was determined for each individual oocyte by liquid scintillation counting after the time points indicated and are expressed relative to the initial 100%. Each time point represents the mean and s.e.m. of ten oocytes. To calculate the relative transport rate in per cent per minute, linear regression was performed. Each data point in Fig. 1a and Extended Data Fig. 9c represents the transport rate of one biological replicate using oocytes collected from different *X. laevis* females. GraphPad Prism V 9.3 was used for statistical analyses.

Reporting summary

Further information on research design is available in the Nature Research Reporting Summary linked to this paper.

Data availability

Atomic models have been deposited in the Protein Data Bank (PDB) and cryo-EM maps have been deposited in the Electron Microscopy Data Bank (EMDB) under the following accession numbers. Apo outward state in peptidisc: PDB 7QP9 and EMDB EMD-14115, IAA-bound outward state in peptidisc: PDB 7QPA and EMDB EMD-14116, NPA-bound inward state in peptidisc: PDB 7QPC and EMDB EMD-14117, and apo outward state in detergent: EMDB EMD-14118. Source data are provided with this paper.

34. Lyons, J. A., Shahsavar, A., Paulsen, P. A., Pedersen, B. P. & Nissen, P. Expression strategies for structural studies of eukaryotic membrane proteins. *Curr. Opin. Struct. Biol.* **38**, 137–144 (2016).
35. Tomasiak, T. M. et al. General qPCR and plate reader methods for rapid optimization of membrane protein purification and crystallization using thermostability assays. *Curr. Protoc. Protein Sci.* **77**, 29.11.1–29.11.14 (2014).
36. Carlson, M. L. et al. The Peptidisc, a simple method for stabilizing membrane proteins in detergent-free solution. *eLife* **7**, e34085 (2018).
37. Ung, K. L., Alsarraf, H., Kremer, L. & Blaise, M. MmpL3, the trehalose monomycolate transporter, is stable in solution in several detergents and can be reconstituted into peptidiscs. *Protein Express. Purif.* **191**, 106014 (2022).
38. Bazzone, A. & Barthmes, M. Functional characterization of SLC transporters using solid supported membranes. *Methods Mol. Biol.* **2168**, 73–103 (2020).
39. Punjani, A., Rubinstein, J. L., Fleet, D. J. & Brubaker, M. A. cryoSPARC: algorithms for rapid unsupervised cryo-EM structure determination. *Nat. Methods* **14**, 290–296 (2017).
40. Baek, M. et al. Accurate prediction of protein structures and interactions using a three-track neural network. *Science* **373**, 871–876 (2021).
41. Pettersen, E. F. et al. UCSF Chimera—a visualization system for exploratory research and analysis. *J. Comput. Chem.* **25**, 1605–1612 (2004).
42. Emsley, P., Lohkamp, B., Scott, W. G. & Cowtan, K. Features and development of Coot. *Acta Crystallogr. D* **66**, 486–501 (2010).

43. Trabuco, L. G., Villa, E., Mitra, K., Frank, J. & Schulten, K. Flexible fitting of atomic structures into electron microscopy maps using molecular dynamics. *Structure* **16**, 673–683 (2008).
44. Kidmose, R. T. et al. Namdinator—automatic molecular dynamics flexible fitting of structural models into cryo-EM and crystallography experimental maps. *IUCrJ* **6**, 526–531 (2019).
45. Adams, P. D. et al. PHENIX: a comprehensive Python-based system for macromolecular structure solution. *Acta Crystallogr. D* **66**, 213–221 (2010).
46. Moriarty, N. W., Grosse-Kunstleve, R. W. & Adams, P. D. electronic Ligand Builder and Optimization Workbench (eLBOW): a tool for ligand coordinate and restraint generation. *Acta Crystallogr. D* **65**, 1074–1080 (2009).
47. Chen, V. B. et al. MolProbity: all-atom structure validation for macromolecular crystallography. *Acta Crystallogr. D* **66**, 12–21 (2010).
48. Prisant, M. G., Williams, C. J., Chen, V. B., Richardson, J. S. & Richardson, D. C. New tools in MolProbity validation: CaBLAM for CryoEM backbone, UnDowser to rethink 'waters,' and NGL Viewer to recapture online 3D graphics. *Protein Sci.* **29**, 315–329 (2020).
49. Sobolev, O. V. et al. A global Ramachandran score identifies protein structures with unlikely stereochemistry. *Structure* **28**, 1249–1258.e2 (2020).
50. Ashkenazy, H. et al. ConSurf 2016: an improved methodology to estimate and visualize evolutionary conservation in macromolecules. *Nucleic Acids Res.* **44**, W344–W350 (2016).
51. Pei, J., Kim, B.-H. & Grishin, N. V. PROMALS3D: a tool for multiple protein sequence and structure alignments. *Nucleic Acids Res.* **36**, 2295–2300 (2008).
52. Bond, C. S. & Schüttelkopf, A. W. ALINE: a WYSIWYG protein-sequence alignment editor for publication-quality alignments. *Acta Crystallogr. D* **65**, 510–512 (2009).
53. Holm, L. DALI and the persistence of protein shape. *Protein Sci.* **29**, 128–140 (2020).
54. Lemoine, F. et al. NGPhylogeny.fr: new generation phylogenetic services for non-specialists. *Nucleic Acids Res.* **47**, W260–W265 (2019).
55. Fastner, A., Absmanner, B. & Hammes, U. Z. Use of *Xenopus laevis* oocytes to study auxin transport. *Methods Mol. Biol.* **1497**, 259–270 (2017).

Acknowledgements We acknowledge the EMBION Cryo-EM Facility at iNANO, Aarhus University, for time under application ID 0137, where all data was collected with the assistance of A. Beggild, J. Lykkegaard Karlsen and T. Boesen. We also thank eBIC (proposal BI27980) for data collection on the detergent PN8 sample. This project has received funding from the European Research Council (ERC) under the European Union's Horizon 2020 research and innovation programme (grant agreement no. 101000936) to B.P.P. U.Z.H. is funded by the Deutsche Forschungsgemeinschaft (HA3468/6-1 and HA3468/6-3) and SFB924. D.L.S. is funded by the National Institutes of Health (R35 GM144109).

Author contributions Sample preparation: K.L.U. and M.W. Electron microscopy data collection and analysis: K.L.U., M.W., E.D., D.L.S. and B.P.P. Activity assays: D.P.J., L.S., M.K. and U.Z.H. Manuscript preparation: K.L.U., M.W., D.L.S., UZ. H. and B.P.P.

Competing interests The authors declare no competing interests.

Additional information

Supplementary information The online version contains supplementary material available at https://doi.org/10.1038/s41586-022-04883-y.

Correspondence and requests for materials should be addressed to Ulrich Z. Hammes or Bjørn Panyella Pedersen.

Peer review information *Nature* thanks Dolf Weijers and the other, anonymous, reviewer(s) for their contribution to the peer review of this work. Peer review reports are available.

New Phytologist

Research

A novel chemical inhibitor of polar auxin transport promotes shoot regeneration by local enhancement of HD-ZIP III transcription

Saiqi Yang[1], Marjolein de Haan[1], Julius Mayer[1], Dorina P. Janacek[2], Ulrich Z. Hammes[2], Brigitte Poppenberger[3] and Tobias Sieberer[1]

[1]Research Unit Plant Growth Regulation, TUM School of Life Sciences, Technical University of Munich, 85354 Freising, Germany; [2]Plant Systems Biology, TUM School of Life Sciences, Technical University of Munich, 85354 Freising, Germany; [3]Biotechnology of Horticultural Crops, TUM School of Life Sciences, Technical University of Munich, 85354 Freising, Germany

Author for correspondence:
Tobias Sieberer
Email: tobias.sieberer@tum.de

Received: *18 November 2021*
Accepted: *21 April 2022*

New Phytologist (2022)
doi: 10.1111/nph.18196

Key words: auxin, chemical genetics, cytokinin, HD-ZIP III, *Helianthus annuus*, pluripotency, polar auxin transport, shoot regeneration.

Summary

- *De novo* shoot organogenesis is a prerequisite for numerous applications in plant research and breeding but is often a limiting factor, for example, in genome editing approaches. Class III homeodomain-leucine zipper (HD-ZIP III) transcription factors have been characterized as crucial regulators of shoot specification, however up-stream components controlling their activity during shoot regeneration are only partially identified.
- In a chemical genetic screen, we isolated ZIC2, a novel activator of HD-ZIP III activity. Using molecular, physiological and hormone transport analyses in *Arabidopsis* and sunflower (*Helianthus annuus*), we examined the molecular mechanism by which the drug promotes HD-ZIP III expression.
- ZIC2-dependent upregulation of HD-ZIP III transcription promotes shoot regeneration in *Arabidopsis* and is accompanied by the induction of shoot specifying factors WUS and RAP2.6L and a subset of cytokinin biosynthesis enzymes. ZIC2's effect on HD-ZIP III expression and regeneration is based on its ability to limit polar auxin transport. We further provide evidence that chemical modulation of auxin efflux can enhance *de novo* shoot formation in the regeneration recalcitrant species sunflower.
- Activation of HD-ZIP III transcription during shoot regeneration depends on the local distribution of auxin and chemical modulation of auxin transport can be used to overcome poor shoot organogenesis in tissue culture.

Introduction

Plants show a remarkable ability to regenerate in response to loss or damage of body parts. When organ forming apical meristems are lost, they can be reestablished in a process called *de novo* organogenesis (Ikeuchi *et al.*, 2019). *De novo* organogenesis is critical for plants as sessile organisms to survive adverse environmental conditions. Moreover, this process is exploited for the breeding and clonal propagation of crops and also represents a crucial prerequisite for plant biotechnological approaches such as genome editing. However, the limited or variable regeneration competence of plant tissues *in vitro* is still a main bottleneck in the application of these methodologies (Altpeter *et al.*, 2016).

De novo organogenesis is a hormone-controlled process and consists of different phases. A well-established standard system employs a two-step protocol in which first a pluripotent cell mass, called callus, is formed (Ikeuchi *et al.*, 2013). The callus induction medium (CIM) is rich in the plant hormone auxin and triggers the proliferation of cells with an identity reminiscent of lateral root primordia. Subsequent transfer on cytokinin-rich shoot induction medium (SIM) results in the conversion of callus cells into functional shoot meristems. This is mediated by a complex patterning process, where areas of different hormone responses are established and a functional stem cell niche is formed. In recent years the temporal and spatial sequences have been described and several factors involved in this self-organizing process have been identified (Radhakrishnan *et al.*, 2018; Ikeuchi *et al.*, 2019), however a full mechanistic understanding is currently lacking and the cause for the strong genotypic variation in the regenerative responsiveness is not resolved.

A key regulatory step in *Arabidopsis* shoot regeneration is the local induction of the homeodomain transcription factor WUSCHEL (WUS), whose expression domain defines the organizing center (OC) of the shoot stem cell niche (Mayer *et al.*, 1998; Sugimoto *et al.*, 2019). Cytokinin in the SIM activates B-type ARABIDOPSIS RESPONSE REGULATORS (ARRs), who induce WUS expression by direct binding to its promoter (Meng *et al.*, 2017; T. Q. Zhang *et al.*, 2017). The locally

restricted expression of WUS is mediated by the class III homeodomain-leucine zipper (HD-ZIP III) family of transcription factors, which physically interact with B-type ARRs at the WUS promoter (T. Q. Zhang *et al.*, 2017). Next to WUS, HD-ZIP III proteins also affect the expression of other shoot identity-conferring transcription factors including SHOOT MERISTEMLESS and RAP2.6L (Shi *et al.*, 2016; Yang *et al.*, 2018). Thus, spatially restricted activation of HD-ZIP III activity is an important prerequisite of shoot regeneration, but the molecular basis of this activation is not fully understood.

Class III homeodomain-leucine zipper proteins are not only crucial for *de novo* shoot regeneration but also represent key determinants of shoot identity during embryogenesis (Prigge *et al.*, 2005; Grigg *et al.*, 2009; Smith & Long, 2010). The expression domains of HD-ZIP III family members are confined to the apical central domain of the developing embryo by the activity of the mir165/166 family of micro-RNAs (miRNAs) (Smith & Long, 2010; Miyashima *et al.*, 2013). This spatial expression pattern is further enforced by the function of AGO10, which dampens the effect of miRNA165/166 in the area of the future shoot meristem (Liu *et al.*, 2009; Zhu *et al.*, 2011). An additional level of regulation is executed by the LITTLE ZIPPER (ZPR) family of microProteins who represent direct transcriptional targets of HD-ZIP III proteins and in turn repress their activity by physical interaction (Wenkel *et al.*, 2007; Kim *et al.*, 2008).

Notably, HD-ZIP III proteins also possess two distinct putative small molecule ligand domains, implicating the presence of further yet unknown modes of regulation (Magnani & Barton, 2011). The steroidogenic acute regulatory protein-related lipid transfer (START) domain was first characterized in animal proteins where they bind diverse hydroponic compounds (Schrick *et al.*, 2014). The C-terminal MEKHLA domain belongs to the superfamily of Per-ARNT-Sim-like (PAS-like) domains (Mukherjee & Burglin, 2006). Per-ARNT-Sim domains can act as sensors of diverse stimuli and regulate the activity of effector domains present in the same protein (Moglich *et al.*, 2009). The HD-ZIP III-specific ligands for these domains are not known to date but it was speculated that the binding status modulates their transcriptional activity as well as their dimerization behavior (Magnani & Barton, 2011; Schrick *et al.*, 2014).

In an attempt to identify novel mechanisms of HD-ZIP III regulation, we performed a reporter based small molecule screen for compounds, which increase the activity of HD-ZIP III *in planta*. We identified a novel plant growth regulator that promotes HD-ZIP III function by stimulating their transcriptional expression. Application of the compound during tissue culture enhances the shoot regeneration response of *Arabidopsis* in an HD-ZIP III-dependent manner. We further provide evidence that the regenerative function of the compound is based on its ability to limit polar auxin transport. Finally, we show that chemical modulation of auxin transport can significantly enhance shoot regeneration in sunflower (*Helianthus annuus* L.), an important oil crop, in which genetic transformation and genome editing is currently difficult to achieve due to its poor shoot formation capacity in tissue culture (Zhang & Finer, 2015).

Materials and Methods

Plant materials and growth conditions

Unless stated otherwise, *Arabidopsis thaliana* (L.) Heynh. seeds were plated and plants grown as described in the literature (Yang *et al.*, 2018). Previously published plant lines used in this study: *phb-1d* (McConnell *et al.*, 2001), *rev-10d*, *rev-6 phb-13 phv-11* (Prigge *et al.*, 2005), *pZPR::ZPR3::β-glucuronidase* (*GUS*) and *35S::ZPR3* (Wenkel *et al.*, 2007), *pWUS::GUS* (Gross-Hardt *et al.*, 2002), *pRAP2.6L::RAP2.6L:GUS* (Yang *et al.*, 2018), *pPHB>>GFP*, *pMIR165A::GFP* and *pMIR166A::GFP* (Carlsbecker *et al.*, 2010), *gPHB::GUS* (Gillmor *et al.*, 2010), *pIPT1::GUS* and *pIPT5::GUS* (Miyawaki *et al.*, 2004), *pIPT7::GFP* (Takei *et al.*, 2004), *pARR5::GUS* (D'Agostino *et al.*, 2000), *TCS::GFP* (Muller & Sheen, 2008), *DR5::GUS* (Ulmasov *et al.*, 1997), *DR5rev::GFP* and *pPIN1::GUS* (Friml *et al.*, 2003), *pPIN1::PIN1:GFP* (Benkova *et al.*, 2003).

Chemical screen

Compounds of a custom assembled chemical library (www.chembridge.com) were tested in half-strength Murashige & Skoog (MS) liquid medium under the growth conditions described earlier at a final concentration of 25 μM. The *pZPR3::GUS* seeds were germinated in the presence of the compounds until day 10. Seedlings were subjected to GUS staining and analyzed with a stereomicroscope (SZX10; Olympus, Tokyo, Japan). ZIC2 (Chembridge ID: 5131153) and the described structural analogs were re-ordered from MolPort (www.molport.com) with the following ID numbers: ZIC2 (000-246-311), T1 (000-759-143), T2 (002-287-475), T3 (000-251-109), T4 (001-534-280), T5 (002-251-423), T6 (009-332-327), T7 (000-205-112), L1 (009-030-711), L2 (000-650-194), P1 (000-246-278), P2 (009-146-001), P3 (001-679-944), P4 (009-509-050,), P5 (000-780-505).

Gene constructs

Polymerase chain reaction (PCR) was performed with proofreading thermostable polymerase (Thermo Fisher Scientific, Waltham, MA, USA), and all clones were confirmed by sequencing. For generation of *pZPR3::GUS*, the 3132 bp promoter region of *ZPR3* gene (AT3G52770) was amplified with primers pZPR3F(PstI) and pZPR3R-2(BamHI) and subcloned into pGEM-T Easy (Promega, Madison, WI, USA). The fragment was excised using PstI and BamHI and ligated into pPZP-GUS-1 (Diener *et al.*, 2000). At least 10 independent *pZPR3::GUS* transgenic lines were generated, which showed the same tissue-specific expression pattern. For generation of *pZPR3::LUC* the 3132 bp upstream promoter region of *ZPR3* gene (AT3G52770) was amplified with primers pZPR3F(PstI) and pZPR3R-2(NcoI) and inserted as PstI/NcoI fragments into corresponding cloning sites of the transient expression vector pGreenII 0800-LUC (Hellens *et al.*, 2000). To create effector vectors 35S::PHB-YFP and 35S::REV-YFP, the open reading frame (ORF) of PHABULOSA (AT2G34710) and REVOLUTA (AT5G60690) were amplified

by PCR using PHB ORF F (EcoRV)-PHB ORF R (NotI) and REV ORF F (EcoRV) and REV ORF R (NotI), respectively. The fragments were subcloned into pGEM-T Easy. Subsequently, the PHB ORF and REV ORF were transferred via EcoRV and NotI into pGWR8-YFP (Rozhon *et al.*, 2010), and NotI excised the yellow fluorescent protein (YFP) sequence of pGWR8-YFP out. YFP (from pGWR8-YFP) was subcloned into NotI site of pGWR8-PHB and pGWR8-REV.

GUS staining

GUS staining was performed as previously described (Yang *et al.*, 2018). The seedlings were stained at 37°C for various periods of time depending on the reporter strength. After staining the tissue was dehydrated with 70% ethanol. Samples were analyzed using a stereomicroscope (SZX10; Olympus).

Fluorometric MUG assay

The *pZPR3::GUS* seedlings were grown on half-strength MS medium (½MS) under the growth conditions described earlier containing 25 µM of ZIC2 or the described structural analogs. The roots were harvested and flash-frozen in liquid nitrogen. The MUG assay was performed as previously described (He *et al.*, 2018).

Fluorescence microscopy

Images of *pPHB>> GFP, TCS::GFP, pIPT7::GFP, pPIN1::PIN1:GFP* and *DR5rev::GFP* tissues were generated using a TCS SP8 (Leica Microsystems, Wetzlar, Germany) or a FV1000 (Olympus) confocal laser-scanning microscope. Green fluorescent protein (GFP) was excited at 488 nm and emission was analyzed between 500–535 nm.

Protoplast transactivation assay

Protoplasts were isolated and transformed as described in Yoo *et al.* (2007). Thus, 14 h after transformation, protoplasts were harvested by centrifuging at 100 ***g*** for 2 min at room temperature and flash-frozen in liquid nitrogen. Luciferase assays were performed using a Dual-Luciferase Reporter Assay System (Promega) with a Lumat LB9501 luminometer (Berthold, Bad Wildbach, Germany) for signal quantification.

Lugol staining

Roots of 7-d-old seedlings were stained with Lugol's solution (Sigma-Aldrich) for 3 min, then transferred to clearing solution (chloral hydrate : water : glycerol, 8 : 3 : 1, v/v) and imaged immediately with a stereomicroscope (SZX10; Olympus).

Auxin transport assay

Auxin transport measurement was performed based on a previous protocol with minor modifications (Xiao & Offringa, 2020). Four 2.5-cm segments from the basal part of 15-cm long wild-type (WT) Col-0 inflorescence stems were placed in inverted orientation in 30 µl of auxin transport buffer (0.5 nM indole-3-acetic acid (IAA), 1% sucrose, 5 mM MES, pH 5.5) with either solvent control, 50 µM naphtylphtalamic acid (NPA) or 50 µM ZIC2 for 1 h, then transferred to 30 µl of auxin transport buffer with either solvent control, 50 µM NPA or 50 µM ZIC2 containing 2 µM [^{14}C] IAA (Biotrend, Köln, Germany), allowed to incubate for 1 h and subsequently transferred to 30 µl of auxin transport buffer without [^{14}C] IAA and incubated for another 4 h. Segments were cut into 5-mm pieces, the bottom piece (0–5 mm) was discarded and the remaining pieces were placed separately into 2 ml of Ultima-Flo AF (no. 6013589; PerkinElmer, Waltham, MA, USA) for overnight maceration. [^{14}C] IAA was quantified using a Tri-Carb 2800TR liquid scintillation analyzer (PerkinElmer).

PIN transport assay

The transport assays for PIN1 and PIN3 in oocytes were performed as previously described (Fastner *et al.*, 2017). ZIC2 (10 µM final internal concentration) was coinjected with ^{3}H-IAA (RC Tritec, Teufen, Switzerland).

Arabidopsis shoot regeneration assay

The assay was performed based on a previous protocol with minor modifications (Che *et al.*, 2006). *Arabidopsis* seeds were germinated and grown for 8 d on ½MS under long day conditions. Root segments of 1.5–2 cm were cut, transferred to CIM (full strength MS medium including B5 vitamins (Duchefa, Haarlem, the Netherlands) supplemented with 0.5 g l^{-1} MES (pH set to 5.7), 2% sucrose, 2.2 µM 2,4-dichlorophenoxyacetic acid, 0.2 µM kinetin and 0.8% agar) and incubated under constant light (80 µmol s^{-1} m^{-2}, 21°C) for 4 d. The root explants were then transferred to shoot induction medium (full strength MS medium including B5 vitamins (Duchefa) supplemented with 0.5 g l^{-1} MES (pH set to 5.7), 2% sucrose, 2.5 µM isopentenyladenine, 0.45 µM IAA and 0.8% agar) and incubated under constant light (80 µmol s^{-1} m^{-2}, 21°C) for 16 d.

Sunflower shoot regeneration assay

The sunflower regeneration protocol was modified based on previous protocols (Sujatha *et al.*, 2012; Radonic *et al.*, 2015). Seeds from the *Helianthus annuus* L. inbred line HA89 were rinsed with 70% ethanol, soaked in 5% sodium hypochlorite (NaOCl) containing 0.05% Tween 20 for 15 min with mild shaking, followed by three washes with sterile double-distilled water (ddH_2O). The seeds were de-coated after 30 min soaking in sterile ddH_2O, re-sterilized and germinated overnight on ½MS in the dark at 26°C. Then the seed radicles were cut off and the internal thin membrane was removed. The rest of the seed was separated longitudinally along the embryo axis, and the leaf primordia at the base of the cotyledons were removed. The cotyledons were placed on coculture medium (MS medium with B5 vitamins (Duchefa; pH set to 5.8) with 3% sucrose and 3 g l^{-1} phytagel, supplemented with 2.0 mg l^{-1} isopentenyladenine, 0.5 mg l^{-1} IAA and 0.1 mg l^{-1} thidiazuron) with the adaxial side in contact with the medium. The cotyledon explants were cultured at 30 µmol m^{-2} s^{-1} light intensity, at 24°C (±2°C) under long day conditions (16 h : 8 h) for 10 d, then subcultured on coculture medium for another 11 d. The shoot apical meristem (SAM) cluster area was measured with ImageJ software. For shoot elongation, explants were transferred to coculture medium supplemented with 0.1 mg l^{-1} gibberellic acid (GA_3) for 2 wk.

Quantitative real-time PCR

Approximately 50 mg of *Arabidopsis* seedling material or 200 mg of sunflower cotyledon explants were collected, shock-frozen in liquid nitrogen and homogenized with a Retsch mill (Verder Scientific, Haan, Germany). RNA extraction, complementary DNA (cDNA) synthesis and quantitative polymerase chain reaction (qPCR) were done as described in Yang *et al.* (2018). Sequences of oligos used for qPCR can be found in Supporting Information Table S1. Data were normalized to At*UBC* (*AT5G25760*) or *HaACT7* (*LOC110909803*) and measured in at least three technical replicates.

Scanning electron microscopy

Sunflower seed explants were incubated in FAA fixative (50% ethanol, 10% acetic acid, 5% formaldehyde) overnight at 4°C, dehydrated through a graded ethanol series and subsequently subjected to supercritical point drying using an EM CPD300 (Leica, Wetzlar, Germany). Explants were mounted on conductive adhesive tabs (Plano, Wetzlar, Germany). Pictures were taken with a T-3000 scanning electron microscope (Hitachi, Tokyo, Japan).

Histology

The histological analysis was performed as previously described (De Smet *et al.*, 2004). Tissues were fixed overnight at 4°C in FAA (5% (v/v) formaldehyde, 5% (v/v) acetic acid, and 50% (v/v) ethanol). Samples were then dehydrated in a graded ethanol series and embedded with Technovit 7100 (Heraus Kulzer, Hanau, Germany) according to the manufacturer's instructions. A series of 5–7 µm thick transverse sections was made with a Leica RM2255 Microtome. Sections were transferred to microscopic slides (Marienfeld, Lauda-Königshofen, Germany), stained in Ruthenium red solution (0.05%) for 50 s and rinsed with water. Stained sections were analyzed with a microscope (BX-61; Olympus).

Statistics

All statistical parameters of the performed experiments are shown in the figures or figure legends, including number of samples (*n*), type of statistical tests and methods used. Statistical significance is denoted by lower case letters, stars or the shown *P*-values. Statistical analysis was performed with Prism8 software (GraphPad, San Diego, CA, USA).

Results

Identification of ZIC2 in a screen for compounds that activate the expression of the HD-ZIP III direct target gene ZPR3

There is circumstantial evidence that HD-ZIP III activity is regulated by unknown signaling molecules, through interaction with the putative ligand binding domains found in these proteins (Magnani & Barton, 2011; Schrick *et al.*, 2014). We reasoned that a small molecule screen for activators of HD-ZIP III function might not only provide information about the structural requirements to interact with these domains but also might lead to the identification of novel chemical tools, to improve shoot regeneration in recalcitrant crop plants.

To this end we screened a library of 9000 structurally diverse chemicals for compounds, which induce the activity of a transcriptional GUS reporter for the HD-ZIP III direct target gene *ZPR3* (Fig. 1a). Application of 3-chloro-*N*-(1,5-dimethyl-3-oxo-2-phenyl-2,3-dihydro-1H-pyrazol-4-yl)-1-benzothiophene-2-carboxamide (CAS-RN: 301157-28-8) at a concentration of 25 µM (Fig. 1b), drastically increased pZPR3::GUS activity in seedling roots (Fig. 1c) and we therefore named the substance ZPR3 Inducing Compound 2 (ZIC2). ZIC2 also enhanced the expression of the translational reporter pZPR3::ZPR3:GUS, in the root and the shoot meristem region (Fig. 1d) and significantly increased endogenous *ZPR3* transcript levels in WT seedlings treated for 24 h with the chemical (Fig. 1e).

Next, we assessed the concentration range in which ZIC2 affects ZPR3 expression (Fig. S1a). Root meristem specific activity of pZPR3::GUS was visibly increased at a concentration of 1 µM ZIC2 and gradually became more intense at higher concentrations. We also analyzed the kinetics of ZIC2-mediated pZPR3::GUS induction in liquid medium (Fig. S1b). A slight increase of ZPR3 expression in the central root meristem was already visible after 1 h of ZIC2 exposure and after 3–6 h the pZPR3::GUS activity was clearly elevated in the central root meristem and the root differentiation zone. In the shoot tissues the ZPR3 reporter activity was upregulated after 24 h under these conditions (Fig. S1b).

To specify the cell types affected by ZIC2-mediated ZPR3 induction we analyzed reporter activity in transversal sections of root meristems. In untreated controls pZPR3::GUS activity was faintly detectable in the xylem and the adjacent procambial cells (Fig. 1f) substantially overlapping with the expression domains of HD-ZIP III transcription factors (Carlsbecker *et al.*, 2010). The reporter activity strongly increased in these tissues after 24 h of ZIC2 treatment and even expanded to the phloem and pericycle cells (Fig. 1f). Long-term ZIC2 treatment provoked a strong proliferation of stele cells in the distal root meristem, which showed intense reporter expression (Fig. 1g). Taken together, ZIC2 rapidly induces ZPR3 transcription in a dose-dependent manner in tissues of HD-ZIP III expression.

New Phytologist (2022)
www.newphytologist.com

© 2022 The Authors
New Phytologist © 2022 New Phytologist Foundation

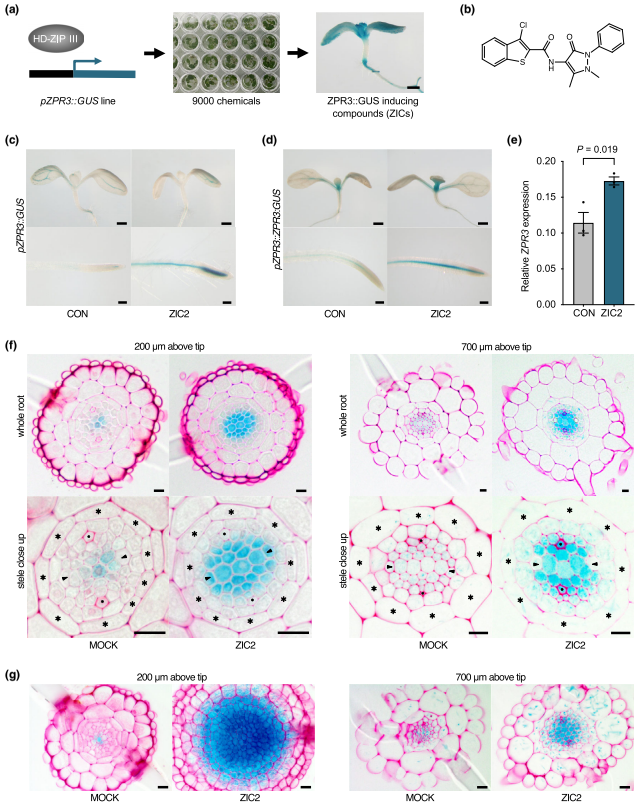

Fig. 1 Identification of ZIC2 in a screen for compounds inducing expression of the class III homeodomain-leucine zipper direct target gene ZPR3 in *Arabidopsis*. (a) Schematic representation of the screening procedure. pZPR3::GUS seedlings were germinated in liquid medium containing 9000 structurally diverse compounds at a concentration of 25 µM and subsequently ZPR3::GUS activity was subsequently determined 7 d after germination (DAG). (b) Molecule structure of ZIC2 (3-chloro-*N*-(1,5-dimethyl-3-oxo-2-phenyl-2,3-dihydro-1H-pyrazol-4-yl)-1-benzothiophene-2-carboxamide). (c) pZPR3::GUS activity in seedlings at 7 DAG, grown on solid medium containing solvent only (CON) or 25 µM ZIC2. (d) pZPR3::ZPR3:GUS activity in seedlings grown for 8 d on solid ½MS medium and then transferred for 24 h to liquid ½MS medium CON or 25 µM ZIC2. (e) Quantitative polymerase chain reaction (qPCR) analysis of ZPR3 expression in seedlings grown for 9 d on solid ½MS medium and then transferred for 24 h to liquid ½MS medium CON or 25 µM ZIC2 (means ± SEM; $n = 3$). *P*-value is indicated above bars (unpaired Student's two-tailed *t*-test). (f) Short-term effect of ZIC2 on tissue-specific ZPR3::GUS activity in root meristems. Transversal sections at the indicated positions of GUS-stained root tips from 7-d-old *pZPR3::GUS* seedlings. Before harvest plants were grown for 24 h in liquid medium containing solvent only (mock) or 25 µM ZIC2. Asterisks, endodermis; arrowheads, protoxylem; closed circles, phloem centre. (g) Long-term effect of ZIC2 on tissue-specific ZPR3::GUS activity in root meristems. Transversal sections of GUS-stained root tips of 7-d-old *pZPR3::GUS* seedlings grown in the absence (mock) or presence (ZIC2) of 25 µM ZIC2. Bars: (a, c, d) 500 µm; (f, g) 10 µm.

Structural requirements of ZIC2 function

To define the structural requirements for ZIC2 to activate ZPR3 expression we tested 14 structural variants showing modifications either in the thiobene ring, linker region, or the pyrazole substructure of the molecule (Fig. S2a). Whereas the linker and pyrazole variants did not show obvious induction of pZPR3::GUS activity in root tips, reporter expression was increased in the presence of T1, T3, T4, T5 and T6 (Fig. S2b,c). Quantification of GUS activity using the MUG assay revealed significant induction of root specific reporter expression by T1, T3 and T6 with all being in a similar range as ZIC2 (Fig. S2f). Since ZIC2 negatively affects primary root elongation we also quantified root lengths of seedlings grown in the presence of the ZIC2 analogs. From the thiobene variants, T1, T3 and T6 showed the strongest negative impact on root growth (Fig. S2d). The pyrazole variant P4 also significantly suppressed root elongation, however in combination with a general toxic effect on seedling growth (Fig. S2e). Taken together, modifications in the linker and pyrazole part of ZIC2 causes loss of ZPR3 induction and root growth inhibition, whereas the thiobene moiety appears to be less important for ZIC2 function.

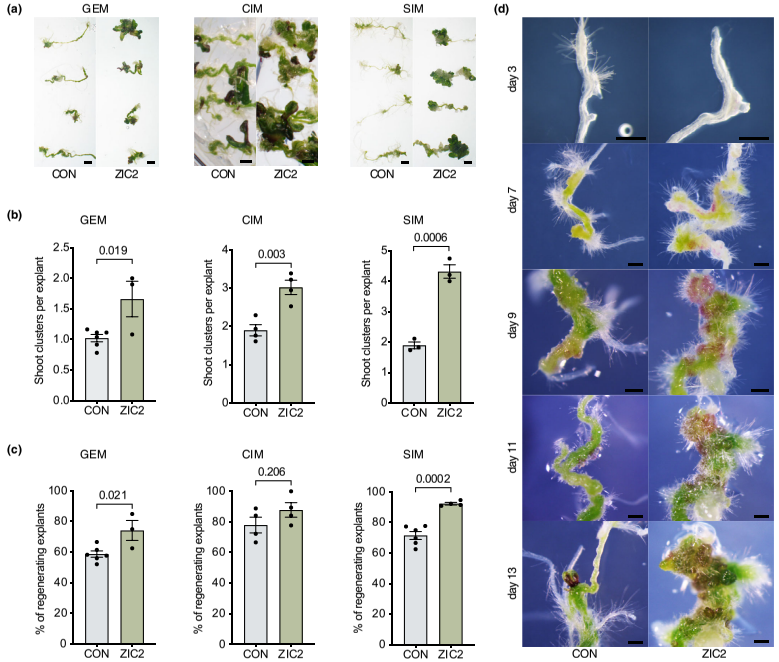

Fig. 2 ZIC2 induces shoot regeneration in *Arabidopsis*. (a) Shoot regeneration assay with root explants from wild-type (WT) seedlings where ZIC2 (25 µM) was applied to the germination medium (GEM), the callus induction medium (CIM) or the shoot induction medium (SIM). Representative explants were photographed 13 d (GEM) or 20 d (CIM and SIM) after transfer on SIM. CON, containing solvent only. (b) Quantification of regenerated shoot clusters per explant from the regeneration assay shown in (a). Data are from at least three independent experiments (means ± SEM). *P*-value is indicated above bars (unpaired Student's two-tailed *t*-test). (c) Quantification of percentage of explants with regenerated shoots from the regeneration assay shown in (a). Data are from at least three independent experiments (means ± SEM). *P*-value is indicated above bars (unpaired Student's two-tailed *t*-test). (d) Phenotypes of explants cultured on SIM CON or 25 µM ZIC2 for the indicated number of days. Bar, 500 µm.

ZIC2 promotes shoot regeneration in *Arabidopsis*

Since ZIC2 induces the transcription of the HD-ZIP III-regulated gene ZPR3 and HD-ZIP III function has been shown to be rate-limiting for shoot regeneration, we tested the effect of the chemical in a standard *Arabidopsis* regeneration assay. In this assay, seeds are germinated on ½MS medium, root explants are then transferred to CIM followed by an incubation on SIM. When ZIC2 was applied only during the germination phase, it negatively affected explant size (Fig. 2a), but still induced the formation of a significant higher number shoot clusters (Fig. 2a,b) and also increased the percentage of regenerating explants compared to the control (Fig. 2c). Adding ZIC2 only to the CIM enhanced the density of formed shoots per explant (Fig. 2a,b) but the number of responding explants was not significantly increased (Fig. 2c). The strongest effects were observed when ZIC2 treatment was restricted to the SIM, where two-times more shoot clusters were formed compared to the control group (Fig. 2a,b) and also the ratio of responding explants was considerably higher (Fig. 2c). Closer inspection of the explants over time revealed that ZIC2 in the SIM suppresses the outgrowth of lateral roots and instead provokes a slightly faster and much more pronounced formation of anthocyanin rich shoot pro-meristems without having an obvious effect on the callus proliferation rate (Fig. 2d). Notably, ZIC2 did not provoke short-term induction of DR5::GUS or pARR5::GUS reporter activities indicating that the compound's effect on regeneration is not based on direct auxin or cytokinin-like activities of the molecule (Fig. S3a,b). Finally, we also tested the three thiobene analogs of ZIC2 in the shoot regeneration assay, which have shown induction of ZPR3::GUS activity. Whereas T1 and T3 rather dampened the shoot regeneration rate, T6 exerted a significant promotive effect to a similar extend as ZIC2 (Fig. S4a,b).

ZIC2 promotes shoot regeneration in a HD-ZIP III-dependent manner

Next, we asked, whether HD-ZIP III proteins are required for the promotive effect of ZIC2 on shoot regeneration. To this end

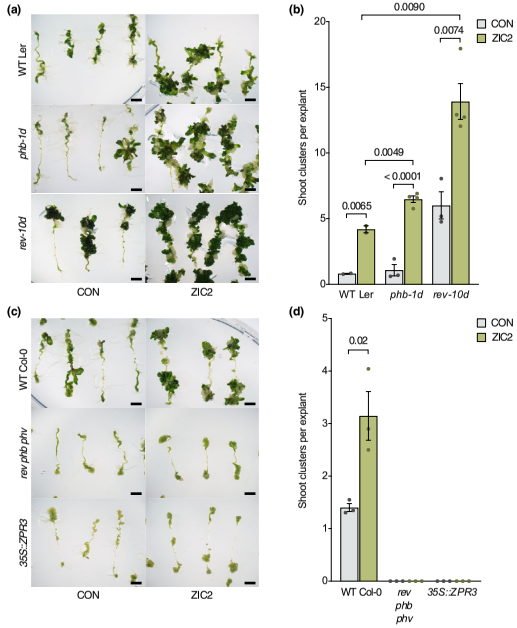

Fig. 3 The promotive effect of ZIC2 on *Arabidopsis* shoot regeneration depends on class III homeodomain-leucine zipper transcription factors. (a) Shoot regeneration phenotypes of wild-type (Ler), *phb-1d* and *rev-10d* explants cultivated on shoot induction medium (SIM) containing solvent only (CON) or 25 μM of ZIC2. Photographs were taken 16 d after transfer on SIM. (b) Quantification of shoot regeneration rate (shoot clusters per explant) in wild-type (Ler), *phb-1d* and *rev-10d* explants cultivated on SIM CON or 25 μM of ZIC2. Bars show means ± SEM from at least two independent experiments ($n \geq 12$ for each experiment). *P*-value is indicated above bars (unpaired Student's two-tailed *t*-test). (c) Shoot regeneration phenotypes of wild-type (Col-0), *rev phb phv* and *35S::ZPR3* explants cultivated on SIM CON or 25 μM of ZIC2. Photographs were taken 16 d after transfer on SIM. (d) Quantification of shoot regeneration rate (shoot clusters per explant) in wild-type (Col-0), *rev phb phv* and *35S::ZPR3* explants cultivated on SIM CON or 25 μM of ZIC2. Bars show means ± SEM from at least three independent experiments ($n \geq 12$ for each experiment). *P*-value is indicated above bars (unpaired Student's two-tailed *t*-test). Bar, 2 mm.

we analyzed the ZIC2-mediated regeneration response in different genotypes with altered HD-ZIP III activities. Mutation of the miRNA165/166-binding site in *phb-1d* results in ectopic accumulation of PHB (Mallory *et al.*, 2004). ZIC2-treated *phb-1d* explants showed a significantly higher shoot regeneration rate compared to the ZIC2 treated WT control whereas the untreated samples showed a similar response in our assay (Fig. 3a,b). The miRNA-resistant *rev-10d* gain-of-function allele already exerted pronounced shoot formation under control conditions (Fig. 3a, b). However, ZIC2 treatment further enhanced the response to the brink of saturation, since there was barely any explant area left not covered with leaf primordia. To test the ZIC2 effect in plant lines with reduced HD-ZIP III function we employed the triple mutant *rev phb phv*. In accordance with a previous study (T. Q. Zhang *et al.*, 2017) *rev phb phv* explants were not able to regenerate shoots under control conditions (Fig. 3c,d). ZIC2 application

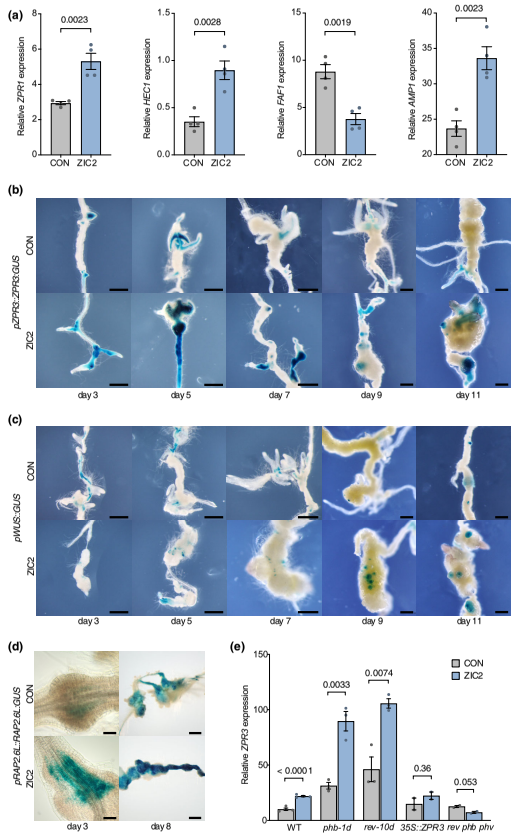

Fig. 4 ZIC2 causes advanced expression of Class III homeodomain-leucine zipper direct target genes in *Arabidopsis*. (a) Quantitative polymerase chain reaction (qPCR) expression analysis of indicated genes in roots of seedlings grown for 9 d on solid ½MS medium and then transferred for 24 h to liquid ½MS medium containing solvent only (CON) or 25 μM ZIC2. Data from four biological repeats are shown (means ± SEM). *P*-value is indicated above bars (unpaired Student's two-tailed *t*-test). (b) pZPR3::ZPR3:GUS activity in explants cultured on shoot induction medium (SIM) CON or 25 μM ZIC2 for the indicated number of days. (c) pWUS::GUS activity in explants cultured on SIM CON or 25 μM ZIC2 for the indicated number of days. (d) pRAP2.6L::RAP2.6L:GUS activity in explants cultured on SIM CON or 25 μM ZIC2 for the indicated number of days. (e) qPCR analysis of ZPR3 expression in roots of the indicated genotypes grown for 9 d on solid ½MS medium and then transferred for 24 h to liquid ½MS medium CON or 25 μM ZIC2. Data from two to four biological repeats are shown (means ± SEM). *P*-value is indicated above bars (unpaired Student's two-tailed *t*-test). Bars: (b, c and right panel in d) 500 μm; (left panel in d) 50 μm.

did not alleviate this effect. To test the ZIC2 response in a line with a minimal residual level of REV/PHB/PHV function we used *35S::ZPR3*. Again, ZIC2 was fully ineffective to promote regeneration of shoots in this genotype, supporting the conclusion that ZIC2 function is dependent on the presence of HD-ZIP III activity (Fig. 3c,d).

ZIC2 causes advanced expression of HD-ZIP III direct target genes

To assess, whether ZIC2 affects HD-ZIP III-dependent transcriptional activity on a broader level, we analyzed the expression of additional genes, directly controlled by HD-ZIP III transcription factors (Reinhart *et al.*, 2013; Weits *et al.*, 2019). A 24-h treatment with ZIC2 caused significant upregulation of ZPR1, HEC1 and AMP1 in root tissues (Fig. 4a). Long-term treatment of root explants on SIM showed ZIC2-dependent upregulation of ZPR3 expression at all tested time points (Fig. 4b). In contrast, upregulation of the HD-ZIP III target WUS (T. Q. Zhang *et al.*, 2017) became apparent only between day 7 and 9 after transfer on SIM containing ZIC2 (Fig. 4c). Finally, we also followed the expression of RAP2.6L in response to ZIC2, an AP2 transcription factor with a rate limiting effect on shoot regeneration, whose transcription is directly activated by HD-ZIP III proteins (Che *et al.*, 2006; Yang *et al.*, 2018). GUS-activity of a RAP2.6L-specific reporter was elevated in the presence of ZIC2 from day 3 onward and cumulated at day 8 under the used conditions (Fig. 4d).

To interrogate, whether the observed induction of HD-ZIP III target genes by ZIC2 is indeed dependent on HD-ZIP III activity, we compared the amplitude of ZPR3 activation in different HD-ZIP III gain and loss of function alleles by qPCR (Fig. 4e). As expected, *ZPR3* messenger RNA (mRNA) levels were elevated in *phb-1d* and *rev-10d* compared to WT. In both genotypes ZIC2 application for 24 h resulted in a further boost of ZPR3 transcript levels (Fig. 4e). In contrast, ZIC2 induction of ZPR3 transcripts (qPCR specific for non-transgenic mRNAs) was diminished in *35S::ZPR3* and absent in *rev phb phv* (Fig. 4e).

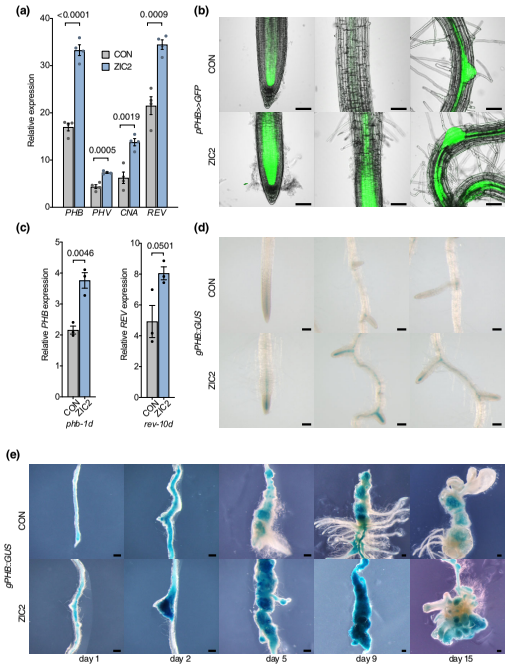

Fig. 5 ZIC2 promotes the transcription of Class III homeodomain-leucine zipper proteins. (a) Quantitative polymerase chain reaction (qPCR) expression analysis of indicated genes in roots of seedlings grown for 9 d on solid ½MS medium and then transferred for 24 h to liquid ½MS medium containing solvent only (CON) or 25 μM ZIC2. Data from four biological repeats are shown (means ± SEM). *P*-value is indicated above bars (unpaired Student's two-tailed *t*-test). (b) pPHB>>GFP fluorescence in roots of seedlings grown for 5 d on solid ½MS medium and then transferred for 48 h to liquid ½MS medium CON or 25 μM ZIC2. (c) qPCR expression analysis of indicated genes in roots of *phb-1d* (left graph) and *rev-10d* (right graph) seedlings grown for 9 d on solid ½MS medium and then transferred for 24 h to liquid ½MS medium CON or 25 μM ZIC2. Data from three biological repeats are shown (means ± SEM). *P*-value is indicated above bars (unpaired Student's two-tailed *t*-test). (d) gPHB::GUS activity in roots of seedlings grown for 7 d on solid ½MS medium and then transferred for 24 h to liquid ½MS medium CON or 25 μM ZIC2. (e) gPHB::GUS activity in explants cultured on shoot induction medium (SIM) CON or 25 μM ZIC2 for the indicated number of days. Bars: (b) 50 μm; (d) 100 μm; (e) 200 μm.

ZIC2 induces HD-ZIP III transcription

To test whether ZIC2 affects HD-ZIP III function at the protein level, e.g. by interacting with one of the ligand binding domains, we overexpressed PHB and REV in protoplasts and compared the induction rates of the ZPR3 promoter in the presence of increasing concentrations of ZIC2 (Fig. S5). Neither PHB nor REV-dependent activation of the pZPR3::LUC reporter changed in the presence of ZIC2 indicating that the compound does not primarily affect HD-ZIP III protein function.

A 24 h ZIC2 treatment of seedlings rather caused a significant increase of transcript levels of all four tested members of the HD-ZIP III family (Fig. 5a). Analysis of the pPHB>>GFP reporter in ZIC2-treated roots revealed a stronger fluorescence in the original expression domain, as well as a lateral expansion in the root meristem (Fig. 5b). Increased reporter activity was also visible in the stele along the root axis (Fig. 5b). The ZIC2-mediated induction of transcription was also detectable in the miRNA-resistant HD-ZIP III mutants *phb-1d* and *rev-10d* (Fig. 5c), indicating that ZIC2 acts in a miRNA165/166-independent manner. Consistent with this assumption, 24 h ZIC2 treatment did not drastically change the expression patterns of pMIR165A::GFP and pMIR166A::GFP in the root meristem endodermis (Fig. S6a,b). After 48 h the reporter activities became more restricted to the proliferation zone, which appeared to be a consequence of the morphological change of the meristem. Enhanced *PHB* transcription levels by ZIC2 application in roots correlated with higher PHB protein accumulation as denoted by the stronger GUS activity of the gPHB::GUS reporter (Fig. 5d). We also monitored gPHB::GUS activity in root explants shifted on SIM containing ZIC2 (Fig. 5e). From day 2 onward, strong reporter activation could be observed in proliferating areas in ZIC2-treated explants, which were localized in bigger but also more irregular foci compared to the mock control. Reporter expression further intensified in ZIC2-treated explants from day 5 to day 9 causing strong GUS staining of the entire propagule, whereas reporter activity in the control was restricted to separated patches.

ZIC2 induces the expression of a subset of cytokinin biosynthesis enzymes during shoot regeneration

PHB has been shown to promote the expression of a subset *IPT* genes in the root apical meristem, which code for rate limiting enzymes of cytokinin biosynthesis (Dello Ioio *et al.*, 2012). ZIC2 treatment significantly elevated the transcript levels of *IPT1*, *IPT3* and *IPT7* in roots (Fig. S7a). Consistent with the qPCR data, pIPT1::GUS and pIPT7::GFP activity was increased in the basal stele, 24 h after addition of ZIC2, and the expression domains of the reporters expanded to the whole root meristem area after prolonged ZIC2 treatment (Fig. S7b,c). The elevated expression of *IPT* genes correlated with a higher activity of the cytokinin-responsive reporter pARR5::GUS in root meristematic tissues (Fig. S7d). Next, we monitored IPT reporter expression in root explants during the shoot regeneration process. A ZIC2-dependent increase of pIPT1::GUS activity was first apparent 5 d after transfer on SIM and further intensified at day 7 to day 10 (Fig. S7e). IPT7::GFP fluorescence was also clearly elevated in the outer layers of explants grown on ZIC2-containing SIM (Fig. S7f). Using TCS::GFP and pARR::GUS, we could detect a ZIC2-mediated stronger cytokinin response in explant tissue domains showing the pronounced IPT1 and IPT7 expression levels (Fig. S7g,h). Notably, the expression of IPT5, a gene which has been reported to be not controlled by PHB (Dello Ioio *et al.*, 2012), did not change in ZIC2 treated root meristems or explants (Fig. S8a,b).

Fig. 6 ZIC2 inhibits polar auxin transport. (a) Root growth phenotypes of 6-d-old wild-type seedlings grown on ½MS medium containing solvent only (CON) or the indicated concentrations of ZIC2. (b) Effect of ZIC2 on root gravitropic response. Five-day-old wild-type seedlings were transferred on vertical half-strength MS agar plates containing the indicated concentrations of either ZIC2 or naphtylphtalamic acid (NPA) and then cultured for further 19 h. After rotating plates by an angle of 90° against vertical direction plants were further incubated for 8 h. Root angles were measured, grouped into 22.5° classes and plotted as circular histograms. (c) Quantification of primary root growth of 5-d-old wild-type seedlings transferred on vertical plates with ½MS medium CON or the indicated concentrations of NPA or ZIC2. Increase in root length was measured 48 h after transfer (means ± SEM; $n \geq 20$). Different letters over the error bars indicate significant differences ($P < 0.05$; one-way ANOVA followed by Tukey's multiple comparison tests). (d) Quantification of primary root length of wild-type seedlings germinated for 4 d on ½MS medium and then transferred on vertical plates with ½MS medium CON or the indicated concentrations of NPA or ZIC2. Root length was measured 4 d after transfer (means ± SEM; $n \geq 8$). Different letters over the error bars indicate significant differences ($P < 0.05$; one-way ANOVA followed by Tukey's multiple comparison tests). (e) Quantification of lateral root primordia of wild-type seedlings germinated for 4 d on ½MS medium and then transferred on vertical plates with half-strength MS medium CON or the indicated concentrations of NPA or ZIC2. Root primordia were counted 4 d after transfer (means ± SEM; $n \geq 8$). Different letters over the error bars indicate significant differences ($P < 0.05$; one-way ANOVA followed by Tukey's multiple comparison tests). (f) Quantification of lateral root primordia of wild-type seedlings geminated for 4 d on ½MS medium and then transferred on vertical plates with half-strength MS medium CON or the indicated concentrations of NPA or ZIC2. Root primordia were counted 8 d after transfer (means ± SEM; $n \geq 8$). Different letters over the error bars indicate significant differences ($P < 0.05$; one-way ANOVA followed by Tukey's multiple comparison tests). (g) Lugol-staining of 7-d-old wild-type primary root tips treated with the indicated concentrations of NPA and ZIC2. Plants were germinated for 4 d on ½MS medium and then transferred to drug-containing ½MS medium for 3 d. (h) Effect of NPA and ZIC2 on DR5::GUS activity (upper panel) pARR5::GUS activity (middle panel) and pPIN1::GUS activity (lower panel) in root tips of wild-type seedlings. Plants were germinated for 4 d on ½MS medium and then transferred on ½MS medium CON, 25 μM NPA or 25 μM ZIC2. GUS staining was performed 4 d after transfer. (i) Transport of carbon-14 (^{14}C)-labelled indole-3-acetic acid (IAA) in 2.5-cm wild-type inflorescence stem pieces. Data from at least three biological repeats are shown (means ± SEM). Data were analysed using one-way ANOVA followed by Tukey's multiple comparison tests. Significant differences ($P < 0.05$) are indicated by different letters in each segment group. Bars: (a) 0.5 mm; (g, h) 100 μm.

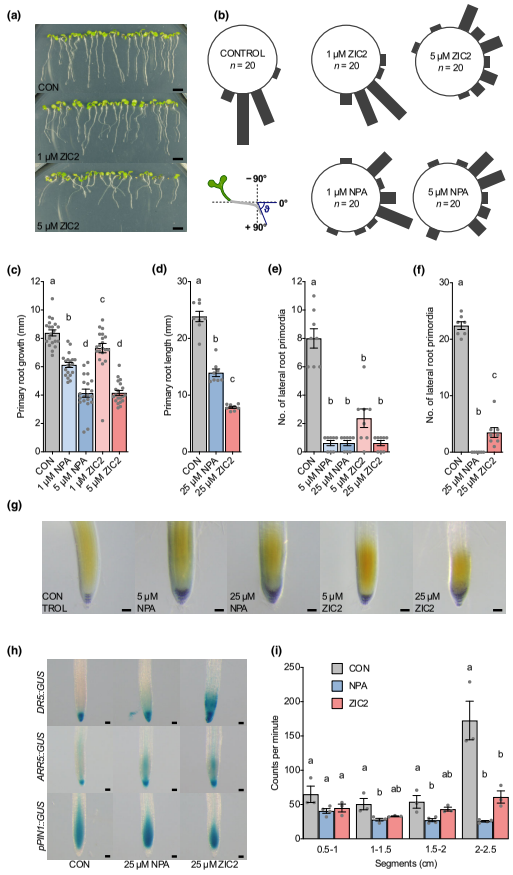

ZIC2 inhibits polar auxin transport

Seedlings grown on ZIC2-containing medium showed a defect in root gravitropism. This defect was already clearly apparent at a concentration of 1 µM and was fully developed at a concentration of 5 µM (Fig. 6a). ZIC2 inhibited root gravitropism in a concentration range comparable with the polar auxin transport inhibitor NPA (Fig. 6b). Block of polar auxin transport by NPA also suppresses primary root growth as well as the formation of lateral root primordia (Rashotte *et al.*, 2000; Casimiro *et al.*, 2001). Both processes are also affected by ZIC2 (Fig. 6c–f). ZIC2 application also caused the formation of additional starch granule-containing columella cell layers (Fig. 6g), a hallmark of NPA-treated root meristems (Sabatini *et al.*, 1999). These anatomical changes triggered by the two drugs were accompanied by highly congruent alterations in DR5::GUS, ARR5::GUS and pPIN1::GUS expression patterns of root tips (Figs 6h, S9a). Moreover, ZIC2 led to enhanced DR5::GUS activity in the margins of cotyledons (Fig. S9b), another feature provoked by auxin transport inhibitor treatment (Bao *et al.*, 2004). Finally, we compared the movement of radioactively labelled auxin through inflorescence stems pretreated with either NPA or ZIC2. Both compounds blocked accumulation of the [^{14}C]-IAA in the basal segments of treated stems (Fig. 6i). However, in contrast to NPA (Abas *et al.*, 2021), ZIC2 did not significantly alter PIN1/3 auxin transport activities in *Xenopus* oocytes (Fig. S10a,b). Taken together, ZIC2 provokes NPA-like growth defects and inhibits polar auxin transport *in planta*, but does not directly affect PIN auxin transport in a heterologous test system.

Block of auxin transport by NPA causes accumulation of HD-ZIP III transcripts and enhances shoot regeneration in *Arabidopsis*

To test, whether the promotive effect of ZIC2 on HD-ZIP III expression and shoot regeneration is due to its impact on polar auxin transport, we analyzed the effect of NPA on these processes. Increasing concentrations of NPA caused strengthening and broadening of the pZPR3::GUS expression pattern in the root tip as observed for ZIC2 (Fig. 7a). Accordingly, NPA and ZIC2 exhibited the same inductive effect on gPHB::GUS activity resulting in strong reporter expression in the proliferating stele tissues of the RAM (Fig. 7b). Moreover, addition of NPA to the shoot induction medium led to a significantly higher shoot cluster number in a concentration range between 1 and 25 µM (Fig. 7c,d). The higher regeneration rate was accompanied by stronger and broader ZPR3 and PHB expression domains, which subsequently co-localized with the higher number of regenerating shoots (Fig. 7e,f).

Altered auxin responses in ZIC2-treated explants correlate with the suppression of root development and a subsequent higher rate of shoot formation

To better understand how ZIC2-mediated inhibition of auxin transport leads to the enhanced shoot regeneration rate we monitored auxin responses during the regeneration process. In the first 5 d on SIM, DR5rev::GFP activity was prevalent in the proliferating pericycle cells and the reporter activity appeared slightly stronger after treatment with the drug (Fig. S11a). Thereafter, DR5 reporter expression marked root primordium formation in the control sample, which did not occur in the presence of ZIC2 (Fig. S11a,b). The inability to form functional root primordia on ZIC2 was also reflected in altered PIN1 expression patterns. pPIN1::GUS activity was present in deformed non-growing protuberances (Fig. S11c). These structures showed unorganized pPIN1::PIN:GFP localization in contrast to the root primordia in the control samples (Fig. S11d). However, 12 d after transfer, new PIN1 and DR5 expression domains appeared at a higher density on the surface of ZIC2-treated explants compared to the control samples, representing incipient shoot meristems (Fig. S11b,c,e). Taken together, auxin transport inhibition by ZIC2 interferes with root primordia formation and promotes HD-ZIP III expression, which activates a developmental program favorable for shoot regeneration.

ZIC2 and NPA promote *de novo* shoot formation in the regeneration recalcitrant species sunflower

To assess, whether ZIC2 improves *de novo* shoot formation in regeneration recalcitrant plant species, we tested the compound in sunflower using cotyledons as explants (Sujatha *et al.*, 2012). ZIC2 caused a significant increase in the size of forming shoot meristem clusters (Fig. 8a–d). This correlated with a higher level of *HaWUS* expression in ZIC2-treated explants (Fig. 8i). The higher density of regenerated meristems also resulted in a higher number of outgrowing shoots when transferred on gibberellin-containing shoot elongation medium (Fig. 8j). Moreover, ZIC2 application also raised the percentage of shoot regenerating explants (Fig. 8e). A dose response experiment revealed 10 µM as the most favorable concentration in respect to SAM cluster size as well as regeneration frequency (Fig. 8g,h). We also tested the structural analogs of ZIC2 in sunflower and consistent with the results in *Arabidopsis* (Fig. S4), only T6 exerted a promotive effect in the recalcitrant crop (Fig. 8f).

Finally, NPA also considerably enhanced *de novo* shoot formation, when applied in our sunflower regeneration protocol, in a comparable concentration range as ZIC2 (Fig. 8k–m). Thus, pharmacological modulation of auxin transport can be used to improve shoot regeneration rates in the recalcitrant species sunflower.

Discussion

De novo shoot regeneration enables plants to continue organogenesis even after massive damage of their body structures. Moreover, it constitutes the foundation of biotechnical methods central for basic plant research and crop breeding. In this work we identified ZIC2 as a novel small molecule modulator of polar auxin transport to induce the expression of HD-ZIP III proteins and thereby to promote the rate of shoot regeneration in *Arabidopsis*. Our results provide insight that local HD-ZIP III induction in explant tissue, is controlled by auxin gradients formed by polar transport of the hormone. We moreover show that this knowledge can be applied to enhance *in vitro* shoot formation in the regeneration-recalcitrant crop sunflower.

ZIC2 inhibits polar auxin transport *in planta* and provokes morphological and molecular phenotypes closely related to the auxin efflux inhibitor NPA. NPA directly targets PIN auxin efflux carriers and interferes with their activity by affecting their dimerization behavior (Abas *et al.*, 2021; Teale *et al.*, 2021).

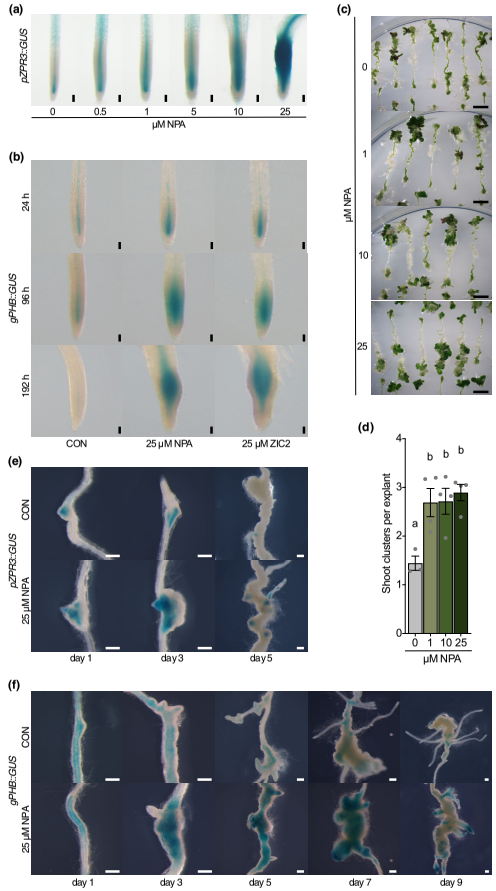

Fig. 7 Block of auxin transport by naphthylphthalamic acid (NPA) causes accumulation of Class III homeodomain-leucine zipper transcripts and enhances shoot regeneration in *Arabidopsis*. (a) pZPR3::GUS activity in primary roots of wild-type seedlings 8 d after germination (DAG) grown on the indicated concentrations of NPA. (b) gPHB::GUS expression in primary roots of wild-type plants grown for the indicated times on medium containing only the solvent dimethyl sulfoxide (DMSO) (CON), 25 μM NPA or 25 μM ZIC2. Plants were germinated on ½MS medium and transferred on compound-containing media at 4 DAG. (c) Shoot regeneration phenotypes of wild-type explants cultivated on shoot induction medium (SIM) containing the indicated concentrations of NPA. Photographs were taken 16 d after transfer on SIM. (d) Quantification of shoot regeneration rate (shoot clusters per explant) in wild-type explants cultivated on SIM containing the indicated concentrations of NPA. Bars show means ± SEM from at least three independent experiments ($n \geq 12$ for each experiment). Different letters over the error bars indicate significant differences ($P < 0.05$; one-way ANOVA followed by Tukey's multiple comparison tests). (e) pZPR3::GUS activity in explants cultured on SIM containing solvent only (CON) or 25 μM NPA for the indicated number of days. (f) gPHB::GUS activity in explants cultured on SIM CON or 25 μM NPA for the indicated number of days. Bars: (a, b) 100 μm; (c) 5 mm; (e, f) 200 μm.

However, in contrast to NPA, ZIC2 does not impede the activity of heterologous expressed PIN proteins suggesting that ZIC2 impacts on auxin transport by a different molecular mechanism. This finding is consistent with the low structural similarity of ZIC2 to NPA and other members of the phytotropin family of auxin transport inhibitors (Katekar *et al.*, 1981). ZIC2 neither shows structural resemblance to other classical auxin transport inhibitors such as 2,3,5-triiodobenzoic acid (TIBA) or morphactin nor to more recently identified compounds we found in the literature (Rojas-Pierce *et al.*, 2007; Kim *et al.*, 2010; Tsuda *et al.*, 2011; Nishimura *et al.*, 2012; Steenackers *et al.*, 2017). We therefore postulate that ZIC2 represents a novel type of polar auxin transport inhibitor. Future studies should clarify whether ZIC2 specifically acts on other known NPA targets involved in auxin transport such as the ABCB family of multidrug efflux proteins (Noh *et al.*, 2001) or affects yet unknown regulators of this process.

Local induction of HD-ZIP III expression in explants has been shown to be a prerequisite for the establishment of shoot stem cell niches (T. Q. Zhang *et al.*, 2017). However, how this domain

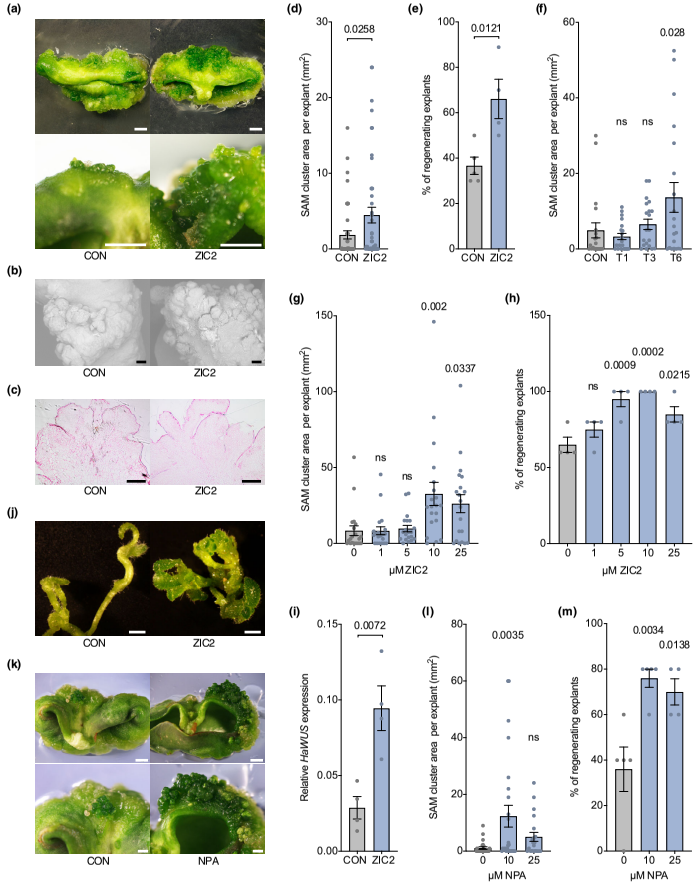

Fig. 8 ZIC2 enhances shoot regeneration in sunflower. (a) Shoot regeneration phenotypes of sunflower cotyledon explants cultivated on regeneration medium containing solvent only (CON) or 25 μM ZIC2. Photographs were taken 21 d after transfer on regeneration medium. Overview pictures are shown in upper panel, close up views of regenerating areas are shown in lower panel. (b) Scanning electron micrographs of regenerating areas of sunflower cotyledon explants cultivated on regeneration medium CON or 25 μM ZIC2 for 21 d. (c) Transversal sections of regenerating areas of sunflower cotyledon explants cultivated on regeneration medium CON or 25 μM ZIC2 for 35 d. (d) Quantification of shoot apical meristem (SAM) cluster area of sunflower cotyledon explants cultivated on regeneration medium CON or 25 μM ZIC2 for 21 d (means ± SEM, $n \geq 45$). *P*-value is indicated above bars (unpaired Student's two-tailed *t*-test). (e) Percentage of regenerating sunflower cotyledon explants on regeneration medium CON or 25 μM ZIC2. Data from at least four independent repeats are shown (means ± SEM). *P*-value is indicated above bars (unpaired Student's two-tailed *t*-test). (f) Quantification of SAM cluster area of sunflower cotyledon explants cultivated on regeneration medium CON or 25 μM of the ZIC2 analogs T1, T3 or T6 (means ± SEM, $n \geq 20$). Relevant *P*-values obtained from significance test against the control treatment are indicated above bars (ns, not significant; one-way ANOVA followed by Dunnett's multiple comparison test). (g) Quantification of SAM cluster area of sunflower cotyledon explants cultivated on regeneration medium containing the indicated concentrations of ZIC2 for 21 d (means ± SEM, $n \geq 20$). Relevant *P*-values obtained from significance test against the control treatment are indicated above bars (ns, not significant; one-way ANOVA followed by Dunnett's multiple comparison test). (h) Percentage of regenerating sunflower cotyledon explants on regeneration medium containing the indicated concentrations of ZIC2 for 21 d. Data from four independent repeats are shown (means ± SEM). Relevant *P*-values obtained from significance test against the control treatment are indicated above bars (ns, not significant; one-way ANOVA followed by Dunnett's multiple comparison test). (i) Quantitative polymerase chain reaction (qPCR) expression analysis of *HaWUS* in sunflower cotyledon explants cultivated for 21 d on shoot regeneration medium CON or 25 μM ZIC2. Data from four biological repeats are shown (means ± SEM). *P*-value is indicated above bars (unpaired Student's two-tailed *t*-test). (j) Regenerated shoots from sunflower cotyledon explants cultivated on regeneration medium CON or 25 μM ZIC2 for 21 d and then transferred on shoot elongation medium for 45 d. (k) Shoot regeneration phenotypes of sunflower cotyledon explants cultivated on regeneration medium CON or 25 μM naphthylphthalamic acid (NPA). Photographs were taken 21 d after transfer on regeneration medium. Overview pictures are shown in upper panel, close up views of regenerating areas are shown in lower panel. (l) Quantification of SAM cluster area of sunflower cotyledon explants cultivated on regeneration medium containing the indicated concentrations of NPA for 21 d (means ± SEM, $n \geq 20$). Relevant *P*-values obtained from significance test against the control treatment are indicated above bars (ns, not significant; one-way ANOVA followed by Dunnett's multiple comparison test). (m) Percentage of regenerating sunflower cotyledon explants on regeneration medium containing the indicated concentrations of NPA for 21 d. Data from four independent repeats are shown (means ± SEM). Relevant *P*-values obtained from significance test against the control treatment are indicated above bars (one-way ANOVA followed by Dunnett's multiple comparison test). Bars: (a, j, k) 2 mm; (b, c) 250 μm.

specific induction of HD-ZIP III expression is achieved was not resolved so far. Our analysis of ZIC2 function revealed that the formation of auxin gradients by auxin efflux carriers plays an important role in the transcriptional activation of PHB and its paralogs in explants on SIM. ZIC2-mediated altered distribution of auxin in the explant might directly enhance HD-ZIP III transcription in broader domains, resulting in a higher number of independent shoot stem cell niches formed. Previous studies have provided evidence that auxin controls HD-ZIP III expression. In the SAM, the expression of REV is upregulated by simultaneous application of NPA and the synthetic auxin NAA (Caggiano *et al.*, 2017). During the formation of the primary vascular system and the vascular cambium auxin maxima define the expression domains of HD-ZIP III members (Donner *et al.*, 2009; Ursache *et al.*, 2014; Smetana *et al.*, 2019). In contrast, during the establishment of the shoot stem cell niche in the embryo and the leaf axil, HD-ZIP III expression is rather specified in domains of low auxin response (Shi *et al.*, 2016; Z. Zhang *et al.*, 2017). Although we monitored changes in the expression pattern of auxin responsive DR5::GUS/GFP reporters in ZIC2-treated explants, we could not clearly link the onset and location of ectopic HD-ZIP III expression to areas of enhanced or reduced auxin responsiveness in these tissues. Future time-lapse co-expression experiments of HD-ZIP III reporters with different auxin response detection systems might help to further resolve this issue.

The original aim of the performed small molecule screen was to identify chemicals, which modulate HD-ZIP III activity by direct binding to one of the putative ligand binding domains present in the protein. Our work, however, revealed that ZIC2 promotes HD-ZIP III transcription by compromising auxin transport rather than post-translationally controlling the activity of these proteins. In previous work it has been shown that HD-ZIP III expression and activity is under tight control at different regulatory levels including miRNA165/166, AGO10 and ZPR proteins (Ramachandran *et al.*, 2017). Due to this tight control, overexpression of HD-ZIP III WT versions does not lead to severe phenotypes like root-shoot conversion or leaf adaxialization phenotypes (Magnani & Barton, 2011). Consistent with this, we do not observe such phenotypes in seedlings treated with ZIC2. Nevertheless, in the process of *de novo* shoot regeneration the transcriptional stimulation by ZIC2 in explants is followed by enhanced and ectopic accumulation of PHB, and this upregulation appears to be sufficient to trigger ectopic shoot stem cell niche formation. The disclosed impact of auxin distribution on HD-ZIP III expression during shoot regeneration will help to further resolve the transcriptional regulation of this important class of transcription factors.

The ZIC2-mediated activation of HD-ZIP III expression is accompanied by an induction of their downstream targets WUS and RAP2.6L, crucial drivers of shoot regeneration (Che *et al.*, 2006; T. Q. Zhang *et al.*, 2017; Yang *et al.*, 2018). In addition, we observed a concerted transcriptional activation of members of the IPT family of cytokinin biosynthesis enzymes resulting in stronger cytokinin responses in regenerating explants. This activation is in agreement with the observation that in the root meristem PHB induces the transcription of IPT1 and IPT7 (Dello Ioio *et al.*, 2012). Thus, in the context of *de novo* shoot regeneration, this downstream effect of HD-ZIP III activity might reinforce the establishment of shoot stemness by enhancing tissue-specific cytokinin responses including B-type ARR activity. Based on these findings, we postulate that during shoot regeneration HD-ZIP III contributes to WUS activation in a dual manner, by binding to its promoter and by enhancing the activity of their transcriptional interaction partners, the B-type ARRs.

Due to their impact on plant growth and development it is not surprising that PAT inhibitors have been previously tested in organ regeneration experiments in plant tissue culture but the spectrum of observed effects was quite controversial. Consistent with our results, studies in different species revealed a promotive effect of PAT inhibitors on shoot regeneration. In *Arabidopsis* cotyledons, NPA treatment increased the capacity of shoot formation under high light conditions (Nameth *et al.*, 2013) and application of TIBA significantly promoted *de novo* shoot regeneration from cucumber cotyledon explants (Shukla *et al.*, 2014). A positive effect of NPA was also reported for the regeneration of shoots from epicotyl cuttings in different citrus cultivars (Hu *et al.*, 2017). Other studies, however, revealed a clear negative impact of TIBA or NPA on the process of *de novo* shoot regeneration (Murashige, 1965; Cheng *et al.*, 2013). These contradictory results potentially originate from the differences in used explant types, application time points and inhibitor concentrations and this might also be the reason that PAT inhibitors are yet not commonly perceived as regeneration promotive agents. The type of response most likely depends on the levels and distribution of endogenous IAA in the explant and the presence of externally applied auxin in the medium. Moreover, the timepoint and concentration of PAT inhibitor treatment might be crucial to trigger the establishment of the stem cell niche in the early phase of regeneration but to not interfere with the process of leaf formation at later stages. Optimization of application parameters and systemic comparison of different PAT inhibitors with different uptake kinetics and tissue half-lives will reveal to which extent these chemicals can help to overcome regeneration recalcitrance in crop plants and thus a major bottle neck in modern plant breeding.

Acknowledgements

This work was supported by a grant from the German Federal Ministry of Education and Research (BMBF 031B0554 to TS) and grants from the German Research Foundation DFG (SI 2323/2-1 to TS and HA3468/6-3 to UZH). The authors thank Ykä Helariutta and Michael Prigge for providing seed material. The authors also thank Jesica Fabro for contributing to the set-up of the chemical screen as part of her Master thesis. The authors thank Irene Ziegler and Shuyao Chen for technical assistance. Light microscopy was performed at the Center for Advanced Light Microscopy (CALM) at the TUM School of Life Sciences.

Author contributions

TS conceived the study. SY, MdH, JM, DPJ, UZH and TS performed experiments. SY, MdH, JM, UZH, BP and TS evaluated the data and SY and TS performed the statistical analyses. TS drafted the manuscript, which was reviewed and edited by all coauthors.

ORCID

Ulrich Z. Hammes https://orcid.org/0000-0002-3663-4908
Brigitte Poppenberger https://orcid.org/0000-0003-1020-0500
Tobias Sieberer https://orcid.org/0000-0002-4462-9260
Saiqi Yang https://orcid.org/0000-0002-6425-3731

Data availability

All data associated with this manuscript will be made available upon request.

References

Abas L, Kolb M, Stadlmann J, Janacek DP, Lukic K, Schwechheimer C, Sazanov LA, Mach L, Friml J, Hammes UZ. 2021. Naphthylphthalamic acid associates with and inhibits PIN auxin transporters. *Proceedings of the National Academy of Sciences, USA* **118**: e2020857118.

Altpeter F, Springer NM, Bartley LE, Blechl A, Brutnell TP, Citovsky V, Conrad L, Gelvin SB, Jackson D, Kausch AP *et al.* 2016. Advancing crop transformation in the era of genome editing. *Plant Cell* **28**: 1510–1520.

Bao F, Shen J, Brady SR, Muday GK, Asami T, Yang Z. 2004. Brassinosteroids interact with auxin to promote lateral root development in *Arabidopsis*. *Plant Physiology* **134**: 1624–1631.

Benkova E, Michniewicz M, Sauer M, Teichmann T, Seifertova D, Jurgens G, Friml J. 2003. Local, efflux-dependent auxin gradients as a common module for plant organ formation. *Cell* **115**: 591–602.

Caggiano MP, Yu X, Bhatia N, Larsson A, Ram H, Ohno CK, Sappl P, Meyerowitz EM, Jonsson H, Heisler MG. 2017. Cell type boundaries organize plant development. *eLife* **6**: e27421.

Carlsbecker A, Lee J-Y, Roberts CJ, Dettmer J, Lehesranta S, Zhou J, Lindgren O, Moreno-Risueno MA, Vatén A, Thitamadee S *et al.* 2010. Cell signalling by microRNA165/6 directs gene dose-dependent root cell fate. *Nature* **465**: 316–321.

Casimiro I, Marchant A, Bhalerao RP, Beeckman T, Dhooge S, Swarup R, Graham N, Inzé D, Sandberg G, Casero PJ *et al.* 2001. Auxin transport promotes *Arabidopsis* lateral root initiation. *Plant Cell* **13**: 843–852.

Che P, Lall S, Nettleton D, Howell SH. 2006. Gene expression programs during shoot, root, and callus development in *Arabidopsis* tissue culture. *Plant Physiology* **141**: 620–637.

Cheng ZJ, Wang L, Sun W, Zhang Y, Zhou C, Su YH, Li W, Sun TT, Zhao XY, Li XG *et al.* 2013. Pattern of auxin and cytokinin responses for shoot meristem induction results from the regulation of cytokinin biosynthesis by AUXIN RESPONSE FACTOR3. *Plant Physiology* **161**: 240–251.

D'Agostino IB, Deruere J, Kieber JJ. 2000. Characterization of the response of the *Arabidopsis* response regulator gene family to cytokinin. *Plant Physiology* **124**: 1706–1717.

De Smet I, Chaerle P, Vanneste S, De Rycke R, Inze D, Beeckman T. 2004. An easy and versatile embedding method for transverse sections. *Journal of Microscopy* **213**: 76–80.

Dello Ioio R, Galinha C, Fletcher A, Grigg S, Molnar A, Willemsen V, Scheres B, Sabatini S, Baulcombe D, Maini P *et al.* 2012. A PHABULOSA/cytokinin feedback loop controls root growth in *Arabidopsis*. *Current Biology* **22**: 1699–1704.

Diener AC, Li H, Zhou W, Whoriskey WJ, Nes WD, Fink GR. 2000. Sterol methyltransferase 1 controls the level of cholesterol in plants. *Plant Cell* **12**: 853–870.

Donner TJ, Sherr I, Scarpella E. 2009. Regulation of preprocambial cell state acquisition by auxin signaling in *Arabidopsis* leaves. *Development* **136**: 3235–3246.

Fastner A, Absmanner B, Hammes UZ. 2017. Use of *Xenopus laevis* oocytes to study auxin transport. *Methods in Molecular Biology* **1497**: 259–270.

Friml J, Vieten A, Sauer M, Weijers D, Schwarz H, Hamann T, Offringa R, Jurgens G. 2003. Efflux-dependent auxin gradients establish the apical-basal axis of *Arabidopsis*. *Nature* **426**: 147–153.

Gillmor CS, Park MY, Smith MR, Pepitone R, Kerstetter RA, Poethig RS. 2010. The MED12-MED13 module of Mediator regulates the timing of embryo patterning in *Arabidopsis*. *Development* **137**: 113–122.

Grigg SP, Galinha C, Kornet N, Canales C, Scheres B, Tsiantis M. 2009. Repression of apical homeobox genes is required for embryonic root development in *Arabidopsis*. *Current Biology* **19**: 1485–1490.

Gross-Hardt R, Lenhard M, Laux T. 2002. WUSCHEL signaling functions in interregional communication during *Arabidopsis* ovule development. *Genes & Development* **16**: 1129–1138.

He J, Xu M, Willmann MR, McCormick K, Hu T, Yang L, Starker CG, Voytas DF, Meyers BC, Poethig RS. 2018. Threshold-dependent repression of SPL gene expression by miR156/miR157 controls vegetative phase change in *Arabidopsis thaliana*. *PLoS Genetics* **14**: e1007337.

Hellens RP, Edwards EA, Leyland NR, Bean S, Mullineaux PM. 2000. pGreen: a versatile and flexible binary Ti vector for *Agrobacterium*-mediated plant transformation. *Plant Molecular Biology* **42**: 819–832.

Hu W, Fagundez S, Katin-Grazzini L, Li Y, Li W, Chen Y, Wang X, Deng Z, Xie S, McAvoy RJ *et al.* 2017. Endogenous auxin and its manipulation influence in vitro shoot organogenesis of citrus epicotyl explants. *Horticulture Research* **4**: 17071.

Ikeuchi M, Favero DS, Sakamoto Y, Iwase A, Coleman D, Rymen B, Sugimoto K. 2019. Molecular mechanisms of plant regeneration. *Annual Review of Plant Biology* **61**: 377–406.

Ikeuchi M, Sugimoto K, Iwase A. 2013. Plant callus: mechanisms of induction and repression. *Plant Cell* **25**: 3159–3173.

Katekar GF, Nave JF, Geissler AE. 1981. Phytotropins: III. NAPHTHYLPHTHALAMIC ACID BINDING SITES ON MAIZE COLEOPTILE MEMBRANES AS POSSIBLE RECEPTOR SITES FOR PHYTOTROPIN ACTION. *Plant Physiology* **68**: 1460–1464.

Kim JY, Henrichs S, Bailly A, Vincenzetti V, Sovero V, Mancuso S, Pollmann S, Kim D, Geisler M, Nam HG. 2010. Identification of an ABCB/P-glycoprotein-specific inhibitor of auxin transport by chemical genomics. *Journal of Biological Chemistry* **285**: 23309–23317.

Kim YS, Kim SG, Lee M, Lee I, Park HY, Seo PJ, Jung JH, Kwon EJ, Suh SW, Paek KH *et al.* 2008. HD-ZIP III activity is modulated by competitive inhibitors via a feedback loop in *Arabidopsis* shoot apical meristem development. *Plant Cell* **20**: 920–933.

Liu Q, Yao X, Pi L, Wang H, Cui X, Huang H. 2009. The *ARGONAUTE10* gene modulates shoot apical meristem maintenance and establishment of leaf polarity by repressing miR165/166 in *Arabidopsis*. *The Plant Journal* **58**: 27–40.

Magnani E, Barton MK. 2011. A per-ARNT-sim-like sensor domain uniquely regulates the activity of the homeodomain leucine zipper transcription factor REVOLUTA in *Arabidopsis*. *Plant Cell* **23**: 567–582.

Mallory AC, Reinhart BJ, Jones-Rhoades MW, Tang G, Zamore PD, Barton MK, Bartel DP. 2004. MicroRNA control of *PHABULOSA* in leaf development: importance of pairing to the microRNA 5′ region. *EMBO Journal* **23**: 3356–3364.

Mayer KF, Schoof H, Haecker A, Lenhard M, Jurgens G, Laux T. 1998. Role of *WUSCHEL* in regulating stem cell fate in the *Arabidopsis* shoot meristem. *Cell* **95**: 805–815.

McConnell JR, Emery J, Eshed Y, Bao N, Bowman J, Barton MK. 2001. Role of *PHABULOSA* and *PHAVOLUTA* in determining radial patterning in shoots. *Nature* **411**: 709–713.

Meng WJ, Cheng ZJ, Sang YL, Zhang MM, Rong XF, Wang ZW, Tang YY, Zhang XS. 2017. Type-B ARABIDOPSIS RESPONSE REGULATORs specify the shoot stem cell niche by dual regulation of WUSCHEL. *Plant Cell* **29**: 1357–1372.

Miyashima S, Honda M, Hashimoto K, Tatematsu K, Hashimoto T, Sato-Nara K, Okada K, Nakajima K. 2013. A comprehensive expression analysis of the *Arabidopsis MICRORNA165/6* gene family during embryogenesis reveals a conserved role in meristem specification and a non-cell-autonomous function. *Plant and Cell Physiology* **54**: 375–384.

Miyawaki K, Matsumoto-Kitano M, Kakimoto T. 2004. Expression of cytokinin biosynthetic isopentenyltransferase genes in *Arabidopsis*: tissue specificity and regulation by auxin, cytokinin, and nitrate. *The Plant Journal* **37**: 128–138.

Moglich A, Ayers RA, Moffat K. 2009. Structure and signaling mechanism of Per-ARNT-Sim domains. *Structure* **17**: 1282–1294.

Mukherjee K, Burglin TR. 2006. MEKHLA, a novel domain with similarity to PAS domains, is fused to plant homeodomain-leucine zipper III proteins. *Plant Physiology* **140**: 1142–1150.

Muller B, Sheen J. 2008. Cytokinin and auxin interaction in root stem-cell specification during early embryogenesis. *Nature* **453**: 1094–1097.

Murashige T. 1965. Effects of stem-elongation retardants and gibberellin on callus growth and organ formation in tobacco tissue culture. *Physiologia Plantarum* **18**: 665–673.

Nameth B, Dinka SJ, Chatfield SP, Morris A, English J, Lewis D, Oro R, Raizada MN. 2013. The shoot regeneration capacity of excised *Arabidopsis* cotyledons is established during the initial hours after injury and is modulated by a complex genetic network of light signalling. *Plant, Cell & Environment* **36**: 68–86.

Nishimura T, Matano N, Morishima T, Kakinuma C, Hayashi K-I, Komano T, Kubo M, Hasebe M, Kasahara H, Kamiya Y *et al.* 2012. Identification of IAA transport inhibitors including compounds affecting cellular PIN trafficking by two chemical screening approaches using maize coleoptile systems. *Plant and Cell Physiology* **53**: 1671–1682.

Noh B, Murphy AS, Spalding EP. 2001. Multidrug resistance-like genes of *Arabidopsis* required for auxin transport and auxin-mediated development. *Plant Cell* **13**: 2441–2454.

Prigge MJ, Otsuga D, Alonso JM, Ecker JR, Drews GN, Clark SE. 2005. Class III homeodomain-leucine zipper gene family members have overlapping, antagonistic, and distinct roles in *Arabidopsis* development. *Plant Cell* **17**: 61–76.

Radhakrishnan D, Kareem A, Durgaprasad K, Sreeraj E, Sugimoto K, Prasad K. 2018. Shoot regeneration: a journey from acquisition of competence to completion. *Current Opinion in Plant Biology* **41**: 23–31.

Radonic LM, Lewi DM, Lopez NE, Hopp HE, Escandon AS, Bilbao ML. 2015. Sunflower (*Helianthus annuus* L.). *Methods in Molecular Biology* **1224**: 47–55.

Ramachandran P, Carlsbecker A, Etchells JP. 2017. Class III HD-ZIPs govern vascular cell fate: an HD view on patterning and differentiation. *Journal of Experimental Botany* **68**: 55–69.

Rashotte AM, Brady SR, Reed RC, Ante SJ, Muday GK. 2000. Basipetal auxin transport is required for gravitropism in roots of *Arabidopsis*. *Plant Physiology* **122**: 481–490.

Reinhart BJ, Liu T, Newell NR, Magnani E, Huang T, Kerstetter R, Michaels S, Barton MK. 2013. Establishing a framework for the Ad/abaxial regulatory network of *Arabidopsis*: ascertaining targets of class III homeodomain leucine zipper and KANADI regulation. *Plant Cell* **25**: 3228–3249.

Rojas-Pierce M, Titapiwatanakun B, Sohn EJ, Fang F, Larive CK, Blakeslee J, Cheng Y, Cuttler S, Peer WA, Murphy AS *et al.* 2007. *Arabidopsis* P-glycoprotein19 participates in the inhibition of gravitropism by gravacin. *Chemistry & Biology* **14**: 1366–1376.

Rozhon W, Mayerhofer J, Petutschnig E, Fujioka S, Jonak C. 2010. ASKtheta, a group-III *Arabidopsis* GSK3, functions in the brassinosteroid signalling pathway. *The Plant Journal* **62**: 215–223.

Sabatini S, Beis D, Wolkenfelt H, Murfett J, Guilfoyle T, Malamy J, Benfey P, Leyser O, Bechtold N, Weisbeek P *et al.* 1999. An auxin-dependent distal organizer of pattern and polarity in the *Arabidopsis* root. *Cell* **99**: 463–472.

Schrick K, Bruno M, Khosla A, Cox PN, Marlatt SA, Roque RA, Nguyen HC, He C, Snyder MP, Singh D *et al.* 2014. Shared functions of plant and mammalian StAR-related lipid transfer (START) domains in modulating transcription factor activity. *BMC Biology* **12**: 70.

Shi B, Zhang C, Tian C, Wang J, Wang Q, Xu T, Xu Y, Ohno C, Sablowski R, Heisler MG *et al.* 2016. Two-step regulation of a meristematic cell population acting in shoot branching in *Arabidopsis*. *PLoS Genetics* **12**: e1006168.

Shukla PS, Das AK, Jha B, Agarwal PK. 2014. High-frequency in vitro shoot regeneration in *Cucumis sativus* by inhibition of endogenous auxin. *In Vitro Cellular & Developmental Biology-Plant* **50**: 729–737.

Smetana O, Mäkilä R, Lyu M, Amiryousefi A, Sánchez Rodríguez F, Wu M-F, Solé-Gil A, Leal Gavarrón M, Siligato R, Miyashima S *et al.* 2019. High levels of auxin signalling define the stem-cell organizer of the vascular cambium. *Nature* **565**: 485–489.

Smith ZR, Long JA. 2010. Control of *Arabidopsis* apical-basal embryo polarity by antagonistic transcription factors. *Nature* **464**: 423–426.

Steenackers W, Klima P, Quareshy M, Cesarino I, Kumpf RP, Corneillie S, Araújo P, Viaene T, Goeminne G, Nowack MK *et al.* 2017. cis-Cinnamic acid is a novel, natural auxin efflux inhibitor that promotes lateral root formation. *Plant Physiology* **173**: 552–565.

Sugimoto K, Temman H, Kadokura S, Matsunaga S. 2019. To regenerate or not to regenerate: factors that drive plant regeneration. *Current Opinion in Plant Biology* **47**: 138–150.

Sujatha M, Vijay S, Vasavi S, Reddy PV, Rao SC. 2012. Agrobacterium-mediated transformation of cotyledons of mature seeds of multiple genotypes of sunflower (*Helianthus annuus* L.). *Plant Cell Tissue and Organ Culture* **110**: 275–287.

Takei K, Ueda N, Aoki K, Kuromori T, Hirayama T, Shinozaki K, Yamaya T, Sakakibara H. 2004. AtIPT3 is a key determinant of nitrate-dependent cytokinin biosynthesis in *Arabidopsis*. *Plant and Cell Physiology* **45**: 1053–1062.

Teale WD, Pasternak T, Dal Bosco C, Dovzhenko A, Kratzat K, Bildl W, Schwörer M, Falk T, Ruperti B, V Schaefer J *et al.* 2021. Flavonol-mediated stabilization of PIN efflux complexes regulates polar auxin transport. *EMBO Journal* **40**: e104416.

Tsuda E, Yang H, Nishimura T, Uehara Y, Sakai T, Furutani M, Koshiba T, Hirose M, Nozaki H, Murphy AS *et al.* 2011. Alkoxy-auxins are selective inhibitors of auxin transport mediated by PIN, ABCB, and AUX1 transporters. *Journal of Biological Chemistry* **286**: 2354–2364.

Ulmasov T, Murfett J, Hagen G, Guilfoyle TJ. 1997. Aux/IAA proteins repress expression of reporter genes containing natural and highly active synthetic auxin response elements. *Plant Cell* **9**: 1963–1971.

Ursache R, Miyashima S, Chen Q, Vaten A, Nakajima K, Carlsbecker A, Zhao Y, Helariutta Y, Dettmer J. 2014. Tryptophan-dependent auxin biosynthesis is required for HD-ZIP III-mediated xylem patterning. *Development* **141**: 1250–1259.

Weits DA, Kunkowska AB, Kamps NCW, Portz KMS, Packbier NK, Nemec Venza Z, Gaillochet C, Lohmann JU, Pedersen O, van Dongen JT *et al.* 2019. An apical hypoxic niche sets the pace of shoot meristem activity. *Nature* **569**: 714–717.

Wenkel S, Emery J, Hou BH, Evans MM, Barton MK. 2007. A feedback regulatory module formed by *LITTLE ZIPPER* and *HD-ZIPIII* genes. *Plant Cell* **19**: 3379–3390.

Xiao Y, Offringa R. 2020. PDK1 regulates auxin transport and *Arabidopsis* vascular development through AGC1 kinase PAX. *Nature Plants* **6**: 544–555.

Yang S, Poretska O, Sieberer T. 2018. ALTERED MERISTEM PROGRAM1 restricts shoot meristem proliferation and regeneration by limiting HD-ZIP III-mediated expression of RAP2.6L. *Plant Physiology* **177**: 1580–1594.

Yoo SD, Cho YH, Sheen J. 2007. *Arabidopsis* mesophyll protoplasts: a versatile cell system for transient gene expression analysis. *Nature Protocols* **2**: 1565–1572.

Zhang TQ, Lian H, Zhou CM, Xu L, Jiao Y, Wang JW. 2017. A two-step model for de novo activation of *WUSCHEL* during plant shoot regeneration. *Plant Cell* **29**: 1073–1087.

Zhang ZF, Finer JJ. 2015. Sunflower (*Helianthus annuus* L.) organogenesis from primary leaves of young seedlings preconditioned by cytokinin. *Plant Cell Tissue and Organ Culture* **123**: 645–655.

Zhang Z, Tucker E, Hermann M, Laux T. 2017. A molecular framework for the embryonic initiation of shoot meristem stem cells. *Developmental Cell* **40**: 264–277 e264.

Zhu H, Hu F, Wang R, Zhou X, Sze SH, Liou LW, Barefoot A, Dickman M, Zhang X. 2011. *Arabidopsis* Argonaute10 specifically sequesters miR166/165 to regulate shoot apical meristem development. *Cell* **145**: 242–256.

Supporting Information

Additional Supporting Information may be found online in the Supporting Information section at the end of the article.

Fig. S1 Effect of ZIC2 concentration and application time on the induction of pZPR3::GUS activity.

Fig. S2 ZIC2 structure/function analysis.

Fig. S3 ZIC2 does not show direct cytokinin or auxin activity.

Fig. S4 Effect of ZIC2 analogs on *Arabidopsis* shoot regeneration.

Fig. S5 Effect of ZIC2 on post-transcriptional class III homeodomain-leucine zipper activity.

Fig. S6 Effect of ZIC2 on pMIR165A::GFP and pMIR166A::GFP fluorescence in primary root meristems.

Fig. S7 ZIC2 induces the expression of a subset of cytokinin biosynthesis enzymes during *Arabidopsis* shoot regeneration.

Fig. S8 Effect of ZIC2 on pIPT5::GUS activity in primary root meristems and during shoot regeneration.

Fig. S9 Naphtylphtalamic acid-like effects of ZIC2 on auxin responses in *Arabidopsis* seedlings.

Fig. S10 Effect of ZIC2 on PIN-mediated ^{3}H-IAA efflux in *Xenopus* oocytes.

Fig. S11 Effect of ZIC2 and naphtylphtalamic acid on auxin responses during regeneration.

Table S1 Oligos used in quantitative real-time polymerase chain reaction experiments.

Please note: Wiley Blackwell are not responsible for the content or functionality of any Supporting Information supplied by the authors. Any queries (other than missing material) should be directed to the *New Phytologist* Central Office.